NUMERICAL ANALYSIS OF PILE-SUPPORTED GEOGRID-REINFORCED EMBANKMENTS ON SOFT GROUNDS

Thesis

Submitted in partial fulfilment of the requirements for the degree of

DOCTOR OF PHILOSOPHY

By

RADHIKA M. PATEL

DEPARTMENT OF CIVIL ENGINEERING

NATIONAL INSTITUTE OF TECHNOLOGY KARNATAKA

SURATHKAL, MANGALORE-575025

JANUARY 2022

NUMERICAL ANALYSIS OF PILE-SUPPORTED GEOGRID-REINFORCED EMBANKMENTS ON SOFT GROUNDS

Thesis

Submitted in partial fulfilment of the requirements for the degree of

DOCTOR OF PHILOSOPHY

By

RADHIKA M. PATEL

(155090CV15F07)

Under the guidance of

Dr. B.R. JAYALEKSHMI and Dr. R. SHIVASHANKAR

DEPARTMENT OF CIVIL ENGINEERING

NATIONAL INSTITUTE OF TECHNOLOGY KARNATAKA

SURATHKAL, MANGALORE-575025

JANUARY 2022

D E C L A R A T I O N

I hereby *declare* that the Research Thesis entitled "**Numerical analysis of pile-supported geogrid-reinforced embankments on soft grounds"** which is being submitted to the **National Institute of Technology Karnataka, Surathkal** in partial fulfilment of the requirements for the award of the Degree of **Doctor of Philosophy** in **Civil Engineering**, is a *bonafide report of the research work carried out by me.* The material contained in this Research Thesis has not been submitted to any University or Institution for the award of any degree.

RADHIKA M. PATEL

(Register No: 155090CV15F07)

Department of Civil Engineering

Place: NITK Surathkal

Date: 24/01/2022

CERTIFICATE

This is to *certify* that the Research Thesis entitled "**Numerical analysis of pile-supported geogrid-reinforced embankments on soft grounds**" submitted by **RADHIKA M. PATEL,** (Register Number: **155090CV15F07**) as the record of the research work carried out by her, *is accepted as the Research Thesis submission* in partial fulfilment of the requirements for the award of degree of **Doctor of Philosophy.**

02/02/2022

Prof. B.R.Jayalekshmi

Research Guide
Professor
Department of Civil Engineering
NITK, Surathkal

2/2/22

Prof. R. Shivashankar

Research Guide
Professor
Department of Civil Engineering
NITK, Surathkal

NATIONAL INSTITUTE OF TECHNOLOGY KARNATAKA, SURATHKAL
DEPT. OF CIVIL ENGG.

02/02/2022

Prof. B.R.Jayalekshmi

Chairman-DRPC
Head of the Department
Department of Civil Engineering
NITK, Surathkal

Chairman (DRPC)
Department of Civil Engineering
National Institute of Technology Karnataka, Surathkal
Mangalore - 575 025, Karnataka, INDIA

DEDICATED TO MY GUIDES, FAMILY AND FRIENDS

ACKNOWLEDGEMENT

First and above all I would like to thank the almighty for bestowing upon me the choicest blessings and providing me the capability to proceed successfully in my life.

Since its inception, NITK Surathkal has always been a harbinger of educational excellence and research throughout the country. I am extremely fortunate to be associated with this great institution.

I would like to express my deep sense of gratitude to my guide and research supervisor Dr. B.R. Jayalekshmi, Professor and Head, Department of Civil Engineering, NITK Surathkal, for giving me an opportunity to pursue my research work under her valuable guidance. Without her constant supervision and persistence, this thesis would not have been possible.

With great pleasure I acknowledge my sincere gratitude to my research supervisor Dr. R. Shivashankar, Professor, Civil Engineering Department, NITK Surathkal, for all his inspiration, relentless guidance, encouragement and help in successful completion of the research program. His keen engineering and scientific insight has helped me enormously in improving the technical content and practical relevance of the thesis.

I am greatly indebted to RPAC members, Prof. M. C. Narasimhan of civil engineering department and Prof. Subba Rao from department of water resources and ocean engineering for their timely evaluation and valuable suggestions during the progress of the research work.

I am thankful to Dr. Palanisamy T, Secretary DRPC. I take this opportunity to thank former department heads namely, Prof. K. N. Lokesh, Prof. Venkat Reddy, Prof. Varghese George and Prof. K. Swaminathan for their timely help during my entire research period.

I sincerely thank Prof. Katta Venkataramana, Professor, Civil Engineering Department, NITK Surathkal, for his continuous and wholehearted support during my entire research period.

I gratefully acknowledge the support and help rendered by Mr. Anil Sagar, Ms. Sreya M. V. Mr. Sachin, Mr. M. Harsha Ms. Pranitha (Junior research scholars, Civil engineering department) Ms. Sreelekshmy Sreedevi, Ms. Surya N. R, Mr. Somanna (Former M.Tech. Students of GTE) Mr. Shreyas (Former M.Tech student, ST) for the successful completion of my research work. Special thanks to my friends Mr. Pandith

Aradhya, Dr. Rashma R. S. V, Ms. Arpitha, Dr. Anaswara S, Dr. Shreyasvi, Dr. Gayana, Dr. Sowmya, Dr. Uma S, Dr. Vajreshwari, Dr. Archana J. Sateesh and Dr. Suman Saha for their help in the successful completion of my research. I thank all my friends at NITK who were always supportive and friendly to me. I sincerely thank my seniors Dr. Jisha and Dr. Chinmayi for clarifying my software related issues. I also wish to thank my M.Tech friend, Dr. Deviprasad B. S for clarifying my doubts.

I wish to thank my cousin Mr. Basavaraj K. Y and Mr. Ashokan K, Co-director, Acufore engineering services organization for helping me in learning the software. I am thankful to my cousin Dr. Darshan G. P for his valuable suggestions regarding research.

I also like to extend my gratitude to all the teaching faculty and supporting staff of the civil engineering department, for their encouragement, help and support provided during the research work. I sincerely thank Mr. Subhash, computer lab staff, for his help to run the models in the lab. My thanks are also due to the office staff of Civil Engineering Department.

I would like to express my sincere gratitude to the authorities of NITK Surathkal, for providing me excellent facilities and comfortable stay in the campus.

I thank my mother, Mrs. Girija G. M for the great sacrifices she has done for my education and bright future. I thank my father, Mr. A. C. Mruthyunjaya who always inspired me and gave freedom in following my career dreams. I thank my husband, Mr. Avinash A. S and my in laws for the forbearance and full hearted support offered me during my studies, without which my research dreams wouldn't have been fulfilled. I thank my brother Mr. Rahul M. Patel and all my cousins for their whole hearted support to the completion of this research. I also like to extend my thanks to all my uncles and aunts for their help and support provided during this research. More than anything, I would like to thank my one and half year old little star Miss Preksha R. Avinash, who patiently cooperated, when her mother was busy with the research and studies.

I would like to thank all my professors, teachers, colleagues, friends, and my students for making me what I am today. Let me, in the end pay sincere thanks to all from whom I had received or receiving positive vibes, support, co-operation and encouragement in life.

Radhika M. Patel

ABSTRACT

In recent decades, the column supported embankments are often constructed at places where soft clay exists within a considerable depth and the construction of roads or rail roads or bridge approach roads is of great demand due to rapid increase of industrialization and urbanization. The column supported embankment has many advantages over the other conventional consolidation based techniques. Such as, these embankments can be constructed at a stretch without prolonged time delay and the embankment loads are directly transferred to the hard strata through piles. Geosynthetics has several advantages for improving the soft grounds, among them providing geogrids as basal-reinforcement below the embankments constructed over soft subsoils of shallow depth is one of the well-known technique. The basal-reinforcements can also be provided above the piles instead of pile caps or raft above piles. The geosynthetics can also be provided in the embankment body to steepen the embankment side slopes. The response of these basal or body-reinforced embankments with or without pile supports under static loading conditions is well-addressed in literature. Most of the studies on dynamic response of these embankments considered cyclic loads or sinusoidal loads to represent traffic loading. Though there are studies available on the seismic response of these embankments, the response of these embankments considering full 3-Dimensional finite element model subjected to time-history loading of different earthquakes is not yet addressed. Hence, in the present study both static and seismic response of basal or body reinforced embankments with and without pile supports are studied using 3-dimensional finite element analysis.

In the first part of the study, the response of basal geogrid-reinforced pile-supported embankments subjected to self-weight and traffic load are studied using 3-dimensional finite element models. The influence of various parameters such as, embankment height, geogrid tensile modulus, pile length, pile type and pile spacing are studied. Based on the results of numerical analysis, the modifications to the soil arching coefficient (C_c) including the effect of pile length and pile spacing are proposed and compared with the existing analytical equations. Crest settlements, toe lateral displacements, differential settlements at crest, stress distribution ratio, lateral stress

distribution ratio and coefficient of lateral pressure along embankment height were considered to analyse the response of these embankments. The analysis of results indicates that, the end-bearing pile supported embankments performs better than floating pile supported embankments in terms of settlements, differential settlements and lateral displacements even at larger pile spacing. The addition of basal geogrid could further reduce the settlements and lateral displacements in the embankment. The analytical equation for C_c proposed based on the 3-dimensional finite element analysis results considered the effect of pile spacing, which the earlier methods did not consider. Hence the proposed analytical equation could able to give the more accurate results of pile loads than the existing methods. The crest centre settlements were further increased by the addition of traffic load.

These basal geogrid-reinforced pile-supported embankments should stand safe during disastrous situations like earthquakes. Hence the second part of the study analyses the seismic response of basal geogrid-reinforced pile-supported embankments subjected to seismic excitations. Time-history analysis was performed on the 3-Dimensional finite element models of basal geogrid-reinforced pile-supported embankments. The seismic response of embankment in terms of vertical and lateral displacements, differential settlements, vertical and lateral stress distribution on pile and the foundation soil between piles, amplification coefficient, lateral earth pressure along the embankment height and the pore water pressure are studied by considering the height of embankment, side slope of embankment, basal geogrid tensile modulus, length of pile, spacing of pile and type of pile. The analysis of results shows that the embankment height is an important parameter to consider in the seismic design of basal geogrid reinforcement. 4 m high embankment experiences very less differential settlements caused by seismic excitations among the different embankment heights considered. About 8 % reduction of toe lateral displacements are observed by the addition of basal geogrid. But the embankment with pile supports shows a reduction of 40.8 % and the combination of both pile supports and basal geogrid could reduce 46 % of toe lateral displacements. Addition of basal geogrid increases both vertical and lateral stresses on piles due to seismic excitations. The variation of coefficient of lateral pressure along the embankment elevation is random for the considered parameters, this indicates that the formation of soil arching in a geogrid reinforced pile supported

embankment subjected to seismic loading is not uniform like in the case of self-weight analysis.

Basal geosynthetic-reinforcements are the most commonly used ground improvement technique for the embankments constructed over shallow depth soft clays. The width of the basal-reinforcement provided should be adequate to withstand lateral sliding, rotational failure and excessive settlements under both static and seismic loading conditions. In the third part of the study, an attempt has been made to study the optimum width of basal geosynthetic-reinforcement subjected to both static and seismic loading conditions. Finite element models of basal geosynthetic-reinforced embankments including the effect of embankment height, embankment side slope, tensile modulus of geosynthetic, number of layers of geosynthetic, stiffness of embankment fill, stiffness of foundation soil and intensity of seismic loading were studied. Based on the results of crest settlements, toe lateral displacements and lateral displacements at the crest, the required width and tensile modulus of basal geogrid were identified. Basal geogrid having a minimum tensile modulus of 500 kN/m with a width equal to the base width (B) of embankment is found to be sufficient to reduce settlements at places where static loading is predominant or in low seismic regions. Basal geogrid of width equal to 'B+H' having tensile modulus of 4000 kN/m is recommended to reduce the lateral displacements in embankments at active seismic regions. Further reduction of about 6 % in lateral displacements are seen by providing 4 layers of basal geogrid with a total tensile modulus equal to 4000 kN/m.

The geosynthetics are also used as embankment body-reinforcements to steepen the embankment side slopes. These slopes are stable under static loading conditions but, under seismic loading conditions, repairable damages or sometimes complete failure of slopes may occur. Hence the present study is also extended to analyse the seismic response of body-reinforced embankments considering the effect of embankment side slope and foundation soil stiffness using finite element analysis. From the analysis it is observed that, in unreinforced embankments the face lateral displacements increase as the steepness of slope increases and the embankment above soft soil displaces more than the embankment on stiff soil.

Keywords: Pile-supported embankments, Basal geosynthetic, Finite element method, soft marine clay, Soil arching coefficient, Body-reinforced embankments, Slope stability, Seismic excitations, Stress distribution ratio, Lateral stress distribution ratio

CONTENTS

List of Figures

List of Tables

NOMENCLATURE

Abbreviations

APDL Ansys Parametric Design Language

ASTM American Standard Testing Manual

BSI British Standards Institution's

DEM Discrete element method

FEM Finite Element Method

GGS German Geotechnical Society's

GRPES Geosynthetic reinforced piled embankment systems

GRS Geosynthetic reinforced soil

IRC Indian Road Congress

IS Indian Standard

LA Limit Analysis

LDRR Lateral Displacement Reduction Ratio

LSDR Lateral stress distribution ratio

PFA Pulverized Fuel Ash

PGA Peak ground acceleration

PPPeBOTDA Pulse-pepumpe Brillouin optical time domain analysis

SDR Stress distribution ratio

Notations

a Pile cap width or diameter

A Area of pile or pile cap

A_n The field controlling the viscous dampers along normal direction in the boundary

A_{t1} & A_{t2} The fields controlling the viscous dampers along tangential direction in the boundary

b centre line spacing of piles

c' Effective cohesion

C_c Coefficient of soil arching

f_{fs} Partial factor for soil density (1.3)

f_q Partial load factor for external applied loads (1.3)

H Embankment height

J	Geosynthetic tensile stiffness
K	Coefficient of lateral earth pressure
K_o	Coefficient of Earth pressure at rest
K_a	Coefficient of active earth pressure
K_p	Coefficient of passive earth pressure
l	Length of floating pile
L_{crit}	Critical length of pile
L_T	Reinforcement length at the top
L_B	Reinforcement length at bottom
P	Load over pile
q	Surcharge load over embankment
Q_p	Allowable load carrying capacity of each pile in the pile group
r	Radius of pile
R	Pile spacing/2
RF_{CR}	Reduction factor due to creep,
RF_{ID}	Reduction factor due to installation damage
RF_D	Reduction factor due to durability.
s	Pile centre to centre spacing
S_{3D}	Stress reduction ratio
S_{reinf}	Settlement of soil with pile and geogrid reinforcement
$S_{unreinf}$	Settlement of soil without pile and geogrid reinforcement
S_{edge}	Settlement of soil at the edge of embankment crest
S_{centre}	Settlement of soil at the centre of embankment crest
t	trap-door's width
T_{ult}	Ultimate tensile strength of the reinforcement
v_p	P-wave velocity of the considered medium
v_s	S-wave velocity of the considered medium
W	Weight per unit length
W_s	External surcharge loading
$\overline{x}$	Depth of neutral plane
α	Amplification coefficient
β	Slope depicted in Fig. 1.2(b)

γ	Unit weight of embankment soil
γ'	Density of foundation soil
σ_p	Vertical stress on the pile
σ_s	Vertical stress on the foundation soil
σ_v	Average vertical stress at embankment base
σ_z	Vertical effective stress
τ_{xz}	Shear stress on the xz plane of the soil element
ρ	Density of soil medium
φ	Angle of internal friction of the soil
Φ'	Soil Friction angle
Φ'_f	Factored soil friction angle

CHAPTER 1

INTRODUCTION

1.1 GENERAL

Rapid increase of industrialization and urbanization leads to the construction of new roads and bridges on soft unfavourable grounds, which also leads to the rehabilitation and widening of existing roads. Soft soils are unable to sustain heavy loads because of their low shearing resistance and high compressibility. These soils undergo large amount of settlements due to consolidation. In the case of bridges, loads are transferred to the unyielding strata by deep foundations and the embankment adjacent to it rests on a yielding strata subjected to ground water table variations, erosion, self-weight of embankment and traffic loads. This causes huge differential settlements at the junction of the bridge deck and the approach embankment on either side of the bridge. Due to this differential settlement an uneasy bump will be experienced at the entrance and exit of the bridge causing discomfort for the drivers and passengers.

To resolve all these issues related to road and bridge constructions and their rehabilitation, a variety of techniques are available nowadays. They are preloading, vertical drains, use of light weight fill materials for the embankment fill, replacing the soft foundation soil with suitable fill material (good inorganic soil) and steepening embankment slope. All these ground improvement methods require quite some time to improve the ground because they are consolidation based techniques or they are much labour oriented. But the use of reinforced earthen embankments (or mechanically stabilized earth retaining walls) with or without pile foundations overcome most of the drawbacks of the above mentioned techniques.

Depending on the depth of soft soil extent and the purpose of embankment, the embankments are stabilized with the following (i) only basal geosynthetic, (ii) The combination of basal geosynthetic and pile-supports, if the embankment side slopes need to be steepened or if there is a need of high embankments without berms, (iii) Provision of body reinforcement across the embankment slopes is a reliable solution.

1.2 BASAL GEOSYNTHETIC-REINFORCED EMBANKMENT

The use of geosynthetics in civil engineering constructions has wide range of applications. It can significantly increase the safety factor, improve the performance, and reduce costs in comparison with conventional construction alternatives. In case of embankments on extremely soft foundations, geosynthetics can permit construction to take place at sites where conventional construction alternatives would be either impossible or prohibitively expensive. Geosynthetics are particularly useful in road pavement construction and the earthworks associated with road construction.

The construction of embankments on poor compressible lands is a challenging task for the engineers due to shear failure of soft subsoil, sliding/rotation of embankment fill or subsoil, excessive vertical settlements, and lateral displacements. To prevent these failures, the use of geosynthetic reinforcement at the base level of the embankment is a suitable solution for shallow compressible subsoils. The addition of basal geosynthetic improves the shear resistance of both embankment as well as foundation soil. The provision of basal geosynthetic helps to keep the settlements caused by the embankment weight within the permissible limits of settlements and thereby controlling the total settlements caused by the consolidation of soft subsoil. Hence, the function of basal geosynthetic to spread the embankment loads over a large area of subsoil is necessary until most of the consolidation settlements of subsoil gets over. Fig.1.1 depicts the time-dependent behaviour of basal-reinforcement.

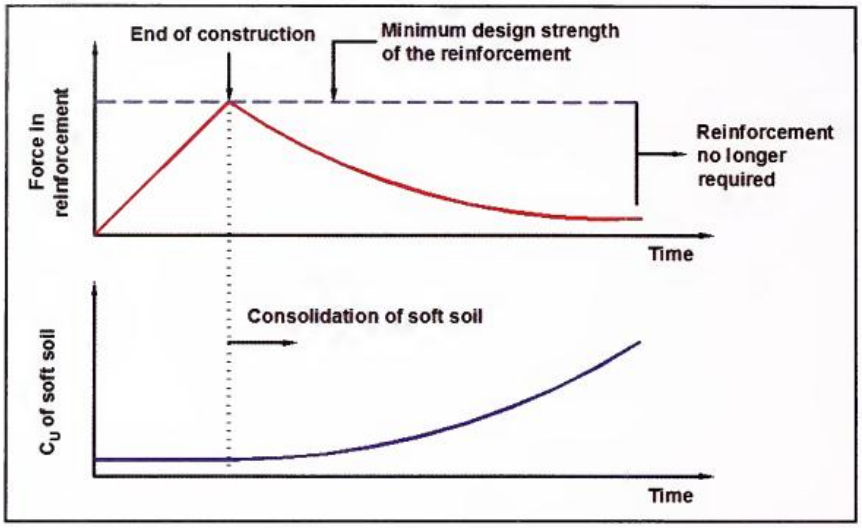

Figure 1. 1 Time-dependent behaviour of basal geosynthetic-reinforcement (IRC: 113-2013)

The reinforcement provided at the base of embankment should be able to withstand the shear failure of foundation soil, lateral sliding of embankment fill and the rotational failure of embankment slope. Hence, the reinforcement should have adequate tensile strength and sufficient width to withstand these failures under different loading conditions like self-weight of embankment, traffic loads and seismic excitations. There are several studies and guidelines available on these embankments subjected to self-weight and traffic loads. Seismic response of these basal-geosynthetic reinforced embankments needs to be studied further in determining the suitable width of basal-reinforcement to withstand the failures caused by seismic excitations. An attempt has been made in the present study to analyse the suitable width and tensile strength of basal-reinforcement including several parameters subjected to self-weight and seismic loading conditions.

1.3 BASAL GEOSYNTHETIC-REINFORCED PILE-SUPPORTED EMBANKMENT

The main purpose of providing pile foundations is to carry and transfer loads into strong bearing strata when good bearing strata is not available at shallow depth by end bearing action and skin friction. Because of rapid growth in infrastructure, researchers are coming-up with various advantages of pile foundations in civil engineering construction. Such as, construction of multi-storey buildings, construction of towers, construction of buildings in expansive clays, construction in loose sands, sheet piles in the construction of dams, construction of bridges, construction of harbours, contiguous piles in retaining wall construction and to check the seepage, micropiles in slope stability, embankment construction in soft clays and so on.

Whenever the soft clays extend to a considerable depth and the construction of embankments on such deep soft clay deposits is necessarily on demand, the construction of embankment with basal geosynthetic-reinforcement along with pile supports is a very good solution. This is due to the numerous advantages of these embankments over other conventional methods. Such as, these basal geosynthetic-reinforced embankments with or without pile foundations can be built at a stretch without prolonged time period with maximum reduction in total and differential settlements. These embankments can be constructed irrespective of the soil properties in the site because most of the loads are transferred by piles to the hard strata through

soft problematic soils. Moreover pile foundations withstand larger loads than any other product used in ground improvement techniques.

The geosynthetic-reinforced piled embankment design mainly consists of the design of embankment geometry (height of embankment, side slopes, presence or absence of berms) stability check, geosynthetic reinforcement, facing element (in case of back to back vertical faced retaining walls as approach embankments), pile dimensions (centre-to-centre spacing between the piles, length of piles and inclination of piles). The reinforced piled embankments transfer the external loads as well as embankment loads by the soil arching mechanism. In this mechanism, the basal reinforcement will be acting as a flexible raft which helps in transferring the embankment loads to the pile foundations.

1.4 MECHANISM OF LOAD TRANSFER

The external load, for example from the traffic and the embankment load above the soil arch is transferred to the piles via the soil arching mechanism. The embankment load below the soil arch will be taken by the geosynthetic and will be directed to the piles via geosynthetic tension. The piles transfer the load to the deeper and stiffer soil stratum. Thus, the soft soil experiences little force and therefore compaction because the forces are transferred through the geosynthetic and the piles. The amount of load transferred to piles depends on different factors such as the transfer platform thickness, inclusion spacing, surcharge, compressibility of the underlying soft soil, and secant stiffness of the geosynthetic material.

In summary, the mechanisms of load transfer can be considered as a combination of embankment soil arching, tensioned membrane or stiffened platform effect of geosynthetic, and stress concentration due to the stiffness difference between pile and soil. Each component depends on a number and tensile stiffness of geosynthetic reinforcement layers, properties of embankment fill and foundation soils, and elastic moduli of pile materials etc.

1.5 SOIL ARCHING

Arching is the ability of a material to transfer loads from one location to another in response to a relative displacement between the locations (McNulty, 1965) (Fig.1.2).

The existing guidelines for the design of reinforced piled embankments (such as the British Standards Institution's(BSI) BS8006-1 (BSI 2010) and German

Geotechnical Society's(GGS) EBGEO (GGS 2010), Nordic guidelines etc.) are based on several soil arching theories given by Terzaghi, Guido et al. (1987), Carlsson (1987), Hewlett and Randolph (1988), Jones et al. (1990) . All these methods are explained below in brief.

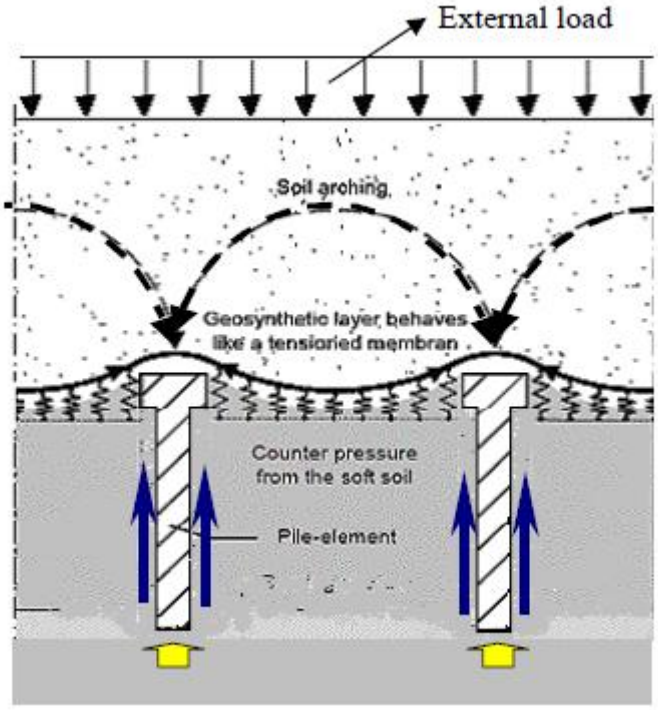

Figure 1. 2 The idea of reinforced piled embankment (Satibi, S. 2007)

1.5.1 Terzaghi's Method

Arching effects are described by Terzaghi based on his experiment on the trap door effects. As shown in Fig.1.3, based on the vertical equilibrium of a soil element, one can write:

$$(\sigma_z + d\sigma_z).t - \sigma_z .t + 2\tau_{xz}\, dz - dW = 0 \qquad (1.1)$$

where:

σ_z is the vertical effective stress,

τ_{xz} is the shear stress on the xz plane of the soil element,

t is trap-door's width,

W is soil weight per unit length.

It can be simplified as

$$d\sigma_z .t = \gamma . tdz - 2\tau_{xz}\, dz , \qquad (1.2)$$

Where: γ is the unit weight of soil.

According to the Mohr-Coulomb failure criterion, shear stress at failure can be expressed as

$$\tau_{xz} = c' + \sigma_x .\tan\phi' \quad (1.3)$$

with c' and ϕ' are the effective cohesion and friction angle of the soil. The effective horizontal stress as a function of vertical effective stress is $\sigma_x = \sigma_z$. K. Hence Eq. (1.2) can be written as follows:

$$d\sigma_z . t = \gamma . t.dz - 2(c' + \sigma z . K \tan\phi')dz \quad (1.4)$$

Dividing both sides of Eq. (1.4) with σ_z and s we get a differential equation as below

$$\frac{d\,\sigma z}{\sigma z} = \frac{\gamma}{\sigma z} dz - \frac{2c\prime}{t.\sigma z} dz - \frac{2K.\tan\phi'}{t} dz \quad (1.5)$$

The solution for the differential equation is as follows:

$$\sigma_z = \frac{t.(\gamma - 2.\frac{c'}{t})}{2.K.tan\phi'} . \left[1 - e^{-2K\tan\phi'.\frac{z}{t}}\right] + p.e^{-2K\tan\phi'.\frac{z}{t}} \quad (1.6)$$

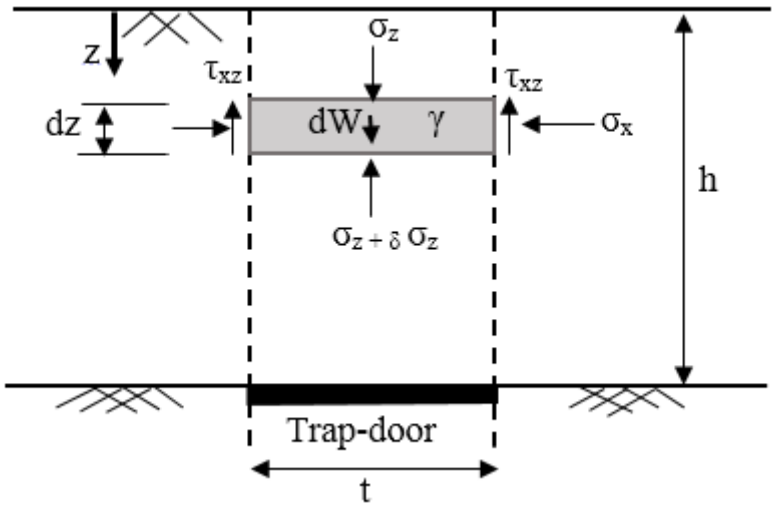

Figure 1. 3 Description of soil arching analysis with Terzaghi's method

Based on the experimental results, Terzaghi determined that the K value is 1. The solution in Eq.(1.6) gives an exponentially increasing vertical effective stress within the embankment fill between the two rigid foundations. Due to arching, the vertical stress acting on the ground surface below the embankment is much lower than the geostatic vertical stress.

1.5.2 Guido et al. Method (1987)

This method is derived from plate loading tests. For the three-dimensional condition, this method assumes that the load spreads through the fill layer at an angle of 45^0 and geosynthetic reinforcement is required to support the weight of a soil pyramid which is not supported by piles. Russell and Pierpoint(1997) derived an expression for the stress reduction ratio for this method, as shown in Eq. (1.7).

$$S_{3D} = \frac{(s-a)}{3\sqrt{2}\,H} \tag{1.7}$$

Where:

S_{3D} is the stress reduction ratio,

s is the pile spacing,

a is the pile cap width,

H is the embankment height.

1.5.3 Carlsson's Method (1987)

The Nordic guidelines follows this method for designing the geosynthetic reinforced piled embankments. This method considers a wedge of soil whose cross-sectional area under the arching soil can be approximated by a wedge with an internal angle at the apex of the wedge equal to 30º as shown in Fig.1.4.

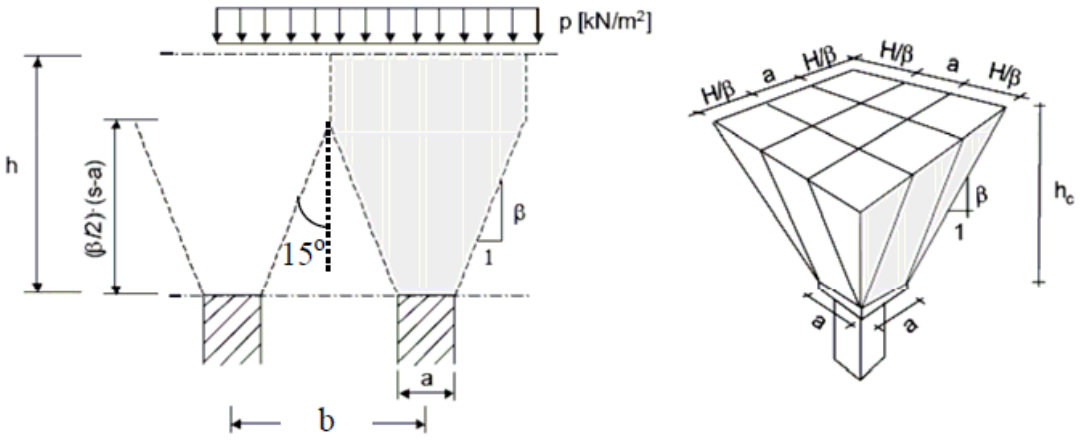

(a) **(b)**

Figure 1. 4 Soil wedge model: (a) 2D and (b) 3D (Satibi, S. 2007)

This method adopts a critical height approach such that any additional overburden above the top of the wedge is transferred directly to the columns. For a 2D

approach, with the height of the embankment above the triangular area, the weight of the soil wedge per unit length can be calculated as:

$$W = \frac{(b-a)^2}{4tan15^0}\gamma \quad (1.8)$$

Where:

W is the weight per unit length (out of plane direction of Fig.1. 4(a),

a is the width of square pile caps,

b is the centerline spacing of piles,

γ is the unit weight of the embankment.

The calculated soil wedge weight is the load on the geosynthetic layer. Rest of the embankment load is carried by the piles. Svano et al. (2000) proposed a method considering the 3-D effect as shown in Fig.1.4 (b). The weight of soil mass per pile cap side that will be transferred to the geosynthetics can be calculated as follows:

$$W_s = \frac{\gamma}{2a}\{b^2\mathrm{H} - \frac{1}{6\tan\beta}[(\mathrm{a} + \mathrm{H}\tan\beta)^3 - \mathrm{a}^3]\} \quad (1.9)$$

Where:

W_s is the weight of soil per pile cap side (half pyramid),

H is the height of embankment,

β is the slope depicted in Fig. 1.4(b).

1.5.4 Hewlett and Randolph Method (1988)

Hewlett and Randolph method assumes that the arching in an embankment forms an arching shell with a shape of hemispherical dome as shown in Fig. 1.5(a) and 1.5(b). The thickness of the arching shell is (b/√2) in the section of diagonal spacing of the squared pile grid. b is the width of a squared pile. Due to the soil arching, soil stresses are assume to be redistributed in this arching shell only. Outside the shell, the stress distribution is similar to initial stress distribution. This means that above and below the arching shell, the stress is increasing linearly with depth.

Failure of the arching is assume to occur only at crown of the arch or at the pile cap. Equilibrium analyses at the two positions lead to two equations for the stress acting on the surface of the sub soil, σ_s as presented in the following:

a) Equilibrium analysis at the crown of arch

The analysis is in plane strain of arching shell with spherical geometry. Vertical equilibrium of soil at the crown of the arch as shown in Fig.1.5 (a) requires that:

$$\frac{d\sigma_r}{dr} + \frac{2(\sigma_r - \sigma_\theta)}{r} = -\gamma \tag{1.10}$$

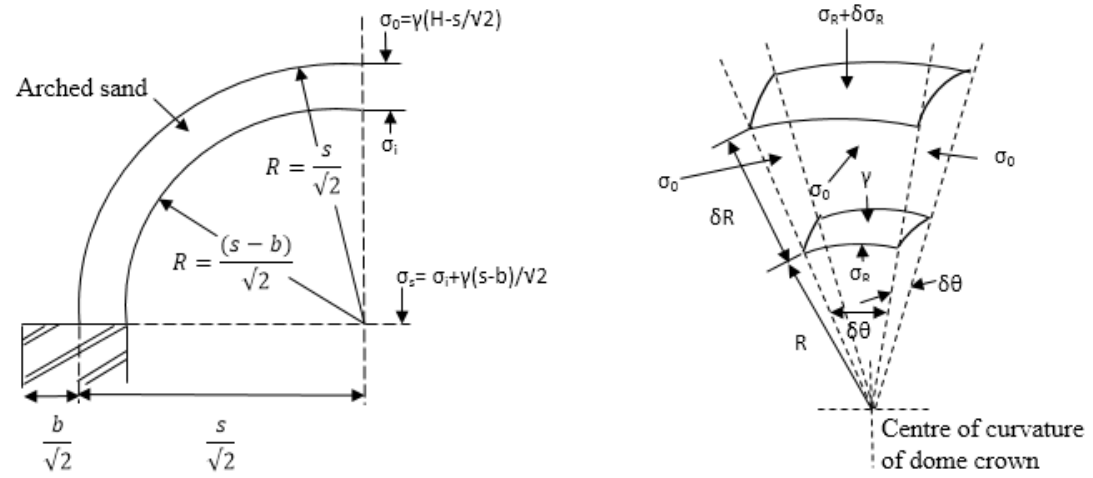

(a)

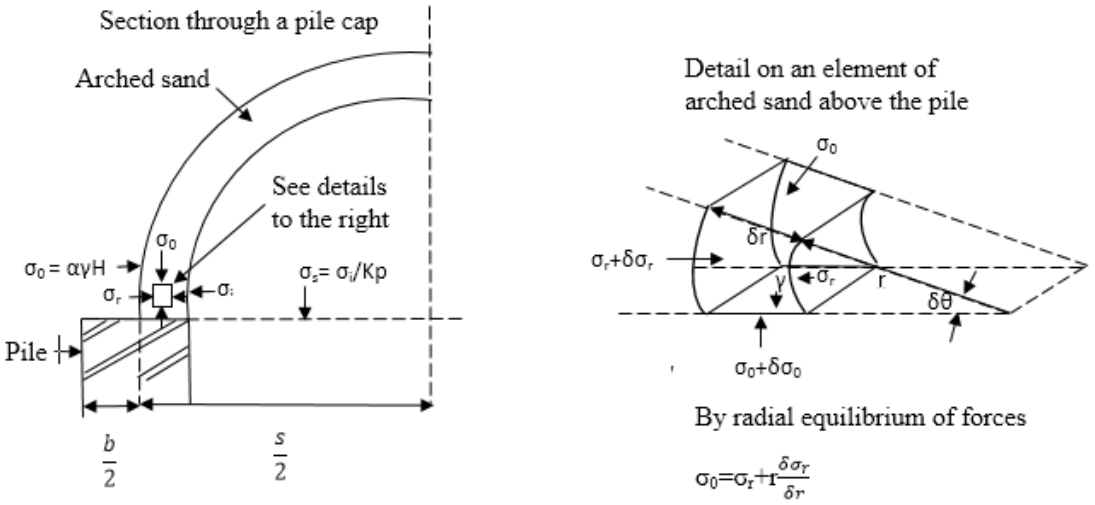

(b)

Figure 1. 5 Soil arching (a) Equilibrium analysis at crown of arch (b) Equilibrium analysis at just above pile cap (Satibi S. 2007)

Where: $\sigma_\theta = K_p . \sigma_r$, and Kp is the Rankine's passive earth pressure coefficient which is equal

to $(1+ \sin \phi') / (1- \sin \phi')$. The inner radius is $R = (s - b)/\sqrt{2}$ and the outer radius is $R = s /\sqrt{2}$ with s is the centre-to-centre pile spacing. The corresponding vertical stresses are σ_i and $\gamma (H – s/\sqrt{2})$ as shown in Fig. 1.5(a), where H is the height of the embankment. Solving the Eq. (1.10) subjected to the boundary conditions of inner and outer radius gives:

$$\sigma_i = \left[\gamma(1-\delta)^{2(K_p-1)}\right].\left[H - \frac{s}{\sqrt{2}}\left(\frac{\mathrm{K_p}-2}{2\mathrm{K_p}-3}\right)\right] + \gamma\frac{\mathrm{s-b}}{\sqrt{2}(2\mathrm{K_p}-3)} \quad (1.11)$$

With δ is b/s. The total pressure acting on the subsoil σ_s is:

$$\sigma_s = \sigma_i + \gamma(s-b)/\sqrt{2} \quad (1.12)$$

b) Equilibrium analysis at the pile cap

At the pile cap, the vault comprises four plane strain arches, each occupying a quadrant of the cap. The equilibrium analysis is in plane strain at the pile cap section as shown in Fig.1.5 (b). The pressure acting on the subsoil, σ_s due to this equilibrium analysis is as below:

$$\sigma_s = \frac{\gamma H}{\frac{2K_p}{K_p+1}.\left[(1-\delta)^{(1-K_p)} - (1-\delta).\left(1-\delta.K_p\right)\right] + (1+\delta^2)} \quad (1.13)$$

The larger stress acting on the surface of subsoil is determined by the larger value between the result from Eq. (1.12) and Eq. (1.13). The Hewlett and Randolph formula gives a typical vertical stress distribution of the embankment fill along the centre of the arching dome as shown in Fig.1.5 (a-b).

1.5.5 Kempfert et al. (1997)

Kemfert et al. (1997) proposed the multi shell arching theory. This theory is based on the idea of the Hewlett and Randolph approach, with a modification for low-height embankments using multi shell arching theory. In the new approach, Kempfert et al. considers domed arches spanning between columns or pile caps.

1.5.6 Jones et al. (1990)

Jones et al. (1990) developed an empirical method, which is based on a formula proposed by Marston and Anderson (1913) for soil arching on top of a buried pipe. This method has been adopted by BS 8006. In this Method, the arching is assumed to be semi-spherical dome and it is independent of the type and strength properties of the embankment fill. The ratio of the vertical stress on top of the caps to the average vertical stress at the base of the embankment (P_c'/σ_v') may be estimated as follows:

$$\frac{P_c'}{\sigma_v'} = \left[\frac{C_c a}{H}\right]^2 \quad (1.14)$$

Where:

Cc soil arching coefficient defined as:

1.95 H / a − 0.18 for end-bearing piles

1.5H/ a − 0.07 for friction and other piles

a is the size of the pile caps,

H is the height of the embankment.

These arching theories are based on wide range of assumptions and to better understand the phenomenon of soil arching under both static and dynamic loading conditions, there is a need to study the behaviour of these embankments using full 3-dimensional finite element analysis. Hence, the present study also has focussed on the 3-dimensional finite element analysis of basal geogrid-reinforced pile-supported embankments subjected to static and seismic excitations. Several parameters influencing the load transfer mechanism in these embankments under both static and seismic loading conditions are studied.

1.6 BODY -REINFORCED EMBANKMENT

Among the various advantages of geosynthetics for improving the ground, use of geosynthetic to stabilize the embankment slopes is one of the well-known technique. At places where the construction of embankments with shallow slopes is difficult due to land restrictions and in the construction of high embankments without berms, the use of geosynthetic as a body reinforcement is a reliable solution.

Soil slopes that are quite stable under static conditions can simply collapse during earthquakes due to several reasons, including ground shaking leading to excessive vibrations and deformations, loss of bearing strength of the foundation soil due to liquefaction, and reduction in the safety factor of the slope due to transient shooting up of the pore water pressures. To prevent this, body reinforcements are incorporated into the embankment slope. Hence, the present study also aims to analyse the effect of body-reinforcement in embankments subjected to seismic loading.

1.6 ORGANISATION OF THESIS

The dissertation has nine chapters and the contents of each chapter has been organized as follows:

Chapter 1 – Introduction

This chapter presents a brief overview of the construction of embankments over soft clay deposits using basal/body geosynthetic reinforced embankments with or without pile foundations. It also explains the load transfer and soil arching mechanism in piled embankments subjected to static loading conditions.

Chapter 2 – Literature Review

A brief summary of literature focusing on research carried out related to geosynthetic reinforced embankments with or without pile foundations is presented. It is also attempted to study various experiments, case studies, empirical relations and numerical studies conducted on geosynthetic reinforced embankments with or without pile supports subjected to static as well as dynamic loads.

Chapter 3 – Objectives and Scope of the work

Details of objectives framed for the study and the scope of the present study are elaborated.

Chapter 4 – Methodology

This chapter elaborates the methodology followed in the study towards the fulfilment of the objectives set forth. It gives the details of the idealization of Finite Element models of geosynthetic-reinforced embankments with or without pile-supports. The details of material properties, boundary conditions and application of static and seismic loading are also explained.

Chapter 5 – Response variation of basal geogrid-reinforced pile-supported embankments subjected to self-weight and traffic load

This chapter discusses the observations and the inferences from the analysis carried out on the basal geogrid-reinforced pile-supported embankments subjected to self-weight and traffic load. The quantifications of various parameters are also discussed in this section. Based on the results obtained from the numerical analysis, a new soil arching coefficient is also proposed in this chapter.

Chapter 6 – Response variation of basal geogrid-reinforced pile-supported embankments subjected to seismic excitations

This chapter discusses the observations and the inferences from the analysis carried out on the basal geogrid-reinforced pile-supported embankments subjected to seismic excitations. The effect of embankment height, embankment side slope, geogrid tensile modulus, pile length, pile spacing and type of seismic excitations on the stress distribution and displacement reduction of these embankments subjected to seismic excitations are also discussed.

Chapter 7 – Response variation of basal geogrid-reinforced embankments subjected to static and seismic load

This chapter discusses the observations and the inferences from the analysis carried out on the basal geogrid-reinforced embankments subjected to static and seismic load. The effect of embankment height, embankment side slope, geogrid stiffness, foundation soil stiffness, embankment stiffness and intensity of seismic loading in determining the optimum width of basal geogrid-reinforcement are studied.

Chapter 8 – Response variation of body-reinforced embankments subjected to seismic load

This chapter discusses the observations and the inferences from the analysis carried out on the body-reinforced embankments subjected to seismic load. The behaviour of body-reinforced embankments having different side slope and supported on different foundation soil subjected to seismic excitations are discussed.

Chapter 9 – Conclusions

This chapter summarizes the work that has been carried out. Also, the significant conclusions from the work are presented, highlighting the importance of geosynthetic as basal or body reinforcement and the inclusion of pile foundations for embankment construction on soft clay deposits. The suggestions for future research are also added.

CHAPTER 2

LITERATURE REVIEW

The review of literature is classified into two sections such as studies on basal or body reinforced embankments and the studies on pile supported embankment with basal geogrid.

2.1 BASAL OR BODY-REINFORCED EMBANKMENTS

From literature, several studies are seen on the improved performance of embankment by the addition of basal geosynthetic under static loading conditions. Bonaparte and Christopher (1987) suggested a method of design and construction for the basal geosynthetic-reinforced embankments over weak subsoils. Rowe and Soderman (1987) carried out finite element analysis of embankment constructed over high strength geosynthetic stabilized soft soil. Rowe and Li (1999) analyzed reinforced embankments over soft foundations under undrained and partially drained conditions and observed an increase of 11-38 % in the factor of safety against failure under partially drained conditions when compared to undrained conditions. Rowe and Skinner (2001) numerically examines the effect of uncertainty regarding the drained and undrained strength of the loam foundation material, its stiffness, the thickness of this soft layer and its position with respect to the bottom of the wall in the geosynthetic reinforced retaining wall constructed on a layered soil foundation. Field and laboratory tests, as well as analysis of results by Chai et al. (2002) indicated that the presence of basal geosynthetic reinforcement improved the stability of the embankment. Helwany et al (2003) investigated the potential of GRS bridge abutments to alleviate bridge approach settlements. The study was conducted by the finite element method of analysis using the computer program DACSAR. A parametric study was conducted to examine the effects of different foundation soils, ranging from loose sand to stiff clay, on the performance of a GRS abutment. The study indicated that the finite element computer code DACSAR is a reliable analytical tool for analyzing the performance of GRS bridge abutments and that the GRS abutment is an effective means to reduce differential settlements between the abutment and the approach embankment. Bathurst et al. (2003) conducted large-scale experiments on geosynthetic reinforced and unreinforced

embankments and reported about 1.6-2 times increase of load-carrying capacity in reinforced soil embankments when compared with unreinforced embankments. Yoo and Jung (2004) conducted full-scale experiments to study the behaviour of a geosynthetic-reinforced segmental retaining wall in a tiered configuration. The results show that the interaction between the upper and the lower tiers not only influences the performance of the lower tier, but also that of the upper tier, resulting in large horizontal deformations in the upper tier and strains in reinforcement that can depart significantly from what might be anticipated. Skinner and Rowe (2005) performed numerical analysis on a geosynthetic reinforced retaining wall and bridge abutment constructed over a yielding foundation. The analysis of results show that a geosynthetic reinforced soil wall can withstand the excessive deformations caused by unexpected significant yielding of the foundation soil and even reduce the differential settlement and potential bridge bump effect at the top of the wall. Both field study and numerical analysis by Rowe and Li (2005) reported that the use of basal geosynthetic reinforcement could significantly reduce the creep deformations of the foundation soils. Yoo and Kim (2008) conducted full scale experiments and also performed finite element analysis on a 5 m high segmental geosynthetic reinforced retaining wall subjected to surcharge loading. From the analysis, they observed that, the wall deformation at the allowable bearing pressure of 200 kPa was within the serviceability level demonstrating an excellent load carrying capacity of the reinforced wall. Shukla and Kumar (2008) observed the beneficial effects of prestressing of basal geosynthetic reinforcement in soft subsoils than in stiff subsoils. Magnani et al. (2009) presented the behaviour of two reinforced test embankments built on normally consolidated soft clay and observed the increase in the reinforcement forces with the increase in embankment height. Oliveira et al. (2010) observed the importance of sand blanket than the basal geosynthetic for increasing the embankment stability. Leshchinsky et al. (2010) exhumed and examined the instrumented geogrid-reinforced retaining wall and observed a roughly uniform mobilized maximum tensile strains in the geogrid panels ranging between 3 % to 5 %. The effect of consolidation during the construction of basal geosynthetic reinforced embankment was analysed by considering the cases of undrained and partially drained conditions by Taechakumthorn and Rowe (2013). The use of geosynthetics for basal reinforcement of embankment in locally weak zones reduces the differential settlements

(Benmebarek et al. 2015). . The addition of basal geotextiles reduces the vertical displacements of subsoil and thus prevents the sudden failure of embankment during construction (Zhang et al. 2015). Xie and Leshchinsky (2015) demonstrated a series of numerical simulations using Limit Analysis (LA). An algorithm is developed using LA to find the critical collapse state for the determination of optimal reinforcement placement in Mechanically Stabilized Earth (MSE) walls based on both spacing and concentration - specifically at the toe or crest of the structure. Smith and Tatari (2016) carried out a limit analysis of basal geosynthetic reinforced embankments using the Discontinuity layout optimization technique and compared the results available in the literature. Wang et al. (2018) proposed the earth pressure coefficients for reinforcement loads of vertical geosynthetic-reinforced soil retaining walls under working stress conditions and the obtained reinforcement loads were in good agreement with the numerical and experimental results. Oser et al. (2020) proposed a limit equilibrium method for quantifying the basal reinforced embankment safety against lateral spreading. The requirement of basal geosynthetic is up to the dissipation of excess pore water pressure in the soft subsoil. Hence, Sarsby (2007); Mwasha and Petersen (2010) and Chaiyaput et al. (2014) used the Limited Life Geosynthetics as short-term embankment reinforcement in order to improve the stability of embankment on soft clay.

There are studies on the seismic performance of geosynthetic reinforced embankments also available in the literature. Matsuo et al. (2000) carried out numerical analysis of embankment constructed over liquefiable soils. Hata et al. (2008) proposed a practical method to consider soil strength heterogeneity in computing Newmark sliding block residual displacements of an embankment for seismic design. Okamura et al. (2013) conducted a series of centrifuge experiments on embankments. From the study, it was observed that the soft subsoil consolidation is the major cause of embankment failure during an earthquake. Lin and Yang (2013) studied the dynamic behaviour of railway embankment slope subjected to seismic excitation. Increasing geotextile layers and geotextile stiffness decreases the maximum displacement due to seismic loading (Faizi et al. 2013). Papadimitriou et al. (2014) generated a model based on statistical regression for estimating seismic coefficients for the design of earth dams and high embankments. Lin et al. (2015) observed from shaking table tests that, the

reinforced embankment slope is less sensitive to seismic excitation than the unreinforced embankment slope.

Panah et al. (2015) conducted a series of 1-g shaking table tests on 80 cm high reinforced-soil wall models to determine the seismic behaviour of reinforced soil retaining walls with polymeric strips. They also conducted uniaxial tensile and pullout tests in reduced-scale models to determine the best material to be used instead of polymeric strips in models. The effect of the length of reinforcement, number of steps and shape of the reinforcement arrangement (zigzag vs. parallel) on the failure mode, the wall displacement, and the acceleration amplification factor were investigated. Findings suggest that walls built with extensible reinforcement were flexible and the internal failure mechanism in the reinforced zone for these walls involved a bulging mode. The parallel implementation of reinforcements is more favourable as it decreases the displacements more than 50% before failure compared to the zig-zag arrangement.

Wang et al. (2015) studied the seismic performance of geogrid reinforced rigid retaining walls with saturated backfill sand using large-scale shaking table test models constructed in a large laminar shear container, which included geogrid reinforced rigid retaining walls and unreinforced soil retaining walls. Considering the effects of ground motions, the seismic response of the retaining walls were investigated, along with wall accelerations, lateral displacements of walls, seismic settlements of the backfill sand surfaces, and the excess pore water pressures in the backfill sand and geogrid strains. Comparing the results of the test models indicated that seismic waves with long-time high acceleration values from the far field had greater effects on the seismic behaviours of the reinforced retaining wall than those from the near field, and the geogrid could still effectively improve the seismic resistance deformation abilities of the saturated geogrid reinforced rigid retaining wall. Since the geogrid was a lighter and more flexible mesh structure compared with soils, geogrid layers could decrease the development of excess pore water pressures and accelerate the dissipation of excess pore water pressures. The middle-layer geogrids in the reinforced soil played important roles in the seismic stability of the retaining wall, and the geogrid ends embedded inside the walls were key-parts in the seismic design of the geogrid reinforced rigid retaining wall. Seismic waves from far or mid-far fields must be considered in the seismic designs of geogrid reinforced rigid retaining walls. (The input ground motions of the far and

mid-far fields has long-period high acceleration values, and the input ground motion from the near fault field has short-period high acceleration values).

Vijayasri et al. (2017) analysed the seismic response of pond ash embankment and observed that the pond ash embankment is susceptible to liquefaction for most of the earthquake motions considered. From the experiments and numerical analysis Modoni et al. (2018) observed that, highly compacted gravel embankment fill has exceptionally high resistance against severe earthquakes.

2.2 SUMMARY OF LITERATURE ON BASAL OR BODY-REINFORCED EMBANKMENTS

Many researchers have investigated the failure mechanism of basal geosynthetic-reinforced embankments over soft subsoils subjected to static and seismic loads. But studies on identifying the optimum width of basal geosynthetic under static and seismic loading conditions are not seen. There is a need to explore the behaviour of these basal geosynthetic-reinforced embankments particularly under seismic excitations. Therefore, in the present study, both static and time-history analyses has been performed to examine the behaviour of basal geosynthetic-reinforced embankments with various width of geosynthetic. Construction of earth structures reinforced with geosynthetics has expanded extensively in the last twenty years, also in seismically active areas. Although severe damage was not observed during recent strong earthquakes, the performance of these structures under seismic loading is not fully known. Several studies have been conducted on reduced models using shaking tables. However due to modelling limitations the results are not often very meaningful when seeking to deduce the seismic performance of full scale prototype structures. So the extension of above study to body reinforced embankments is desirable.

2.3 STUDIES ON NUMERICAL ANALYSIS OF GEOSYNTHETIC-REINFORCED PILED EMBANKMENTS

Piled embankments have been existing for a long time, but they have become more popular since 1970s. Since the 1980s, increasing interest in piled embankments has led to an increase in research on rational approaches for load transfer mechanism in these embankments. The load transfer mechanism in these basal geosynthetic reinforced piled embankments is due to soil arching which is the load transfer to the

piles due to the distribution of shear stresses in the embankment soil caused by the stiffness difference of pile foundations and soft foundation soil between piles and tensioned membrane action of geosynthetic (van Eekelen et al. 2011; Bhasi and Rajagopal, 2015). Several soil arching theories on static loading conditions are available in the literature (Terzaghi, 1965; Guido et al. 1987; Russell and Pierpoint, 1997; Carlsson, 1987; Kempfert et al. 1997; Hewlett and Randolph, 1988; van Eekelen et al. 2013) and these theories are adopted by many design codes (BS8006, 2010; EBGEO, 2010; Dutch guidelines etc.) for the design of geosynthetic reinforced piled embankments.

The load transfer mechanism (soil arching effect) is currently assessed using conservative analytical approaches. The reasons for this, according to Jones et al. (1990), are twofold. First, to measure the arching mechanism across adjacent pile caps, simpler analytical approaches rely on empirical equations. Second, the simpler approaches are incapable of adequately accounting for partial foundation support beneath the geosynthetic reinforcement.

Since the load transfer in the pile reinforced embankments is a complex phenomenon, numerical techniques are needed for accurately analyzing their response (Lawson 1992). Full three-dimensional(3D) analyses are required to study the stress concentrations developed at the edge of the pile, the tensile forces, and strains developed in the geosynthetic layer (Smith and Filz 2007;Abdullah and Edil 2007).

Very limited works have been carried out using coupled full 3D analyses considering the pile-soil-reinforcement interaction because carrying out full 3D analyses requires a substantial amount of time and computer memory to perform the calculations (Ariyarathne et al. 2013). Therefore, for practical reasons, many researchers in the past have used unit cell concept to study the performance of piled embankments (Russell and Pierpoint 1997; Han and Gabr 2002; Smith and Filz 2007; Yoo and Kim 2009).

A detailed explanation of the various numerical studies, analytical solutions, case studies and experiments conducted on pile-supported geosynthetic-reinforced embankments in the recent years is presented in this section of thesis.

Han and Gabr (2002) conducted a numerical study to investigate pile-soil-geosynthetic interactions by considering three major influence factors such as: the

height of the fill, the tensile stiffness of geosynthetic, and the elastic modulus of pile material. Analysis results indicated that the soil arching ratio decreases with an increase in the height of embankment fill, an increase in the elastic modulus of the pile material, and a decrease in the tensile stiffness of geosynthetic. The study results also suggest that the stress concentration ratio and maximum tension in geosynthetic increase with increasing the height of embankment fill, increasing the stiffness of geosynthetic, and increasing the elastic modulus of the pile material. The distribution of tension in geosynthetic shows that the maximum tension occurs near the edge of the pile.

Liu et al. (2007) described a case history of a geogrid reinforced pile supported (GRPS) highway embankment and it was back analyzed by carrying out 3-D fully coupled finite-element analysis. Both measured and computed results are compared and discussed. Based on their studies, it is clear that there was a significant load transfer from the soil to the piles due to soil arching. The measured contact pressure acting on the pile was about 14 times higher than that acting on the soil located between the piles. For embankment higher than 2.5 m, predictions of stress reduction ratio based on two common existing design methods (Russell and Pierpoint method and Hewlett and Randolph method) are consistent with the measured values and the 3D numerical simulations. During the construction of the piled embankment, the measured lateral displacement–settlement ratio was only about 0.2. This suggests that the use of GRPS system can reduce lateral displacements and enhance the stability of an embankment significantly.

Han et al. (2007) analysed eight cases of column-supported widened embankments and two untreated foundations. Two-dimensional finite difference software was used after the calibration of the model against a field case study and numerical analyses were conducted to investigate stresses and deformations of the widened embankments over soft soil with or without the remediation of foundation columns. This study shows that the widening of embankment increases shear stresses in the existing embankment towards the widened portion. Foundation columns can provide shear resistance to the shear stress induced by widening of the embankments.

Zing et al. (2008) analysed the lateral behaviour of piles in a pile supported embankment using finite difference method. The results show that pile deflections and

bending moments induced by soil lateral deformation and embankment vertical load were different for piles at different positions under the same embankment.

Huang and Han (2009) conducted three-dimensional coupled mechanical and hydraulic modelling using FLAC3D to consider consolidation and three-dimensional arrangement of columns. The study was based on a well-documented bridge approach embankment reinforced by a layer of geotextile and supported by deep mixed (DM) columns. Their results show that the coupled mechanical and hydraulic modelling is necessary to study the time-dependant behaviour of GRCS embankments under staged construction. The total and differential settlements on the crest of the embankment are much smaller than those at the base of the embankment. The post-construction settlement on the crest is more critical and meaningful for the design of GRCS embankment than that at the base. Also the results show that the strains in the geosynthetic reinforcement in the transverse direction are higher than those in the longitudinal direction and that higher strains develop over the columns in both directions. GRCS foundations have a fast reduction in excess pore water pressure due to a combination of drainage and stress transfer.

Van Eekelen et al. (2011) proposed some modifications to BS8006 in order to eliminate the shortcomings when calculating the line load on the geosynthetic layer. The results of BS8006, Modified BS8006, and the German/Dutch guideline are compared with finite element calculations and field measurements. It is concluded that the results given by the Modified BS8006 are more accurate to those using BS8006.

Van Eekelen et al. (2011) conducted a series of twelve 3D laboratory model tests on piled embankments. In the first part of a two-part study, the measured load distribution, deformation, and strains were presented and analysed. In the second part, the measurements were compared with calculations using EBGEO (2010), and suggestions were given for improvements to this calculation model.

Wang and Mei (2012) studied the seismic performance of micropile-supported embankment and found that micropiles can reduce the seismic response of the embankment.

Han et al. (2012) conducted numerical simulations for the unreinforced and reinforced pile-supported embankments using the discrete element method (DEM). The

study investigated the changes of vertical and horizontal stresses and porosities, the vertical displacements within the embankment fill, and the deflection and tension in the geogrid. The simulation results showed that the coefficient of lateral earth pressure in the embankment fill changed from an initial at rest condition to a passive condition at certain locations after the compression of the compressible soil. The embankment fill dilated during the development of soil arching. The embankment load was transferred to the piles owing to the reorientation of the principal stresses. The results also showed that the geogrid reinforcement significantly reduced the total and differential settlements at the top of the embankment.

Thach et al. (2013) suggested considering the vibrational resonance effect for designing the high-speed railway embankments. Train-induced waves are trapped and dissipated within the pile-supported embankment system reducing vibration amplitudes outside the embankment.

Armstrong et al. (2013) performed three dynamic centrifuge model tests to investigate pile-pinning effects. Each centrifuge model was composed of two identical embankments underlain by liquefiable soil: one with a pile group and the other without. The tests demonstrated that the embankment with a pile group experienced less lateral movement and settlement than the embankment without a pile group.

Han et al. (2014) investigated the properties of soil arching under dynamic load by performing model tests and numerical studies using the FEM. Embankments with different heights under dynamic load were investigated. In numerical analysis, because of the existence of the geogrid, the value of the ratio of the height of the embankment to the centre-to-centre pile distance ensuring the stability of soil arching under dynamic load was 1.4, which is less than the value acquired in model tests, and it indicates that the existence of a geogrid and subsoil can improve the stability of soil arching under dynamic load.

Van Eekelen et al. (2014) validated the analytical model for the design of the geosynthetic reinforcement in a piled embankment with measurements from seven full-scale tests and four series of scaled model experiments. It is concluded that the Concentric Arching model matches the measurements better than the models of Zaeske (2001) or Hewlett and Randolph (1988).

Geogrid embedment increases the lateral performance and reduces the dynamic response of pile foundations, Taha et al. (2015). Han et al. (2015) analyzed the soil arching behaviour of geogrid reinforced pile-supported embankment subjected to cyclic loading.

Bhasi and Rajagopal (2015) examined the performance of geosynthetic reinforced piled embankment systems (GRPES) modelled using three different modelling methodologies (axisymmetric, three-dimensional (3D) column, and full 3D models). The numerical models in this study were calibrated using data from a full-scale field test of GRPESs. The load distribution between different components of the GRPES and the tensile force developed in the geosynthetic reinforcement were compared with the results obtained using various design methods and other analytical results. The numerical analysis was also expanded to look at the tensile force created between the layers of a multilayer GRPES, and the results were compared to the empirical solutions.

They concluded that the measured total loads transferred to the piles were found to agree well with the results of full 3D analyses. The prediction from the axisymmetric and 3D column models were about 27% and 16% higher, respectively. This higher load predicted by the approximate models can be attributed to the effect of vertical boundaries, which comes into play in these models. The measured pressures on the foundation soil are very close to the predictions made by the full 3D finite-element model and the EBGEO method. The soil pressures at the base are not adequately predicted by the approximate numerical models. The reinforcement forces predicted for different heights of embankment estimated from the numerical analyses do not support the assumption that they remain constant when the height of embankment is increased beyond the critical arching height as assumed in BS8006. The BS8006 is extremely conservative for estimation of the reinforcement forces. The modified BS8006 yields geosynthetic forces similar to those predicted by the EBGEO method for embankment heights smaller than the arching height, with a very low modulus of subgrade reaction. The modified BS8006 approach, on the other hand, overestimates the tensile forces when the embankment height is greater than the arching height.

Ariyarathne and Liyanapathirana (2015) investigated the load transfer mechanism of geosynthetic reinforced piled embankments using two-dimensional and three-dimensional finite element analyses, and currently available design methods are compared with the results of the finite element modelling. A comparison of the design methods was carried out using the stress reduction ratio, the geosynthetic tension and pile efficacy, considering different pile diameters and spacing, and embankment heights, which govern the currently available design methods.

Bhasi and Rajagopal (2015) presented the results of numerical investigation into the performance of geosynthetic reinforced embankments supported on end bearing as well as floating piles considering the pile-soil and geosynthetic-soil interaction. 3-D Column models were employed to carry out the parametric studies on factors such as the development of arching, skin friction distribution along the pile length and axial force distribution. Full three-dimensional analyses were carried out to study the overall behaviour of the GRPES system and the results obtained from the analyses were compared with those from British Standard BS8006-2010.

The results indicated that the use of floating piles considerably reduce the settlements and the embankment load transferred through the piles to the foundation soil was found to depend very much on the length of the piles. This aspect needs to be accounted for while calculating the arching factor in the empirical equations.

Chen et al. (2015) conducted experiments on a full-scale high-speed railway embankment model for assessment of the tensile force of the geogrid embedded in the sand cushion. Water bags were distributed around pile caps to create a model of the subsoil. The settlement of the subsoil was determined by the vertical deformation of the water bags. The tensile force of the geogrid, induced by the spreading force of the embankment, and caused by the vertical loads applied to the geogrid, were separately measured by two types of optical fibre sensing approaches, i.e., the pulse-pepumpe Brillouin optical time domain analysis (PPPeBOTDA) and fibre Bragg grating (FBG) sensors. After the completion of the construction of the embankment, the measured tensile force of the geogrid, caused by the spreading force, was about 12% of that calculated by using the BS8006 standard. During the process of subsoil consolidation, the soil arching in the embankment fully develops as the subsoil settlement increases. At the ultimate limit state, the largest tensile force of the geogrid caused by the vertical

loads occurred at the edge of the pile cap, which was about 34% of that calculated by using BS8006. As a design method, BS8006 calculates the tensile force of the geogrid at the ultimate limit state, and the experimental results reveal that the computational procedure specified in BS8006 is safe for determination of the tensile force of the geogrid.

Gao et al. (2016) analysed the effect of direction of P-wave on the seismic response of geogrid reinforced pile-supported embankment using finite element method. The results indicate that in comparison with vertical incidence, the oblique incidence can significantly increase the displacement, velocity and acceleration of key locations in the GRPS embankment. The existence of geosynthetics can alleviate the impact of seismic load on the response of the embankment to a certain degree. Moreover, the number of reinforcement layers and modulus of geogrid also greatly influence the seismic performance of GRPS embankment.

Sheta and Frizzi (2017) conducted FEM analysis on a case study of timber pile supported geogrid reinforced bridge approach embankment in USA. They analysed the embankment for crane loads. Settlements obtained from the numerical analysis indicated acceptable total and differential settlement of the embankment under heavily loaded crane operation, which agreed well with the embankment performance monitored during crane operation.

Dias and Grippon (2017) conducted a numerical study on variable inertia pile supported road near Bourgon-Jallieu (France). From the analysis it was shown that the variable inertia piles are more effective than circular piles of same shaft diameter in terms of vertical settlements reduction and bending moments in the pavement.

Zhuang and Wang (2017) developed an analytical solution for reinforced piled embankments on elastoplastic consolidated soil. They included soil arching effect, reinforcement effect, pile skin friction and consolidation of foundation soil for analysis. Also they compared the analytical solutions with different case studies and showed that the proposed analytical method was capable of finding pore water pressure at different levels, pile skin friction, settlement of pile and foundation soil

Liu et al. (2017) conducted 3D finite element analysis to investigate the time-dependent behaviour of column supported embankments reinforced by viscous reinforcement for different long-term (at 99% degree of consolidation) reinforcement

strains. They showed that a 2% short-term reinforcement strain was optimum in designing the column-supported embankments which corresponds to an approximately 3% long-term reinforcement strain.

Mohamd B. D. Elsawy (2018) simulated a case history of conventional and geogrid-encased stone piles under an embankment using FEM. From the analysis it was observed that most of the consolidation settlements will occured at the time of embankment construction. The encased stone piles show acceleration in the dissipation of excess pore water pressure and increase in stress concentration ratios when compared with conventional stone piles.

Zhuang and Wang (2018) conducted finite element analysis to analyse the dynamic behaviour of soil arching effect in a piled embankment subjected to cyclic train loading. . The analysis of results revealed that, the dynamic load type was found to have an obvious influence on the soil arching effect, in which the settlement increased by approximately 6% when varying the half-sine load type to the sine load type. As expected, the increased vehicle wheel load and velocity aggravated the dynamic vertical stress and settlement of the piled embankment.

Niu et al. (2018) conducted model tests on X-shaped cement concrete pile-supported embankment under M-shaped dynamic trainload. Wang et al. (2018) analyzed the piled embankments under moving shakedown limit loads. Both the studies observed the reduction of soil arching height under dynamic train load when compared to the arching height under static load. Pham and Dias (2019) carried out numerical analysis of piled embankment under cyclic loading to represent traffic load.

Zhuang et al. (2020) analysed the load transfer mechanism in reinforced piled embankment under cyclic loading and unloading using finite element method. From the analysis they observed that, the maximum settlement at the base of the embankment increased to about 23–55% due to cyclic load and slight rebound under unloading when compared with the results under static loads.

Tang et al. (2020) conducted model test to analyse the behaviour of geosynthetic-reinforced pile foundation under long-term dynamic loads. From the test results, they observed that, in thick embankments, the arching kept enhancing under long-term dynamic loading with high load amplitudes.

Meena et al. (2020) studied the dynamic soil arching effects subjected to cycle train induced loading in a pile-supported railway embankment using 2-dimensional finite element model. From the analysis, it is found that the pile modulus, embankment modulus and friction angle has significant effect on the arching mechanism.

2.4 SUMMARY OF LITERATURE ON BASAL GEOSYNTHETIC-REINFORCED PILE-SUPPORTED EMBANKMENTS

Table 2. 1 Summary of literature on basal geosynthetic-reinforced pile-supported embankments

Geosynthetic-reinforced pile-supported embankments under Static loading conditions	
Numerical studies	Han and Gabr (2002); Smith and Filz (2007); Yoo and Kim (2009); Han et al. (2012); Bhasi and Rajagopal (2013); Bhasi and Rajagopal (2015); Lu and Miao (2015); Ariyarathne and Liyanapathirana, (2015); Bhasi and Rajagopal (2015); Zhao et al. (2017); Liu et al. (2017); Yu and Bathurst (2017); Zhang et al. (2019); Wijerathna and Liyanapathirana (2021)
Experimental studies	Van Eekelen et al. (2012 a,b); Briançon and Simon (2012); Xing et al. (2014); Rui et al. (2016); Shen et al. (2017); Rui et al. (2019);
Case studies	Liu et al, (2007); Sheta and Frizzi, (2017)
Analytical studies	Van Eekelen et al. (2013); Zhuang et al. (2014); Zhang et al. (2016); Ghosh et al. (2017); Zhuang and Wang (2017); Zhang et al. (2018)
Geosynthetic-reinforced pile-supported embankments under dynamic loading conditions	
Dynamic train or vehicular load	Thach et al. (2013); Taha et al. (2015); Han et al. (2015); Niu et al. (2018); Wang et al. (2018); Zhuang and Wang (2018); Pham and Dias (2019); Zhuang et al. (2020); Tang et al. (2020); Meena et al. (2020)

Seismic excitations	Wang and Mei (2012); Armstrong et al. (2013); Gao et al. (2016)

2.4.1 Limitations of empirical methods

To simplify the design, all design methods, particularly empirical design methodologies, make assumptions. As a result, several influencing aspects aren't considered. Numerical analysis of piled embankment design can be a useful tool for simulating complex soil-structure interactions.

For instance, for high values of the ratio of pile cap width to pile spacing, the BS 8006 method and the equations given by Bhasi & Rajagopal (2015) can give negative values of soil arching ratio. This imply that these methods are unreliable. Nevertheless, the design results using these equations generally lead to conservative design of piled embankment. The settlement behaviour and horizontal movement of the piled embankment are another important element not covered by empirical design approaches. This is crucial while analysing the embankment's serviceability. Short and long term settling behaviour will be of most importance, especially when using floating piles.

2.4.2 Limitations of numerical methods

Most of the numerical analyses of piled embankments assume that the piles are non-displacement piles although in reality the piles are often displacement piles. This procedure is used because it is not simple to include effect of pile installation in the numerical analyses. Piled embankments are complex soil-structure interaction problems. Numerical methods are considered a powerful tool to reduce the uncertainties and have been used for the piled embankment design. However, the intended outcome is not always followed. To develop an appropriate design approach for modelling piled embankments that includes fewer but more dependable assumptions, more study on numerical analysis of piled embankments is required.

2.4.3 Limitations of dynamic loading conditions

The dynamic response of embankments supported over piles with basal geogrid is analysed by many researchers for cyclic loading conditions to represent train or vehicular loads. Though there are few studies on the seismic behaviour of these embankments, the response of these embankments under seismic excitations is less

addressed and need to be studied further to prevent the large total and differential settlements, lateral spreading, foundation pile failure and basal reinforcement failure.

CHAPTER 3

OBJECTIVES AND SCOPE OF WORK

3.1 PROBLEM IDENTIFICATION AND OBJECTIVES

From the literature survey, it is understood that, the soil arching effect for load transfer in reinforced piled embankments is a very complex phenomenon. The present empirical methods for determining the arching effects are based on wide range of assumptions; hence they fail to produce accurate results. Therefore, the design based on these methods is always under-predicted or over-predicted. Hence, in order to get reliable results, numerical modelling considering the three-dimensional response may be included in the design process. But, there are only few such studies on numerical analysis of geosynthetic reinforced piled embankments/ retaining walls and there is a need of further research in this area. Also, many studies are available on piled embankments with or without basal geogrid to understand their behaviour under static loading conditions. But it is necessary to understand the behaviour under seismic excitations since these structures should stand safe under earthquake also.

Construction of earth structures reinforced with geosynthetics has expanded extensively in the last twenty years, also in seismically active areas. Although severe damage was not observed during recent strong earthquakes, the performance of these structures under seismic loading is not fully known. Several studies have been conducted on reduced models using shaking tables. However due to modelling limitations the results are not often very meaningful when seeking to deduce the seismic performance of full scale prototype structures. So the extension of above study to body reinforced embankments is desirable. Keeping this in view, the following objectives are set for the present work:

1. To analyse the response of basal and/or body reinforced embankments with and without pile foundations

2. To estimate the response variation in terms of total and differential settlements, lateral displacements, stress concentration on pile heads, load transfer to piles, lateral stress distribution between piles and foundation soil, coefficient of lateral pressure variation along embankment elevation

3. To identify the optimum width of basal geogrid based on crest settlements, toe lateral displacements and lateral displacements at the crest.

4. To analyse the slope stability of body-reinforced embankments for various embankment slopes and foundation soil stiffness.

3.2 SCOPE OF THE STUDY

The scope of the study is restricted to the numerical analysis of reinforced embankments with or without piles, subjected to self-weight, traffic loads and dynamic loads. The effect of tensile modulus of reinforcement on the settlement reduction of embankments will be evaluated. The equation for soil arching coefficient including the pile length and pile spacing will be derived. Increase in lateral resistance by the addition of inclined piles with and without geogrid reinforcement will be compared. Slope stability analysis for different embankment slopes including a 90˚ vertical edge with body reinforcement will be evaluated. The effect of type of pile such as end bearing pile and floating pile in reducing the settlements will also be evaluated. The soil arching behaviour under seismic excitations will be analysed. Also the behaviour of embankments for 1940 El Centro earthquake excitation, Lomaprieta earthquake excitation and IS code Zone III spectrum compatible time-history for type III soil condition will be analysed.Suitable width of basal geogrid-reinforcement under seismic excitations will also be evaluated.

CHAPTER 4
METHODOLOGY

The study deals with the construction of embankments over soft soil deposits or the construction of bridge approach embankments. Poor shear strength, very low bearing capacity and excessive settlements are the common problems associated with these soft foundation soils. Depending on the depth of soft soils and the purpose of embankments, shallow ground improvement techniques such as basal geosynthetic-reinforcements or deep ground improvement techniques such as column supports are provided. Due to the fast-infrastructural growth, there are many difficulties in getting the freely available land for the construction of embankments with shallow side slope. Hence to steepen the embankment side slope, geosynthetic-reinforcement across the embankment side slope is one of the reliable ground improvement techniques.

The methodology adopted to study the load transfer mechanism in basal geosynthetic-reinforced piled and body-reinforced embankments subjected to its own weight, traffic loading and seismic excitations is presented in detail in this chapter. Verification of the numerical models, idealization of embankment geometry, material properties, loading and boundary conditions considered are explained in this chapter. The range of parameters considered such as embankment height, embankment side slope, spacing of piles, length of piles and stiffness of geosynthetic are also presented in this chapter.

4.1 NUMERICAL ANALYSIS OF BASAL GEOGRID-REINFORCED PILE-SUPPORTED EMBANKMENTS

At locations where soft compressible soil strata extends to a considerable depth and the construction of embankments over such soils to serve transportation purpose is in demand, construction of embankment with pile supports and basal geogrid is a favourable solution. Because in these embankments, most of the embankment loads will be transferred by pile foundations to the deep stratum by geosynthetic arching action, pile skin friction and end bearing resistance of piles. Also, the use of basal geosynthetic reinforcement will reduce the use of large pile caps and inclined piles near the embankment toe (BS-8006, Gangakhedkar R, 2004) under static loading conditions.

The first step in the numerical modelling is to verify the 3-dimensional finite element model of basal geogrid-reinforced pile-supported embankment created using Ansys Mechanical APDL software. The results of finite element model are compared with the existing results from the literature.

A hypothetical construction of geosynthetic reinforced embankment supported over floating and end bearing piles reported in Bhasi & Rajagopal (2015) is considered for validation. Fig 4.1 represents the cross section of the embankment.

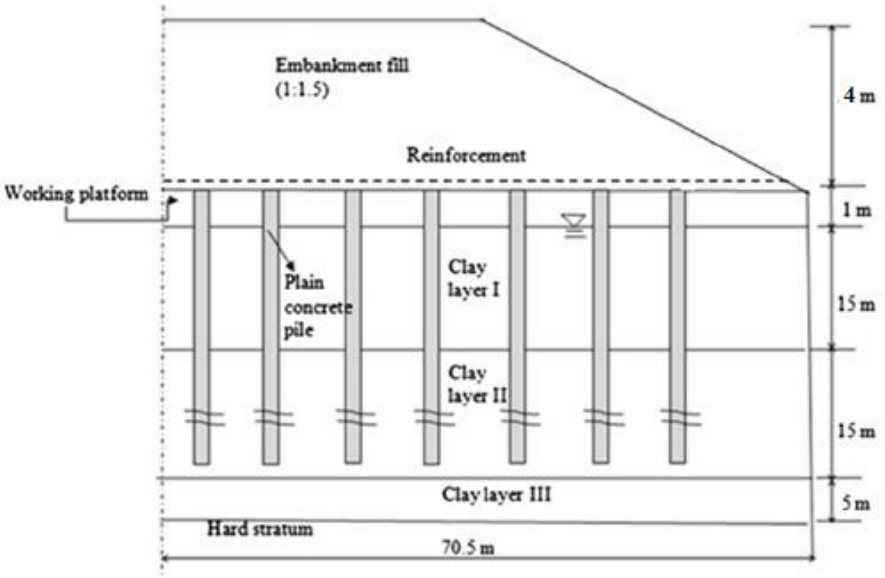

Figure 4.1 Cross section of embankment considered by Bhasi & Rajagopal (2015)

All the clay layers were modelled using modified cam-clay material model including consolidation. To model consolidation, Biot's 3-dimensional consolidation theory was used in the software. The embankment fill and working platform was modelled using Mohr-coulomb material model with drained condition. The soil properties considered were same as given in Bhasi & Rajagopal (2015).Piles of diameter 0.6 m arranged in a square grid pattern at 2.2 m centre-to-centre spacing were used. The pile was modelled as an isotropic linear elastic material with a Young's modulus of 20 GPa, and a Poisson's ratio of 0.15. The geogrid was modelled as an isotropic linear elastic material with a tensile modulus of 1200 kN/m, 4000 kN/m and a Poisson's ratio of 0.3.

Table 4.1 shows the comparison of obtained results from the FEM analysis using ANSYS APDL. It is observed that the difference in results is below 10%, hence similar model and modelling procedure have been used for further studies.

Table 4. 1 Comparison of Numerical (ANSYS) results with Bhasi & Rajagopal (2015)

Pile length	Bhasi & Rajagopal (2015)		Numerical (ANSYS)	
	Surface settlements			
	At Embankment	At Foundation	At Embankment	At Foundation
	mm	mm	mm	mm
Modulus of reinforcement = 1200 kN/m				
15 m	132.5	209.5	137.26	200.85
36 m	54.5	96.0	55.25	93.56
Modulus of reinforcement =4000 kN/m				
15 m	120.5	160.1	126.14	156.14
36 m	49.3	83.8	47.67	80.96

To check the accuracy of pile-soil interaction adopted in the present study, skin friction along the length of piles is compared with the skin friction reported in Bhasi & Rajagopal (2015) (Fig.4.2).

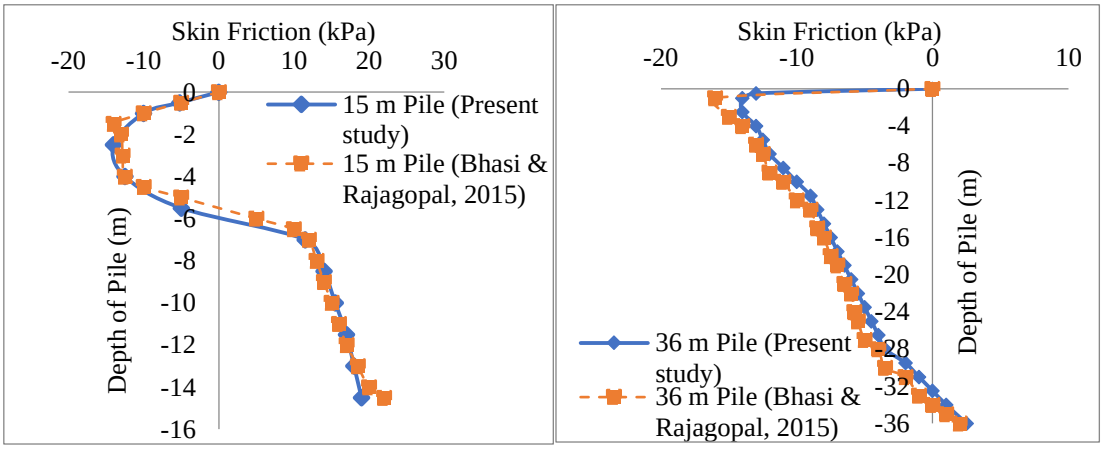

Figure 4.2 Validation of Skin friction along the length of piles with Bhasi & Rajagopal (2015)

To verify the seismic response of generated numerical models, seismic performance of micropile-supported embankment by Wang & Mei (2012) was

considered. Wang & Mei (2012) analysed 2D numerical models of micropile-supported embankment using PLAXIS. For validation, the 3D model was created using ANSYS. Material properties, geometry, boundary conditions and seismic loading considered can be seen in Wang & Mei (2012). Obtained peak acceleration values at the embankment crest for untreated and micropile-supported embankment are compared with the results of Wang & Mei (2012) (Fig.4.3). Obtained peak accelerations were less by 5 % difference compared to the peak acceleration values of Wang & Mei (2012). This validates the numerical model and the same FE modelling was adopted for further seismic response analysis.

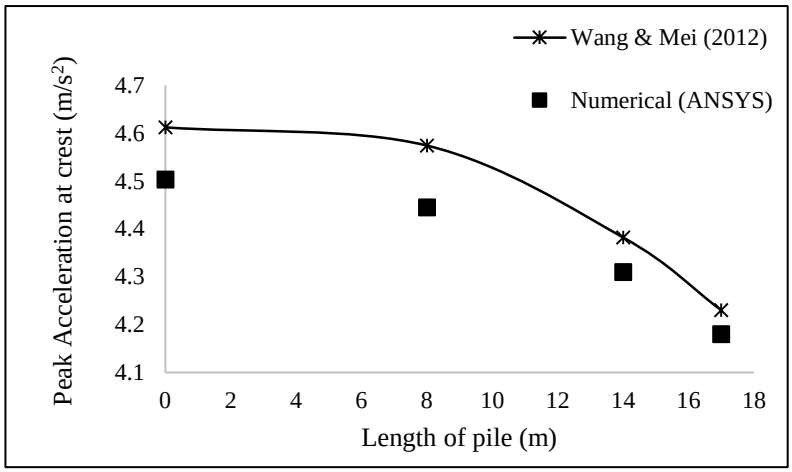

Figure 4.3 Comparison of obtained amplification coefficients with the results of Wang & Mei (2012)

4.1.1 Geometry of basal geogrid-reinforced pile-supported embankment

General purpose finite element (FE) software ANSYS mechanical APDL is capable of doing static, consolidation and time-history analysis for large three-dimensional models. ANSYS is good in simulation and also the time required to perform the dynamic analysis is less in ANSYS. Hence both self-weight, traffic and time-history analysis was performed on the three-dimensional finite element model of the basal geogrid reinforced pile-supported embankment using ANSYS.

Embankments with 3 m, 4 m, 5 m and 6 m height (H) made of pulverized fuel ash (PFA) having 38 m base width and 20 m crest width constructed over 28 m thick soft marine clay were considered for the analysis. Embankment side slope was taken as 1V:2H, 1V:1.5H and 1V:1H. Surface fill of 0.5 m above soft marine clay was laid to construct end bearing concrete piles. A hard stratum of 5 m thickness exists below the

clay layer. The embankment with a finite soil continuum of 342 m width and a depth of 33.5 m having lateral viscous boundaries to represent the infinite soil on lateral boundaries were considered for the analysis. The details of the embankment geometry is shown in Fig.4.4 (a) and a slice of 3-dimensional FE model of geogrid reinforced pile-supported embankment is shown in Fig.4.4 (b).

(a)

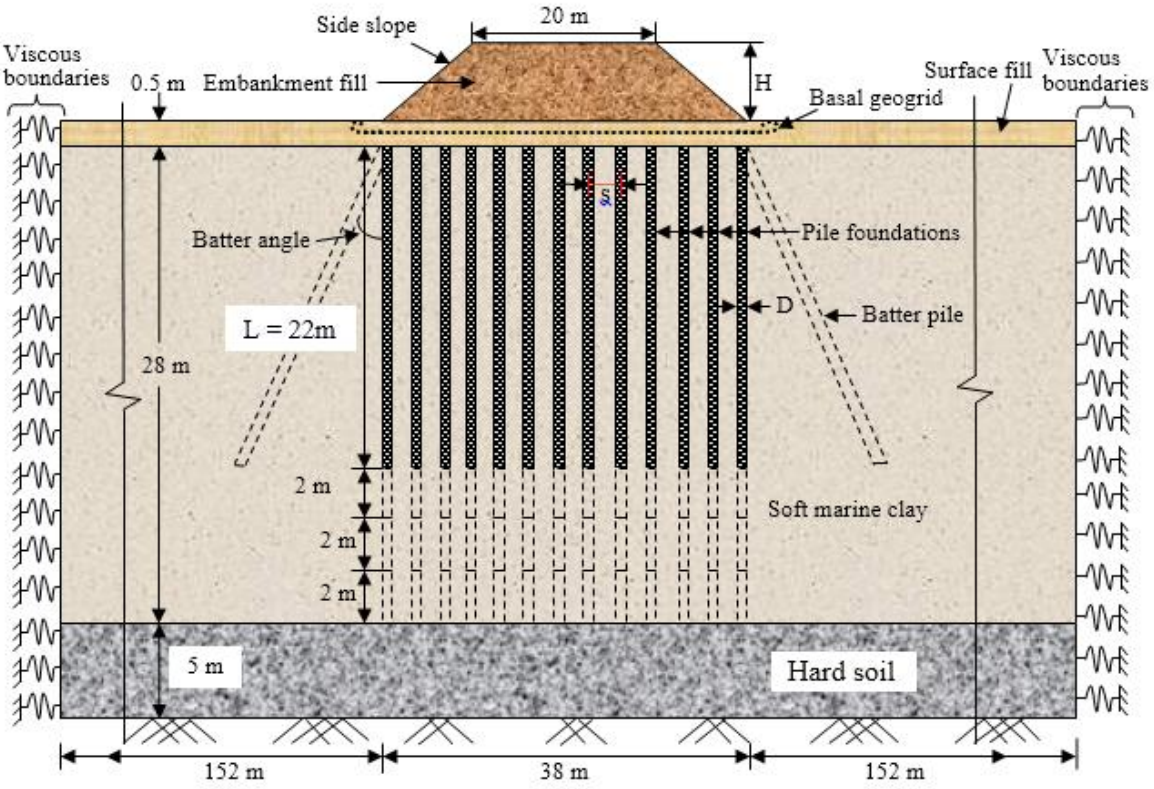

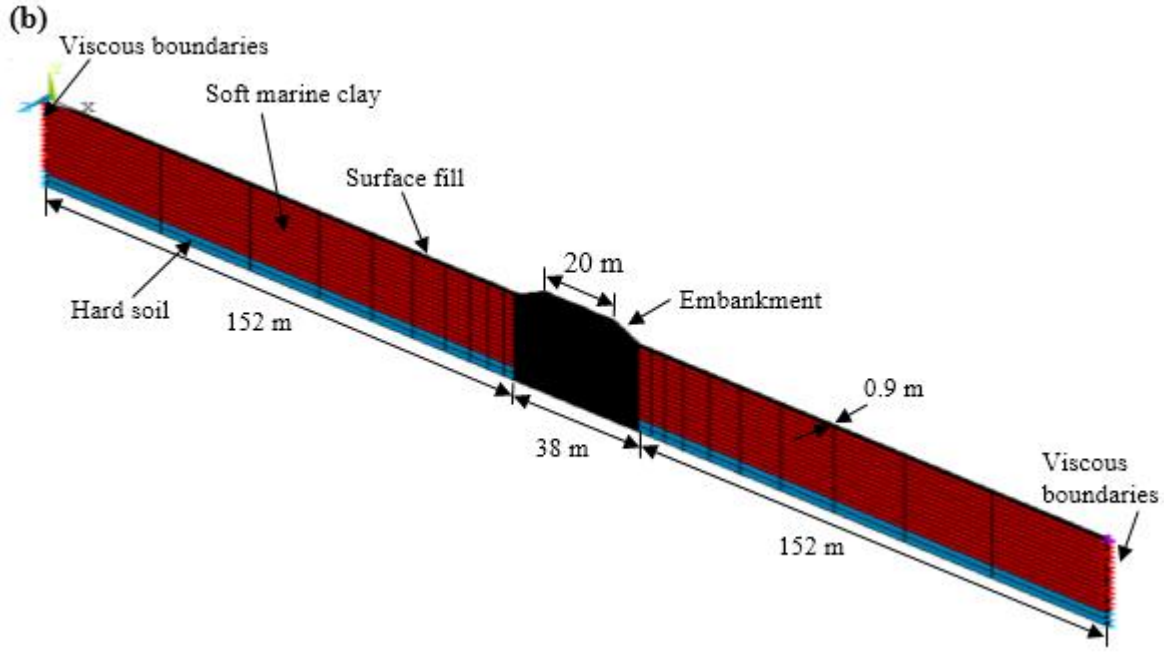

Figure 4.4(a) Details of the Embankment geometry (b) 3-dimensional view of a slice of Finite Element model of embankment

4.1.2 Properties of materials

a) Soil

The properties of PFA, surface fill (Liu et al. 2007), soft marine clay which lies in Cochin (India) region (IRC: 113-2013, Jose et al. 1988) and hard soil considered for the study are listed in Table 4.2. Due to simplicity and reasonable accuracy, studies on the seismic analysis of piled embankments considered Mohr-coulomb material model [Han et al. (2015); Wang & Mei (2012)]. Hence in the present study, Mohr-Coulomb material model with drained condition was used to model PFA and surface fill. Mohr-Coulomb material model including permeability was used to model soft marine clay and hard soil.

Table 4. 2 Soil Properties

Soil type	Unit Weight	Young's Modulus	Poisson's ratio	Cohesion	Angle of internal friction	Permeability	P-wave velocity (v_p)	S-wave velocity (v_s)
	kN/m^3	MN/m^2		kN/m^2		m/s	m/s	m/s
PFA	18.5	20	0.3	10	30˚	-	119.5	63.9

Surface fill	18.5	7	0.3	15	28˚	-	70.7	37.8
Soft marine clay	14	4	0.45	12.5	2˚	5 x 10^{-10}	103.7	31.3
Hard soil	21	250	0.3	50	40˚	5 x 10^{-8}	400.3	213.9

b) Pile Foundations

Both end bearing (28 m) and floating piles (22 m, 24 m, 26 m) were considered for the analysis. The length of floating pile more than the critical length of the pile was considered. An analytical equation developed by Satibi (2009) for critical length of a floating pile is used for this purpose. Critical length is the length of pile at which the entire embankment load is taken by floating pile (Eq .4.1).

$$L_{crit} \approx \sqrt{\frac{2q_{emb}}{\beta\gamma'}} \quad (4.1)$$

Where, $q_{emb} = \gamma H$

$\beta = \frac{2r}{R^2 - r^2} . K . sin\varphi'$

L_{crit} is the critical length of pile.

γ is the density of embankment fill.

γ' is the density of foundation soil.

H is the height of the embankment.

r is the radius of pile.

R = pile spacing/2

K is the coefficient of lateral earth pressure

φ is the angle of internal friction of the foundation soil

The maximum pile spacing's' required to install piles in a square grid pattern according to BS8006-2010 is,

$$s = \sqrt{\frac{Q_p}{(f_{fs}\gamma H + f_q W_s)}} \quad (4.2)$$

Where

Q_p is the allowable load carrying capacity of each pile in the pile group.

f_{fs} is the partial factor for soil density (= 1.3).

Y is the density of embankment fill.

H is the height of the embankment.

f_q is the partial load factor for external applied loads (= 1.3).

W_s is the external surcharge loading.

According to Eq. (4.2) a spacing of up to five times the pile diameter can be provided for the considered embankment height and pile diameter. Also, analyses by Oh & Shin (2007) and Wang et al. (2015) observed that the spacing of three times the diameter is economical and effective in reducing deformations of pile-supported embankments. Hence, 300 mm diameter (D) piles arranged in a 3D, 4D and 5D spaced square grid pattern were considered for the analysis. Piles were modelled as linear elastic isotropic material with modulus of elasticity corresponding to M20 grade concrete, unit weight of 25 kN/m^3 and Poisson's ratio of 0.15.

The presence of batter piles below embankment toe in a pile supported embankment under dynamic loading conditions is beneficial or detrimental need to be studied yet. Hence the study also considers 22 m long 300 mm diameter (D) piles having a batter angle of 0˚, 5˚, 10˚ and 15˚ below embankment toe arranged in a 3D spaced square grid pattern.

Variable head diameter piles are advantageous than the conventional piles with pile cap. They are easy to construct at a stretch. Full 3-dimensional analysis of variable head diameter pile supported embankment with basal geogrid reinforcement was also performed. The details of embankment dimensions, material properties, modelling steps and results are presented in APPENDIX I.

c) Basal geogrid

Parametric study was conducted by varying the geogrid tensile modulus from 0 to 6000 kN/m. Basal geogrid was also modelled as linear elastic isotropic material with Poisson's ratio of 0.3.

4.1.3 Finite element modeling

PFA, surface fill and piles were modelled using SOLID185 element. SOLID185 is an eight noded element with three degrees of freedom at each node: translations in the nodal x, y, and z directions. Soft marine clay and hard soil were modelled using CPT215 element. CPT215 is a coupled pore-pressure mechanical solid element. It is defined by eight nodes having four degrees of freedom at each node: translations in the nodal x, y, and z directions, and one pore-pressure degree of freedom at each corner node. Geogrid

was modelled using SHELL181 element with membrane effect. It is a four noded element with 3 translational degrees of freedom at each node. Enlarged cross-sectional view of the 3-dimensional finite element model of geogrid reinforced pile-supported embankment is shown in Fig.4.5.

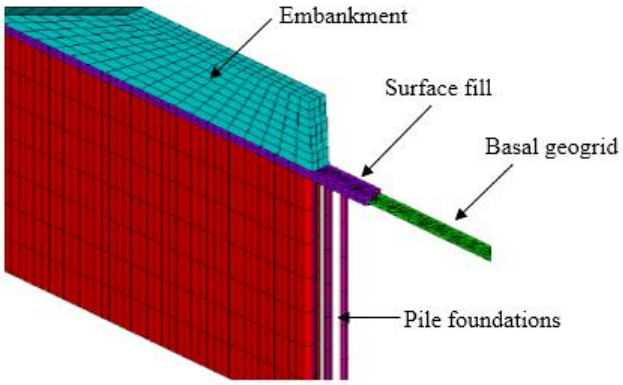

Figure 4.5 Enlarged cross-sectional view of geogrid reinforced pile-supported embankment

4.1.4 Boundary conditions

a) For soil below embankment

i) Static loading

Since the soil is assumed as semi-infinite, the lateral boundaries were restrained for the horizontal deformations and the bottom surface was set as fixed restraining. Liu et al., (2007) had taken the lateral boundary of two times the base width of the embankment for the static analysis. Since time-history analysis was also performed, the lateral boundaries were taken at a distance of four times the width of the embankment so that the waves propagated from the soil cannot reflect back (Ghosh and Wilson, 1969).

ii) Seismic excitations

To simulate the infinite soil medium, viscous boundaries were applied for the lateral boundaries using spring-damper element (Fig.4.6) given by Kianoush and Ghaemmaghami, (2011). To provide the viscous boundaries, COMBIN14 element is used in ANSYS. When the viscous boundaries are considered, the equation of motion with additional damping matrix C^* can be written as follows

$$[M]\{\ddot{x}(t)\} + [C]\{\dot{x}(t)\} + [C^*]\{\dot{x}(t)\} + [K]\{x(t)\} = -[M]\{\ddot{x}_g(t)\} \quad (4.3)$$

Where [M] is the structural mass matrix, [C] is the structural damping matrix, [K] is the structural stiffness matrix, $\{\ddot{x}_g(t)\}$ is the ground acceleration vector, $\{\ddot{x}(t)\}$ is the nodal acceleration vector, $\{\dot{x}(t)\}$is the nodal velocity vector, $\{x(t)\}$ is the nodal displacement vector and [C*] is the special damping matrix that is considered as follows,

$$[C^*] = \begin{bmatrix} A_n \rho v_p & 0 & 0 \\ 0 & A_{t1} \rho v_s & 0 \\ 0 & 0 & A_{t2} \rho v_s \end{bmatrix}$$

Where v_p and v_s are the P-wave and S-wave velocity of the considered medium (Table 4.2), ρ is the density of soil medium, A_n, A_{t1} and A_{t2} are the fields controlling the viscous dampers and the subscripts n and t represent normal and tangential directions in the boundary.

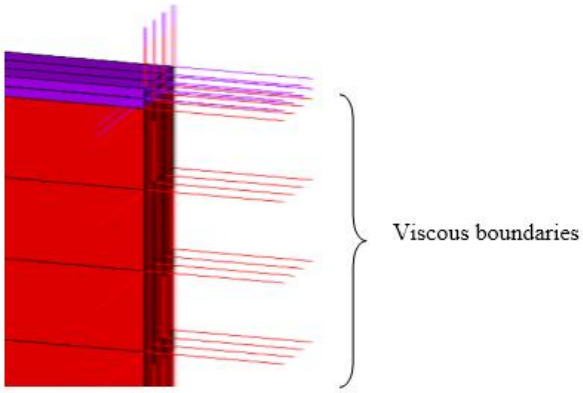

Figure 4.6 Viscous boundaries

b) For soil in the embankment

Both in static and time-history analysis, the embankment slopes were kept unrestrained and the embankment vertical sides across the longitudinal direction were restrained horizontally to consider the continuity along longitudinal direction.

4.1.5 Loading

a) Static loading

Initially, the embankment was analysed for self-weight by providing the gravitational acceleration of 9.81 m/s^2 in the vertical direction along with the mass density of embankment materials until the dissipation of excess pore water pressure so that the settlements are almost constant over time. Later it was analysed for a traffic load of 24 kN/m^2 over the embankment crest (IRC:75-2016). The crest width of 20 m

was considered according to IRC: 6-2014 specifications Class A vehicle on a 4 lane road over the embankment.

b) Seismic excitations

Four different ground acceleration records were used for time-history analysis of geogrid reinforced pile-supported embankments. India has more land area classified as earthquake Zone III under seismic zoning of India. PGA which corresponds to earthquake Zone III is 0.1 g. Hence, an artificial time-history record corresponding to IS code Zone III spectrum with a PGA of 0.1 g was selected. Another two time-history records were collected from the real earthquakes such as the Imperial Valley Earthquake (Elcentro, USA) and Loma Prieta Earthquake (Loma Prieta, USA). Since the embankment is assumed to be constructed at Seismic Zone III in India, the time-history records of real earthquakes taken for the study were scaled down corresponding to the time-history of the design spectrum for Zone III in India with a PGA of 0.1 g as given in IS1893:2016. The time duration corresponding to bracketed duration is taken for the analysis. The ground motion details, acceleration time-history records and the corresponding Fourier spectrum are shown in Table 4.3 and Figs.4.7 (a) – 4.10(a) respectively. Also, to analyse the behaviour of geogrid reinforced pile-supported embankment under strong seismic excitations, the time-history for design spectrum corresponding to IS1893:2016 was scaled to a PGA of 0.35g and used in the time-history analysis. These modified ground motions are designated as Elcentro, Loma Prieta, IS Zone III and IS (0.35 g) hereafter.

Table 4. 3 Ground motion details

Earthquake	Station	Year	Bracketed Duration (sec)	PGA (g)
Imperial Valley	Elcentro	1940	10.26	0.343
Loma Prieta	Loma Prieta	1989	2.72	0.367
IS1893 Zone III	-	-	17.83	0.101
IS1893 Modified	-	-	24.93	0.35

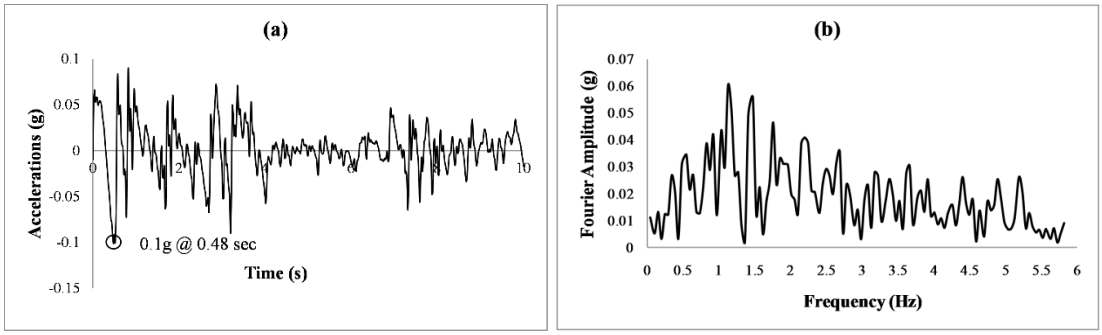

Figure 4.7 (a) Time-history and (b) Fourier spectrum of Elcentro ground motion

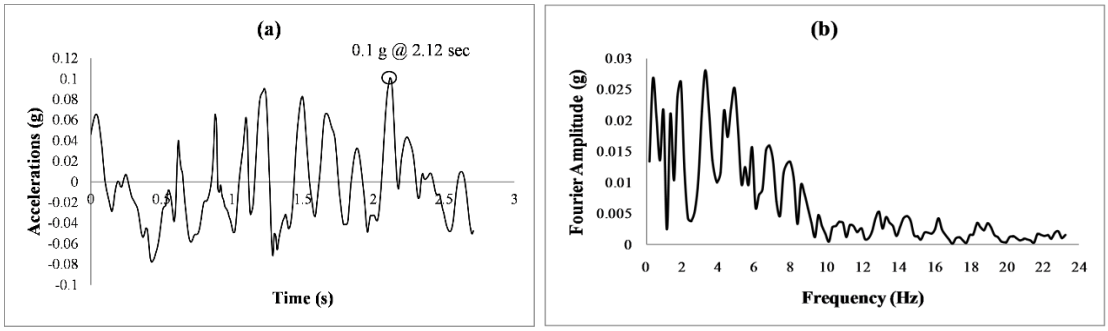

Figure 4.8 (a) Time-history and (b) Fourier spectrum of Loma Prieta ground motion

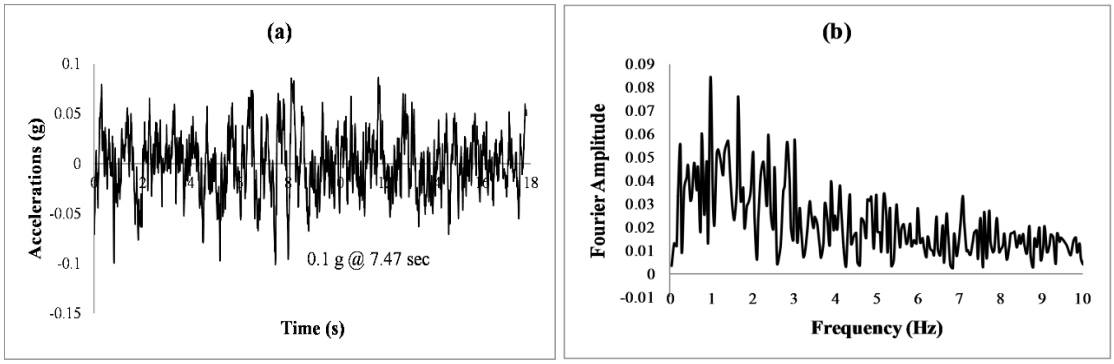

Figure 4.9 (a) Time-history and (b) Fourier spectrum of IS Zone III ground motion

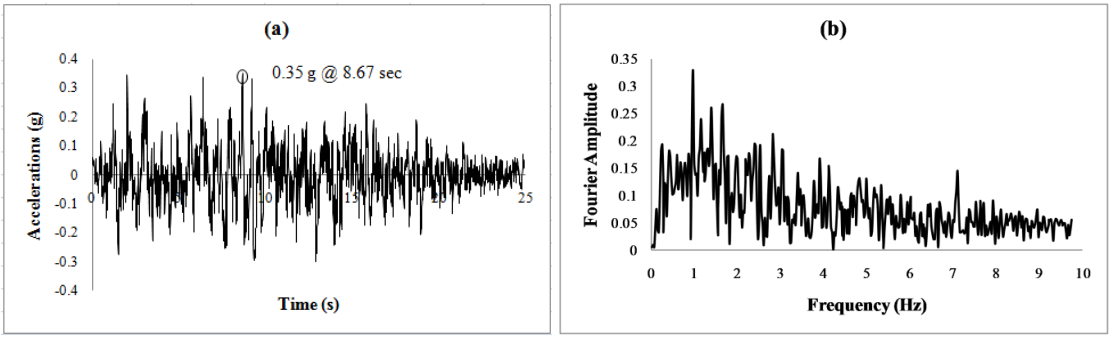

Figure 4.10 (a) Time-history and (b) Fourier spectrum of IS 0.35 g ground motion

4.2 NUMERICAL ANALYSIS OF GEOSYNTHETIC-REINFORCED EMBANKMENTS

The construction of embankments on poor compressible lands is a challenging task for the engineers due to shear failure of soft subsoil, sliding/rotation of embankment fill or subsoil, excessive vertical settlements, and lateral displacements. To prevent these failures, the use of geosynthetic reinforcement at the base level of the embankment is a suitable solution for shallow compressible subsoils. The addition of basal geosynthetic improves the shear resistance of both embankment as well as foundation soil. Parametric studies are conducted to determine the optimum width of basal geosynthetic by considering the geogrid tensile modulus, embankment height, side slope of embankment, Young's modulus of embankment fill and Young's modulus of foundation soil.

To save the land acquired by the shallow slope embankments, the embankments are constructed with very steep and vertical slopes. Embankment fill will not be able to stand freely with such a steep slope and to overcome this problem there are several improvement techniques available. One of the reliable solutions is the provision of geosynthetics in the embankment body as body reinforcement.

This section presents the verification of geosynthetic-reinforced embankment finite element models. A detailed methodology adopted for the numerical analysis of geosynthetic-reinforced embankments also explained here.

Shaking table studies on geosynthetic-reinforced soil slopes by Latha and Varman (2014) was considered for verification of the numerical model under dynamic loads. Shaking table test results of unreinforced and 2-layer geotextiles reinforced 45˚ soil slopes were compared with the numerical simulations. The model slopes were subjected

to 30 cycles of sinusoidal motion having 18.7 mm amplitude and 2 Hz frequency to achieve a base acceleration of 0.3g. 5 % material damping was assumed for the analysis. The slope fill soil was modelled as Mohr-Coulomb material model having unit weight of 18.4 kN/m^3, cohesion of 15 kPa, angle of internal friction of 11˚, Young's modulus of 25 MPa and Poisson's ratio of 0.2. Geotextile's reinforcement was modelled as linear elastic material having 55.5 kN/m ultimate tensile strength, 1 mm thickness and Poisson's ratio of 0.3. The finite element models of unreinforced and 2-layer geotextile-reinforced soil slopes along with the details of slope geometry is shown in Fig.4.11. Plane strain condition was adopted across the slope. The side vertical boundary was restrained against lateral deformations. The bottom boundary was restrained against vertical deformations and the soil slope was unrestrained. Fig.4.12 shows the comparison of results from the analysis of FE model under dynamic excitations with Latha and Varman (2014). The difference in lateral displacements is less than 10 %, this verifies the numerical simulations.

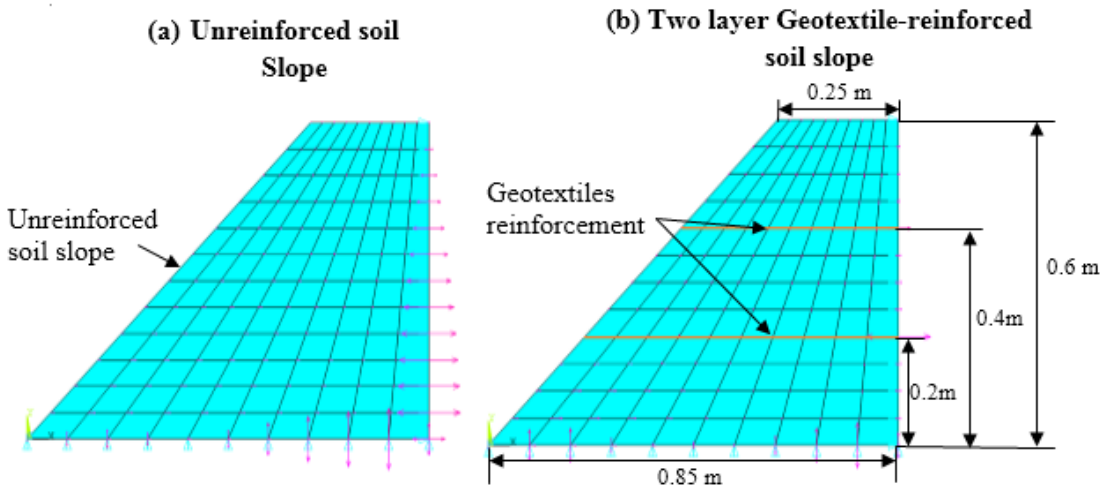

Figure 4.11 Finite element models developed for validation of geosynthetic-reinforced embankment (a) Unreinforced soil slope (b) Two-layer geotextile-reinforced soil slope

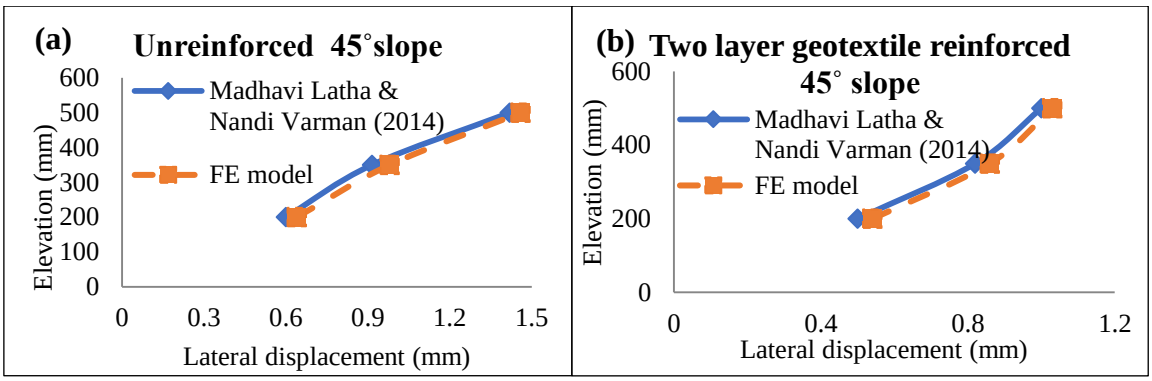

Figure 4.12 Comparison of lateral displacements in FE model with Latha & Varman (2014) (a) Unreinforced slope (b) Reinforced slope

4.2.1 Details of geosynthetic-reinforced embankment geometry

Embankments with 4 m, 6 m, 8 m and 10 m height (H) having 32 m base width (B) and 20 m crest width constructed over 10 m thick clayey foundation soil were considered for the static and time-history analysis. The analysis was carried out for three different side slopes such as 1V:2H, 1V:1H and 1V:0.5H. Basal geogrid was laid at the centre of 0.5 m thick surface fill below the embankment. 10.5 m deep 288 m wide finite soil continuum with lateral viscous boundaries to represent the infinite soil on lateral boundaries were considered below the embankment. Fig.4.13 shows the details of basal geogrid-reinforced embankment.

An embankment of height 6 m supported on 20 m thick foundation soil was analysed for the response under seismic load after reinforcing the same with body reinforcements designed using simple wedge method. The design of body reinforced embankments using simple wedge method is presented in APPENDIX II. The embankment with a slope of 1V:1H supported by soft foundation soil was taken as a representative model to analyse the effect of inclusion of body reinforcement. Effect of slope inclination and foundation soil property was analysed by applying load on embankment models of slopes 1V:1H, 1V:0.5H and 1V:0H. The geometry is given in Fig.4.14.

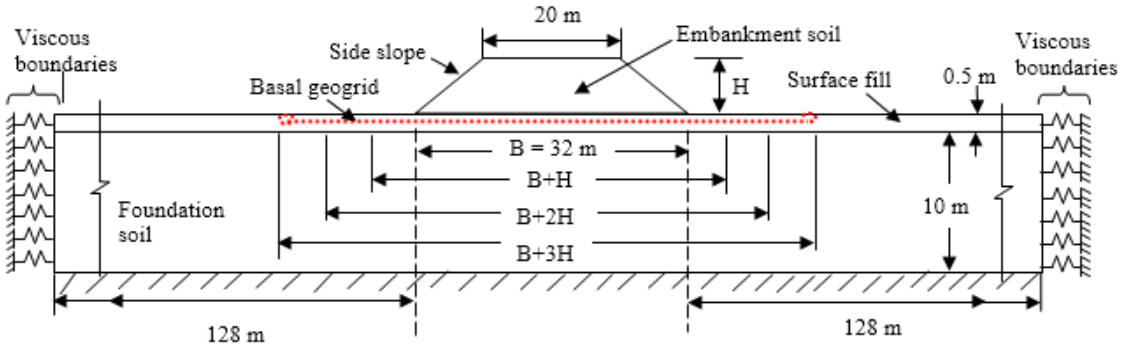

Figure 4.13 Details of basal geogrid-reinforced embankment geometry (Dimensions are not as per scale)

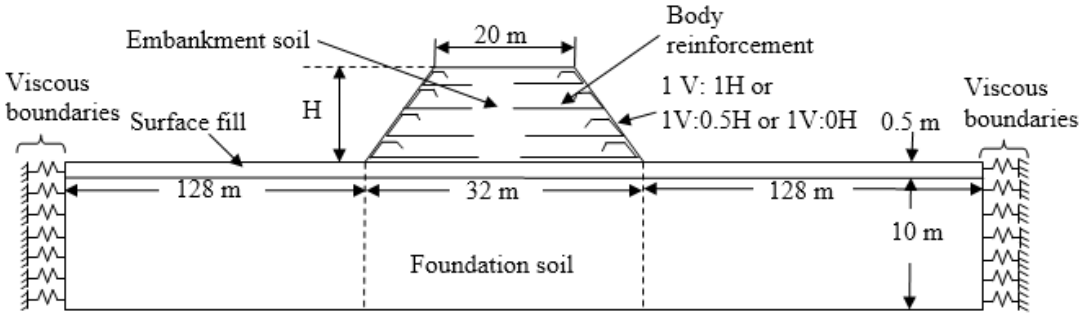

Figure 4.14 Details of body-reinforced embankment geometry (Dimensions are not as per scale)

4.2.2 Finite element model

ANSYS Mechanical APDL was used to perform both static and time-history analysis. Embankment fill, surface fill and soft foundation soil were modelled using PLANE182 element with plane strain condition. PLANE182 is defined by four nodes having translations in the nodal x and y directions. Geogrid reinforcement was modelled using SHELL208 element with membrane action. SHELL208 element is a two noded element with translational degrees of freedom along x and y directions. Fig.4.15 depicts the finite element model of a basal geogrid-reinforced embankment. Similarly, Fig.4.16 (a) depicts the finite element model of body-reinforced embankment and 4.16 (b) shows the enlarged view of body-reinforced embankment.

Since the time taken to run the undrained analysis is very much high compared to drained analysis, only a set of undrained analysis was performed for 6 m high 1V:1H sloped embankment made of ES3 soil having basal geogrid with J = 500 kN/m and supported over FS1 foundation soil having permeability of 5 x 10^{-10} m/s. The embankment was subjected to IS Zone III ground motions. Coupled pore-pressure

element including plane strain condition CPT212 was used to model the foundation soil. It is a four noded element with two translational and one pore water pressure degrees of freedom at each node.

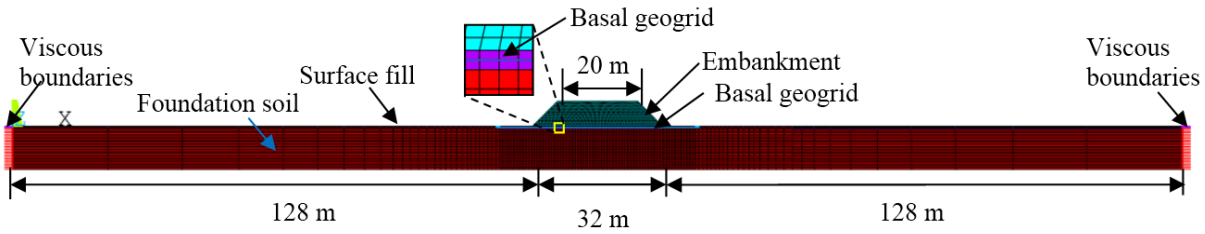

Figure 4.15 Finite element model of basal geogrid-reinforced embankment

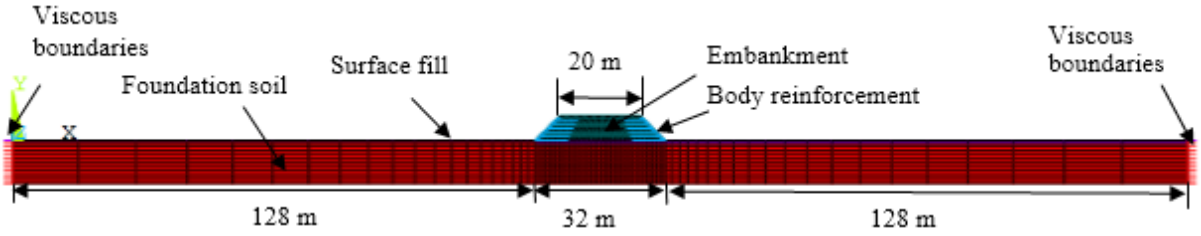

(a)

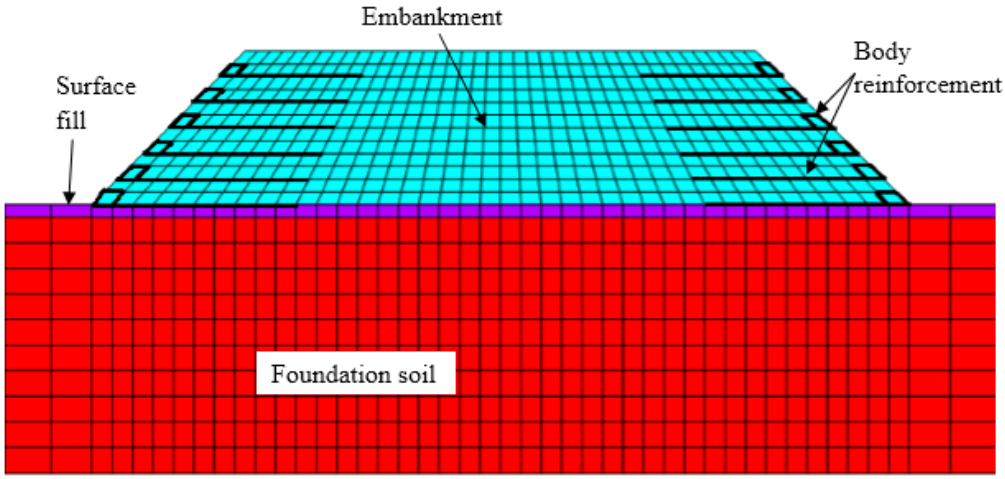

(b)

Figure 4.16 (a) Finite element model of body-reinforced embankment (b) Enlarged view of finite element model of body-reinforced embankment

4.2.3 Materials

a) Soil

The properties of embankment soil (PFA), surface fill and soft foundation soil (Soft marine clay) considered for the analysis are same as listed in Table 4.2.

b) Basal geogrid reinforcement

The width of geosynthetic provided at the base of the embankment should be sufficient to prevent embankment rotational failure, lateral displacements at toe and

vertical settlements of embankment due to static and seismic loads (IRC:113-2013). Therefore, a parametric study was conducted by varying the width of geogrid. The width of geogrid was taken as B, B+H, B+2H and B+3H, where 'B' is the width of base of the embankment and 'H' is the height of the embankment. Fig.4.17 represents the enlarged view of finite element models of embankment annotated with basal geogrid width. Basal geogrid was modelled as a linear elastic isotropic material with Poisson's ratio of 0.3.

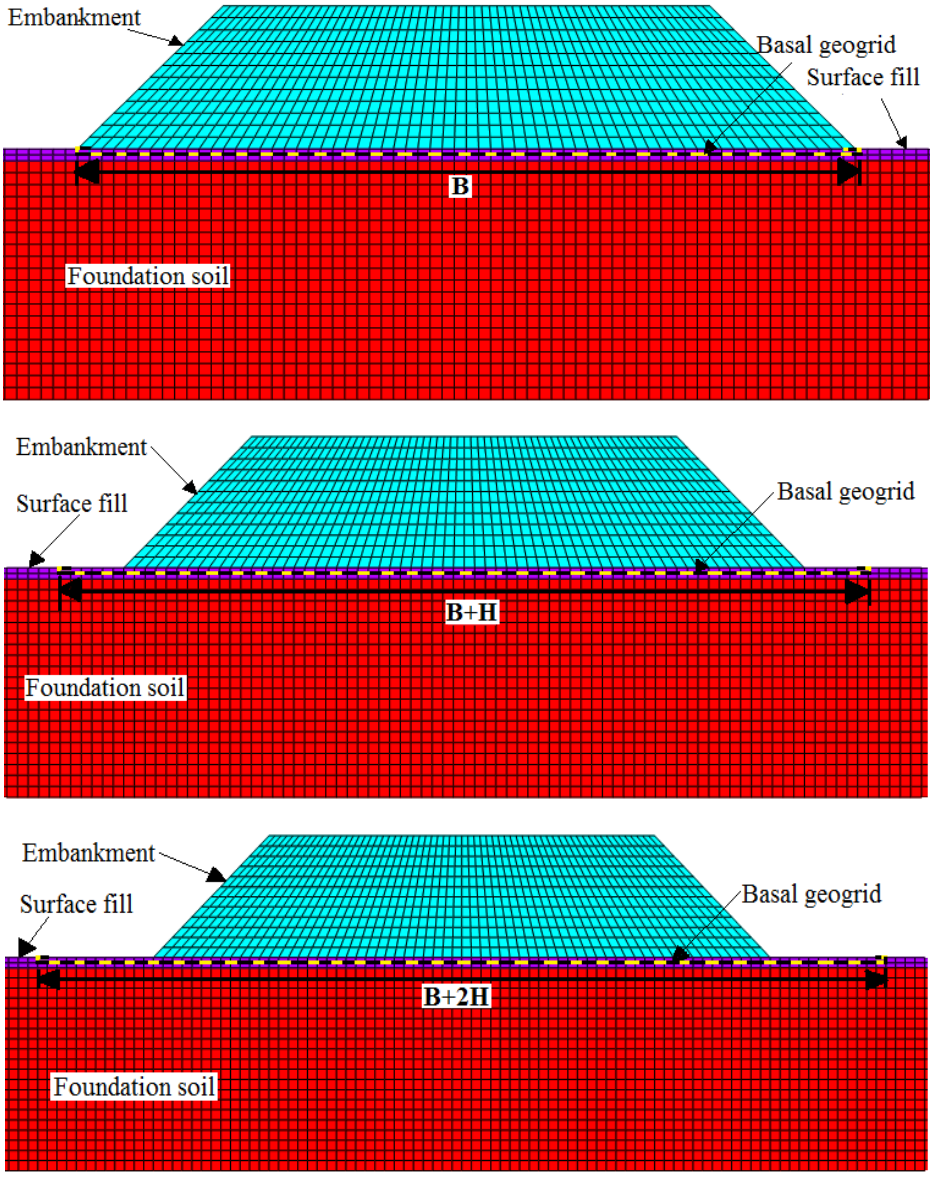

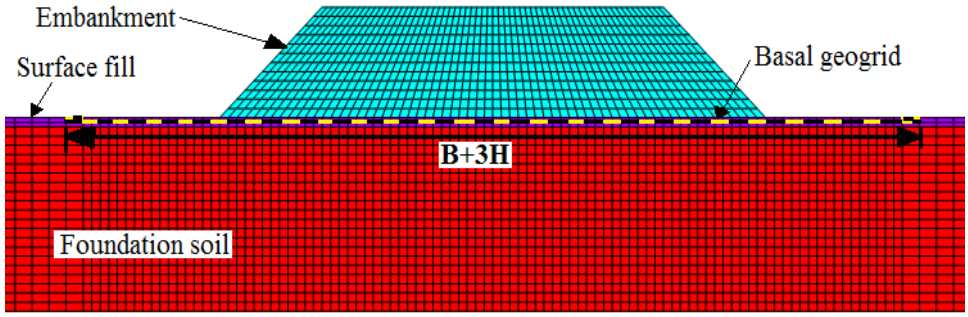

Figure 4.17 Enlarged view of finite element model of embankment showing basal geogrid width

Availability of geogrids with high tensile modulus of 4000 kN/m in the market is rare and geogrids upto 1000 kN/m tensile modulus are most available ones. Hence, the present study also considers to study the behaviour of 4 layer basal geogrid-reinforced embankment having tensile modulus of 1000 kN/m subjected to seismic loading. To provide 4 layers of basal geogrid, 1 m thick surface fill was considered with each layer of geogrid laid at 200 mm spacing. Fig.4.18 shows the finite element model of 4 layer basal geogrid-reinforced embankment and the enlarged view of basal geogrid-reinforcement.

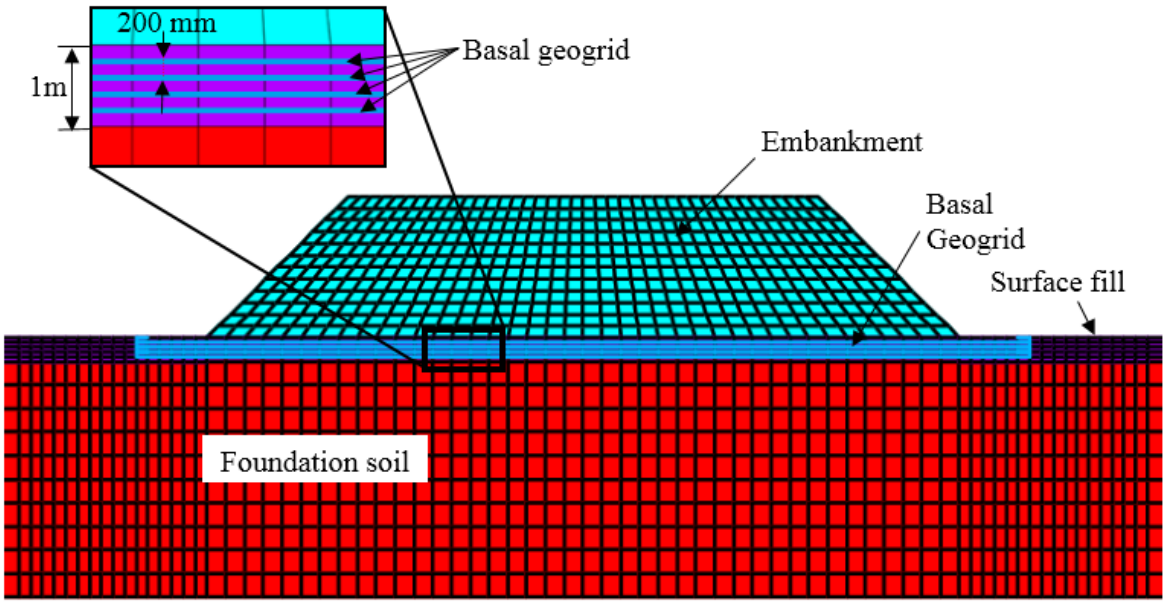

Figure 4.18 Finite element model of 4 layer basal geogrid reinforced embankment and enlarged view of basal geogrid-reinforcement

c) Geogrid as body reinforcement

The embankment body was reinforced with 6 layers of geogrid reinforcement on both sides of embankment slope having 5 m width and 500 kN/m tensile stiffness.

The reinforcement was spaced at 1 m interval along the embankment elevation. Body reinforcement was also modelled as a linear elastic isotropic material with Poisson's ratio of 0.3

4.2.4 Parameters

a) For basal geogrid-reinforced embankment

Parametric study was conducted on embankment models by varying the stiffness of embankment fill, stiffness of foundation soil, embankment height, embankment side slope and basal geogrid stiffness to find the appropriate width of basal geogrid. The embankments were subjected to static and seismic loads. Table 4.4 provides the list of values and notations used for the parameters considered. Young's modulus of embankment soil was adopted corresponding to loose sand and Young's modulus of foundation soil was adopted as a range corresponding to very soft clay to hard clay (Bowles, 2012). Tensile modulus of basal geogrid was varied until the embankment settlements were very small or negligible.

Table 4. 4 Parameters considered for the analysis

Parameters	Values	Notations	Parameters kept constant
Young's modulus (MPa) - Embankment soil	10	ES1	H = 6 m
	15	ES2	Side slope = 1V:1H
	20	ES3	FS1
	25	ES4	J = 500 kN/m
Young's modulus (MPa) - Foundation soil	4 (Very soft clay)	FS1	H = 6 m
	15 (Soft clay)	FS2	Side slope = 1V:1H,
	25 (Medium clay)	FS3	ES3
	50 (Stiff clay)	FS4	J = 500 kN/m
Embankment Height (m)	4	H1	Side slope = 1V:1H
	6	H2	ES3
	8	H3	FS1
	10	H4	J = 500 kN/m
Side slope	1V:1H	1V:1H	H = 6 m
	1V:0.5H	1V:0.5H	ES3, FS1

				J = 500 kN/m
Basal geogrid stiffness (kN/m)	For Static loading 0 to 2000	For Seismic loading 0 to 8000	J	H = 6 m Side slope = 1V:1H ES3 FS1
Earthquake intensity (g)	0.1 g 0.35 g 0.6 g		IS Zone III IS 0.35 g IS 0.6 g	H = 6 m Side slope = 1V:1H ES3, FS1 J = 500 kN/m
Basal geogrid width (m)	0 32 38 44 50		U B B+H B+2H B+3H	All combinations of parameters

b) For body-reinforced embankment

Parametric study was conducted by varying the embankment side slope 1V:1H, 1V:0.5H and 1V:0H and foundation soil stiffness (Table 4.5) in combination with the geogrid stiffness provided to the embankment body.

Table 4. 5 Stiffness of foundation soil

Soil type	Young's Modulus (MPa)	Unit weight (kN/m^3)
Soft foundation soil	4	14
Stiff foundation soil	50	21

4.2.5 Boundary conditions

a) For embankment soil

The embankment side slopes were kept unrestrained both in static and seismic analysis. Plane strain condition was considered along the embankment.

b) For foundation soil and surface fill

i) Under static loading

Plane strain condition along the embankment was considered. The two lateral boundaries were restrained for the horizontal deformations and the bottom surface was restrained in all the three directions.

ii) Under seismic excitations

Similar as basal geogrid-reinforced piled embankments, here in geosynthetic-reinforced embankment analysis, the lateral boundaries were taken at a distance of four times the width of the embankment. To simulate the infinite soil medium, viscous boundaries (Eq.4.3) were applied for the lateral boundaries using spring-damper element COMBIN14 (Fig.4.19)

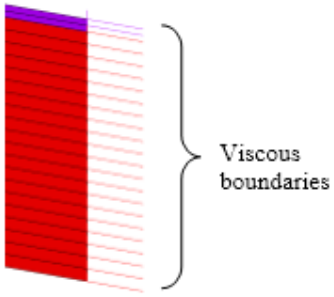

Figure 4.19 Viscous boundaries

4.2.6 Loading

a) For static analysis

Static analysis was done for self-weight by providing the gravitational acceleration of 9.81 m/s^2 in the vertical direction along with the mass density of embankment materials.

b) For seismic analysis

i) Basal geogrid-reinforced embankment

The acceleration time-history record compatible with IS code ground motion corresponding to the elastic design spectrum for Zone III given in IS 1893(Part 1):2016 with a PGA of 0.1 g was selected for the seismic analysis. This is designated as IS Zone III ground motion. Also, the behaviour of basal geogrid-reinforced embankment subjected to different earthquake intensities were analysed by scaling the IS Zone III ground motion to a PGA of 0.35 g and 0.6 g, which are designated as IS (0.35 g) and IS (0.6 g). Time duration corresponding to the bracketed duration was considered for the analysis. The acceleration time-history records and the corresponding Fourier spectrum for IS Zone III and IS (0.35 g) are shown in Figs.4.9 (a) – 4.10(a) and Figs.4.9 (b) – 4.10(b) respectively. IS (0.6 g) ground motion is similar as IS 0.35 g ground motion except a PGA of 0.6 g, hence the acceleration time-history plot for IS 0.6 g ground motion is not presented again.

ii) Body-reinforced embankment

The acceleration time-history record of IS Zone III ground motion scaled to a PGA of 0.35 g was considered for the seismic analysis of body-reinforced embankment. Fig.4.10 (a) and 4.10 (b) presents the acceleration time-history and the corresponding Fourier spectrum of IS (0.35 g) ground motion considered.

4.3 SUMMARY

The methodology followed to evaluate the load transfer mechanism in geogrid-reinforced pile-supported embankments and only geosynthetic-reinforced embankments was detailed in this chapter. The idealization, general assumptions, loading and boundary conditions considered and the analysis carried out to study the static and seismic behaviour of these embankments were elaborated. The chapter presented the proposition put forward to accomplish the objectives outlined in the study.

CHAPTER 5

RESPONSE VARIATION OF BASAL GEOGRID-REINFORCED PILE-SUPPORTED EMBANKMENTS SUBJECTED TO SELF-WEIGHT AND TRAFFIC LOAD

5.1 INTRODUCTION

This chapter presents the results obtained from the 3-dimensional finite element analysis of basal geosynthetic-reinforced embankments with or without pile supports subjected to self-weight and traffic loading.

The response of basal geogrid-reinforced pile-supported embankment in terms of crest settlements, toe lateral displacements, differential settlements at crest, stress distribution ratio, lateral stress distribution ratio, coefficient of lateral pressure under static loading conditions is presented in this section. Also, based on the results of 3-dimensional finite element analysis, an analytical equation for soil arching coefficient (C_c) including the pile spacing is proposed and the obtained results were compared with the existing analytical equations and finite element analysis results.

Embankments of height 3 m, 4 m, 5 m and 6 m having 1V:1.5H side slope supported over 28 m deep soft marine clay improved with floating (22 m, 24 m or 26 m) or end-bearing (28 m) piles arranged in 3D, 4D or 5D spaced square grid pattern (where D is the diameter of pile) and basal geogrid of tensile modulus ranging from 0 to 6000 kN/m are considered for the static (consolidation) analysis under the embankment weight.

5.2 SETTLEMENT AT CREST CENTRE

Fig.5.1 shows the maximum crest centre settlements subjected to consolidation for the weight of embankment. From Fig.5.1 it is noticed that rise in embankment height increases the crest centre settlements and also addition of basal geogrid reduces the crest centre settlements. About 18 % settlement reduction is observed for 6 m high embankment and about 15 % settlement reduction is observed for 3 m high embankment. A minimum geogrid tensile modulus of 500 kN/m is sufficient to reduce the maximum settlements and further increase in tensile modulus beyond 4000 kN/m will not have any effect in reducing settlements. Similar trend in settlements was observed by Han & Gabr, 2002.

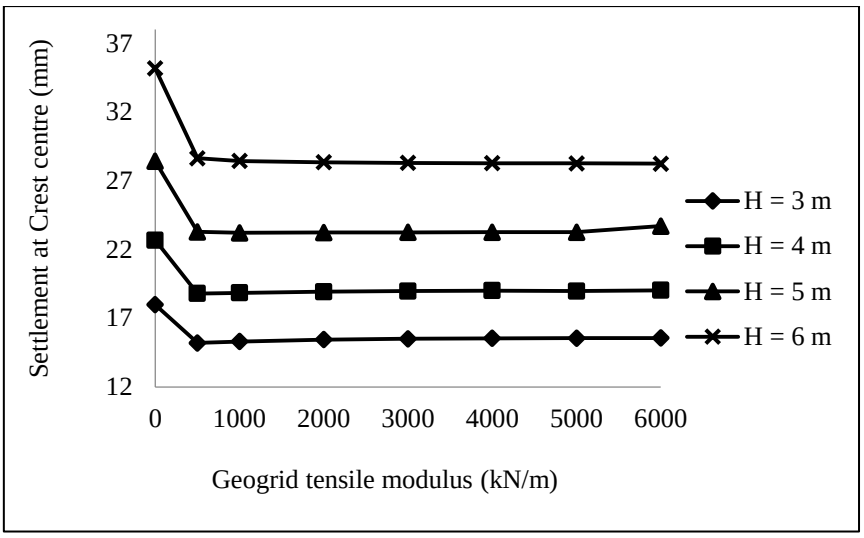

Figure 5. 1 Crest centre settlements for 28 m pile supported embankment

Crest centre settlements for 6 m high embankment supported over 22 m long floating and 28 m long end-bearing piles are shown in Fig.5.2. Similar as Fig.5.1, in case of floating pile-supported (22 m) embankment (Fig.5.2) a minimum geogrid tensile modulus of 500 kN/m is sufficient to reduce the maximum settlements and beyond J = 4000 kN/m further increase in tensile modulus will not have any effect in reducing settlements. From Fig.5.2 it is observed that increase in pile length reduces the crest centre settlements to a greater extent. About 82.3 % decrease in settlements is observed by increasing the pile length from 22 m to 28 m.

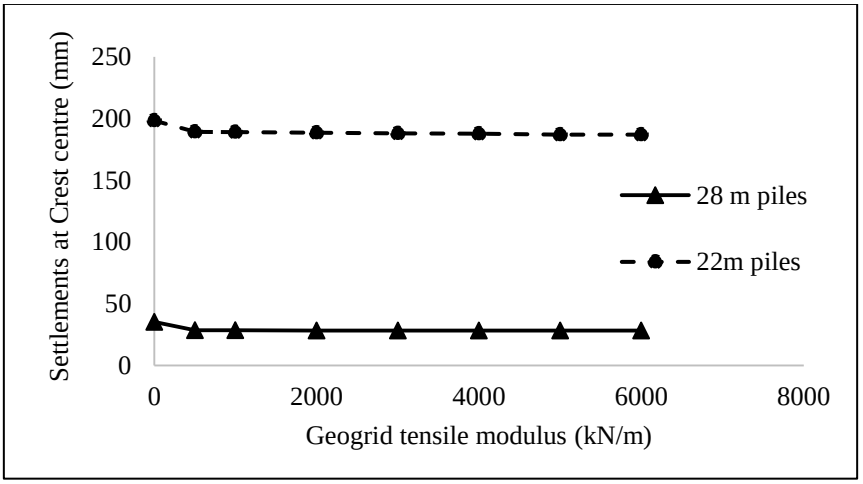

Figure 5. 2 Crest centre settlements for 6 m high embankment

Table 5.1 presents the settlements at crest centre under static loading conditions including various parameters such as pile length, pile spacing, embankment height and presence or absence of basal geogrid. From Table 5.1, it is observed that the

embankment supported over end-bearing piles (28 m) experiences very less crest centre settlements compared with embankment resting over floating piles (22 m, 24 m, 26 m). Even at 5D spacing, 28 m pile supported embankment exhibits less crest centre settlements compared with 3D spaced floating pile supported embankment. Since the 28 m piles offers both end-bearing and frictional resistance the observed crest centre settlements are very less when compared with floating pile supported embankments where only frictional resistance is offered. The basal geogrid acts as a flexible bed over pile foundations, it transfers additional embankment load to piles by membrane action. Hence the provision of basal geogrid helps to lay the piles at higher spacing there by reducing the quantity of concrete and construction charges. 5D spaced pile supported embankment with J = 4000 kN/m experiences less crest centre settlements than unreinforced 3D spaced pile supported embankment. This is because the presence of basal geogrid effectively distributes the embankment load to the pile foundations and the subsoil between piles even at large pile spacing of 5D.

Table 5. 1 Crest centre settlements under static loading conditions

Pile Length (For 6 m high embankment, 3D spacing)	J = 0 kN/m	J = 4000 kN/m
	Crest centre settlements (mm)	
28 m	35.16	28.27
26 m	145.83	138.60
24 m	166.11	158.27
22 m	198.42	187.75
Pile spacing (For 6 m high embankment, 28 m Piles)		
3D	35.16	28.27
4D	43.36	31.35
5D	52.13	34.41
Embankment height (For 3D spaced 28m piles)		
3 m	17.97	15.53
4 m	22.67	19
5 m	28.41	23.25
6 m	35.16	28.27

5.3 STRESS DISTRIBUTION RATIO

Stress distribution ratio (SDR) is defined as the ratio between vertical stresses on the pile to that on the foundation soil between piles measured at same elevation.

$$SDR = \frac{\sigma_p}{\sigma_s} \tag{5.1}$$

Where σ_p is the vertical stress on the pile in kN/m^2 and σ_s is the vertical stress on the foundation soil in kN/m^2.

Figure 5.3 shows the variation in SDR at centre pile head of 28 m long pile (End-bearing) below the embankment for various geogrid stiffness values corresponding to the self-weight of embankment. Increase in geogrid stiffness increases the SDR (Fig.5.3) which indicates the increased load transfer to the piles. Also, the increase in embankment height increases the SDR values. Han and Gabr, (2002) reported similar results. A 6 m high embankment with basal geogrid of tensile modulus 6000 kN/m gives 1377 kPa vertical stress on pile head and 30.2 kPa vertical stress on foundation soil which results in a SDR of 45.6.

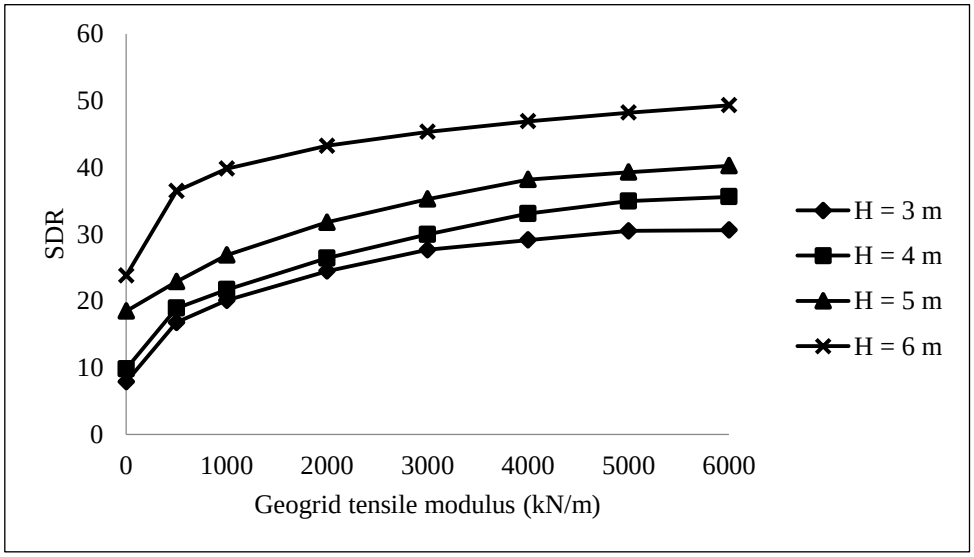

Figure 5. 3 Variation in SDR for 28 m pile supported embankment subjected to its own weight

Fig.5.4 shows the SDR values for 6 m high embankment supported over 22 m (floating) and 28 m (end-bearing) piles. From Fig.5.4 and Table 5.2 it is noticed that increase in pile length increases the SDR value and also irrespective of length of pile increase in geogrid modulus up to 4000 kN/m, SDR value increases. Beyond that

further increase in geogrid tensile modulus is ineffective. When J = 0 kN/m, about 60 % reduction in SDR is observed for 22 m pile supported embankment compared with 28 m pile supported embankment. When J = 4000 kN/m and above, about 43 % reduction in SDR is observed for 22 m pile supported embankment compared with 28 m pile supported embankment.

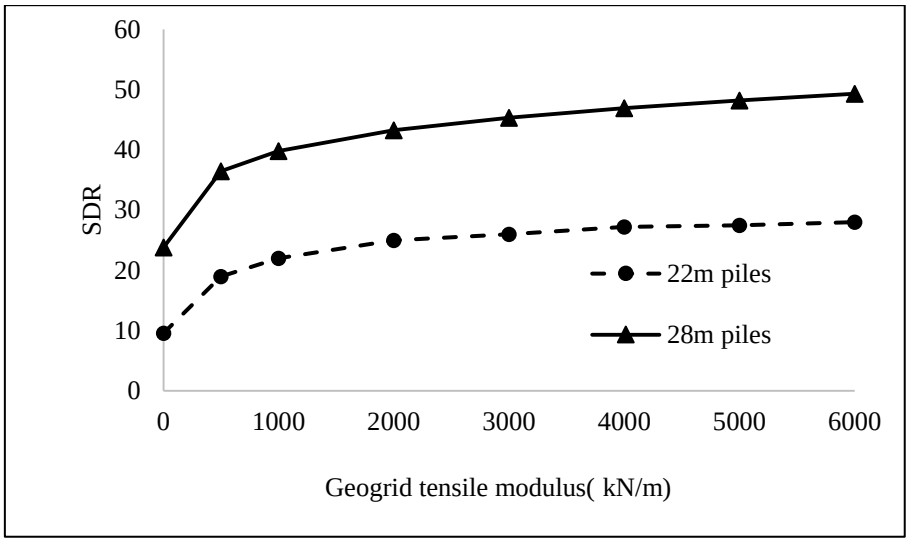

Figure 5. 4 Stress distribution ratio for 6 m high embankment

Table 5.2 presents the variation of SDR for various pile length, pile spacing and embankment height in presence or absence of basal geogrid subjected to embankment self-weight. These SDR values are taken at foundation level below basal geogrid. It is noticed from Table 5.2 that, the decrease in pile length, decrease in embankment height and increase in pile spacing decreases the SDR value. The addition of basal geogrid leads to higher SDR value irrespective of pile length, pile spacing and embankment height. This shows the additional load transfer to the piles due to membrane action of basal geogrid.

Table 5. 2 SDR under static loading conditions

Pile Length (For 6 m high embankment, 3D spacing)	Unreinforced (J = 0 kN/m)	Reinforced (J = 4000 kN/m)
	SDR at foundation level	
28 m	23.8	46.9
26 m	11.57	37.1
24 m	10.36	31.79

22 m	9.54	27.23
Pile spacing (For 6 m high embankment, 28 m Piles)		
3D	23.8	46.9
4D	21.04	35.7
5D	18.9	26.1
Embankment height (For 3D spaced 28m piles)		
6 m	23.8	46.9
5 m	18.48	38.18
4 m	9.82	33.08
3 m	7.88	29.12

Figure 5.5 depicts the plot of SDR versus pile length for 6 m high embankment supported over 3D spaced 28 m end-bearing piles subjected to self-weight of embankment. Increase in basal geogrid stiffness increases the SDR value at foundation level, as the depth increases the SDR values for the considered range of geogrid stiffness becomes equal. Similar trend is observed for various embankment height, pile length and pile spacing considered (Fig.5.6). In case of end-bearing pile (28 m) supported embankment including embankment height variation and pile spacing the maximum SDR is observed at the bottom of pile at a depth 24 m (Fig.5.5 and Fig.5.6). With increase in pile spacing the SDR value at foundation level decreases and at a depth 24 m below foundation level the maximum SDR is observed for 5D spaced pile supported embankment compared with 3D (Fig.5.5) and 4D spaced pile supported embankments. The end-bearing resistance offered by the piles and the high overburden pressure coming on larger spaced piles maybe the reason for maximum SDR at 24 m depth.

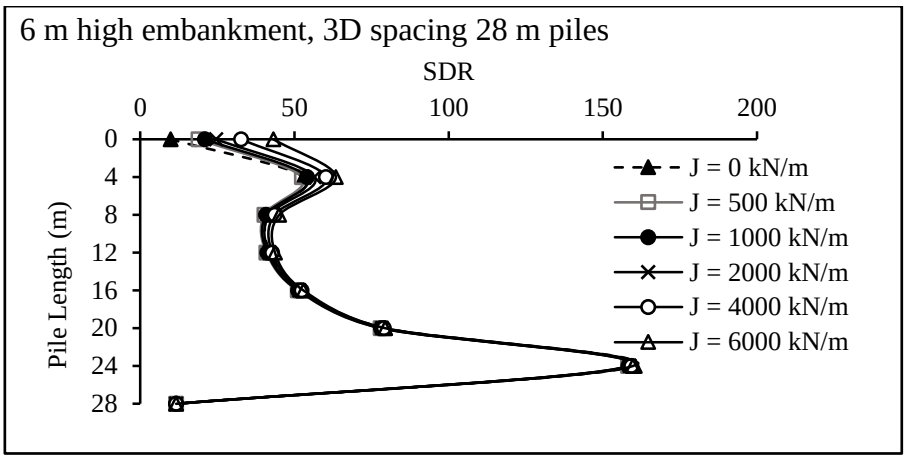

Figure 5. 5 SDR along the length of pile under static loading conditions

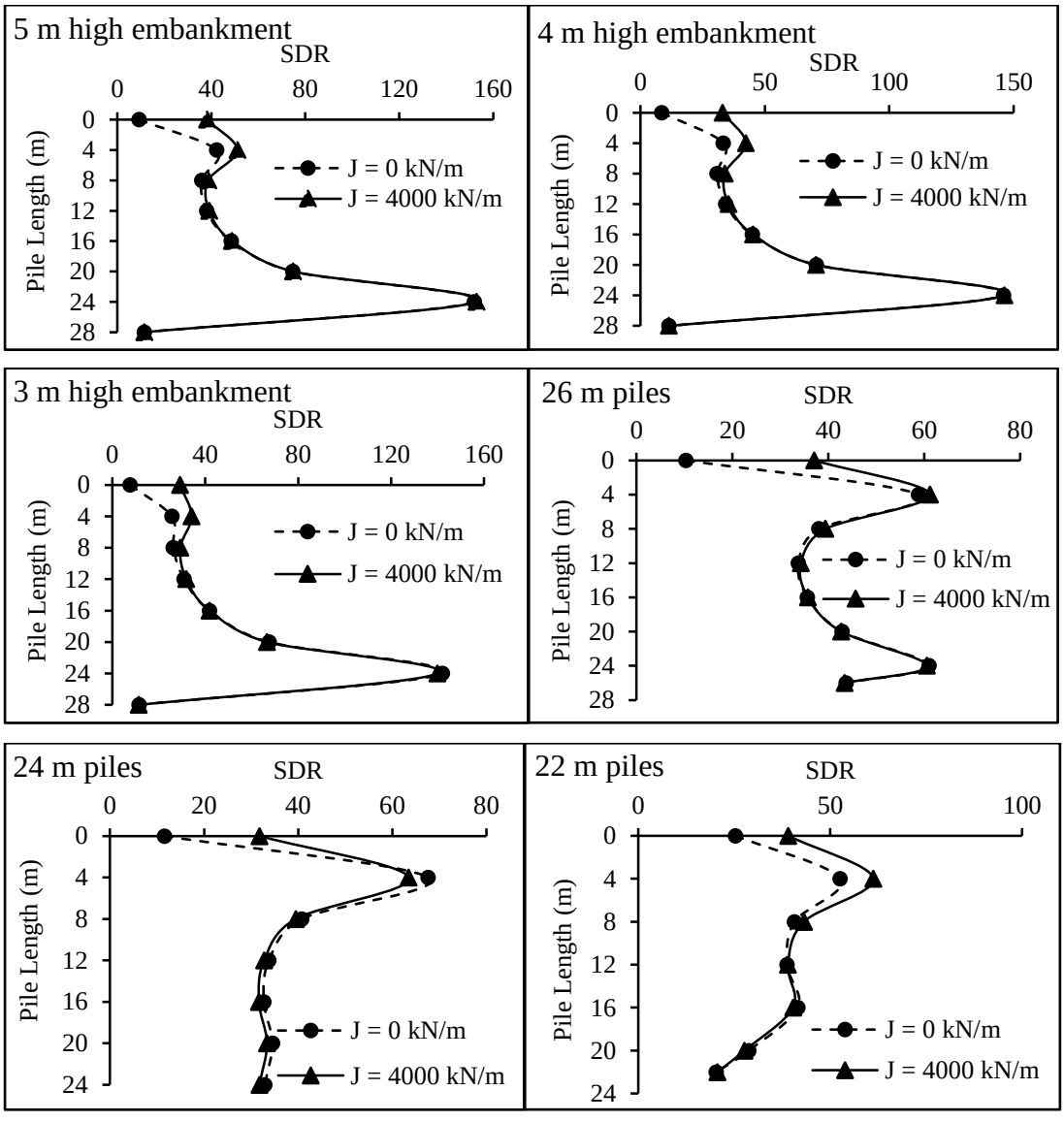

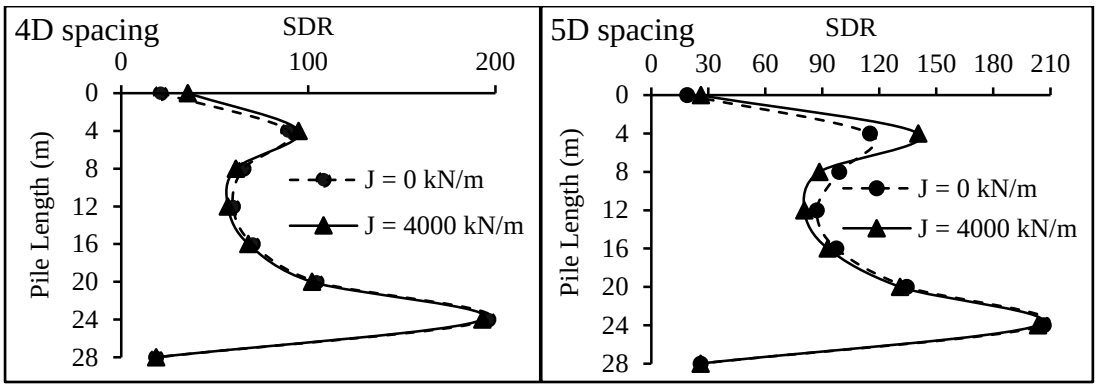

Figure 5. 6 SDR along the length of pile considering embankment height, pile length, pile spacing and geogrid tensile modulus under static loading conditions

5.4 LATERAL STRESS DISTRIBUTION RATIO

Lateral stress distribution ratio (LSDR) is the ratio of lateral stresses on the pile to that on the foundation soil between piles measured at same elevation.

Given by, $$LSDR = \frac{\sigma_{px}}{\sigma_{sx}} \quad (5.2)$$

Where σ_{px} is the lateral stress on pile in kN/m^2 and σ_{sx} is the lateral stress on the foundation soil between piles in kN/m^2.

Figure 5.7 shows the effect of geogrid stiffness and embankment height on LSDR for embankment subjected to its own weight. From Fig.5.7 it is observed that increase in geogrid tensile modulus reduces the LSDR value. Also, the increase in embankment height reduces the LSDR value. Large vertical stresses are observed on piles due to embankment weight. Hence the LSDR values are inversely proportional with SDR values.

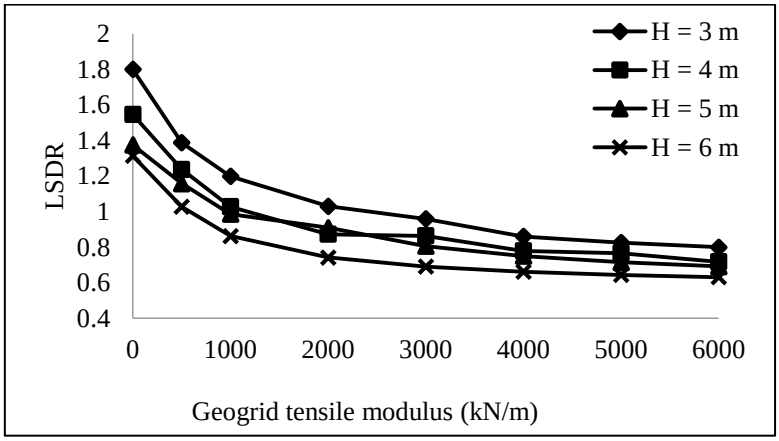

Figure 5. 7 Variation in LSDR for 28 m pile supported embankment subjected to its own weight

Figure 5.8 presents the LSDR variation along the length of pile for 6 m high embankment supported over 3D spaced 28 m piles subjected to static loading. At foundation level the LSDR values reduces with increase in geogrid stiffness and at 4 m depth, the LSDR increases with increase in geogrid stiffness and reaches the maximum. As the depth increases the effect of geogrid stiffness reduces, at depth below 12 m the LSDR values becomes same for the considered geogrid stiffness (Fig.5.8). Similar variation along the length of pile is observed for different embankment height, different pile length and pile spacing (Fig.5.9).

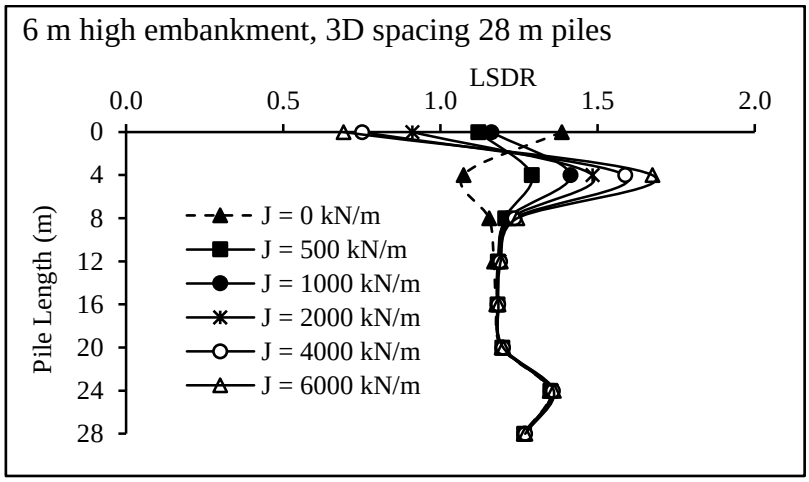

Figure 5. 8 LSDR along the length of pile under static loading conditions

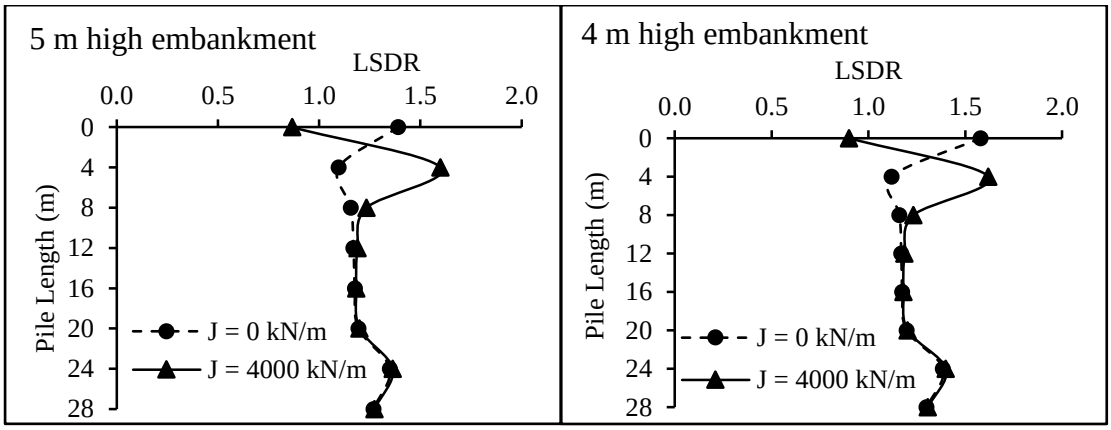

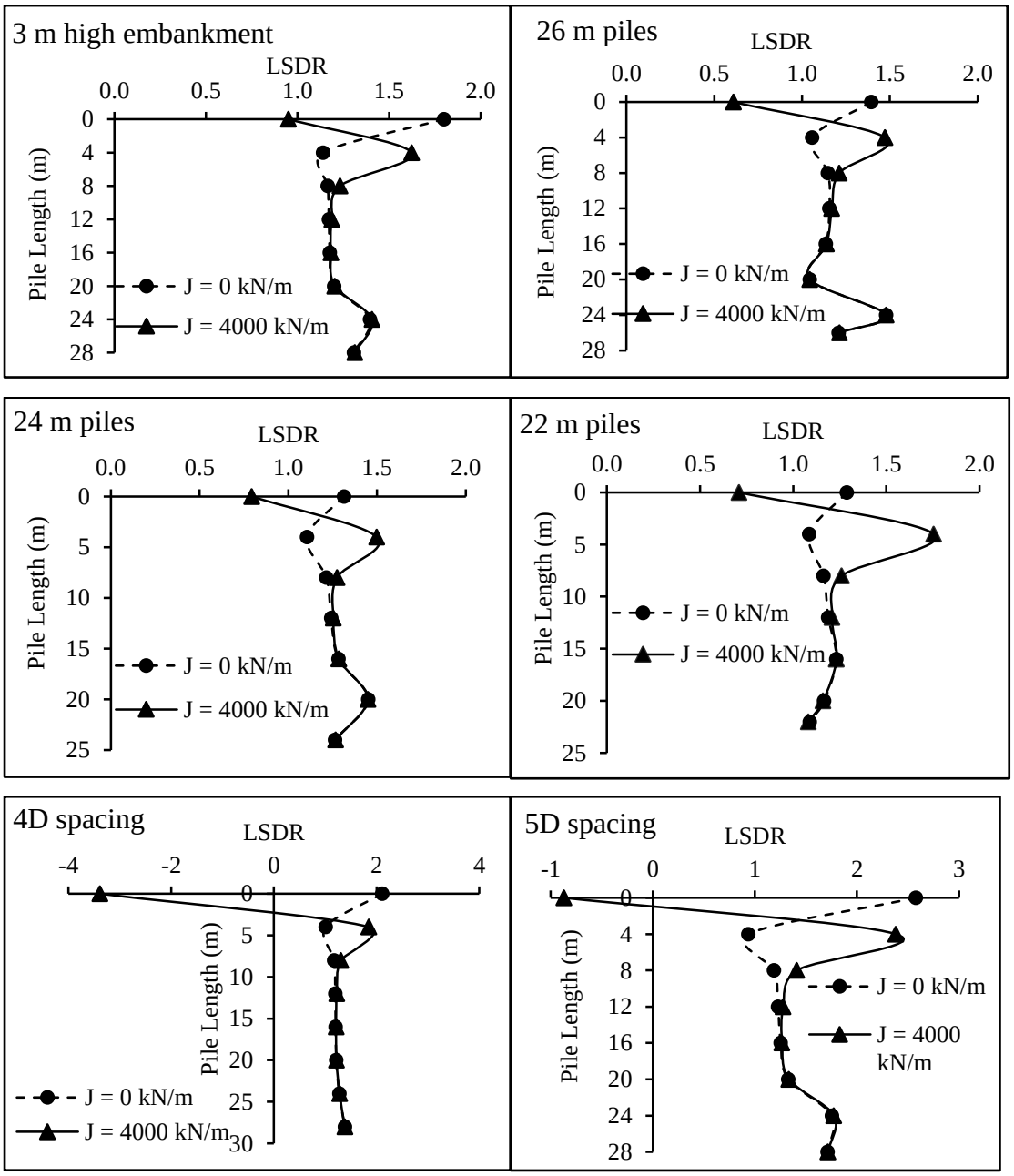

Figure 5. 9 LSDR along the length of pile considering embankment height, pile length, pile spacing and geogrid tensile modulus under static loading conditions

5.5 COEFFICIENT OF LATERAL PRESSURE

Coefficient of lateral pressure (K) is defined as the ratio of lateral stress versus vertical stress at a point in the soil. A plot of coefficient of lateral pressure along embankment height is presented to observe the effect of geogrid tensile modulus, length of piles, spacing of piles and embankment height. The results of K were taken above piles and foundation soil between adjacent piles (Fig.5.10).

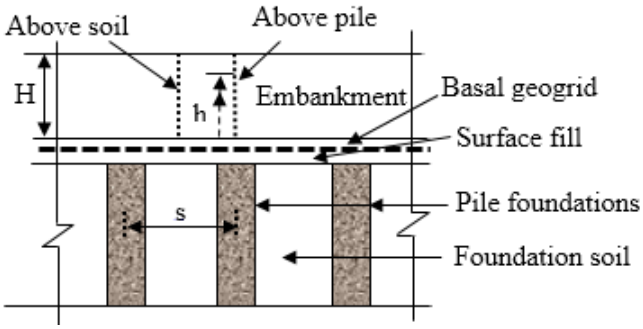

Figure 5. 10 Location where K is measured in the geogrid reinforced pile-supported embankment

The angle of internal friction (ϕ) of embankment fill is 30º.

The corresponding active earth pressure, K_a equal to 0.33. $K_a = \frac{(1-sin\phi)}{(1+sin\phi)}$ (5.3)

Earth pressure at rest K_o equal to 0.5. $K_0 = (1 - sin\phi)$ (5.4)

Passive earth pressure K_p equal to 3. $K_p = \frac{(1+sin\phi)}{(1-sin\phi)}$ (5.5)

Figure 5.11 shows the variation of coefficient of lateral pressure (K) versus normalised embankment height (h/s) above pile and above foundation soil for various basal geogrid stiffness under static loading conditions. 6 m high embankment supported over 3D spaced 28 m end-bearing piles improved subsoil is considered. It is observed from Fig.5.11 that, the K above pile and soil are almost equal to pressure at rest (0.5) up to (h/s) equal to 5. When (h/s) is above 5, the unreinforced (J = 0 kN/m) embankment is giving more lateral earth pressure than the reinforced embankment.

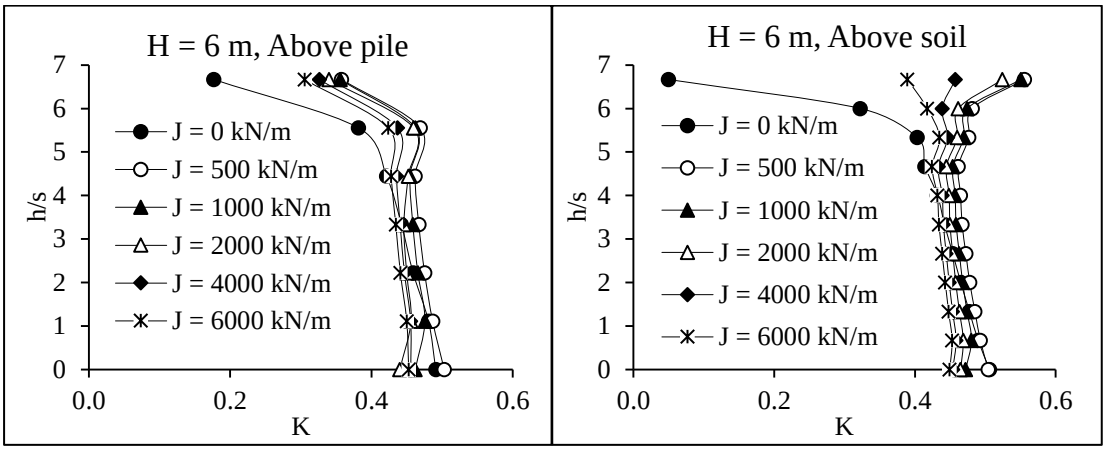

Figure 5. 11 Effect of geogrid stiffness on K along embankment height for 6 m high embankment supported over 3D spaced 28 m piles under static loading conditions

Figure 5.12 presents the plot of K versus (h/s) considering the effect of embankment height for 28 m pile supported embankment subjected to static loading.

From Fig.5.12 it is observed that, the increase in embankment height reduces the K value. This is because of increase in embankment height, the vertical load over piles increases. This results in increased vertical stress over piles and causes less lateral earth pressure above piles and more lateral earth pressure above soil. Addition of basal geogrid further increases the vertical load over piles by membrane action, hence the K values for reinforced embankment are lesser than the unreinforced embankment. At embankment top about 20 %, 50 % and 60 % reduction in K is observed by the addition of geogrid having tensile modulus of 4000 kN/m.

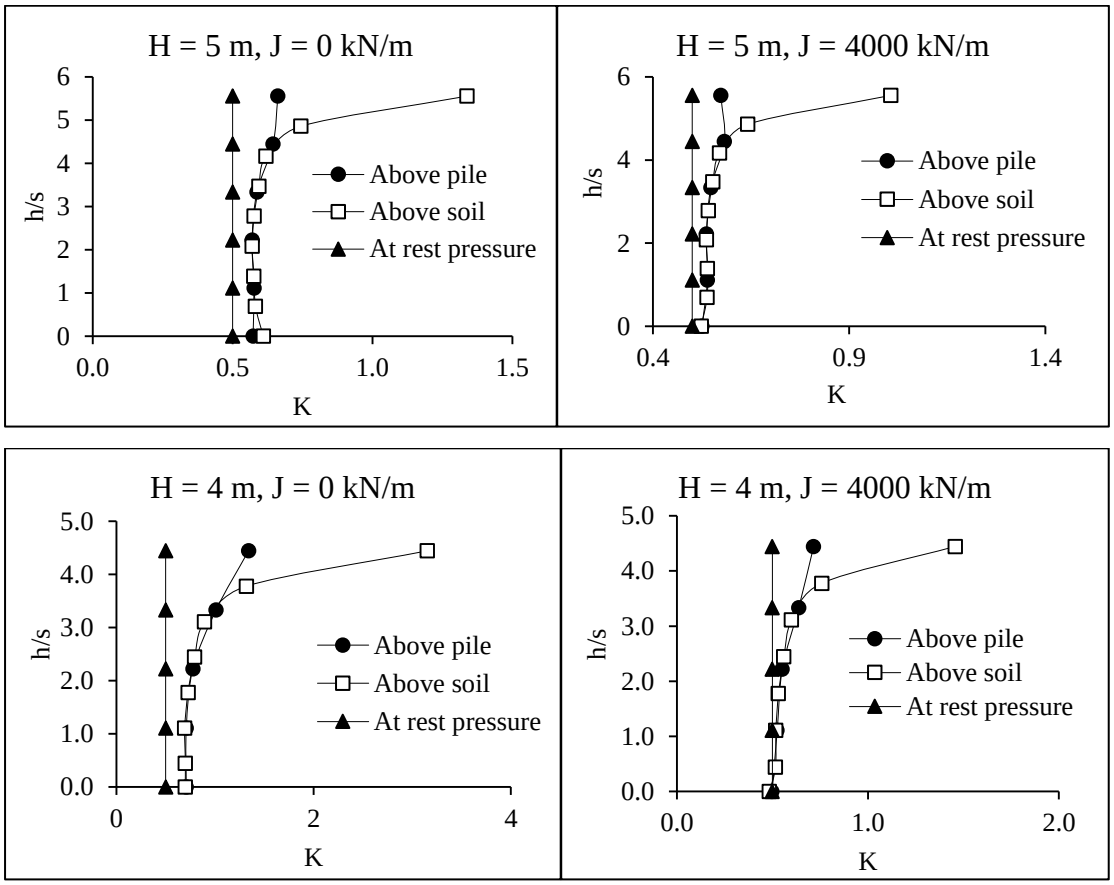

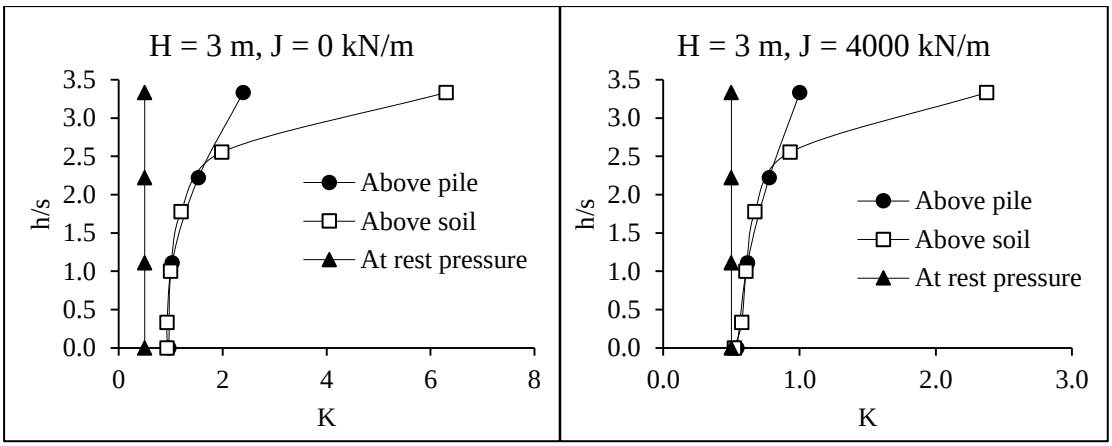

Figure 5. 12 Effect of embankment height in variation of K under static loading

Figure 5.13 presents the plot of K versus (h/s) considering the effect of pile length for piles arranged in 3D spacing, 6 m high embankment subjected to static loading. From Fig.5.13 it is observed that, irrespective of pile length the earth pressure above pile is less than the earth pressure above soil. Also the addition of basal geogrid further reduces the K values.

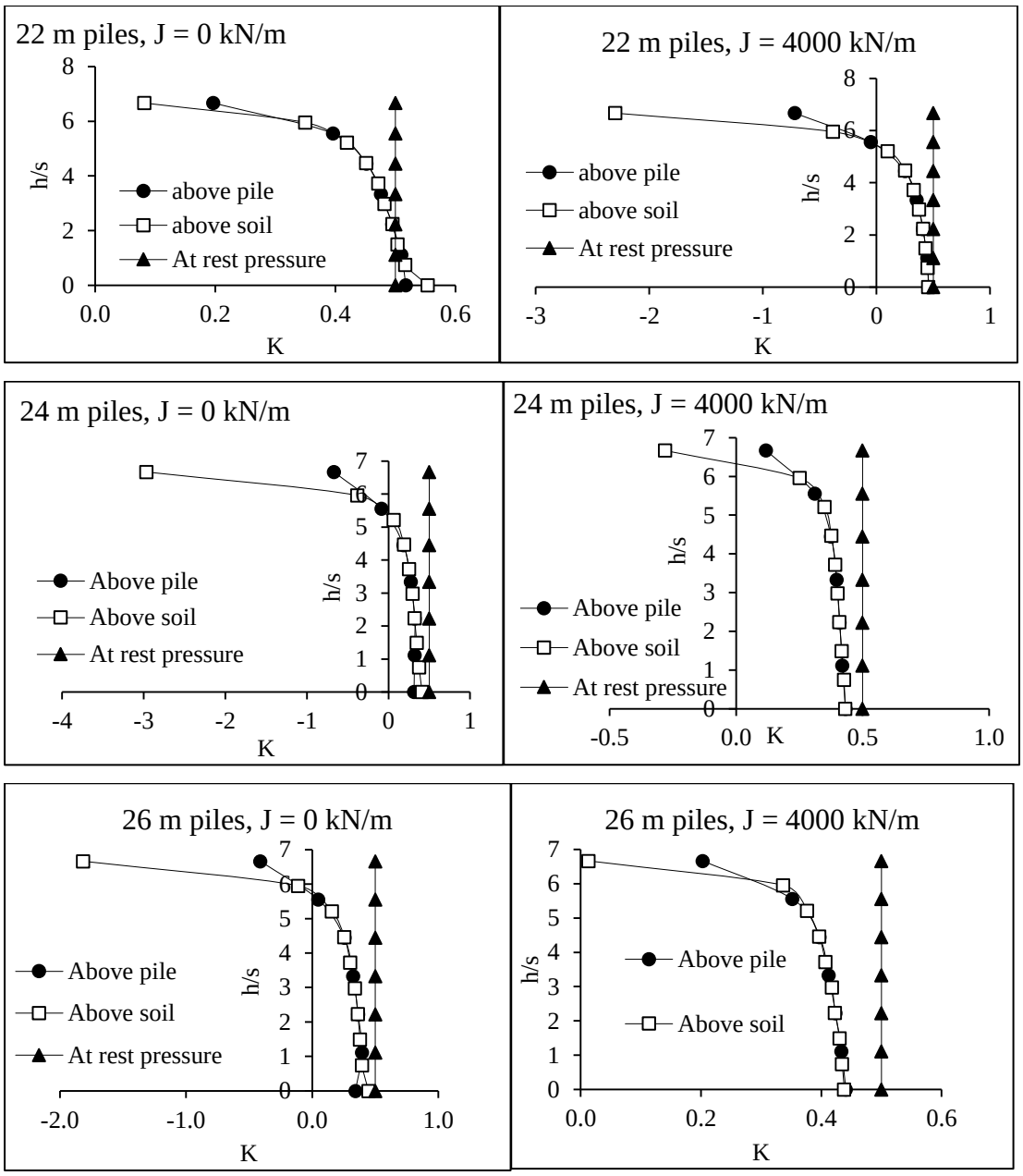

Figure 5. 13 Effect of pile length in variation of K under static loading

Figure 5.14 presents the plot of K versus (h/s) considering the effect of pile spacing for 28 m pile supported 6 m high embankment subjected to static loading. From Fig.5.14 it is observed that, the increase in pile spacing increases the lateral earth pressure above pile and soil. The K values above pile and soil becomes equal at about 1 m height of embankment and continues to be same with increase in embankment height. At the embankment base, the difference in K value above pile and above soil is high for the unreinforced (J = 0 kN/m) embankment compared to reinforced (J = 4000

kN/m) embankment. The addition of reinforcement transfers more vertical stresses to piles and reduces differential settlements at the embankment base by membrane action, hence the difference in K value at the embankment base for reinforced embankment is less than the unreinforced embankment. It is also observed from Fig.5.14 and Fig.5.12 that, higher the pile spacing higher is the difference in K above pile and above soil at embankment base. This indicates the formation of soil arching at the embankment base. Since the piles of diameter 300 mm spaced at 3D or 4D or 5D are analysed, at 3D spacing the soil arch height is less than 1 m and the model has element size of 1 m, hence it was unable to identify the minute variations in K at the embankment base for 3D spacing.

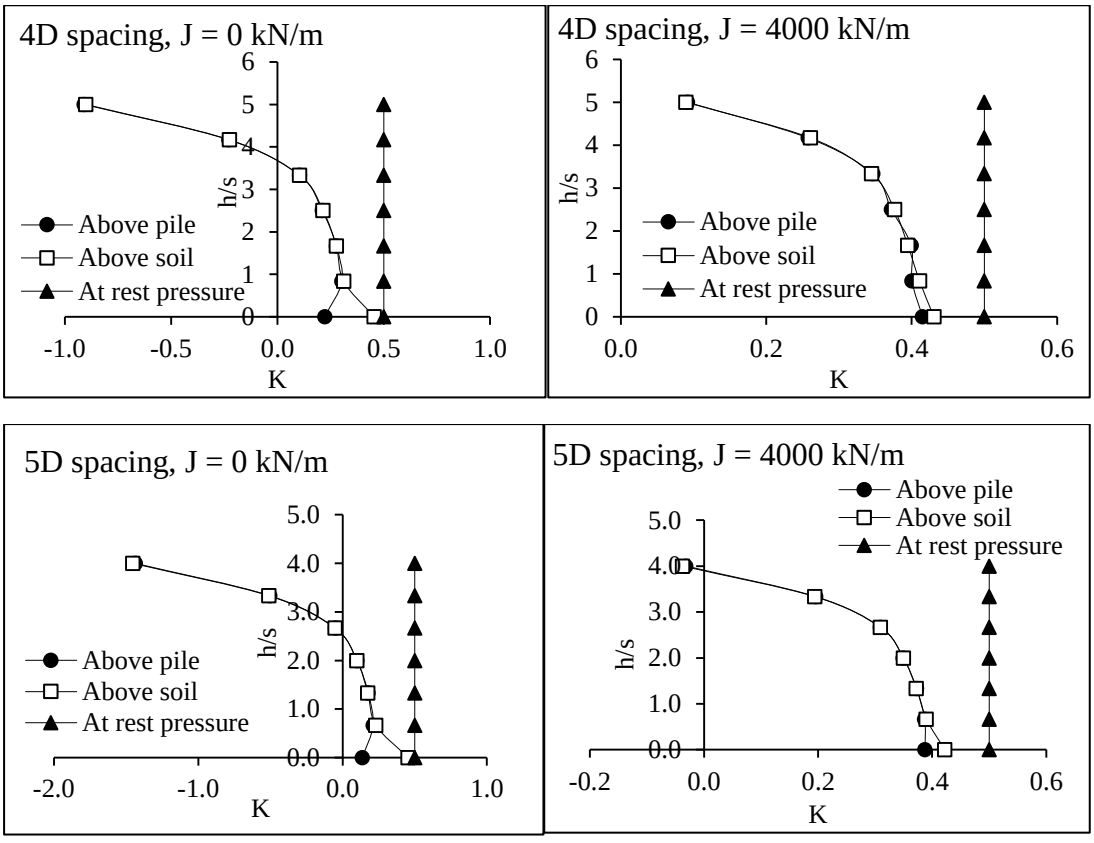

Figure 5. 14 Effect of pile spacing in variation of K under static loading

5.6 TOE LATERAL DISPLACEMENT

Figure 5.15 shows the toe lateral displacements for different embankment heights and different geogrid tensile modulus under static loading conditions. From Fig.5.15 it is noticed that increase in embankment height increases the toe lateral displacements. But the addition of basal geogrid reduces the toe lateral

displacements effectively. More than 70 % reduction in toe lateral displacement is observed for reinforced (J = 4000 kN/m) embankment compared to unreinforced embankment.

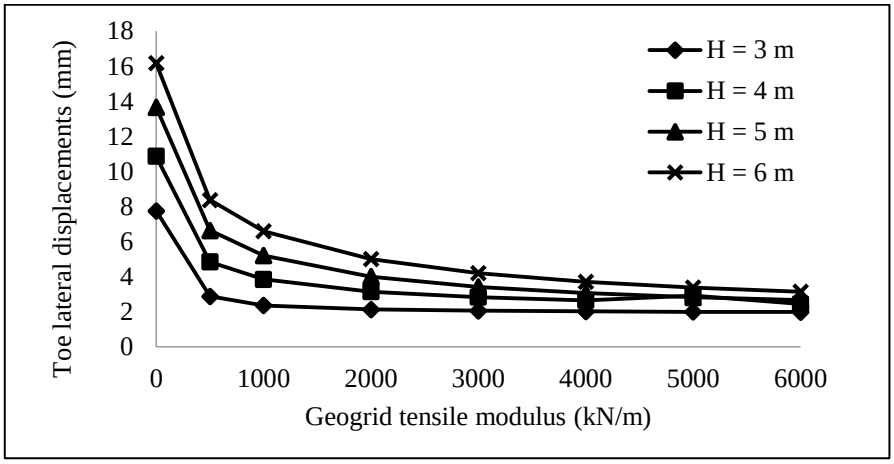

Figure 5. 15 Toe lateral displacements for 28 m pile supported embankment under static loading conditions

Figure 5.16 presents the variation of toe lateral displacements with geogrid tensile modulus for 6 m high embankment supported on floating (22 m) or end-bearing (28 m) pile supported embankment subjected to self-weight of embankment. From Fig.5.16 it is observed that the lateral displacements at toe for 28 m pile supported embankment are less than the lateral displacements at toe for 22 m pile supported embankment. This is due to increase in pile length and end bearing condition not only increases the vertical stability but also increases the lateral stability of soil.

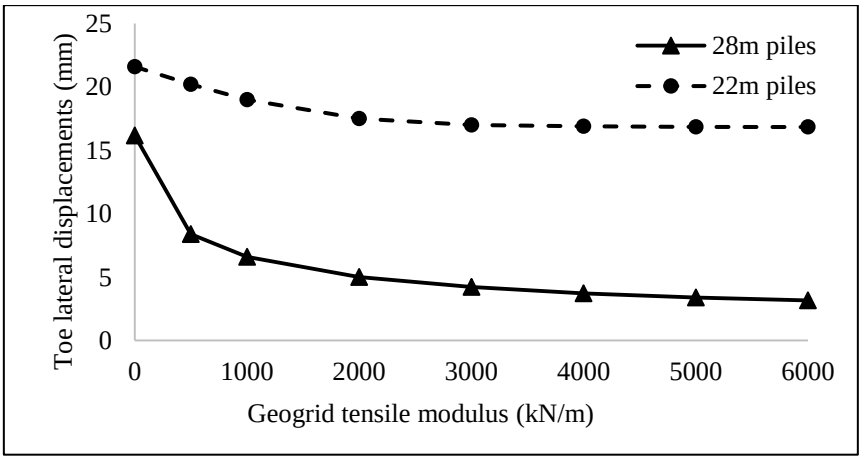

Figure 5. 16 Toe lateral displacements for 6 m high embankment supported on floating (22 m) or end-bearing (28 m) pile supported embankment under static loading

Table 5.3 presents the maximum toe lateral displacements for various embankment heights, pile length, pile spacing and geogrid tensile modulus under static loading conditions. From Table 5.3 it is observed that increase in pile length reduces the toe lateral displacements. End-bearing (28 m) piles are more effective in reducing toe lateral displacements than floating piles. The provision of basal geogrid reduces about 77 % of toe lateral displacements in end-bearing pile supported embankment and about 25 % toe lateral displacements reduction in floating pile supported embankment. Increase in pile spacing and increase in embankment height also increases the toe lateral displacements. From the analysis, it is noticed that end-bearing pile supported embankment with a spacing of 3D along with basal geogrid is the best suited for reducing toe lateral displacements to a maximum extant. Among all the cases listed in Table 5.3, the maximum percentage difference due to geogrid is seen in 6 m high embankment with 3D spaced 28 m piles.

Table 5. 3 Toe lateral displacements under static loading conditions

Pile Length (For 6 m high embankment, 3D spacing)	Unreinforced (J = 0 kN/m)	Reinforced (J = 4000 kN/m)
	Toe lateral displacements (mm)	
28 m	16.18	3.72
26 m	18.64	13.8
24 m	19.17	14.96
22 m	21.6	16.9
Pile spacing (For 6 m high embankment, 28 m Piles)		
3D	16.18	3.72
4D	19.18	9.54
5D	24.7	19.03
Embankment height (For 3D spaced 28m piles)		
3 m	7.75	2.02
4 m	10.87	2.65
5 m	13.67	3.07
6 m	16.18	3.72

5.7 DIFFERENTIAL SETTLEMENTS AT CREST

Differential settlements at crest for 28 m pile supported embankment with different embankment heights and geogrid tensile modulus subjected to static loading is shown in Fig.5.17. It is the settlement difference between crest centre and crest edge. From Fig.5.17 it is observed that 3 m high embankment without basal geogrid experiences maximum differential settlements but the addition of basal geogrid reduces the differential settlements. 4 m high embankment with basal geogrid experiences very less differential settlements.

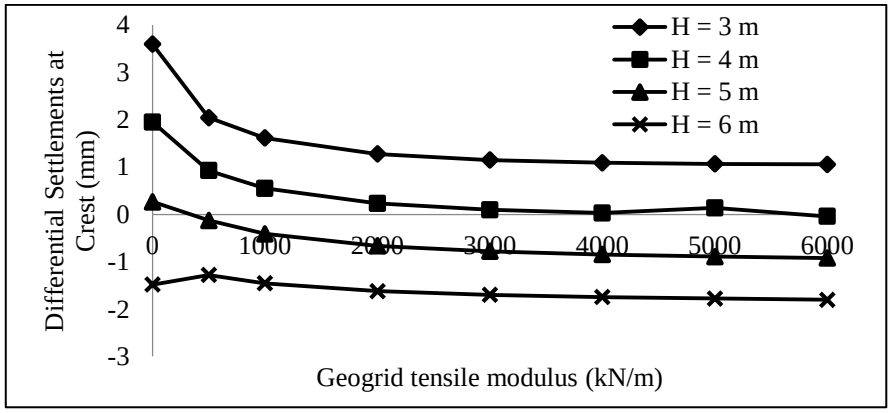

Figure 5. 17 Differential settlements at crest for 28 m pile supported embankment

Figure 5.18 shows the differential settlements at crest for 6 m high embankment supported over 22 m and 28 m piles. From Fig.5.18, it is observed that the embankment supported over 22 m piles will be having more differential settlements than the 28 m pile supported embankment. This indicates that the end bearing condition reduce differential settlements.

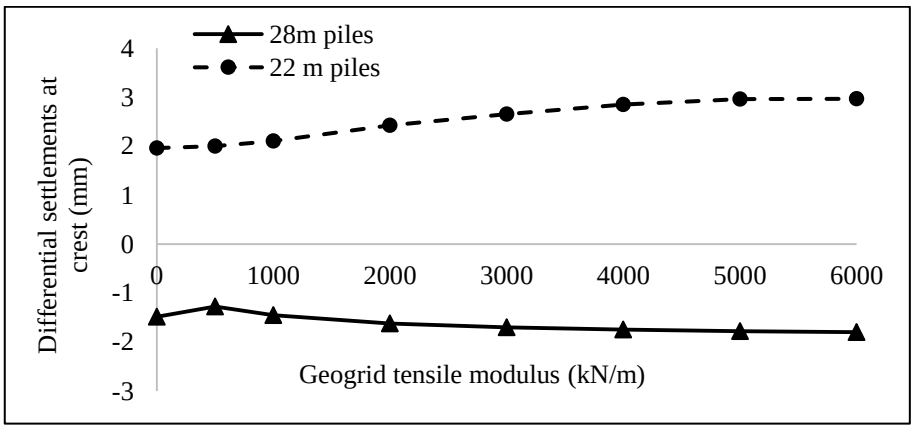

Figure 5. 18 Differential settlements at crest for 6 m high embankment

Table 5.4 presents the maximum differential settlements at embankment crest considering the pile length, pile spacing, embankment height and geogrid tensile modulus under static loading conditions. From Table 5.4 it is observed that, increase in pile length reduces the differential settlements. Also increase in pile spacing increases the differential settlements, but the addition of basal geogrid (J = 4000 kN/m) reduces the differential settlements up to 35 % in 5D spaced pile supported embankment. Overall, 4 m high embankment supported over 3D spaced 28 m piles with a basal geogrid of J = 4000 kN/m experiences very less differential settlements.

Table 5. 4 Differential settlements at crest under static loading conditions

Pile Length (For 6 m high embankment, 3D spacing)	Unreinforced (J = 0 kN/m)	Reinforced (J = 4000 kN/m)
	Differential settlements at crest (mm)	
28 m	1.48	1.74
26 m	1.51	1.75
24 m	1.87	1.78
22 m	1.96	2.85
Pile spacing (For 6 m high embankment, 28 m Piles)		
3D	1.48	1.74
4D	2.42	2.03
5D	3.38	2.2
Embankment height (For 3D spaced 28m piles)		
3 m	3.6	1.1
4 m	1.949	0.029
5 m	0.265	0.846
6 m	1.48	1.74

5.8 COMPARISON OF NUMERICAL RESULTS WITH ANALYTICAL METHODS

5.8.1 Load on pile

Jones et al. (1990) developed an empirical method, which is based on a formula proposed by Marston and Anderson (1913) for soil arching on top of a buried pipe. This

method is adopted by BS8006-1. In this Method, the arching is assumed to be semi-spherical dome and it is independent of the type and strength properties of the embankment fill. According to this method, the load carried by pile foundations is given by,

$$P = \left[\frac{C_c a}{H}\right]^2 \sigma_v' * A \quad (5.6)$$

Where P is the load over pile (kN).

a is the diameter of pile or pile cap (m)

H is the height of embankment (m)

σ_v' is the average vertical stress at embankment base (kN/m^2) equal to (γH+q)

γ is the density of embankment fill (kN/m^3)

q is the surcharge load over embankment (kN/m^2)

A is the area of pile or pile cap (m^2)

C_c is the coefficient of soil arching

BS8006-1 gives separate C_c equations for end-bearing and floating pile supported basal reinforced embankment. Given by,

For end-bearing piles: $C_c = 1.95\left(\frac{H}{a}\right) - 0.18$ (5.7)

For floating piles: $C_c = 1.5\left(\frac{H}{a}\right) - 0.07$ (5.8)

The modifications for BS8006 proposed by van Eekelen et al (2011) (i.e. Modified BS8006) also follows the same arching coefficient equations for calculating the load over piles.

Bhasi & Rajagopal (2015) proposed the modified equations of arching coefficient (C_c) based on the numerically calculated pile loads observed for different lengths of floating and end bearing piles, at the end of construction and at the end of consolidation of foundation soil. As the load transferred to the floating piles are found to be dependent on their length and the location of the neutral plane, these two lengths are incorporated in the equation for arching coefficient of floating piles. Given by,

At the end of construction of embankment

For end-bearing piles: $C_c = 1.8\left(1.95\frac{H}{a} - 0.18\right)$ (5.9)

For floating piles: $C_c = 5.8\left(\frac{\bar{x}}{l}\right)\left(1.5\frac{H}{a} - 0.07\right)$ (5.10)

At the end of consolidation of foundation soil

For end-bearing piles: $C_c = 2.5\left(1.95\frac{H}{a} - 0.18\right)$ (5.11)

For floating piles: $C_c = 7.4\left(\frac{\overline{x}}{l}\right)\left(1.5\frac{H}{a} - 0.07\right)$ (5.12)

C_c values proposed from the Numerical Analysis

From the 3-Dimensional finite element analysis it is noticed that the spacing of piles also have considerable effect on transferring the embankment load to piles. The existing arching coefficients (C_c) are unable to include the spacing of piles. Hence in the present study, based on the results of 3-Dimensional finite element analysis, the equation for arching coefficients (C_c) including the pile length and pile spacing at the end of consolidation of foundation soil are proposed. Given by,

At the end of consolidation of foundation soil

For end-bearing piles: $C_c = 3.2 * s\left(1.95\frac{H}{a} - 0.18\right)$ (5.13)

For floating piles: $C_c = 8 * s\left(\frac{\overline{x}}{l}\right)\left(1.5\frac{H}{a} - 0.07\right)$ (5.14)

Where s is the centre to centre pile spacing (m)

l is the length of floating pile (m)

$\overline{x}$ is the depth of neutral plane (m)

At the end of consolidation of foundation soil, the ratio of depth of neutral plane to the length of floating pile $\left(\frac{\overline{x}}{l}\right)$ is approximately equal to 0.38.

Table 5.5 presents the comparison of numerically obtained load on pile with the existing analytical methods and proposed analytical equations. The load on pile is calculated using Equation. 5.6. Both BS8006 and modified BS use the same arching coefficient (C_c) equations (Equation. 5.7-5.8) to calculate the load on pile. Bhasi & Rajagopal (2015) used their proposed arching coefficient (Cc) equations (Equation. 5.9-5.12) to calculate the load on pile. All these methods will not include the pile spacing in the calculation of load on pile. Hence, in the present study, based on the 3-dimensional finite element analysis, the equations (Equation. 5.13-5.14) for C_c are proposed to calculate load on pile. From Table 5.5 and Fig.5.19 it is noticed that the Load on pile calculated using Bhasi & Rajagopal (2015) over-predicts and BS8006 or Modified BS under-predicts the load on pile when compared with the results obtained by FEA. Since the proposed analytical equation includes pile centre to centre spacing

in the calculation of load on pile, the load on pile obtained from proposed equation are almost equal to the finite element analysis results.

Table 5. 5 Comparison of Numerically obtained load on pile with Analytical Methods and proposed analytical equations

	Load on pile (kN)				
Embankment Height (m)	BS8006	Modified BS	Bhasi & Rajagopal (2015)	Proposed Equation	FEA
	For 3D spaced piles of length 28 m and basal geogrid of tensile modulus 4000 kN/m				
3	14.64	14.64	91.53	29.45	34.58
4	19.62	19.62	122.61	39.63	43.13
5	24.6	24.6	153.7	49.8	51.7
6	29.56	29.56	184.7	60	60.12
Pile Length (m)	For 6 m high embankment supported on 3D spaced piles and basal geogrid of tensile modulus 4000 kN/m				
22					56.84
24	17.53	17.53	138.96	58.33	57.7
26					58.6
28	29.56	29.56	184.7	60	60.12
Pile Spacing	For 6 m high embankment supported on 28 m piles and basal geogrid of tensile modulus 4000 kN/m				
3D				60	60.12
4D	29.56	29.56	184.7	106.6	105.7
5D				166.6	165.2
Tensile modulus of geogrid (kN/m)	For 6 m high embankment supported on 3D spaced 28 m piles				
0					47
500					56
1000					57.5
2000	29.56	29.56	184.7	60	58.86

3000	59.6
4000	60.12
5000	60.53
6000	60.86

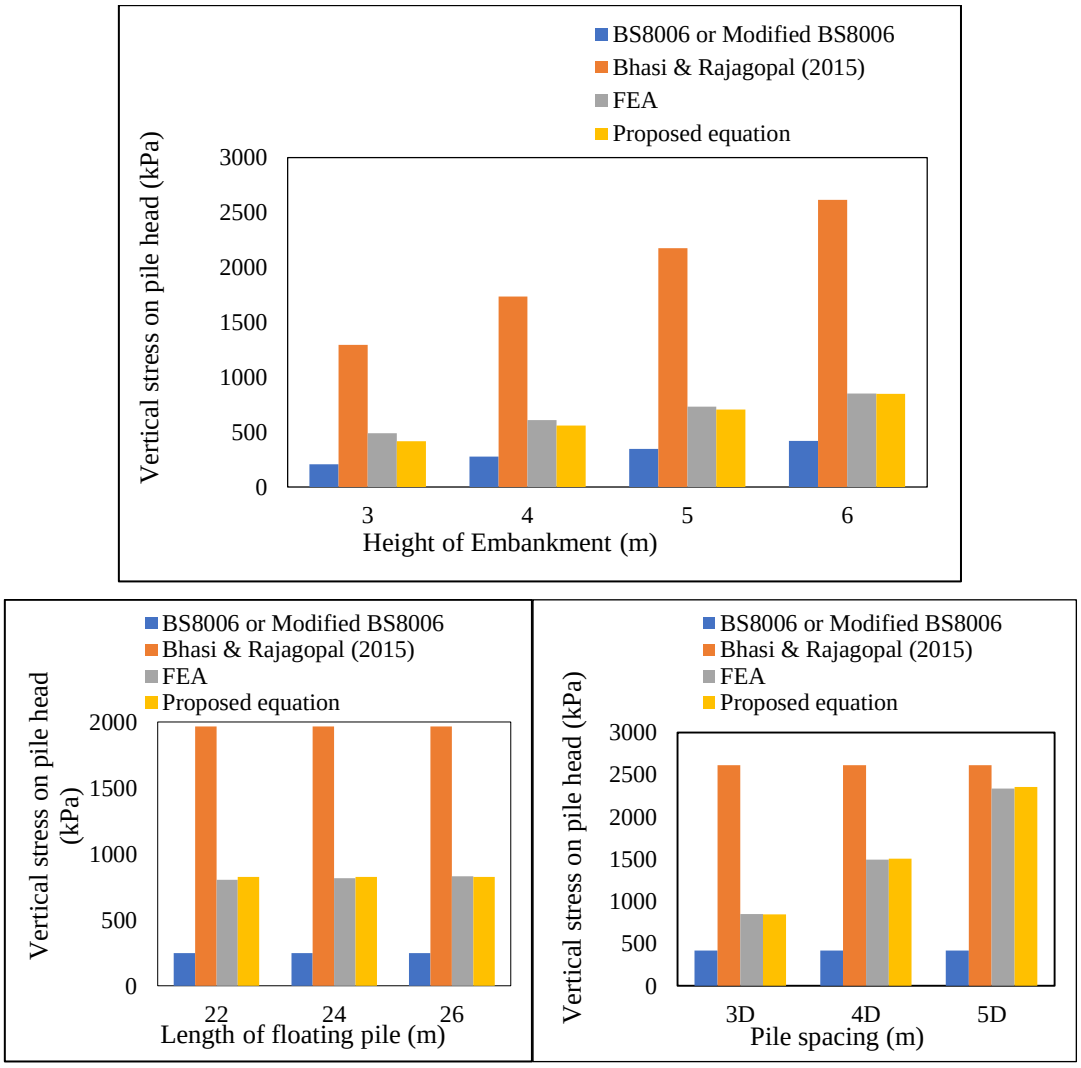

Figure 5. 19 Comparison of calculated vertical stress on pile head using analytical equations and finite element analysis results

5.9 LATERAL DISPLACEMENT OF FOUNDATION SOIL BELOW TOE

Figure 5.20 shows the lateral displacements along the depth of foundation soil below embankment toe subjected to self-weight of embankment considering the effect of pile length, pile spacing and geogrid tensile modulus. 6 m high embankment having 1V:1.5H side slope made of PFA is considered for the analysis. It is observed from

Fig.5.20 that, the increase in pile length reduces the lateral displacement of foundation soil. About 20 % reduction in maximum lateral displacement is observed by increasing the pile length from 22 m to 28 m with or without geogrid. Increase in pile spacing also increases the lateral displacement of foundation soil. About 20 % increase in maximum lateral displacement of foundation soil is observed by increasing the pile spacing from 3D to 5D (Fig.5.20). It is also observed from Fig.5.20 that, the addition of basal geogrid could able to reduce the maximum lateral displacements at the foundation level and as the depth increases, the lateral displacement of reinforced (J = 4000 kN/m) embankment equal to unreinforced (J = 0 kN/m) embankment.

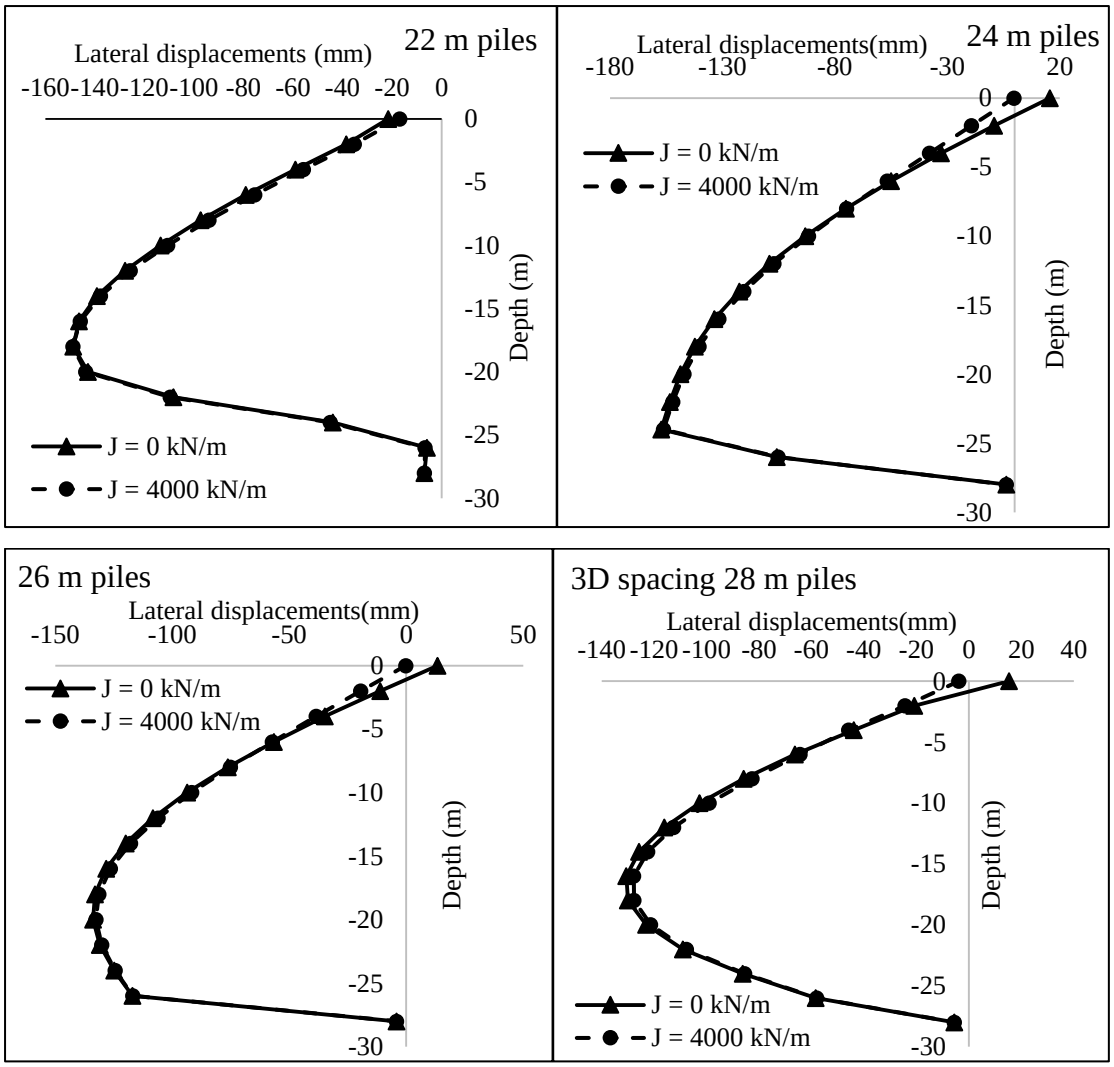

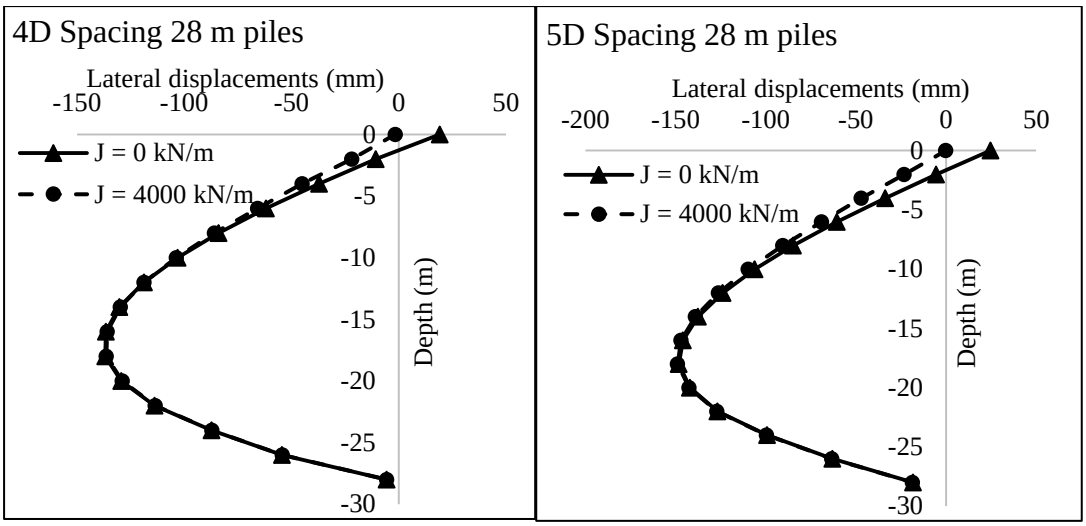

Figure 5. 20 Lateral displacements along the foundation soil below embankment toe subjected to static loading

Figs.5.21 represents the lateral displacements of foundation soil along the depth below toe for embankment without pile supports under static loading conditions. The presence of pile supports below embankment (Fig.5.20) will not allow the foundation soil below embankment to take embankment load and settle. But the foundation soil beside piles just after embankment toe will move towards the piles due to consolidation settlement by its own weight causing negative lateral displacement in the foundation soil (Fig.5.20). But in case of embankment without pile supports, consolidation occurs due to embankment load and causes a positive lateral displacement (Fig.5.21). It is also observed from Fig.5.21 that, the addition of basal geogrid reduces the lateral displacements at foundation level upto 85 % and with increase in foundation soil depth the percentage reduction in lateral displacements by the addition of geogrid also decreases.

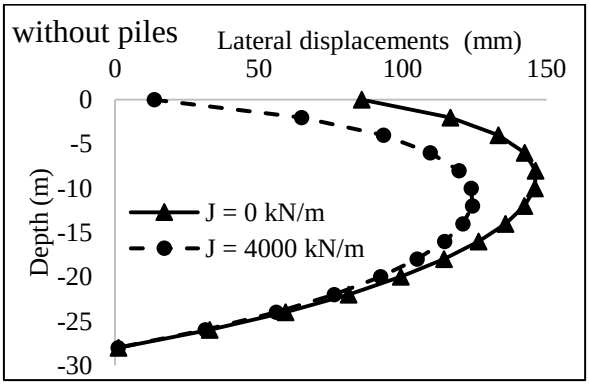

Figure 5. 21 Lateral displacements below embankment toe - without pile supports

5.10 MAXIMUM SETTLEMENT CONTOURS FOR DIFFERENT EMBANKMENT CASES SUBJECTED TO SELF-WEIGHT

Figures.5.22 (a) – 5.22 (e) show the maximum settlement (in m) of 6 m high embankment subjected to self-weight with different types of soil improvement cases considered. From these figures it is observed that addition of geogrid and piles reduces the embankment settlements more effectively.

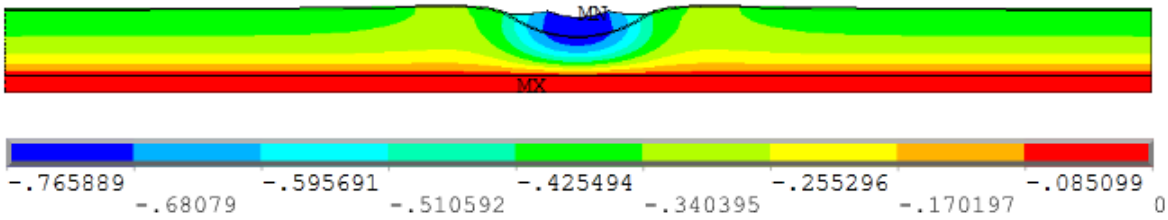

(a) Without piles and geogrid

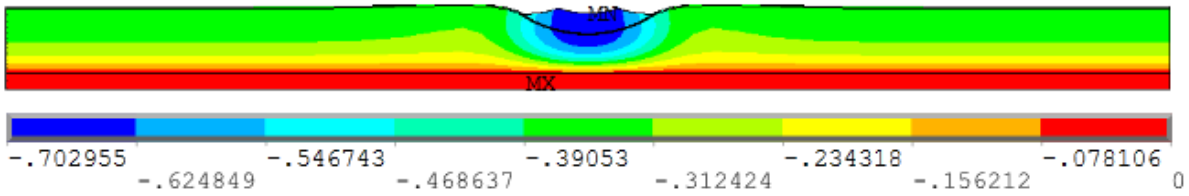

(b) With basal geogrid (J = 4000 kN/m)

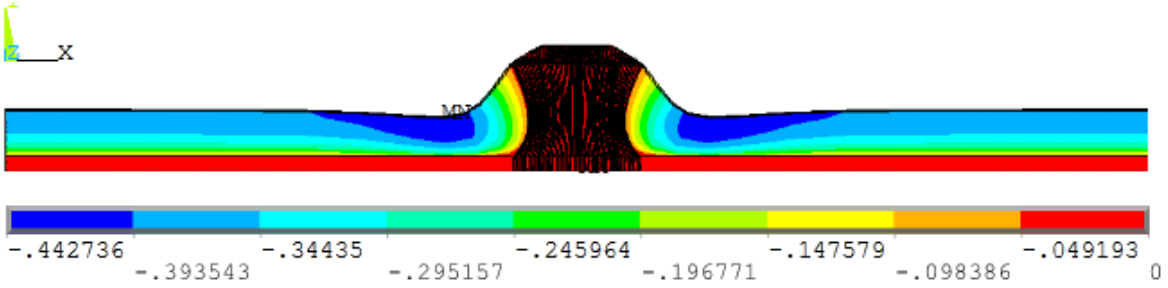

(c) With 28 m piles

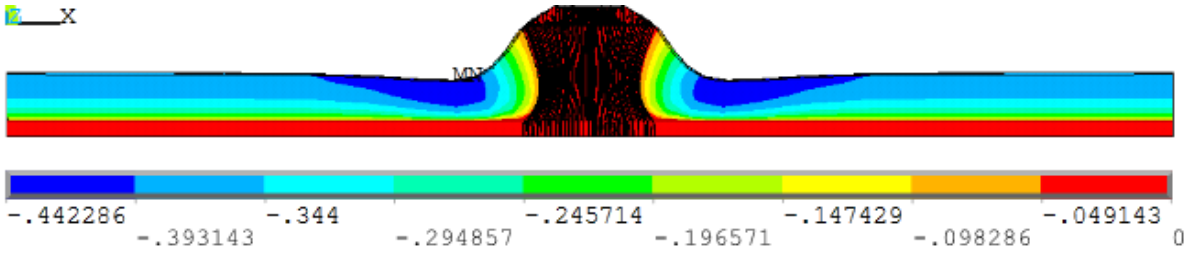

(d) With 28 m piles and basal geogrid (J = 4000 kN/m)

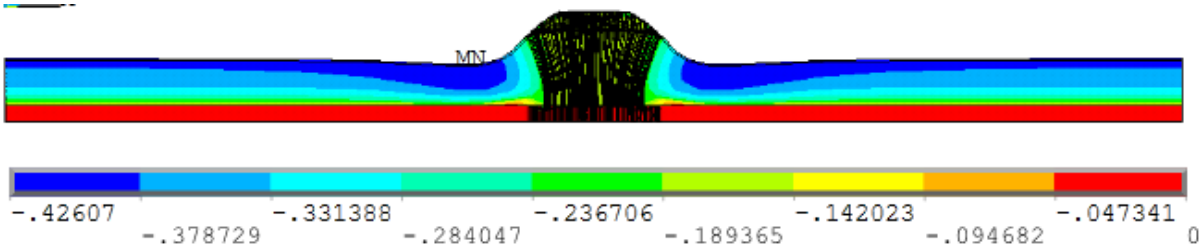

(e) With 22 m piles and basal geogrid (J = 4000 kN/m)

Figure 5. 22 Maximum settlement of 6m embankment subjected to its own weight

5.11 PORE WATER PRESSURE CONTOURS UNDER STATIC LOADING CONDITIONS

Figure 5.23 (a) – 5.23 (b) show the pore water pressure (N/m^2) contours for 22 m (floating pile) and 28 m (end-bearing pile) pile supported embankment with basal geogrid of J = 4000 kN/m. The analysis was performed until the dissipation of excess pore water pressure at the foundation level to be near to zero.

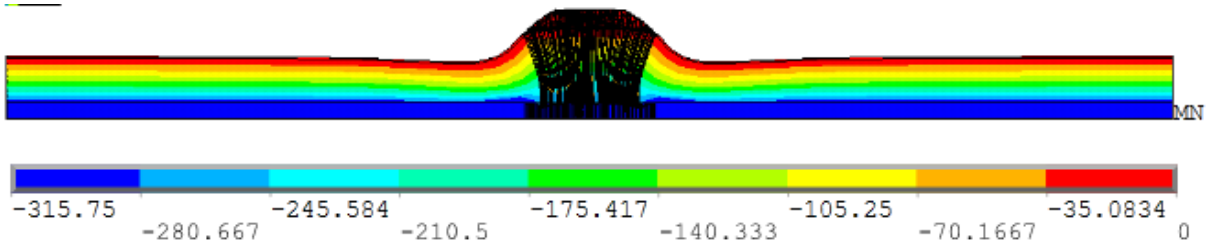

(a) With 22 m piles and basal geogrid (J = 4000 kN/m)

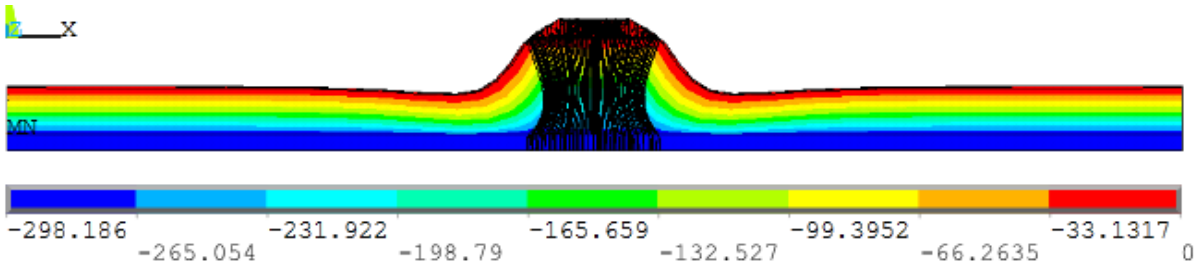

(b) With 28 m piles and basal geogrid (J = 4000 kN/m)

Figure 5. 23 Pore water pressure contour for 6m Embankment subjected to its own weight

5.12 RESPONSE VARIATION OF BASAL GEOGRID-REINFORCED PILE SUPPORTED EMBANKMENTS SUBJECTED TO TRAFFIC LOAD

Self-weight analysis of embankment was performed by providing the gravitational acceleration of 9.81 m/s^2 in the vertical direction along with the mass

density of embankment materials. Later the embankment was analysed for traffic load by applying a uniform pressure of 24 kN/m^2 over the embankment crest (IRC:75-2016).

Figure 5.24 presents the settlements at embankment crest centre subjected to both self-weight and traffic load for 6 m high embankment supported over 28 m (end-bearing) and 22 m (floating) piles including basal geogrid tensile stiffness. From Fig.5.24 it is noticed that the addition of traffic load increases the settlements at crest centre by about 10 mm. For the considered range of geogrid stiffness, about 25 % increase in crest centre settlements are observed for 28 m pile supported embankment and about 5 % increase in crest centre settlements are observed for 22 m pile supported embankment due to the application of traffic load. From Fig.5.24 it is also observed that, the behaviour of embankment by the addition of traffic load is very similar as the behaviour of embankment subjected to self-weight. As compared to self-weight, the traffic load is very small and doesn't contribute considerable variation in settlements. Also there is a need to understand the behaviour of these basal geosynthetic-reinforced pile-supported embankments under dynamic loading conditions. Hence the traffic load analysis was performed only on settlement variation.

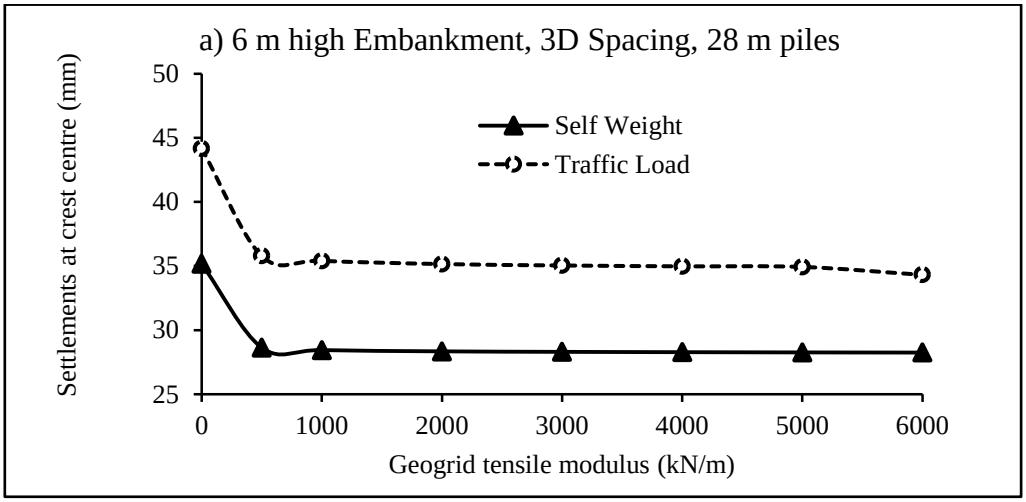

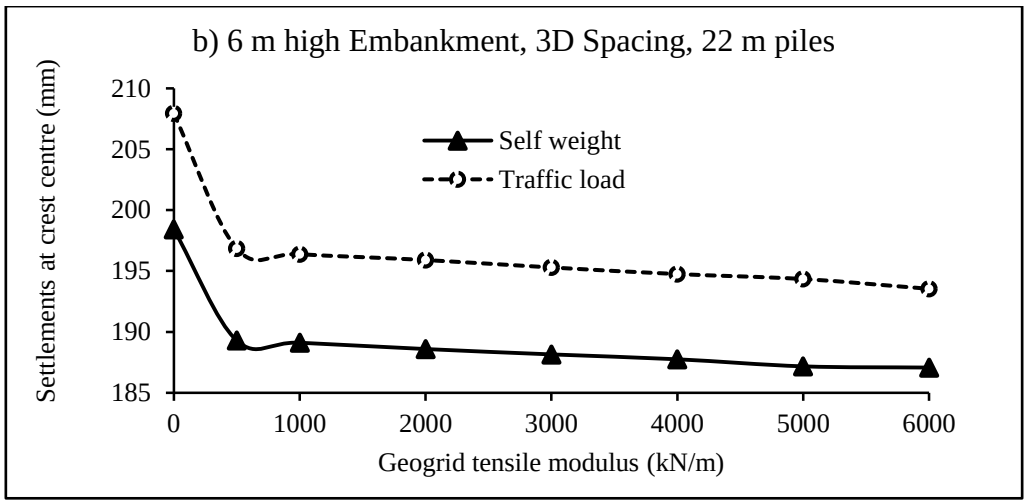

Figure 5. 24 Settlement at crest Centre subjected to traffic load and self-weight of embankment

5.13 SUMMARY

Three-dimensional finite element models of basal geogrid reinforced pile supported embankments subjected to self-weight and also traffic load were analysed in this chapter. The behaviour of these embankments were analysed by considering the embankment height, embankment side slope, basal geogrid tensile modulus, length of piles, spacing of piles and type of piles.

From the static analysis of basal geogrid-reinforced piled embankments it is noticed that, end-bearing pile supported embankments perform better than floating pile supported embankments in terms of settlements, differential settlements and lateral displacements even at larger pile spacing. The addition of basal geogrid further reduces the settlements and lateral displacements in the embankment. The analytical equation for C_c proposed based on the 3-dimensional finite element analysis results incorporates the effect of pile spacing, which the earlier methods did not consider. Hence the proposed analytical equation gives more accurate results of pile loads than the existing methods.

CHAPTER 6

RESPONSE VARIATION OF BASAL GEOGRID-REINFORCED PILE-SUPPORTED EMBANKMENTS SUBJECTED TO SEISMIC EXCITATIONS

6.1 INTRODUCTION

The behaviour of basal geosynthetic-reinforced pile-supported embankments subjected to static loading conditions is very well reported in the literature. On the other side, the behaviour of these embankments subjected to seismic loading need to be addressed in detail considering the three-dimensional system of basal geogrid-reinforced pile-supported embankment with foundation soil. Time-history analysis is one of the most appropriate method to analyse the seismic behaviour of any structure. Hence in the present study also time-history analysis was performed on the 3-dimensoinal finite element models of geosynthetic-reinforced pile-supported embankments. The behaviour of these embankments under seismic excitations was analysed by considering the height of embankment, side slope of embankment, basal geogrid tensile modulus, length of pile, spacing of pile and type of pile (Table 6.1). The response of embankment in terms of vertical and lateral displacements, differential settlements, vertical and lateral stress distribution on pile and the foundation soil between piles, amplification coefficient, lateral earth pressure along the embankment height and the pore water pressure are presented in this section of thesis.

Table 6. 1 Parameters considered for the time-history analysis

Type	Parameters considered
Embankment height (H) in m	3 m, 4 m, 5 m, 6 m
Embankment side slope	1V:2H, 1V:1.5H,1V:1H
Geogrid tensile modulus (J) in kN/m	0, 500, 1000,2000, 3000, 4000, 5000, 6000
Pile length (L) in m	22, 24, 26 (Floating piles) 28 (End-bearing pile)
Pile spacing (s)	3D, 4D, 5D
Pile Batter angle (º)	0º, 5º, 10º, 15º
Seismic excitations	IS 0.35g, IS Zone III, Elcentro, Lomaprieta

6.2 DIFFERENTIAL SETTLEMENTS AT CREST

Differential settlements are the difference in maximum vertical displacements at embankment crest centre and crest edge. Effect of embankment height and geogrid tensile modulus on differential settlements at embankment crest subjected to seismic excitations is seen in Fig.6.1. It is seen that, geogrid tensile modulus of 3000 kN/m in all embankment heights considered is sufficient to reduce the differential settlements. Geogrid tensile modulus beyond 3000 kN/m do not have much effect in reducing the differential settlements under seismic loading conditions. For the considered 3D centre to centre spacing of piles, embankments with height (H) less than 4 m (H/s << 4.5), the soil arches will not form in the embankment fill; there is a direct transfer of loads from embankment fill to piles and foundation soil causing differential settlements. For embankments with height nearly equal to 4 m (H/s ≈ 4.5), complete soil arching will take place and this reduces the differential settlements to a maximum extent. For embankments with height greater than 4 m (H/s >> 4.5), increase in embankment height above soil arching height, increases the differential settlements. Hence 5 m high embankment experiences more differential settlements than 4 m high embankment and 6 m high embankment experiences even more differential settlements.

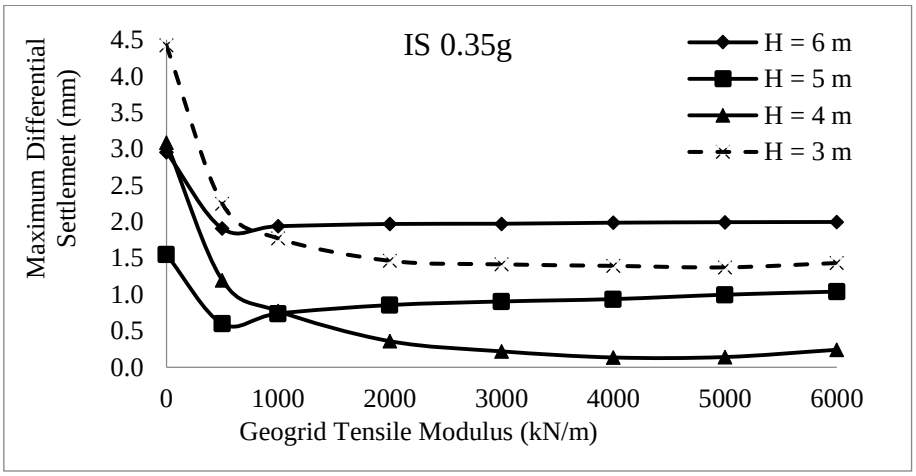

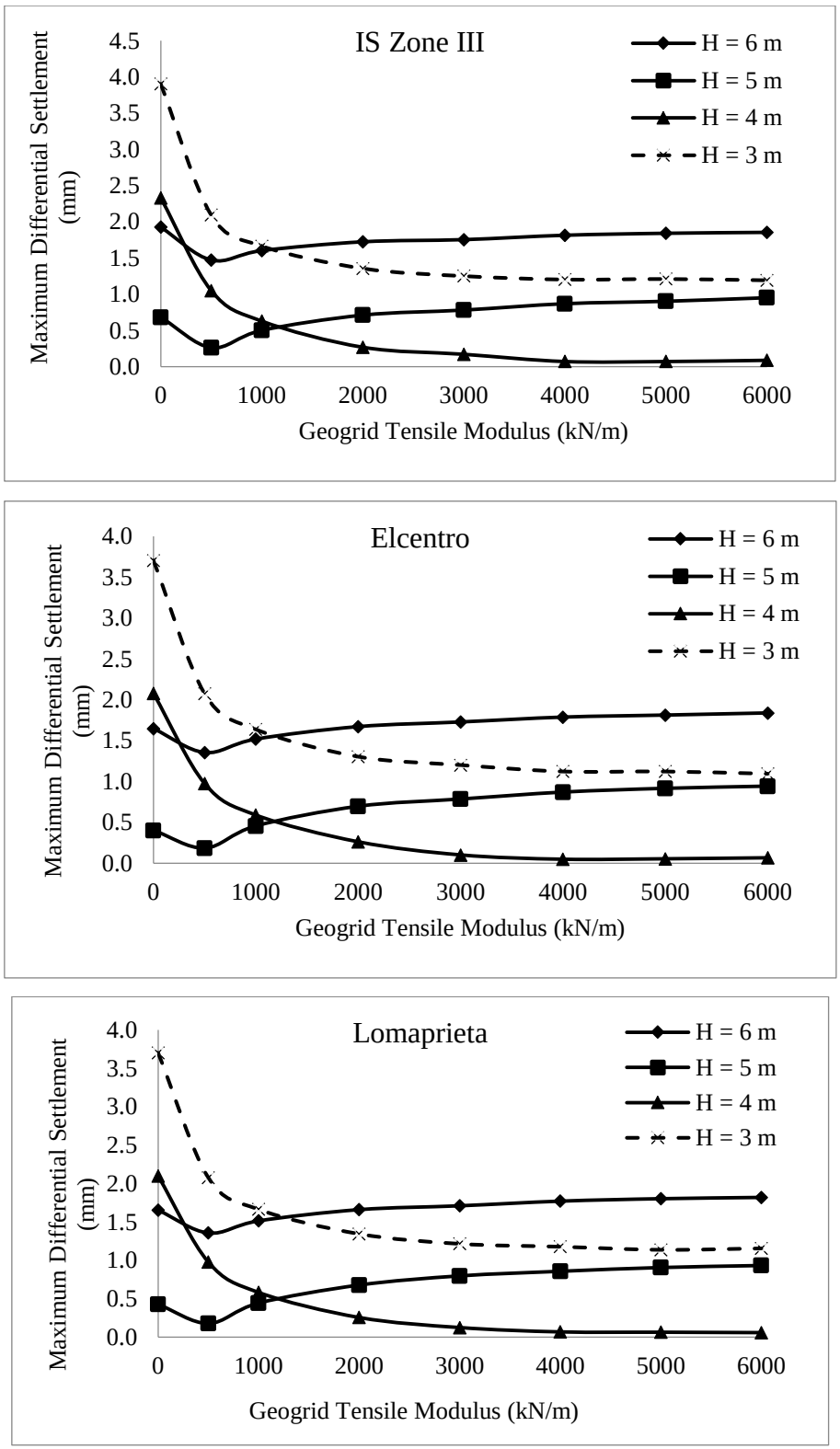

Figure 6.1 Effect of embankment height and geogrid tensile modulus on differential settlements at embankment crest subjected to various seismic excitations

Figure 6.2 depicts the time-history of vertical displacements for 6 m high embankment supported over 3D spaced 28 m pile improved soft foundation soil considering the effect of basal geogrid stiffness. The embankment was subjected to IS (0.35 g) ground motion. From Fig.6.2, it is observed that embankment without basal geogrid experiences more vertical displacements causing more differential settlements but embankment with basal geogrid even with small geogrid tensile modulus of 1000 kN/m reduces the vertical displacements at crest. This reduces the differential settlements at crest. About 35 % reduction in maximum differential settlement is seen by the addition of basal geogrid.

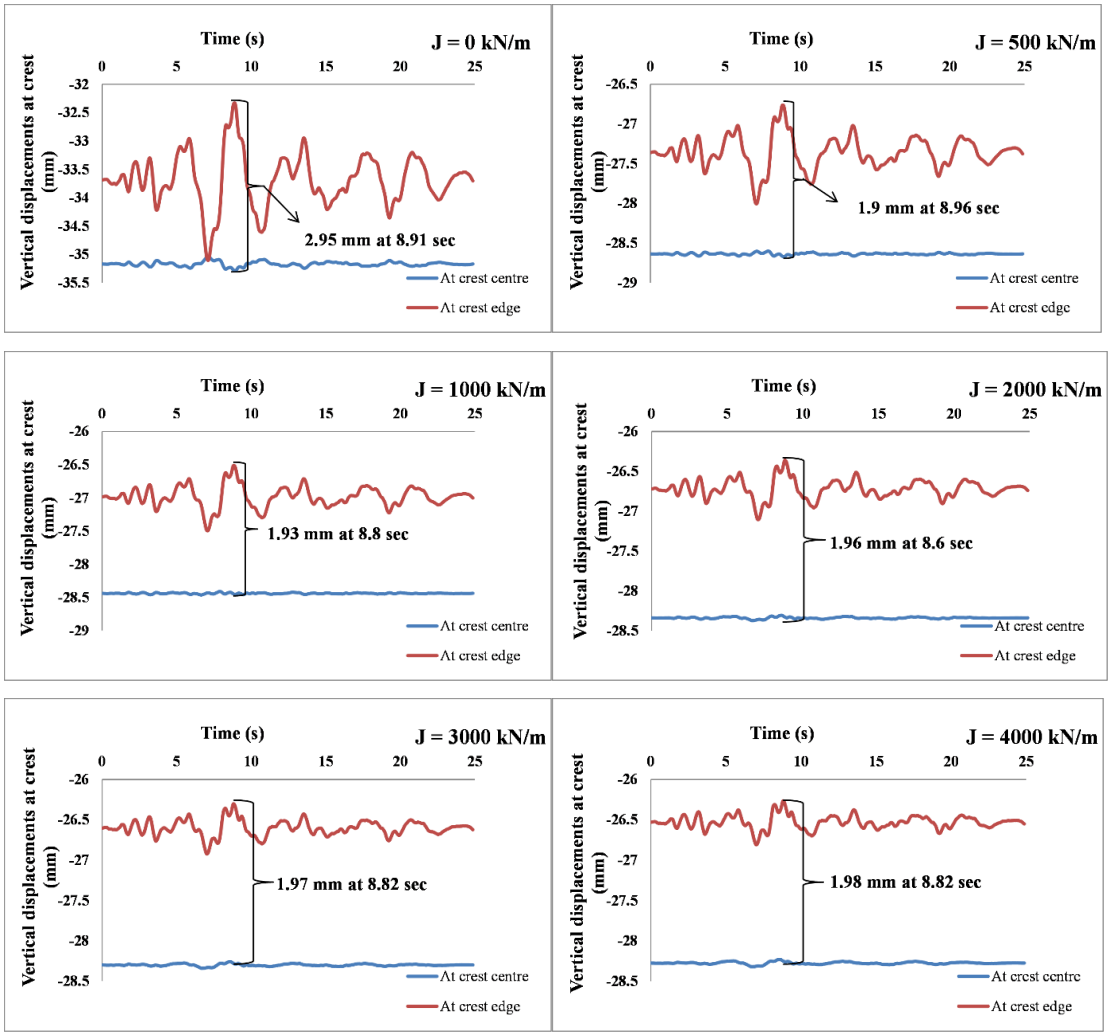

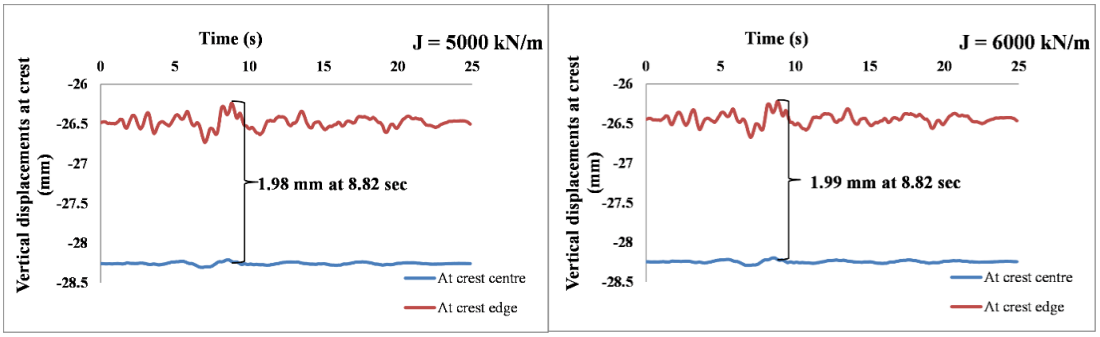

Figure 6.2 Time-history plot of crest vertical displacements for 6 m high embankment supported over 3D spaced 28 m piles considering basal geogrid stiffness subjected to IS (0.35 g) ground motion

Time-history variation of crest vertical displacements considering the effect of embankment height for 3D spaced 28 m pile supported embankments with basal geogrid stiffness of 4000 kN/m subjected to IS (0.35 g) ground motion is shown in Fig.6.3. From Fig.6.3 it is observed that 4 m high embankment experiences very less differential settlements than the other embankment heights considered.

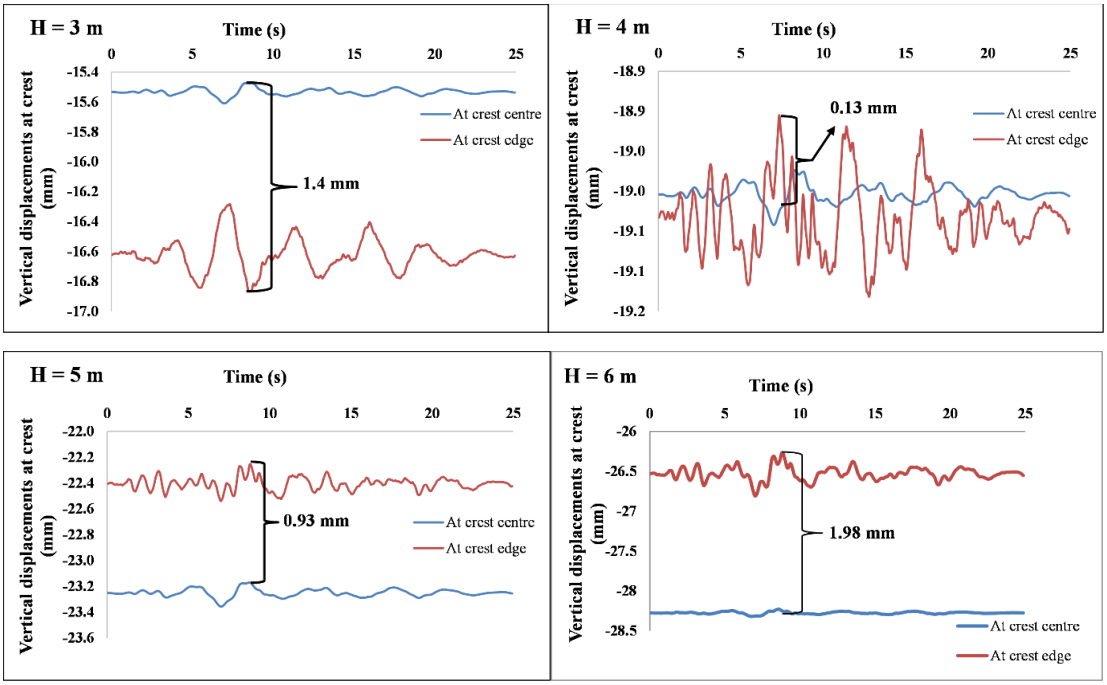

Figure 6.3 Time-history plot of crest vertical displacements for various embankment heights supported over 3D spaced 28 m piles with basal geogrid stiffness of 4000 kN/m subjected to IS (0.35 g) ground motion

Figure 6.4 presents the variation of crest vertical displacements with time considering the effect of pile length in embankments subjected to IS (0.35 g) ground motion. The 6 m high embankment supported over 3D spaced piles with a geogrid

tensile modulus of 4000 kN/m is considered. It is seen from Fig.6.4 that, the increase of pile length reduces the vertical displacements at crest there by reducing the differential settlements. About 5 % reduction in maximum differential settlements are observed by each 2 m increment of pile length. 22 m pile supported embankment without basal geogrid experiences more vertical displacements at crest and this causes more differential settlements. The addition of basal geogrid of tensile stiffness 4000 kN/m for 22 m pile supported embankment reduces about 30 % differential settlements when compared with 22 m pile supported unreinforced embankment.

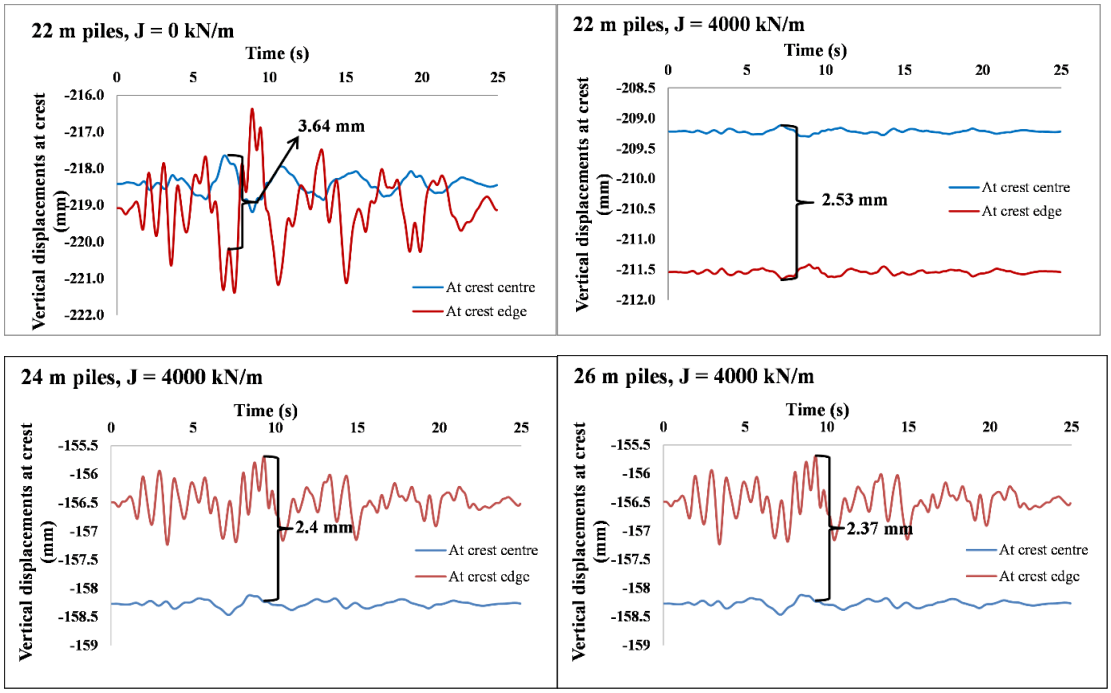

Figure 6.4 Time-history plot of crest vertical displacements for 6 m high embankment supported over 3D spaced floating piles considering basal geogrid stiffness subjected to IS (0.35 g) ground motion

Time-history variation of vertical displacements at embankment crest considering the effect of pile spacing subjected to IS (0.35 g) ground motion is shown in Fig.6.5. 6 m high embankment supported over 28 m pile improved soft marine clay with a basal geogrid of tensile stiffness 4000 kN/m is considered. From Fig.6.5, it is observed that the increase in pile spacing increases the vertical displacements at crest. About 10 % increase in crest vertical displacements are seen by increasing the pile spacing from 4D to 5D. This in turn increases the differential settlements with the increase in pile spacing. About 16% increase in differential settlements are seen by increasing the pile spacing from 4D to 5D. In all the considered pile spacing, the

differential settlements are less than 5 mm due to seismic excitations. Hence, from the study, 3D spacing is recommended at places where there should not be any differential settlements and 5D spacing is recommended at places where differential settlements can occur within permissible limits due to earthquake loading.

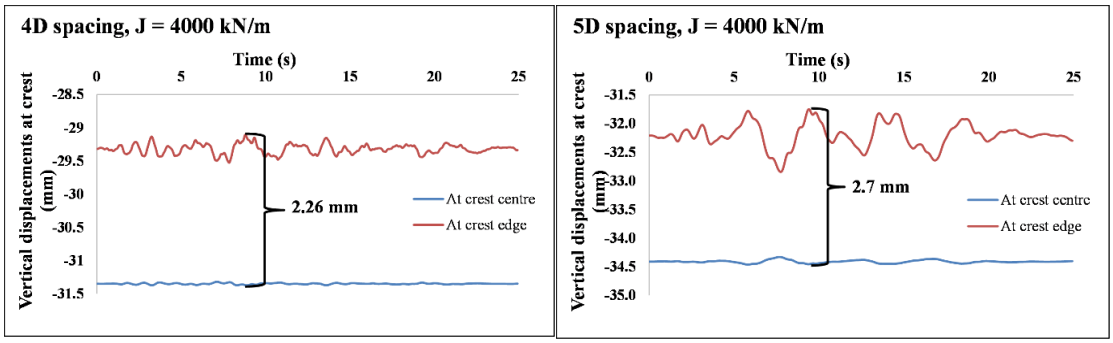

Figure 6.5 Time-history plot of crest vertical displacements for 6 m high embankment supported over different spaced 28 m piles with basal geogrid stiffness of 4000 kN/m subjected to IS (0.35 g) ground motion

Figure 6.6 shows the time-history plot of crest vertical displacements for different embankment side slopes subjected to IS (0.35 g) ground motion. The 6 m high embankment supported over 3D spaced 28 m piles with a basal geogrid stiffness of 4000 kN/m is considered for analyzing the effect of embankment side slope. Change in embankment side slope causes negligible change in vertical displacements at crest centre. But the variation in vertical displacements at crest edge is considerable by varying the embankment side slope. This leads to about 18 % increase in differential settlements by changing the slope from 1V:2H to 1V:1.5H (Fig.6.3, H = 6 m) and about 13 % increase in differential settlements are observed in geometry change by changing the slope from 1V:1.5H to 1V:1H.

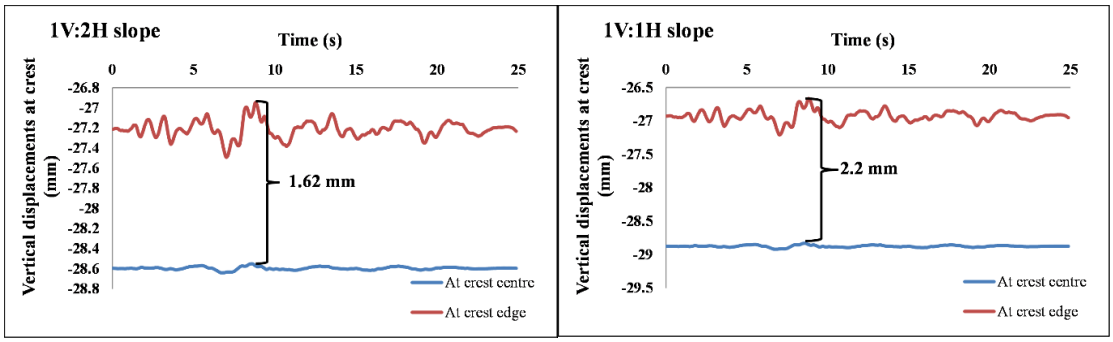

Figure 6.6 Time-history plot of crest vertical displacements for 6 m high embankment with different side slope supported over 3D spaced 28 m piles with basal geogrid stiffness of 4000 kN/m subjected to IS (0.35 g) ground motion

Fig. 6.7 shows the time-history of embankment vertical displacements at crest centre and crest edge for embankments supported over vertical and batter piles subjected to IS (0.35 g) ground motion. For embankment toe supported on 5˚ batter piles, the crest centre and crest edge vertical displacements are about 2 % lesser when compared with the toe supported over 0˚ batter piles. It is also observed from Fig.6.7 that, for embankment toe supported over 0˚ and 5˚ batter piles crest centre vertical displacements are less than the crest edge vertical displacements but in 10˚ and 15˚ batter pile supported embankment, crest centre vertical displacements are more than the crest edge vertical displacements due to the high lateral resistance offered by the higher batter angle. From Fig.6.7, it is noticed that embankment supported over 5˚ batter piles experiences less differential settlements. It is also observed from Fig.6.7 that, the increase in batter angle beyond 5˚ increases the differential settlements at crest.

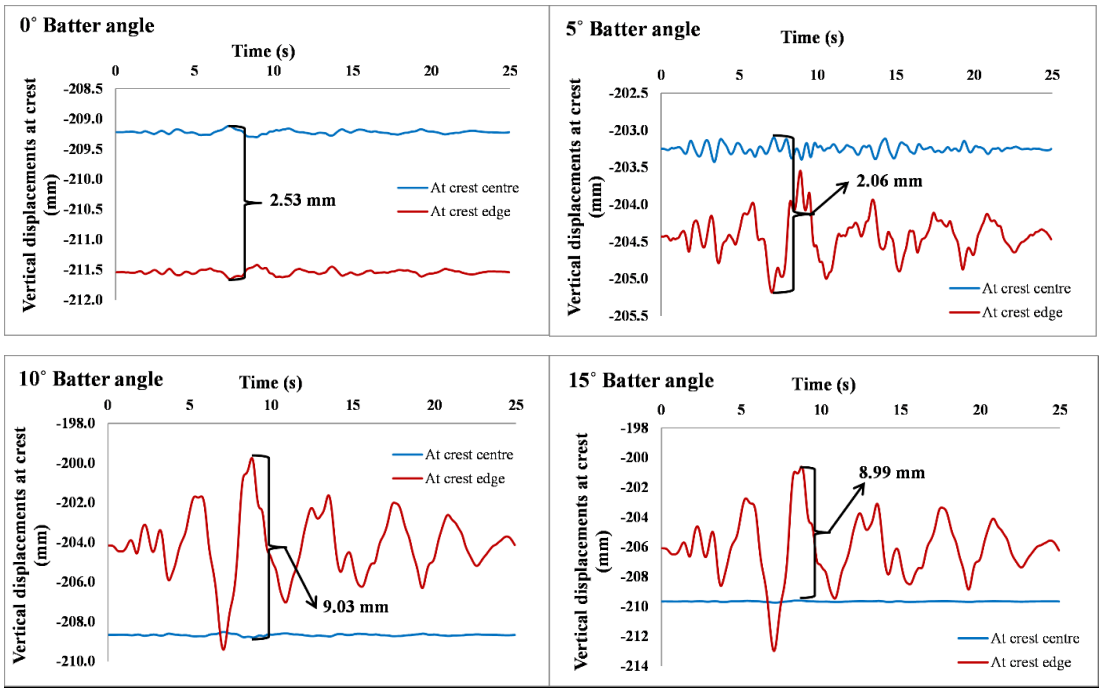

Figure 6.7 Time-history plot of crest vertical displacements for 6 m high embankment supported over 3D spaced 22 m vertical and batter piles with basal geogrid stiffness of 4000 kN/m subjected to IS (0.35 g) ground motion

Fig. 6.8 shows the time history of embankment vertical displacements at crest centre and crest edge with different support conditions subjected to IS (0.35 g) ground motion. The 6 m high embankment having 1V:1.5H side slope supported over 3D spaced 28 m piles and geogrid with J = 4000 kN/m is considered for the analysis. Table 6.2 shows the maximum vertical displacements at embankment crest due to earthquake

loading. From Fig.6.8 and Table 6.2 it is observed that the crest centre and crest edge vertical displacements are very large for the embankment resting over soft clay without basal geogrid and piles. Since the depth of soft clay is very large, the addition of basal geogrid could reduce only 0.3% vertical displacements. But the addition of piles (Fig. 6.2, J = 0 kN/m) could reduce 93.67% and 94% of crest edge and crest centre displacements. Addition of basal geogrid and piles (Fig. 6.2, J = 4000 kN/m) also reduces 93.7% and 94.2% of crest edge and crest centre displacements.

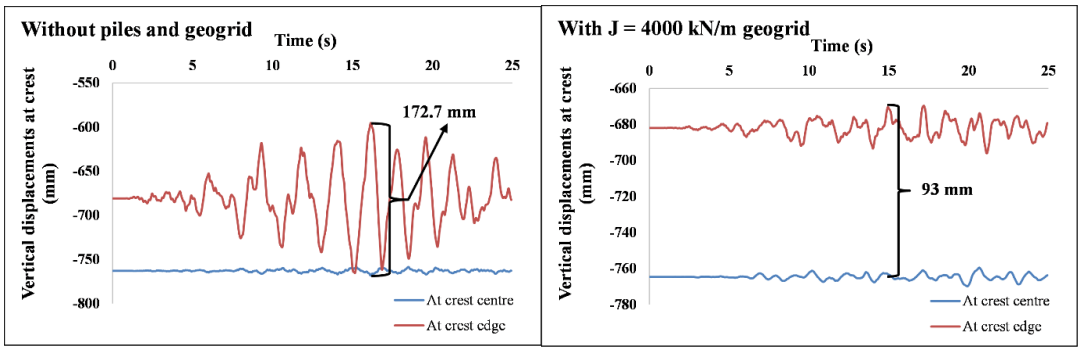

Figure 6.8 Time-history plot of crest vertical displacements for 6 m high embankment with different support conditions subjected to IS (0.35 g) ground motion

Table 6.2 shows the differential settlements at embankment crest subjected to IS (0.35 g) ground motion. It is observed from Fig.6.8 and Table 6.2 that embankment without basal geogrid and piles experiences more differential settlement. About 45 % reduction in maximum differential settlement is observed by adding the basal geogrid. Similar to vertical displacements, addition of piles reduces more than 98% of differential settlements. But further reduction of vertical displacements and about 1 mm reduction in differential settlements is seen by the addition of geogrid along with piles. This is due to the fact that the basal geogrid acts as flexible raft above piles and transfers additional embankment loads to the piles more effectively.

Table 6. 2 Maximum vertical displacements and differential settlements at embankment crest subjected to IS (0.35 g) ground motion

Embankment support condition	Maximum Vertical displacements (mm)		Maximum differential settlements (mm)
	At crest centre	At crest edge	
Without geogrid & Piles	768.14	765.5	172.74
With Geogrid	769.8	696.1	93

With Piles	35.23	35.1	2.95
With Geogrid & Piles	28.3	26.67	1.98

6.3 TOE LATERAL DISPLACEMENTS

Toe lateral displacements variation with time for 6 m high embankment supported over 3D spaced 28 m piles subjected to IS (0.35 g) ground motion considering the effect of basal geogrid stiffness is presented in Fig.6.9. From Fig.6.9 it is observed that the addition of basal geogrid reduces the toe lateral displacements. About 1 % reduction in toe lateral displacements is seen by the addition of basal geogrid having J = 1000 kN/m. Further increase in geogrid tensile modulus up to 4000 kN/m reduces about 9 % toe lateral displacements and geogrid with tensile modulus up to 6000 kN/m reduces 10 % of toe lateral displacements.

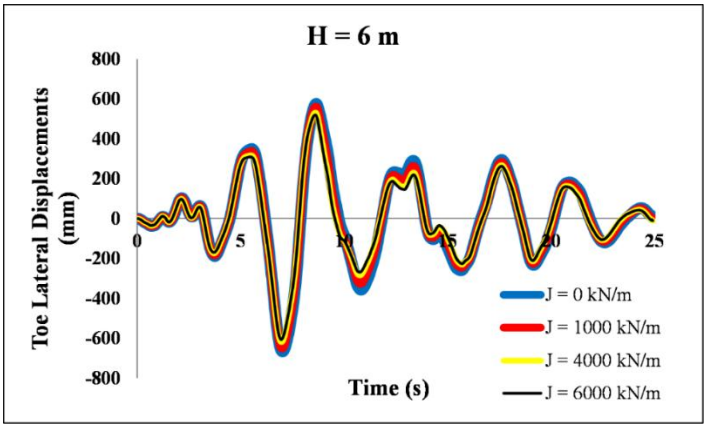

Figure 6.9 Time-history plot of toe lateral displacements for 6 m high embankment supported over 3D spaced 28 m piles considering basal geogrid stiffness subjected to IS (0.35 g) ground motion

Figure 6.10 presents the toe lateral displacements variation with time considering the effect of embankment height subjected to IS (0.35 g) ground motion. 1V:1.5H side sloped embankments supported over 3D spaced 28 m piles with a basal geogrid stiffness of 4000 kN/m are considered to study the effect of embankment height on toe lateral displacements. From Fig.6.10 it is observed that, each 1 m increase in embankment height increases the toe lateral displacements to about 5%.

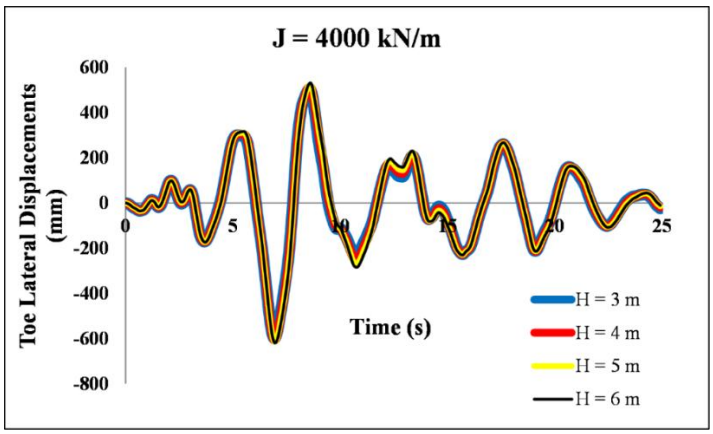

Figure 6.10 Time-history plot of toe lateral displacements considering the effect of embankment height for 3D spaced 28 m pile supported embankment with basal geogrid stiffness of 4000 kN/m subjected to IS (0.35 g) ground motion

Time-history variation of toe lateral displacements considering the effect of pile length for 6 m high embankment with basal geogrid stiffness of 4000 kN/m subjected to IS (0.35 g) ground motion is shown in Fig.6.11. It is observed from Fig.6.11 that, the toe lateral displacements reduces with increase in pile length. About 20 % reduction of toe lateral displacement is seen by increasing the pile length from 22 m to 28 m.

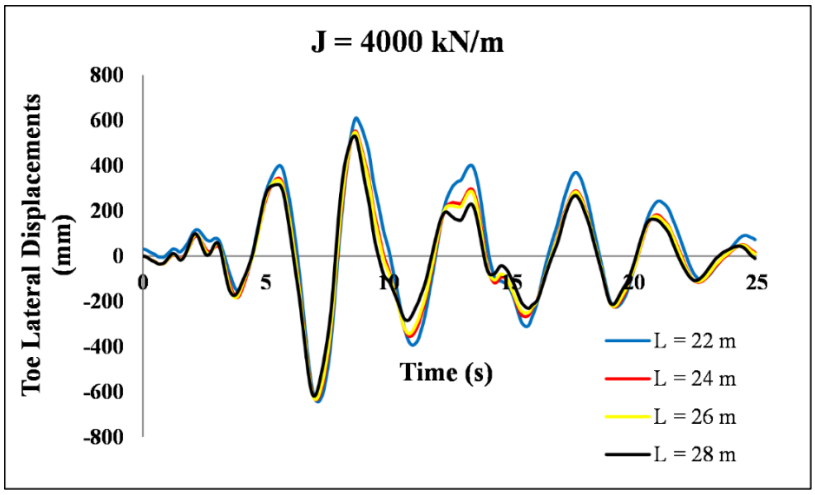

Figure 6.11 Time-history plot of toe lateral displacements considering the effect of pile length for 6 m high embankment supported over 3D spaced piles with basal geogrid stiffness of 4000 kN/m subjected to IS (0.35 g) ground motion

The effect of pile spacing on toe lateral displacements for 6 m high embankment supported over 28 m piles with basal geogrid stiffness of 4000 kN/m subjected to IS (0.35 g) ground motion is shown in Fig.6.12. It is observed from Fig.6.12 that, increase in pile spacing from 3D to 4D increases the toe lateral displacements to about 5 % and a further 5 % increase is observed by increasing the pile spacing from 4D to 5D.

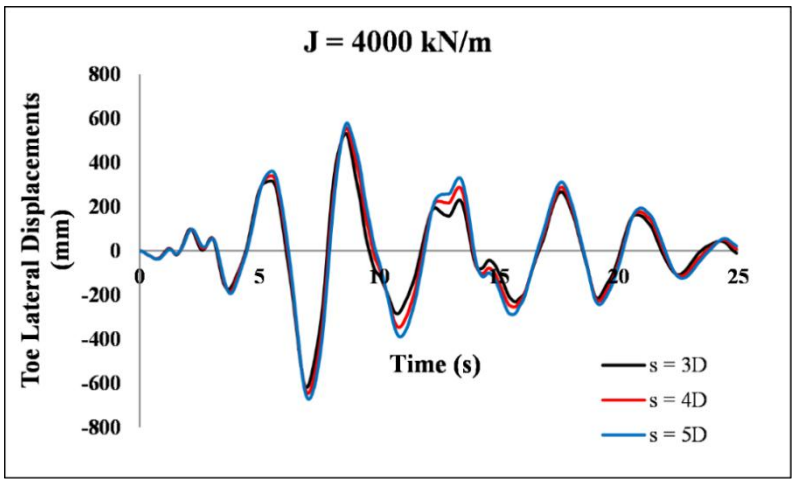

Figure 6.12 Time-history plot of toe lateral displacements considering the effect of pile spacing for 6 m high embankment supported over 28 m piles with basal geogrid stiffness of 4000 kN/m subjected to IS (0.35 g) ground motion

Toe lateral displacements variation with time considering the effect of embankment side slope subjected to IS (0.35 g) ground motion is shown in Fig.6.13. The 6 m high embankment supported over 3D spaced 28 m piles with a basal geogrid having tensile stiffness of 4000 kN/m is considered for the analysis. From Fig.6.13 it is observed that the increase in embankment side slope increases the toe lateral displacements. About 3 % and 8 % increase in toe lateral displacements are observed by increasing the embankment side slope from 1V:2H to 1V:1.5H and 1V:1H.

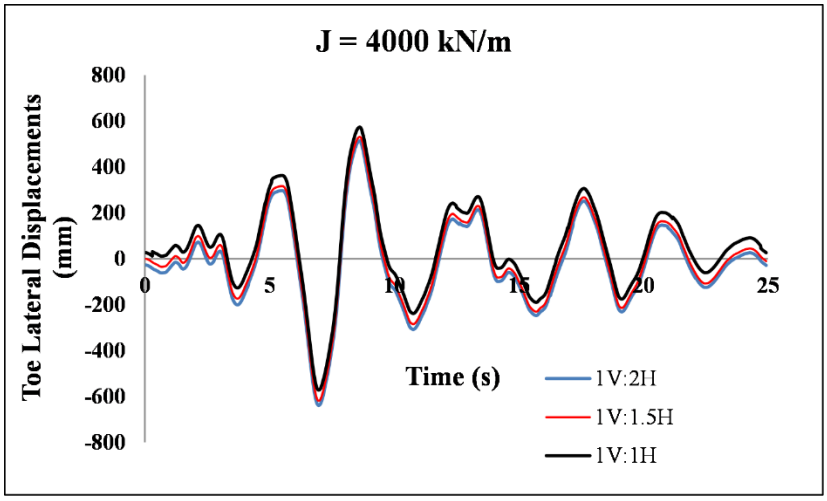

Figure 6.13 Time-history plot of toe lateral displacements considering the effect of embankment side slope for 3D spaced 28 m pile supported embankment with basal geogrid stiffness of 4000 kN/m subjected to IS (0.35 g) ground motion

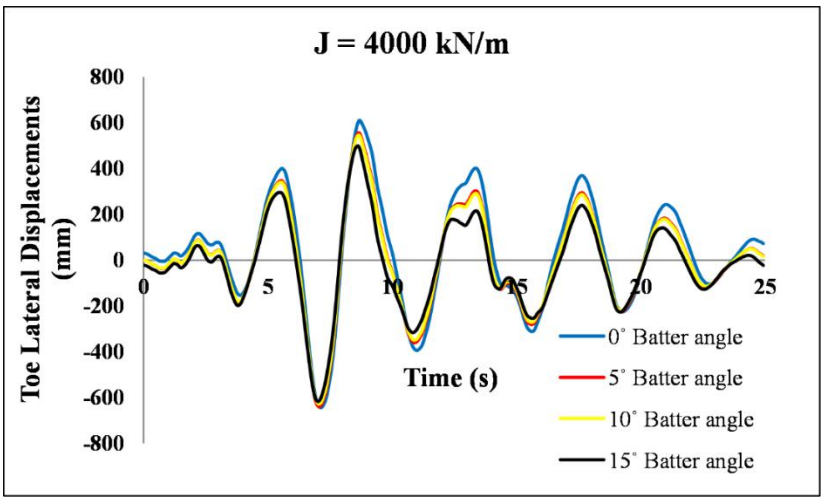

Figure 6.14 Time-history plot of toe lateral displacements for 6 m high embankment supported over 3D spaced 22 m vertical and batter piles with basal geogrid stiffness of 4000 kN/m subjected to IS (0.35 g) ground motion

Figure 6.14 shows the time history of toe lateral displacements for embankments supported over vertical and batter piles. 6 m high embankment supported over 3D spaced 22 m piles with basal geogrid (J = 4000 kN/m) subjected to IS (0.35 g) ground motion is considered for the analysis. From Fig.6.14 it is observed that increase in batter angle reduces the toe lateral displacements. About 4.2 % reduction in toe lateral displacements is seen by increasing the batter angle from 0˚ to 15˚.

Fig.6.15 shows the time history plot of toe lateral displacements for 6 m high embankment with different support conditions subjected to IS (0.35 g) ground motion. From Fig.6.15 it is observed that embankment without pile supports and basal geogrid will be experiencing maximum toe lateral displacements. The embankment with only basal geogrid reinforcement reduces 8 % of toe lateral displacements but the embankment with pile supports reduces 40.8 % and the embankment with pile supports and basal geogrid reduces 46 % of toe lateral displacements.

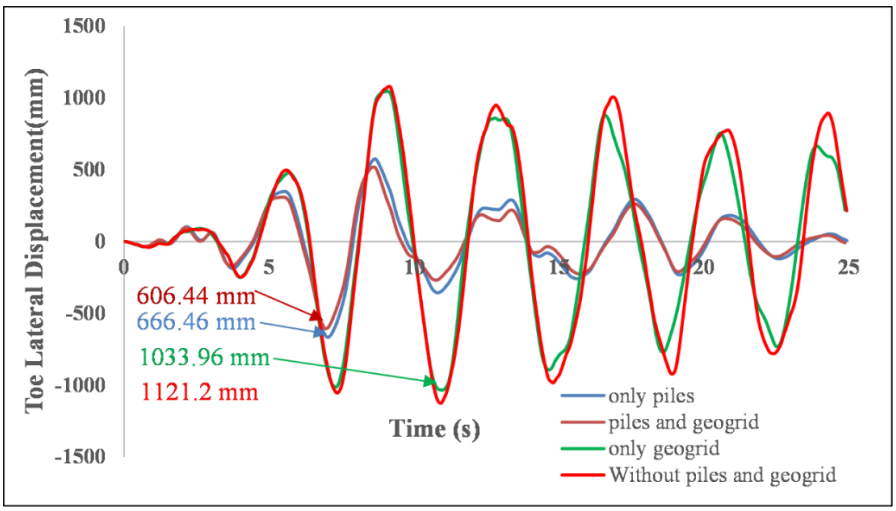

Figure 6.15 Time-history plot of crest vertical displacements for 6 m high embankment with different support conditions subjected to IS (0.35 g) ground motion

6.4 AMPLIFICATION COEFFICIENT

Amplification coefficient (α) is defined as the ratio of maximum acceleration at any time t measured at embankment crest centre to the input maximum acceleration.

Given by $$\alpha = \frac{a_{max(t)}}{a_{max(input)}} \quad (6.1)$$

Fig.6.16 shows the amplification coefficients for different embankment heights and geogrid tensile modulus subjected to seismic excitations. From Fig.6.16 it is observed that an increase in embankment height increases the 'α' value. This is because as the embankment height increases, inertial interaction increases due to added soil mass. This in turn increases the acceleration. It is also observed from Fig.6.16 that, increase in geogrid tensile modulus reduces the 'α' value. This is due to increase in geogrid stiffness increases the whole embankment system stiffness and hence attenuation of acceleration. For the considered earthquake excitations, the behaviour of basal geogrid-reinforced pile-supported embankments in terms of accelerations is same (Fig.6.16). Fig.6.17 shows the crest centre lateral and vertical accelerations for 6 m high embankment supported on 28 m piles subjected to IS (0.35 g) ground motion.

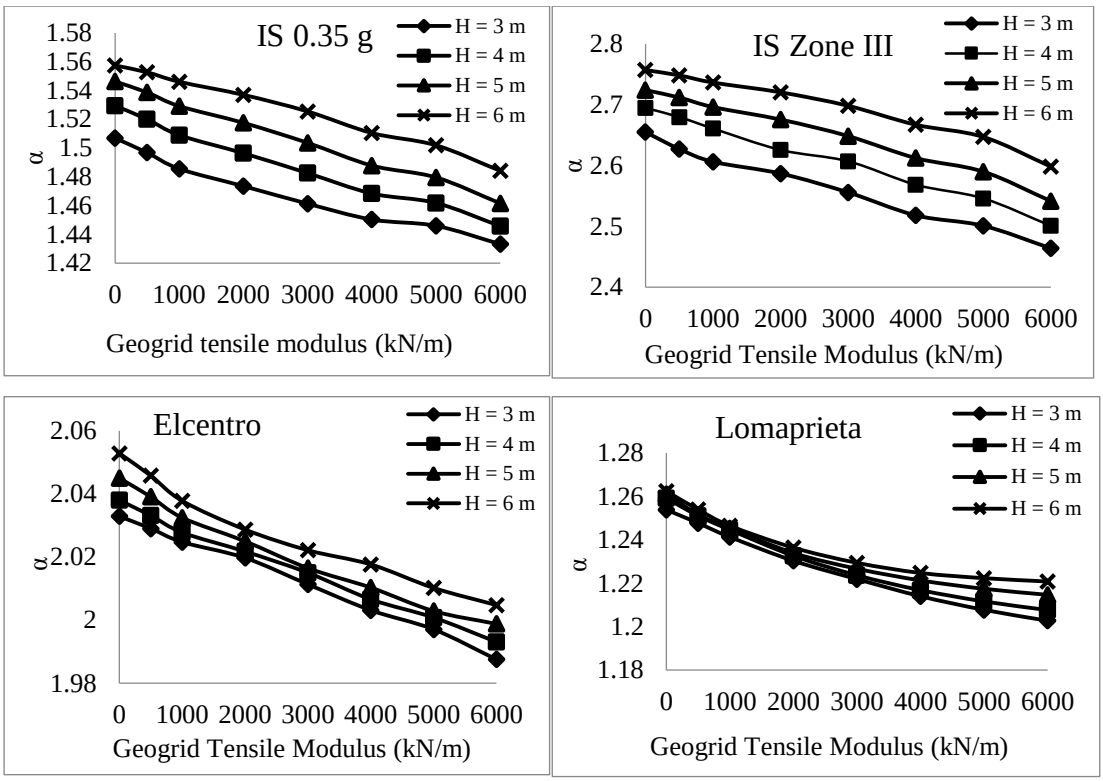

Figure 6.16 Amplification coefficients for different embankment heights and geogrid tensile modulus subjected to seismic excitations.

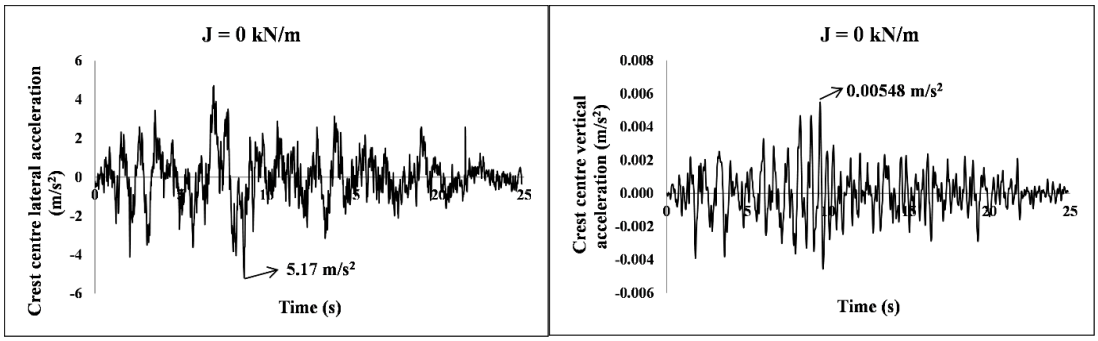

Figure 6.17 Time-history plot of crest centre accelerations for 6 m high embankment supported on 28 m piles subjected to IS (0.35 g) ground motion

Table 6.3 presents the effect of pile length and pile spacing on amplification coefficient. 6 m high embankment having 1V:1.5H side slope supported over pile arranged 3D square grid pattern subjected to IS (0.35 g) ground motion is considered to study the effect of pile length on 'α'. Increase in pile length increases the foundation soil stiffness and this reduces the acceleration in the embankment. Hence, with increase in pile length the 'α' value reduces. 28 m pile supported 6 m high embankment having 1V:1.5H side slope subjected to IS (0.35 g) ground motion is considered to study the effect of pile spacing on 'α'. It is noticed from Table 6.3 that, increasing pile spacing

increases the ‘α’ value due to increased acceleration in the embankment. It is also observed from Table 6.3 that, addition of basal geogrid reduce the ‘α’ value irrespective of pile length and pile spacing.

Table 6. 3 Effect of pile length and pile spacing on amplification coefficient

Pile Length	Amplification coefficient (α)		Pile Spacing	Amplification coefficient (α)	
	J = 0 kN/m	J = 4000 kN/m		J = 0 kN/m	J = 4000 kN/m
22 m	1.5	1.45	3D	1.5	1.45
24 m	1.49	1.44	4D	1.54	1.5
26 m	1.45	1.39	5D	1.587	1.58

Table 6.4 shows the amplification coefficient values for different batter angles and embankment side slopes considered. The 6 m high embankment having 1V:1.5H side slope supported over 22 m vertical and batter piles with a basal geogrid stiffness of 4000 kn/m subjected to IS (0.35 g) ground motion is considered to study the effect of batter angle on ‘α’. From Table 6.4 it is observed that increase in batter angle decreases the acceleration at crest and this in turn reduces the ‘α’ value. 6 m high embankment supported over 3D spaced 28 m piles with a basal geogrid tensile modulus of 4000 kN/m subjected to IS (0.35 g) ground motion is considered to study the effect of embankment side slope on ‘α’ value. Increase in embankment side slope increases the ‘α’ value due to increased crest accelerations (Table 6.4).

Table 6. 4 Effect of batter angle and embankment side slope on amplification coefficient

Batter angle	Amplification coefficient	Embankment side slope	Amplification coefficient
0º	1.45	1V:2H	1.44
5º	1.38	1V:1.5H	1.45
10º	1.36	1V:1H	1.45
15º	1.33	-	-

6.5 STRESS DISTRIBUTION RATIO UNDER SEISMIC LOADING CONDITIONS

As already defined in self-weight analysis, stress distribution ratio (SDR) is the ratio between vertical stresses on the pile to that on the foundation soil between piles measured at same elevation. In the seismic analysis of basal geogrid reinforced pile supported embankments, the SDR was measured at the instant of occurrence of PGA. Figs. 6.18(a) – 6.18 (d) shows the SDR measured at the instant of occurrence of PGA for 3 m to 6 m high embankments subjected to seismic excitations. They are measured at the centre pile head and foundation soil between piles. Maximum SDR values are observed for 3 m (H/s = 3.33) and 4 m (H/s = 4.44) high embankments having basal geogrid tensile modulus of 2000 kN/m and 3000 kN/m. Further increase in geogrid tensile modulus will reduce the SDR value for 3 m and 4 m high embankments. For 5 m (H/s = 5.55) and 6 m (H/s = 6.66) high embankments, increase in geogrid tensile modulus increases the SDR value. Basal geogrid tensile modulus of 3000 kN/m is sufficient to withstand vertical stresses for (H/s) less than or equal to 4.5. Based on the seismic intensity and performance of pile foundations, optimized geogrid tensile modulus should be considered for the final design of geogrid reinforced piled embankment. From Fig.5.3 and Fig.6.18 it is observed that the SDR values obtained by seismic excitations are very high when compared to the SDR obtained by self-weight analysis. This is because of very low vertical stress on foundation soil between piles caused by seismic excitations (Fig.6.19).

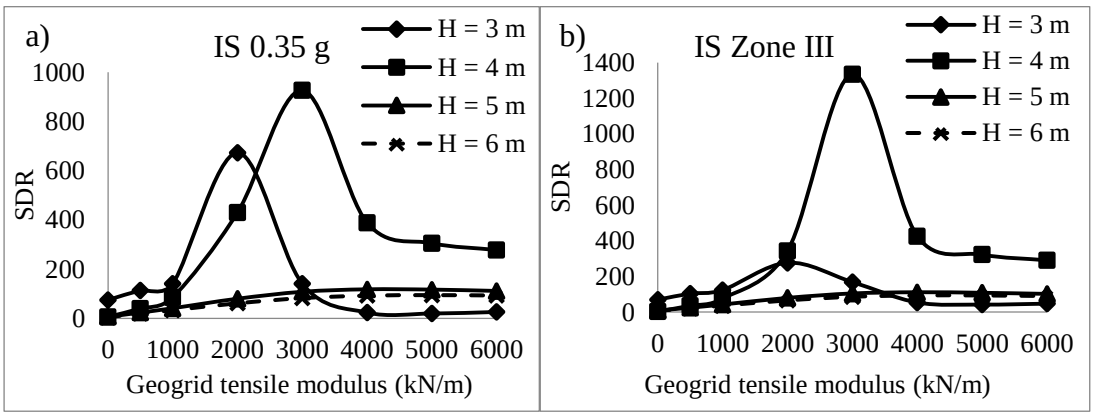

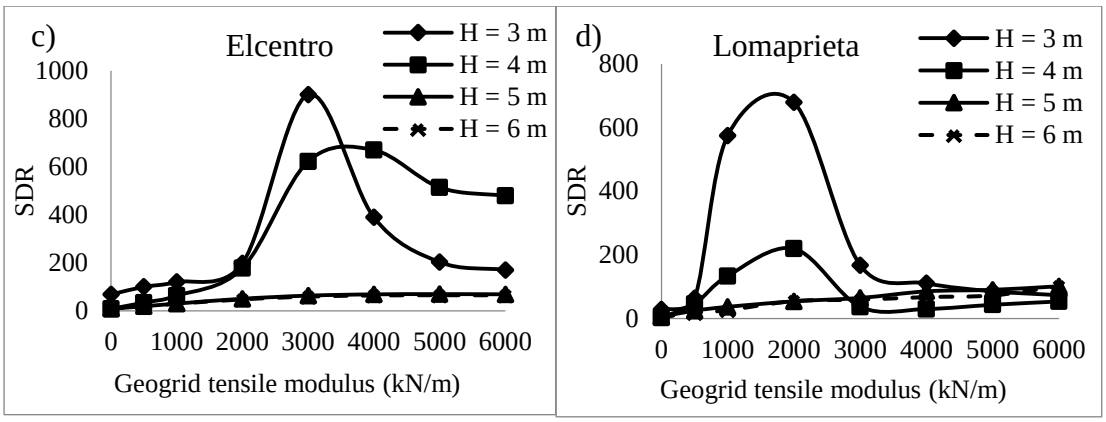

Figure 6.18 Variation in SDR under seismic excitations (a) IS (0.35 g) (b) IS Zone III (c) Elcentro (d) Lomaprieta

Figure 6.19 shows the time-history plot of vertical stress on pile head and foundation soil between piles for 6 m and 3 m high embankment, with and without basal geogrid subjected to IS (0.35 g) ground motion. It is observed from Fig.6.19 that for 3 m high embankment addition of basal geogrid (J = 6000 kN/m) reduces the load transferred to the piles causing lower vertical stresses on piles when compared to the embankment without basal geogrid but for 6 m high embankment addition of basal geogrid increases the load transferred to the piles. Hence, embankment height is an important parameter while designing the basal geogrid to withstand seismic forces in geogrid reinforced piled embankment.

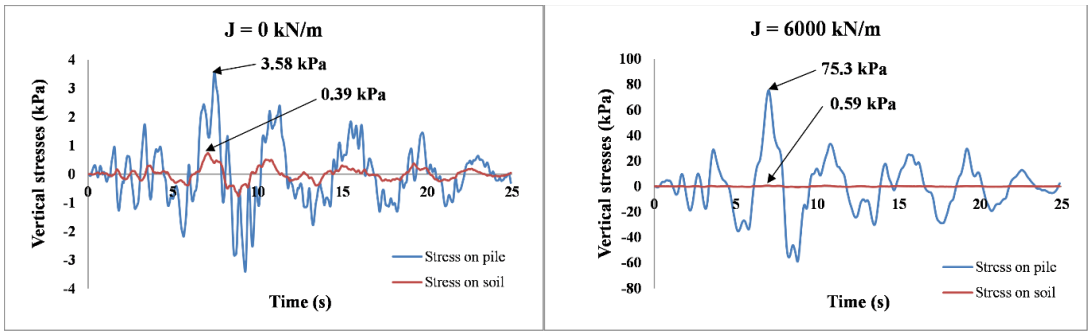

(a) For 6 m high embankment

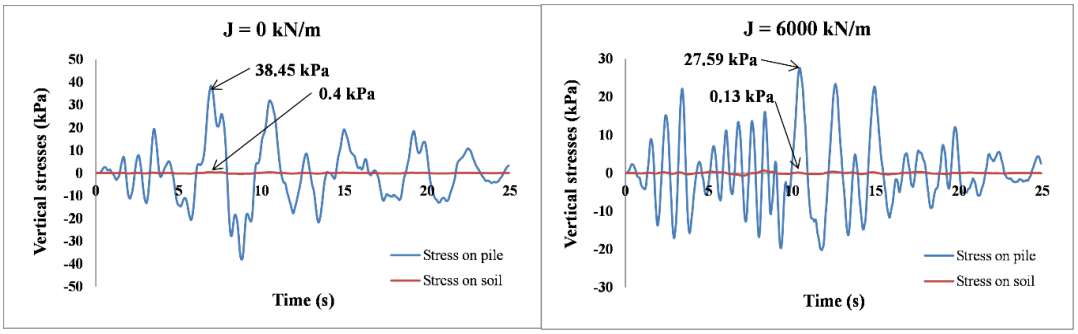

(b) For 3 m high embankment

Figure 6.19 Time-history plot of vertical stress on pile head and foundation soil between piles subjected to IS (0.35 g) ground motion

Figure 6.20 shows the time-history plot of vertical stresses on the centre pile head and foundation soil between piles subjected to seismic loading conditions. Since the time-history plots of remaining embankment heights for the considered earthquake loadings are similar, representative time-history of vertical stresses corresponding to one embankment height is plotted for one earthquake loading. From Fig.6.20 it is observed that increase in basal geogrid modulus increases the vertical stresses except 3 m high embankment (H/s << 4.5). In low embankments, with increase in geogrid stiffness the sandwiched layer of basal geogrid and surface fill behaves as a rigid raft. This causes the direct load transfer from embankment fill to piles and foundation soil. Hence geogrid tensile modulus beyond 3000 kN/m do not have much effect in transferring loads to piles. For 5 m and 6 m high embankments (H/s >> 4.5) increase in geogrid tensile modulus reduces the vertical stresses on foundation soil.

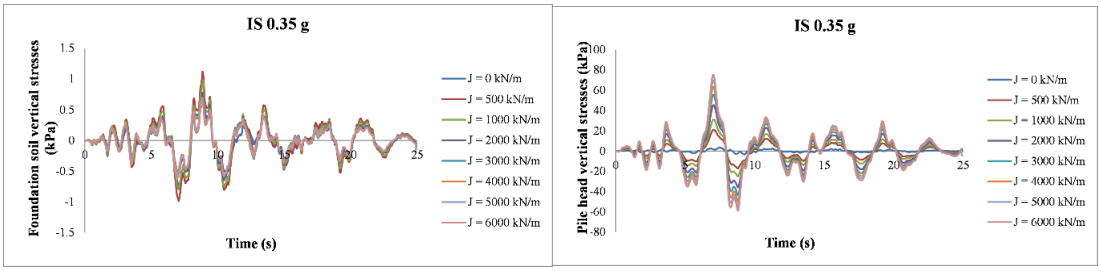

(a) For 6m embankment

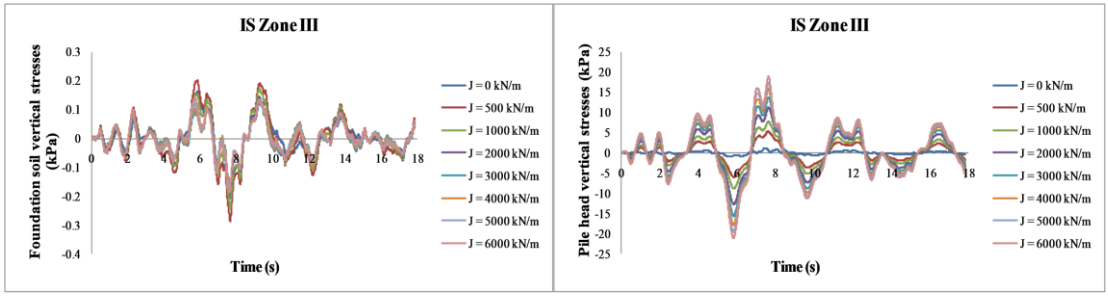

(b) For 5 m embankment

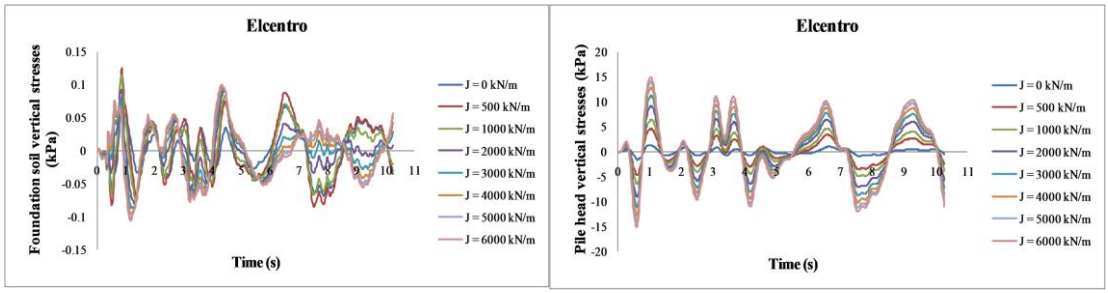

(c) For 4 m embankment

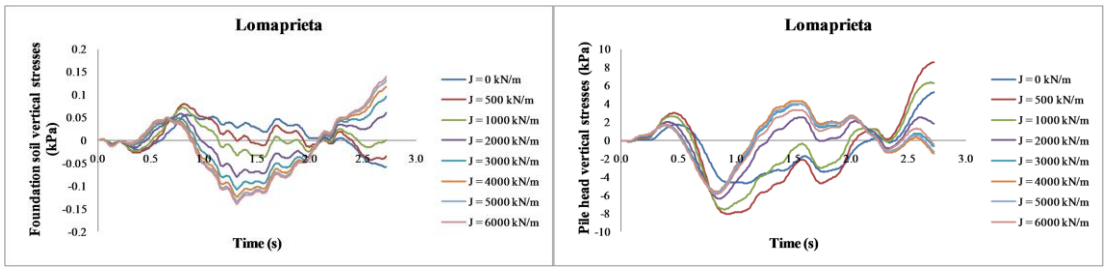

(d) For 3 m embankment

Figure 6.20 Time-history plot of vertical stresses on centre pile and foundation soil subjected to seismic loading

6.6 STRESS DISTRIBUTION BETWEEN PILES AND FOUNDATION SOIL ALONG DEPTH

Maximum SDR along the depth measured for centre pile and foundation soil between piles by varying the embankment height and geogrid tensile modulus are given in Fig.6.21. From Fig.6.21 for embankments with 5 m and 6 m heights, SDR values increase with increase in geogrid tensile modulus. But for 4 m high embankment, SDR values are almost same for geogrid tensile modulus of 2000 kN/m, 4000 kN/m and 6000 kN/m. It is also observed from Fig.6.21 that, higher geogrid tensile modulus reduces the SDR value for 3 m high embankment. This shows that the seismic design of basal geogrid depends on the height of embankment.

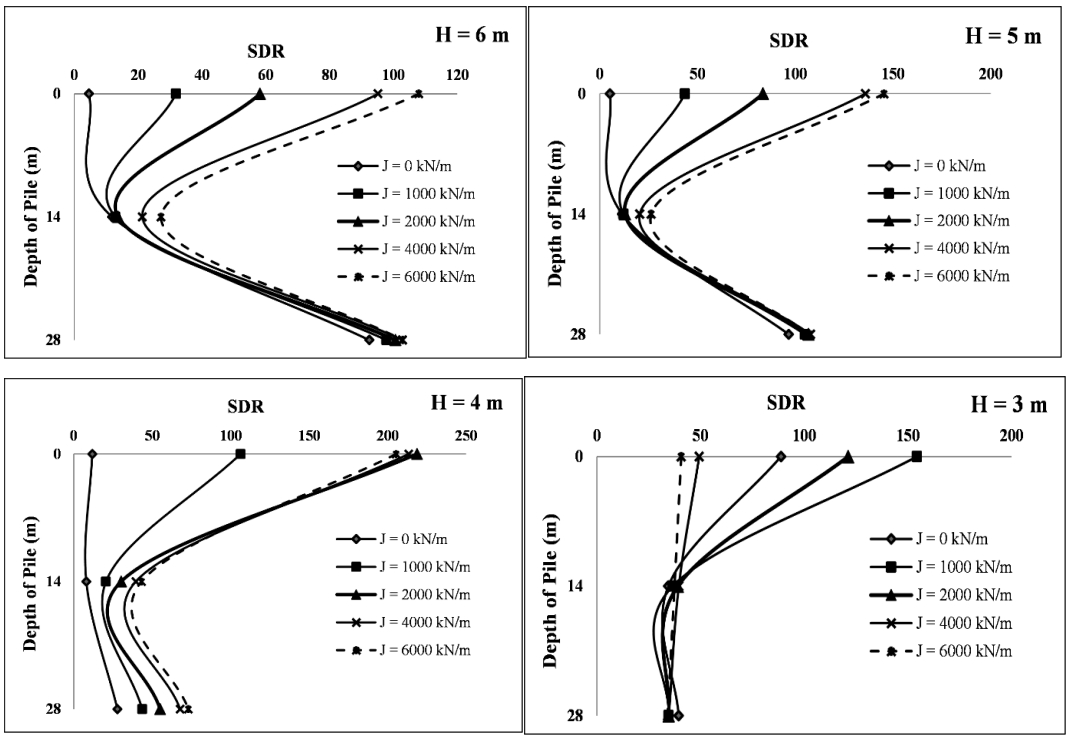

Figure 6.21 Maximum SDR along the depth for different embankment heights and geogrid tensile modulus subjected to IS (0.35 g) ground motion

6.7 LATERAL STRESS DISTRIBUTION RATIO UNDER SEISMIC LOADING CONDITIONS

Lateral stress distribution ratio (LSDR) is the ratio of lateral stress on pile to that on foundation soil between piles measured at same instant of time. LSDR measured at the time of PGA for 3 m to 6 m high embankments under earthquake loads is shown in Fig.6.22 (a) to 6.22 (d). For 5 m and 6 m high embankments, the LSDR values are increasing with the increase of geogrid tensile modulus. In case of 3 m and 4 m high embankments, maximum LSDR is observed for geogrid tensile modulus of 2000 kN/m and 3000 kN/m under IS ground motions. Further increase in geogrid tensile modulus will reduce the LSDR value for 3 m and 4 m high embankments except for Elcentro earthquake excitations (Fig.4.7 (a)). This is due to the Fourier amplitude corresponding to the natural frequency (f = 0.7 Hz) of embankments is very low for Elcentro earthquake excitations. Hence, to withstand the lateral stresses due to earthquakes, a basal geogrid tensile modulus beyond 4000 kN/m is uneconomical for (H/s) less than or equal to 4.5. And for (H/s) greater than 4.5, basal geogrid modulus should be designed by considering the field conditions to withstand lateral stresses.

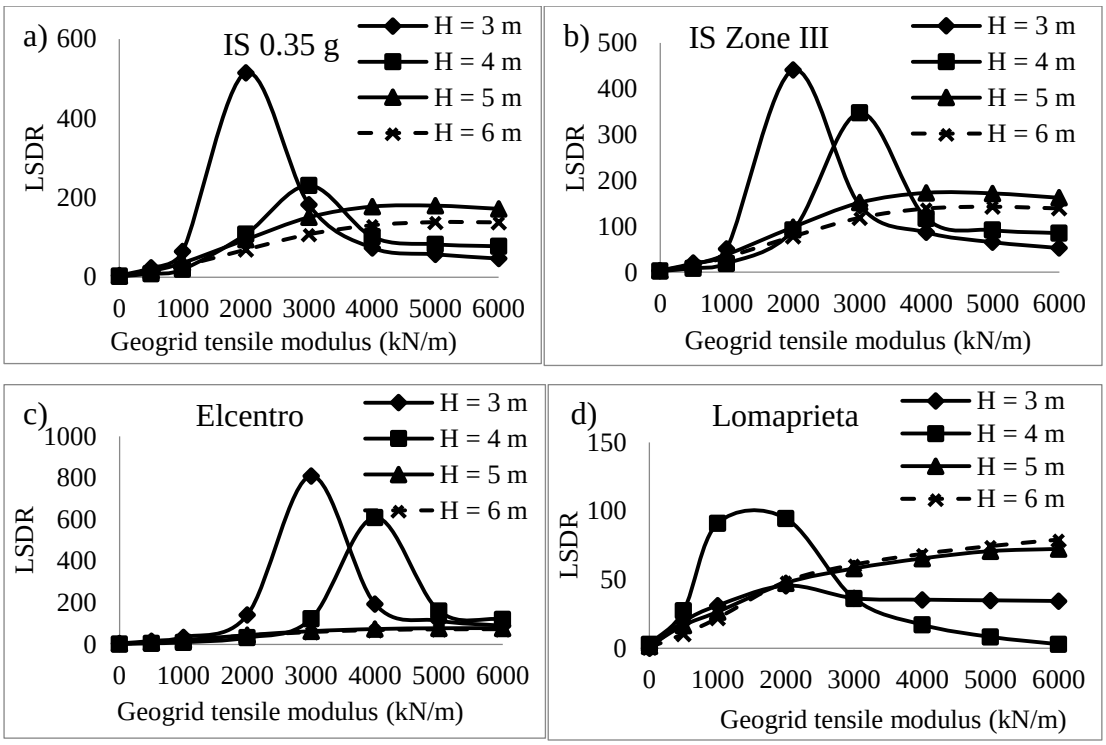

Figure 6.22 Effect of geogrid stiffness and embankment height on LSDR under seismic excitations

Time-history plot of lateral stress on pile head and foundation soil between piles for 6 m and 3 m high embankment, with and without basal geogrid subjected to IS (0.35 g) ground motion are shown in Fig.6.23. For 6 m high embankment, addition of basal geogrid increases the lateral stresses on piles and reduces the lateral stresses on foundation soil. But in 3 m high embankment, addition of basal geogrid (J = 6000 kN/m) increases lateral stresses on both foundation soil and piles.

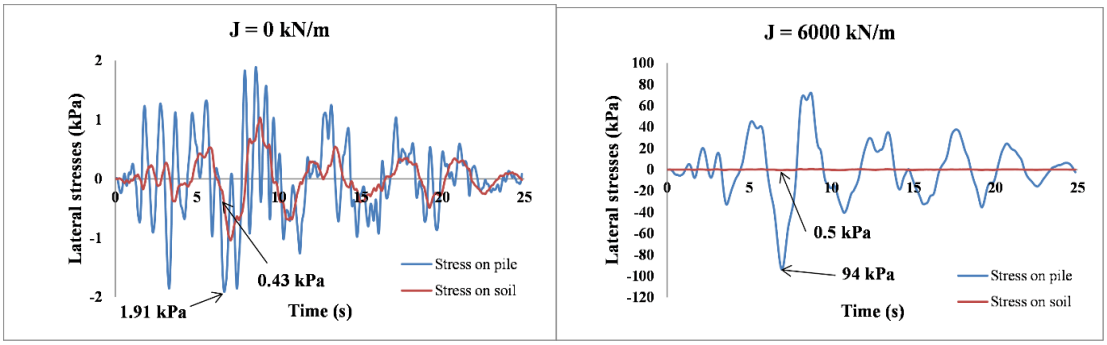

a) For 6 m high embankment

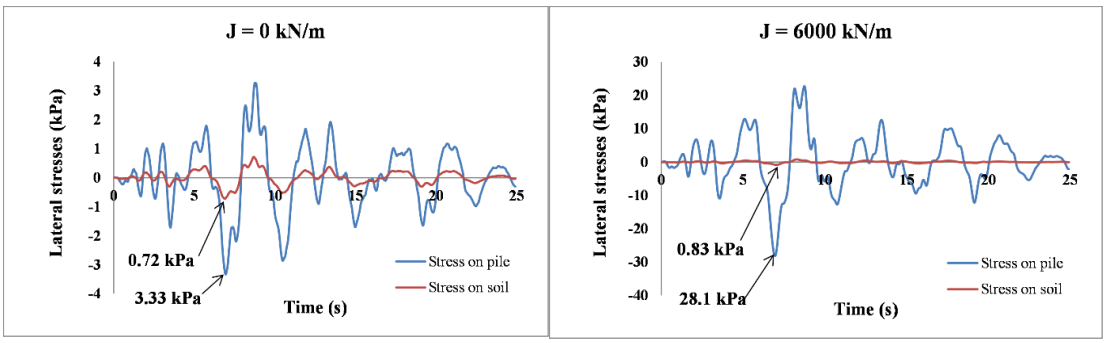

b) For 3 m high embankment

Figure 6.23 Time-history plot of lateral stress on pile head and foundation soil between piles subjected to IS (0.35 g) ground motion

6.8 LATERAL STRESS ALONG THE LENGTH OF PILE

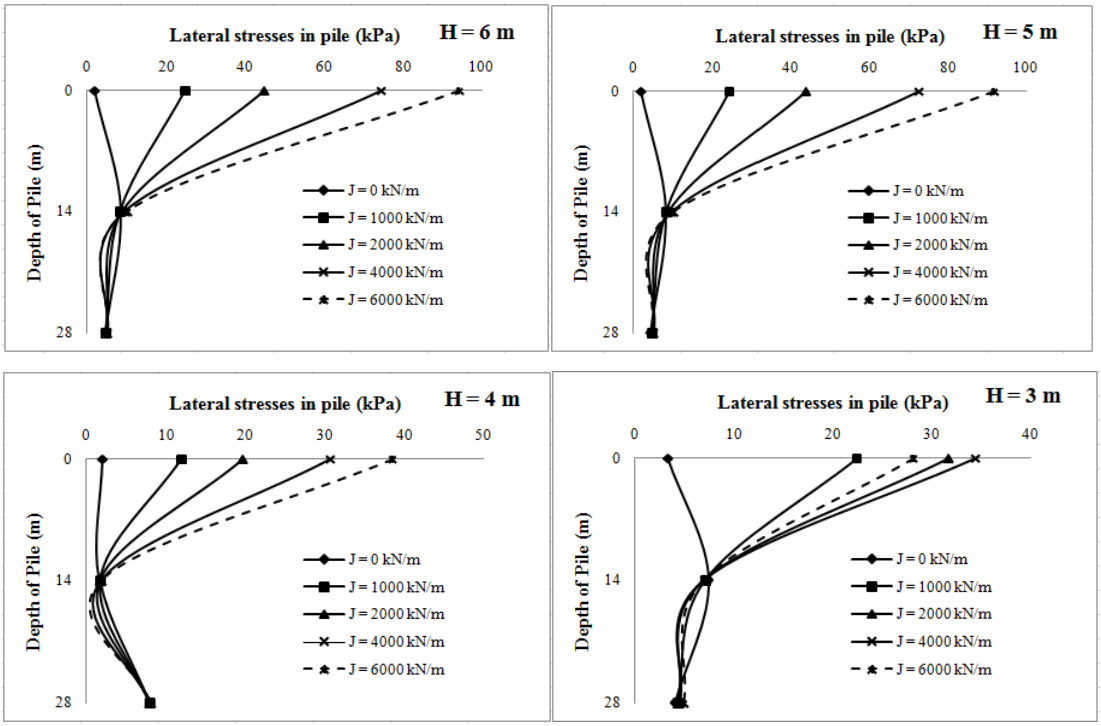

Figure 6.24 Lateral stress along the length of the pile for different embankment heights and geogrid tensile modulus subjected to IS (0.35 g) ground motion

Figure 6.24 shows the maximum lateral stresses along the length of the pile for different embankment heights and geogrid tensile modulus subjected to IS (0.35 g) ground motion. For 4 m, 5 m, and 6 m high embankments lateral stress in piles increases with an increase in geogrid tensile modulus but for 3 m high embankment lateral stress in piles increases with an increase in tensile modulus of geogrid up to 4000

kN/m. Further increase in tensile modulus beyond 4000 kN/m reduces the lateral stresses in piles.

6.9 LATERAL STRESS ALONG THE DEPTH OF FOUNDATION SOIL

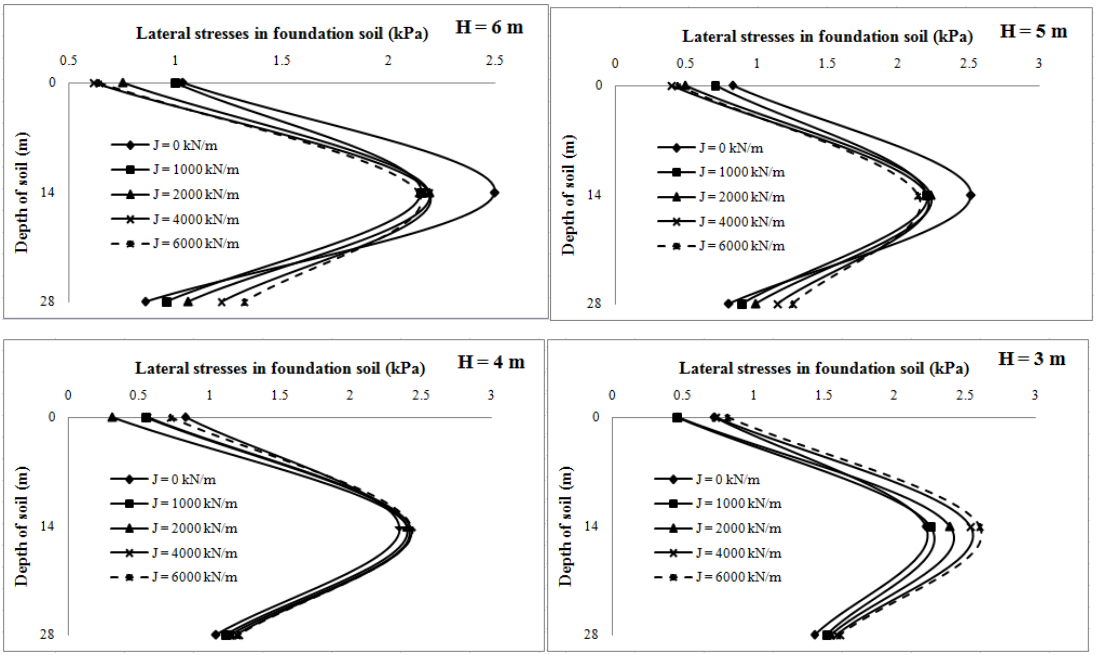

Figure 6.25 Maximum lateral stress along the depth of foundation soil for IS (0.35 g) ground motion

Figure 6.25 shows the maximum lateral stress along the depth of foundation soil for different embankment heights and geogrid tensile modulus subjected to IS ground motion. From Fig.6.25 it is noticed that an increase in geogrid tensile modulus reduces the lateral stresses in the foundation soil for 5 m and 6 m high embankments. Foundation soil in 4 m high embankment experiences almost the same lateral stress at a depth of 14 m and till 28 m for all the geogrid tensile modulus considered. In the case of 3 m high embankment lateral stresses in foundation soil increase with an increase in tensile modulus of geogrid.

Figure 6.26 shows the time-history of lateral stresses on centre pile head and foundation soil between piles subjected to earthquake loading. [Time-history of lateral stresses are also plotted in a similar manner as in Fig.6.20]. Similar to vertical stresses (Fig.6.20), lateral stresses on piles increases with increase in geogrid tensile modulus for all embankment heights considered. For 3 m and 4 m high embankments, the time-history of lateral stresses on foundation soil with geogrid tensile modulus greater than 3000 kN/m changes the path when compared to lateral stresses on foundation soil with

geogrid tensile modulus less than 3000 kN/m. This is due to the higher stiffness value of basal geogrid. Which behaves like a rigid raft below embankment in 3 m and 4 m high embankments and hence lateral stress difference between foundation soil and pile is less.

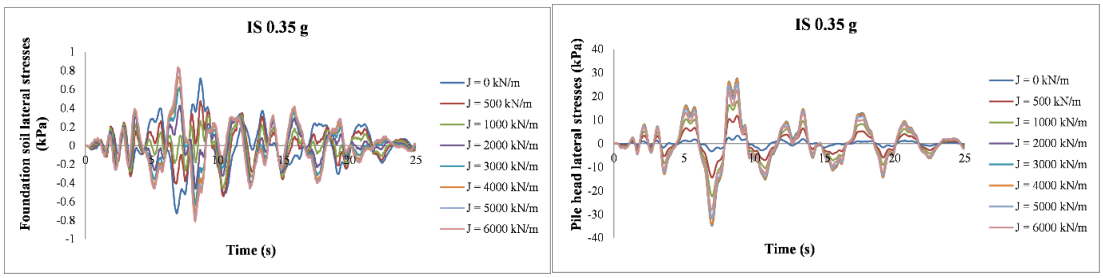

(a) For 3m embankment

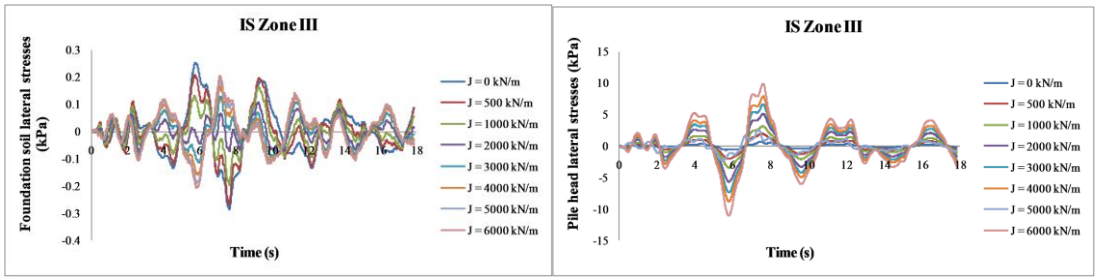

(b) For 4m embankment

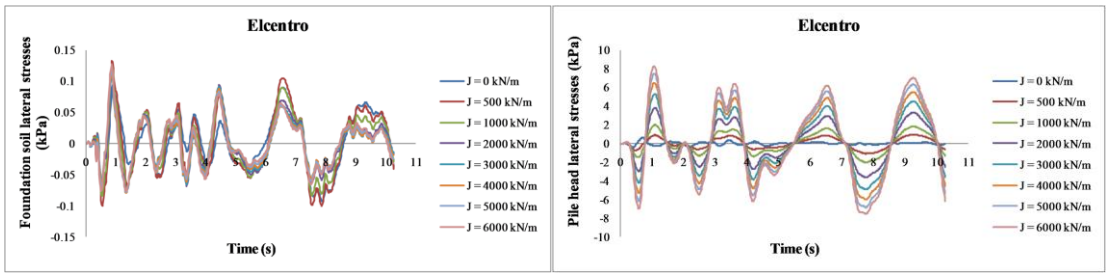

(c) For 5 m embankment

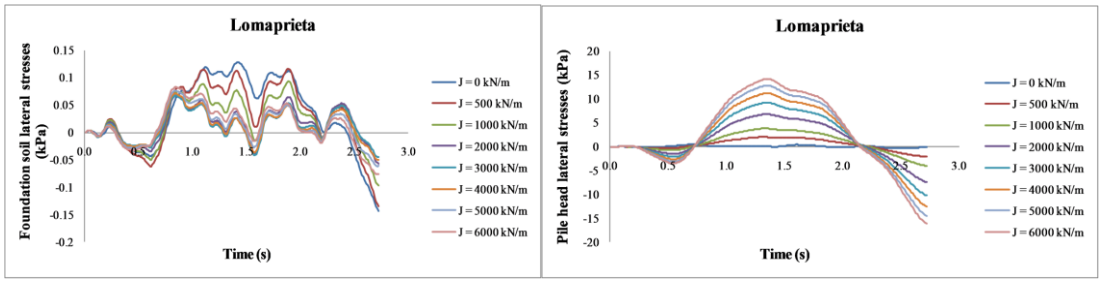

(d) For 6 m embankment

Figure 6.26 Time-history of lateral stresses on centre pile and foundation soil subjected to earthquake loading

6.10 STRESS DISTRIBUTION RATIO AT THE INSTANT OF OCCURRENCE OF PGA

Stress distribution ratio is the ratio between vertical stresses on pile to that on foundation soil between piles. To study the behaviour of embankment vertical stress distribution between piles and foundation soil under seismic loading conditions, SDR versus depth of pile graphs are plotted at the instant of occurrence of PGA. Fig. 6.27 depicts the variation of SDR along the length of pile considering the embankment height, pile length, pile spacing and geogrid tensile modulus at the instant of occurrence of PGA. The embankments were analysed for IS (0.35 g) ground motion. From Fig.6.27 it is noticed that, the presence of basal geogrid (J = 4000 kN/m) helps to transfer additional vertical loads over piles. This causes the increase in SDR values in the presence of basal geogrid when compared with the condition without basal geogrid (J = 0 kN/m). This shows that the presence of basal geogrid not only beneficial under static loading conditions, but also beneficial in distributing seismic loads between foundation soil and piles by its membrane action and flexible raft behaviour.

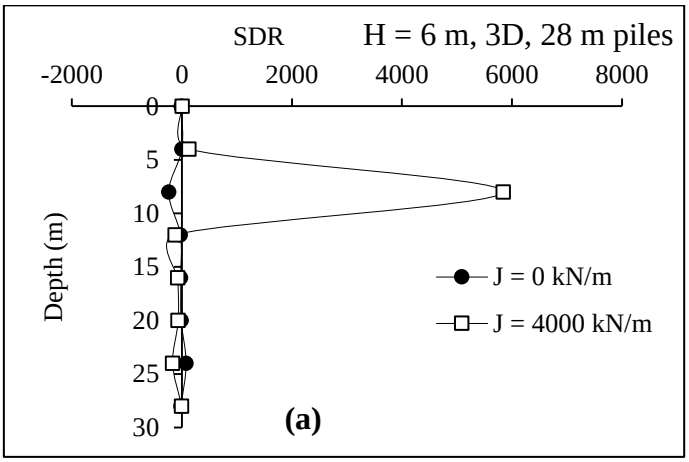

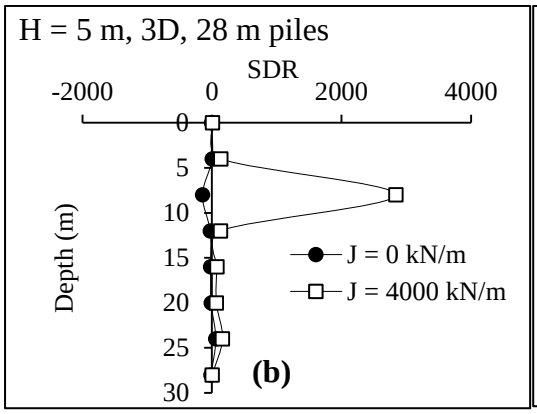

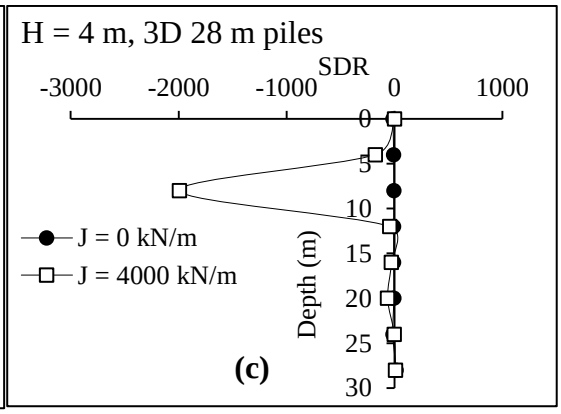

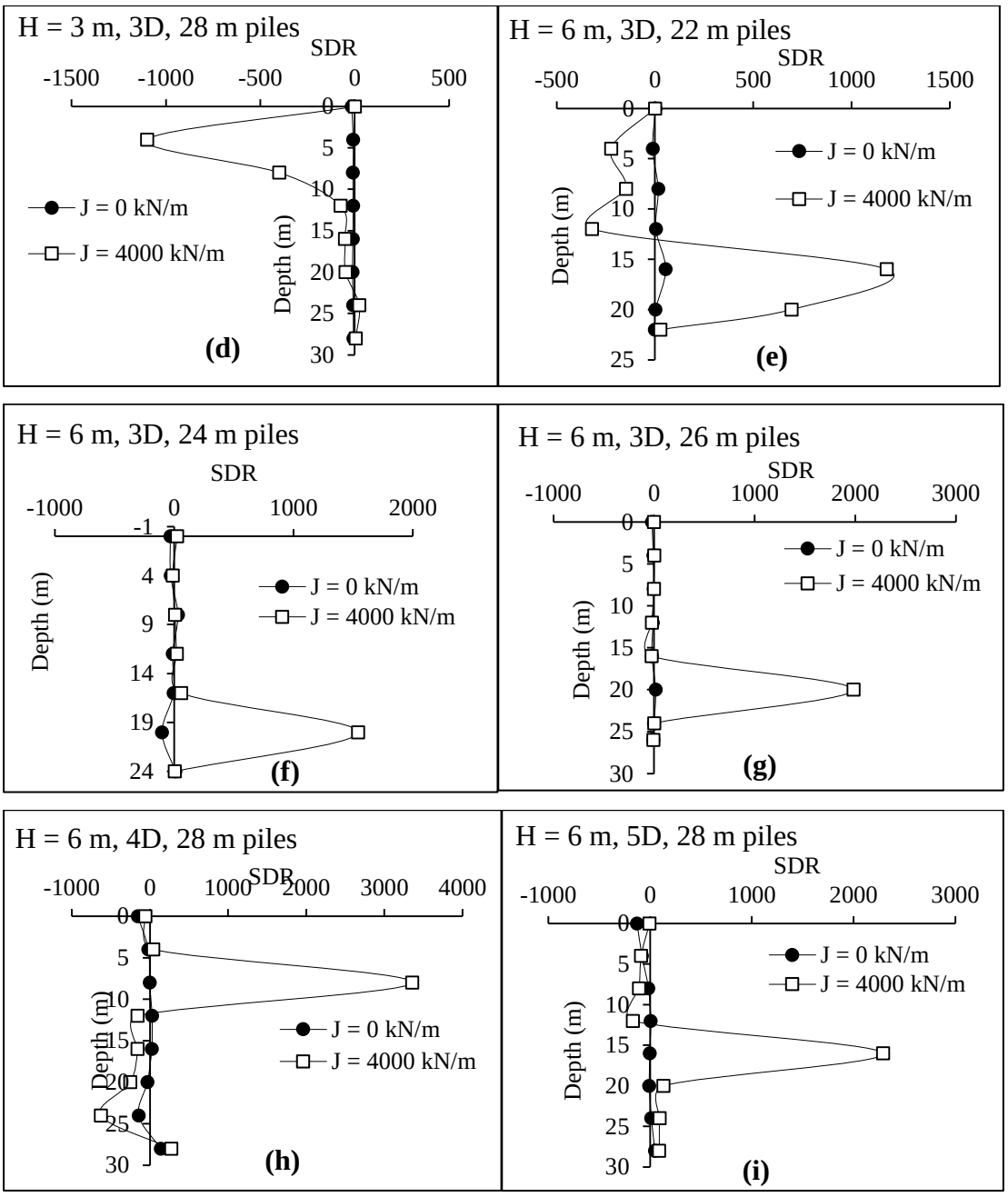

Figure 6.27 SDR along the length of pile

Effect of embankment height on SDR along the length of pile was analysed for 3D spaced 28 m pile supported embankments subjected to IS (0.35 g) ground motion. From Fig.6.27 (a-d) maximum SDR is observed at about 8 m depth for the considered embankment heights. Similar variation of maximum bending moment is observed at a depth of 0.25 L to 0.4 L (where, L is the length of pile) in Chandrasekaran et al (2010). With each 1 m increase in embankment height, about 35 % to 45 % increase in SDR is observed.

Effect of pile length on SDR along the length of pile was analysed for 6 m high embankment supported over 3D spaced piles subjected to IS (0.35 g) ground motion. It is observed from Fig.6.27 that, increase in pile length increases the SDR values. Floating pile supported embankments (22 m, 24 m, 26 m) experience less SDR than the end-bearing (H = 6 m) pile supported embankment. With each increment of 2 m pile length, about 20 % increase in SDR is observed. It is also observed from Fig.6.27 that, in floating pile supported embankments (Fig.6.27, e, f, g), maximum SDR is observed at the bottom level of piles but in end-bearing pile supported embankments (Fig.6.27, a), maximum SDR is observed at the top level of piles. This is because of both end-bearing and frictional resistance offered by the end-bearing piles and only frictional resistance offered by the floating piles.

Effect of pile spacing on SDR along the length of pile was analysed for 6 m high embankment supported over 28 m piles subjected to IS (0.35 g) ground motion. From Fig.6.27 (h, i) it is observed that the increase in pile spacing reduces the SDR along the depth. This is due to the increase in pile spacing increases the area of foundation soil and thus some part of vertical load will also get transferred to the foundation soil causing less SDR values.

6.11 LATERAL STRESS DISTRIBUTION RATIO AT THE INSTANT OF OCCURRENCE OF PGA

Lateral stress distribution ratio is the ratio between lateral stresses on pile to that on foundation soil between piles. To study the behaviour of embankment lateral stress distribution between piles and foundation soil under seismic loading conditions, LSDR versus depth of pile graphs are plotted at the instant of occurrence of PGA. Fig. 6.28 depicts the variation of LSDR along the length of pile considering the embankment height, pile length, pile spacing and geogrid tensile modulus at the instant of occurrence of PGA. The embankments were analysed for IS (0.35 g) ground motion. Similar in Fig.6.27, it is noticed from Fig.6.28 that, the presence of basal geogrid (J = 4000 kN/m) helps to transfer additional lateral loads to piles. This increases the LSDR values in the presence of basal geogrid when compared with the condition without basal geogrid (J = 0 kN/m).

Effect of embankment height on LSDR along the length of pile was analysed for 3D spaced 28 m pile supported embankments subjected to IS (0.35 g) ground

motion. From Fig.6.28 maximum LSDR is observed at about 8 m depth for the considered embankment heights. With each 1 m increase in embankment height, about 50 % to 70 % increase in LSDR is observed.

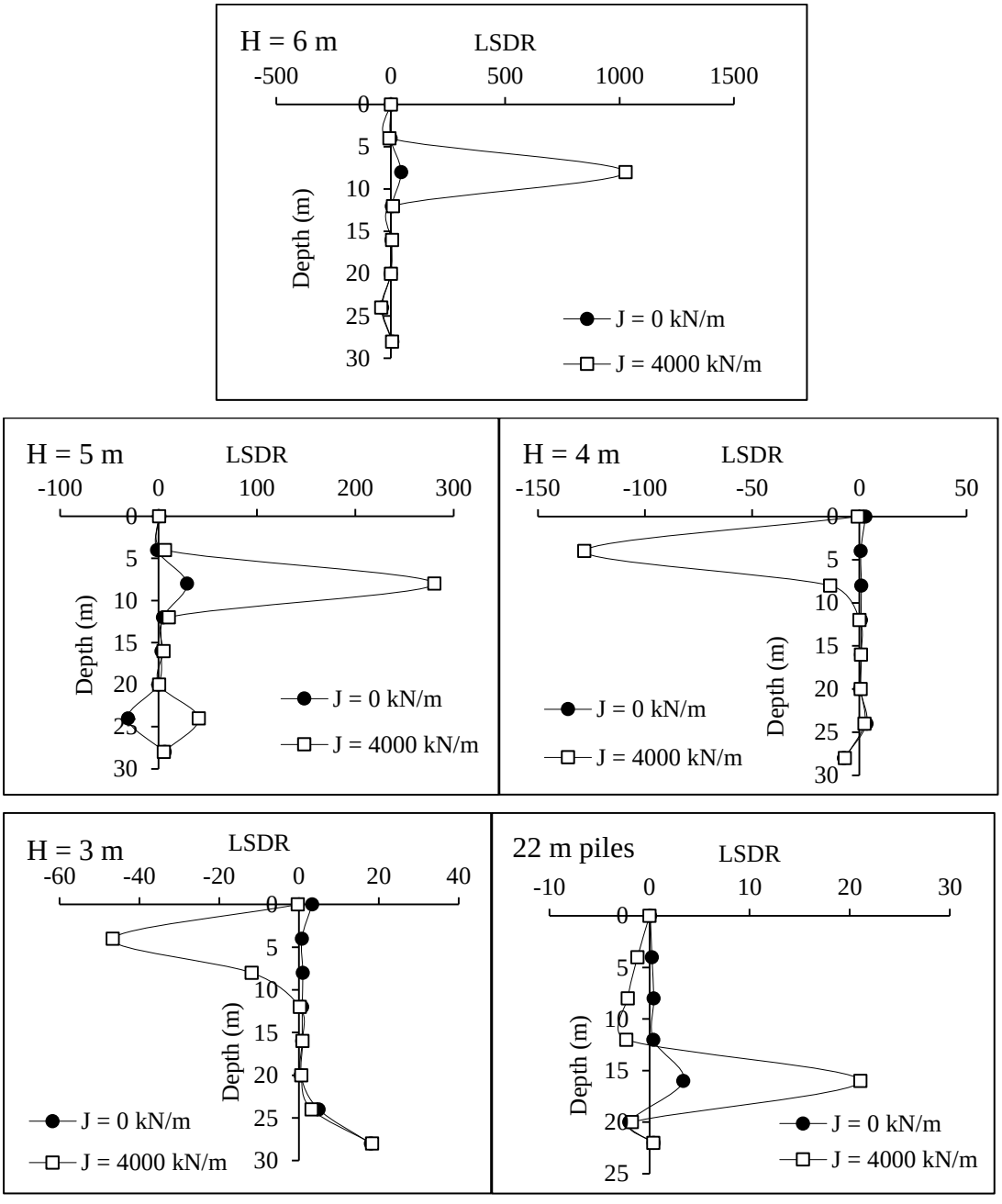

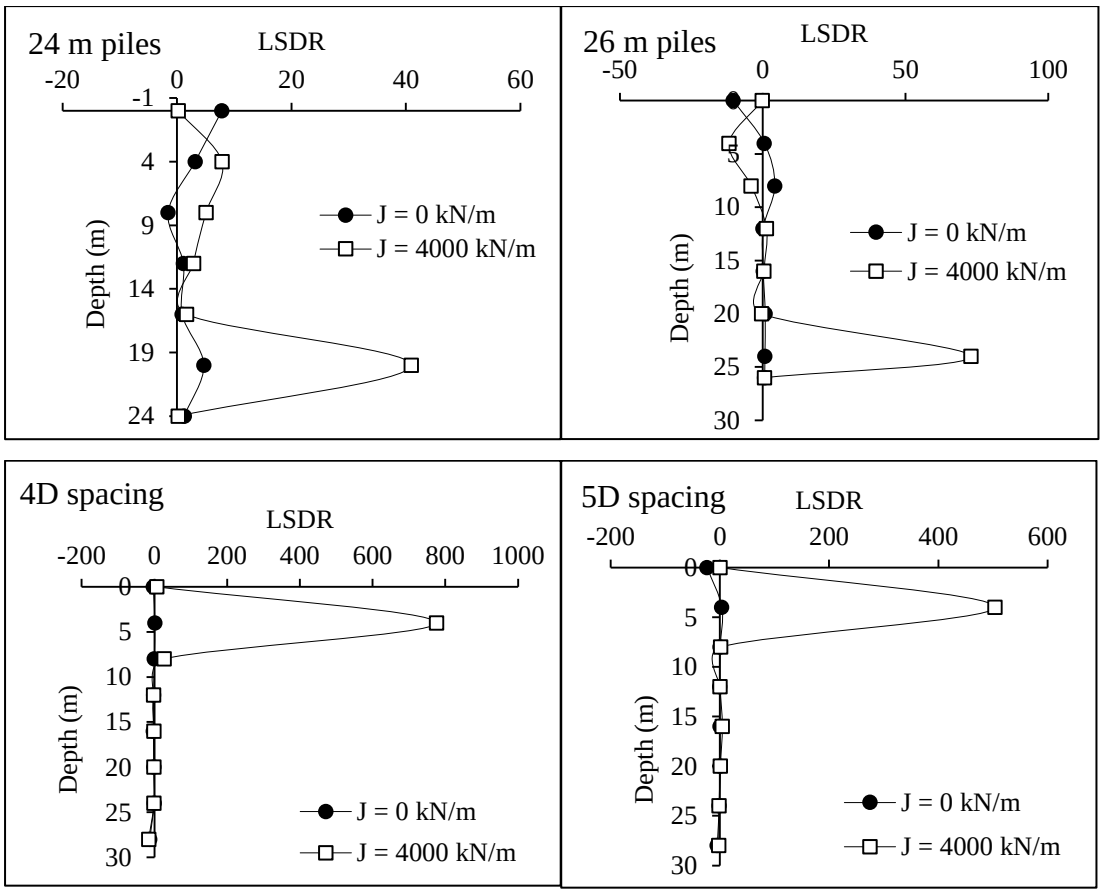

Figure 6.28 LSDR along the length of pile

Effect of pile length on LSDR along the length of pile was analysed for 6 m high embankment supported over 3D spaced piles subjected to IS (0.35 g) ground motion. It is observed from Fig.6.28 that, increase in pile length increases the LSDR values. Floating pile supported embankments (22 m, 24 m, 26 m) experience less LSDR than the end-bearing (H = 6 m) pile supported embankment. With each increment of 2 m pile length, about 50 % increase in LSDR is observed. Similar as SDR (Fig.6.27), it is also observed from Fig.6.28 that, in floating pile supported embankments, maximum LSDR is observed at the bottom level of piles but in end-bearing pile supported embankments, maximum LSDR is observed at the top level of piles.

Effect of pile spacing on LSDR along the length of pile was analysed for 6 m high embankment supported over 28 m piles subjected to IS (0.35 g) ground motion. From Fig.6.28 it is observed that the increase in pile spacing reduces the LSDR along the depth. This is due to the increase in pile spacing increases the area of

foundation soil and thus some part of lateral load will also get transferred to the foundation soil causing less LSDR values.

From both Fig.6.27 and Fig.6.28 it is inferred that the behaviour of piles in terms of vertical and lateral stresses along the depth at any particular instant of time under seismic excitations is similar. Coefficient of lateral pressure (K) along the length of pile and along the depth of foundation soil at the instant of occurrence of PGA also shows the similar variation. The plots of K along the length of pile and depth of foundation soil are given in APPENDIX III.

6.12 COEFFICIENT OF LATERAL PRESSURE ALONG THE EMBANKMENT SUBJECTED TO SEISMIC LOADS

Figure 6.29 shows the effect of geogrid tensile modulus on coefficient of lateral pressure (K) along embankment elevation. 6 m high embankment supported over 28 m piles subjected to IS (0.35 g) ground motion is considered. The K values were measured at the instant of occurrence of PGA. The K values above pile are more for embankment without basal geogrid and the addition of basal geogrid reduces the K value above pile. The reduction of K value above pile continues until the geogrid tensile modulus equal to 4000 kN/m and beyond that further increase in geogrid tensile modulus leads to increase in K value above pile.

It is also observed from Fig.6.29 that, the K values above foundation soil along the embankment elevation increases with increase in geogrid tensile modulus. This indicates that, addition of basal geogrid transfers most of the vertical stresses to the piles causing less K values above piles and more K values above foundation soil in the embankment.

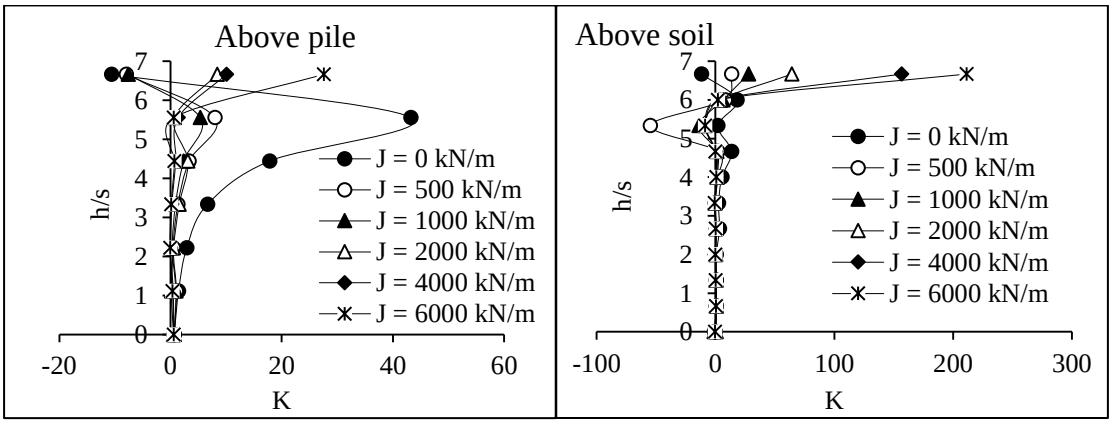

Figure 6.29 Effect of geogrid tensile modulus on K along embankment elevation

Figure 6.30 depicts the effect of embankment height on K along the embankment elevation at the instant of occurrence of PGA. Embankments supported on 3D spaced 28 m piles with and without geogrid subjected to IS (0.35 g) ground motion are considered. From Fig.6.30 it is observed that, the variation of K along the embankment elevation is not similar in all the embankment heights considered. Irrespective of presence or absence of basal geogrid, in 5 m, 4 m, and 3 m high embankments, K values above soil are always greater than the K values above piles. It is also observed from Fig.6.30 that, the K values above pile and above soil cross each other at different elevations in each embankment heights considered. Also the K values above pile and above soil cross each other at different elevations for the same height embankment with and without basal geogrid. This indicates that the formation of soil arches due to stiffness variation of foundation soil and piles under seismic excitations is not uniform along the various embankment heights like in static loading conditions. The inclusion of basal geogrid will also changes the variation of K values along the embankment height.

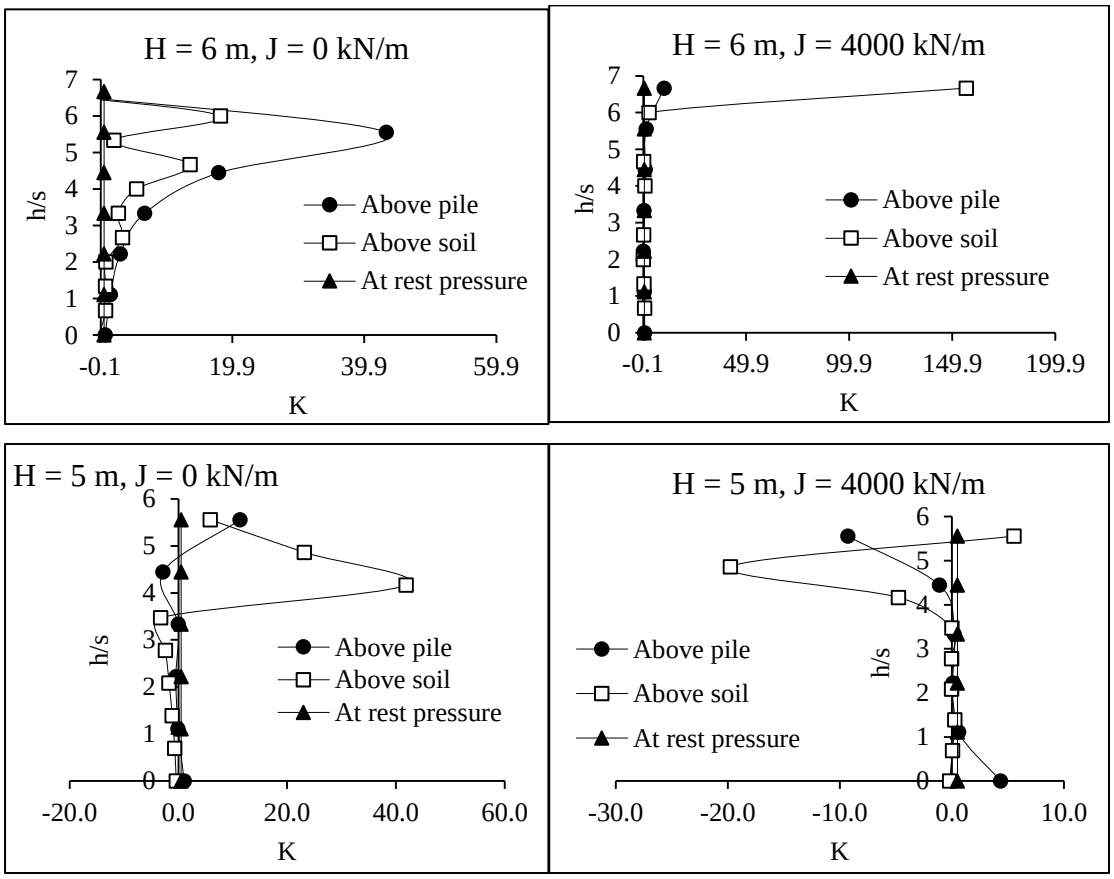

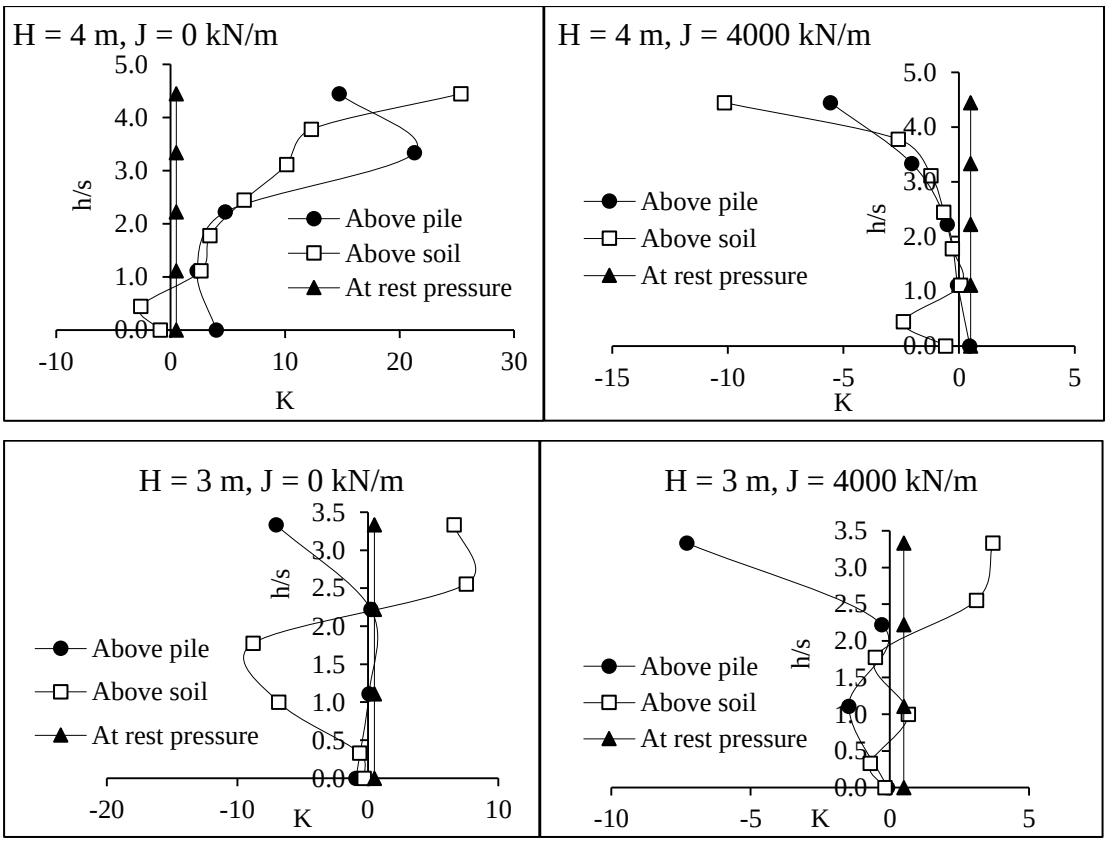

Figure 6.30 Effect of embankment height on K along embankment elevation

Figure 6.31 presents the variation of K along embankment elevation for floating pile (22 m, 24 m & 26 m) supported embankments with and without basal geogrid subjected to IS (0.35 g) ground motion. 6 m high embankment supported over 3D spaced piles is considered to study the effect of pile length on K taken at the instant of occurrence of PGA. The variation of K above soil along embankment elevation is more for 22 m long pile supported embankment. Increase in pile length reduces the variation K above soil along embankment elevation. The variation of K above pile is nearly equal to at rest pressure value (0.5) except at embankment top level.

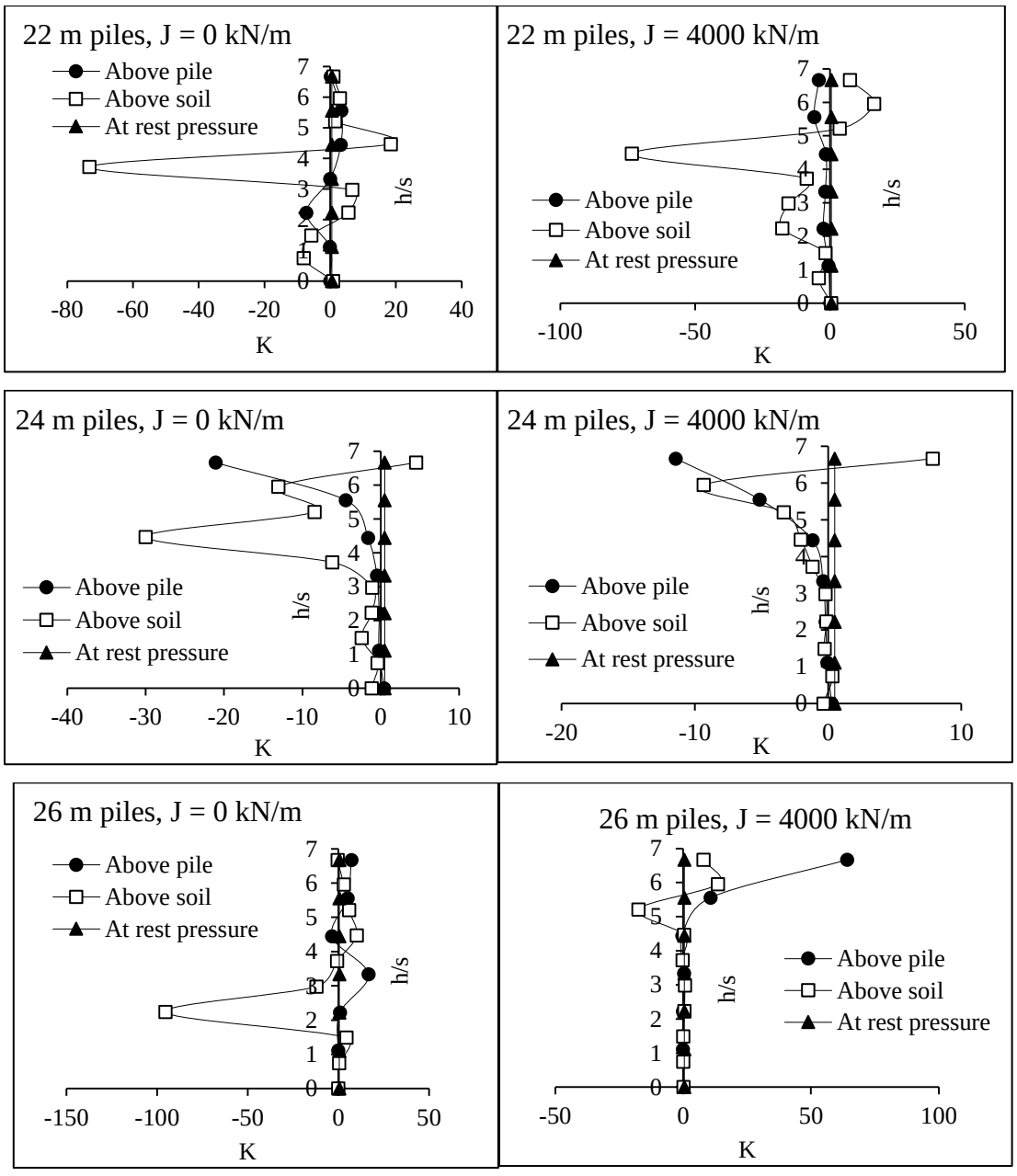

Figure 6.31 Effect of pile length on K along embankment elevation

Figure 6.32 shows the variation of K along embankment elevation considering the effect of pile spacing with and without basal geogrid subjected to IS (0.35 g) ground motion. 6 m high embankment supported over 28 m piles is considered to study the effect of pile spacing on K taken at the instant of occurrence of PGA. From Fig.6.32 it is observed that the increase in pile spacing increases the K value above pile in the presence or absence of basal geogrid. The variation of K value along the embankment elevation is different in each pile spacing arrangements subjected to seismic excitations.

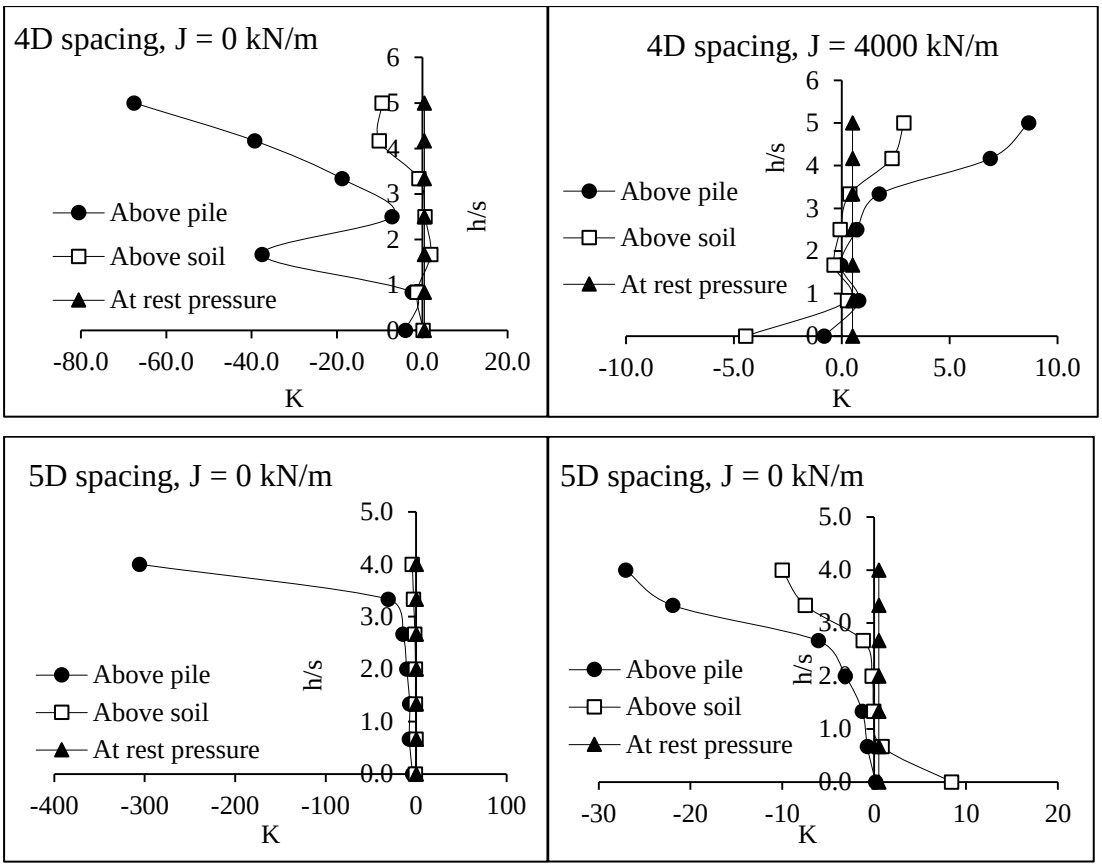

Figure 6.32 Effect of pile spacing on K along embankment elevation

6.13 PORE WATER PRESSURE VARIATION UNDER SEISMIC LOADING CONDITIONS

Figure 6.33 shows the pore water pressure contour (in N/m^2) for 6 m high basal geogrid reinforced pile-supported embankment subjected to IS (0.35 g) ground motions taken at the instant of occurence of PGA. Since the foundation soil is very soft clay, from the present study it was found that the liquefaction possibilities are very less or not there.

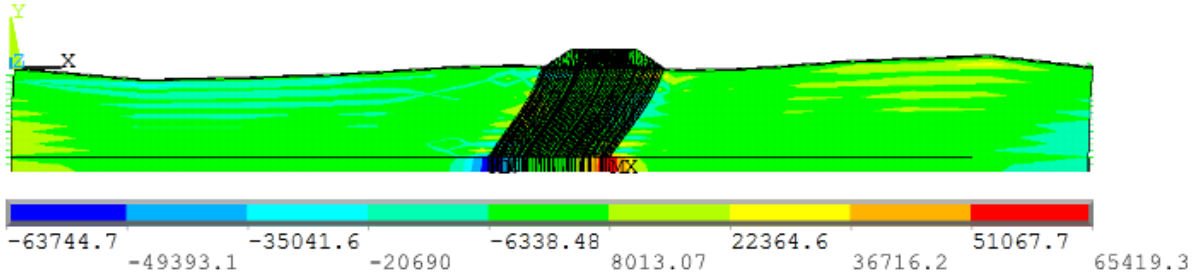

Figure 6.33 Pore water pressure contour under seismic excitations

6.14 LATERAL DISPLACEMENT CONTOURS FOR DIFFERENT EMBANKMENT CASES

Figs. 6.34 (a)- 6.34 (d) shows the lateral displacements (in m) of 6 m high embankment with different types of improvement cases considered subjected to IS ground motion. From these figures it is observed that addition of geogrid and piles could able to reduce the lateral displacements more effectively.

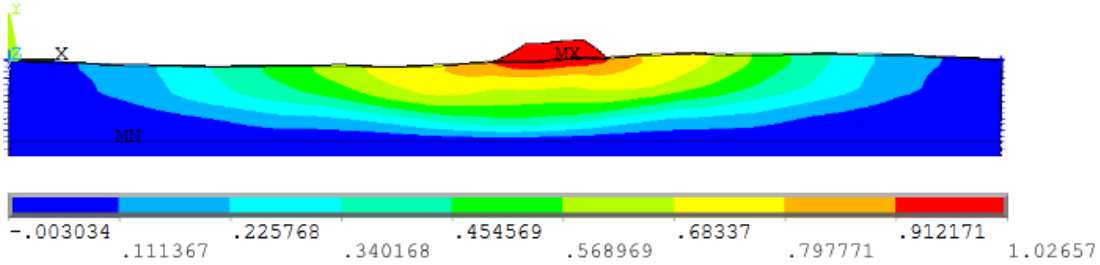

(a) Lateral displacement of 6m Embankment without piles and geogrid

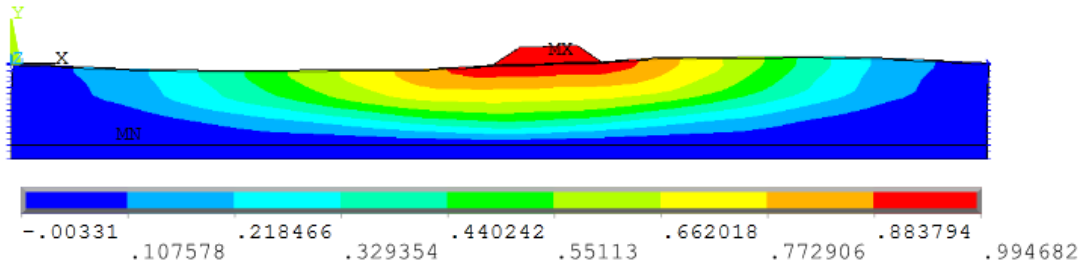

(b) Lateral displacement of 6m Embankment with geogrid

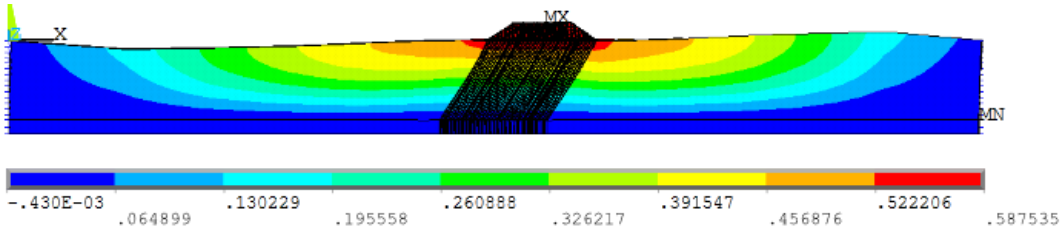

(c) Lateral displacement of 6m Embankment with 28 m piles

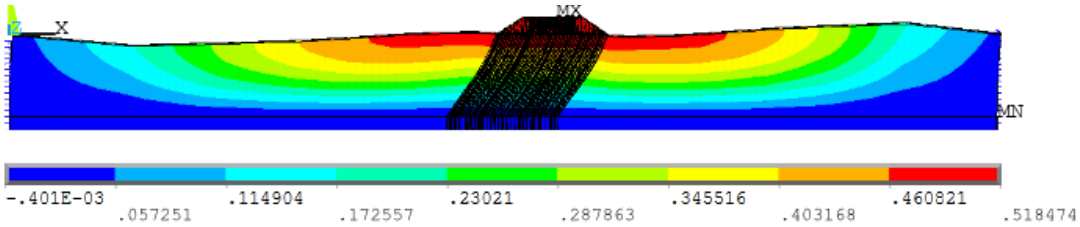

(d) Lateral displacement of 6m Embankment with geogrid and 28 m piles

Figure 6. 34 Lateral displacement contours for different embankment cases

6.17 SUMMARY

Time-history analysis of basal geogrid-reinforced pile supported embankments was performed and results were analysed in this chapter. A detailed parametric study was conducted on 3-dimensional finite element models of embankments considering the effect of embankment height, basal geogrid tensile modulus, pile length, pile spacing, type of pile and type of seismic loads. Embankment lateral displacements, lateral accelerations at crest, differential settlements at crest, vertical and lateral stress distribution between piles and foundation soil and the coefficient of lateral pressure along embankment were analysed under seismic excitations.

The study revealed that the embankment height is an important parameter to consider in the seismic design of basal geogrid reinforcement. For (H/s) less than or equal to 4.5, basal geogrid tensile modulus of 3000 kN/m is sufficient to distribute vertical stresses on pile foundations and soft foundation soil and for (H/s) greater than 4.5, increase in basal geogrid tensile modulus increases the vertical stresses on piles. 4 m high embankment experiences very less differential settlements caused by seismic excitations among the different embankment heights considered. About 8 % reduction of toe lateral displacements are observed by the addition of basal geogrid. The addition of pile supports reduces 40.8 % and the combination of both pile supports and basal geogrid reduces about 46 % of toe lateral displacements. Addition of basal geogrid increases both vertical and lateral stresses on piles due to seismic excitations. The variation of coefficient of lateral pressure along the embankment elevation is random for the considered parameters, this indicates that the formation of soil arching in a geogrid reinforced pile supported embankment subjected to seismic loading is not uniform like what is generally observed under self-weight.

CHAPTER 7

RESPONSE VARIATION OF BASAL GEOGRID-REINFORCED EMBANKMENTS SUBJECTED TO STATIC AND SEISMIC LOAD

7.1 INTRODUCTION

The use of geosynthetic reinforcement at the base level of the embankment is a suitable solution for shallow compressible subsoils. The addition of basal geosynthetic improves the shear resistance of both embankment as well as foundation soil. This chapter presents the results obtained from the finite element analysis of basal geosynthetic-reinforced embankments subjected to static and seismic loading. Time-history analyses was performed to examine the behaviour of basal geosynthetic-reinforced embankments with various width of geosynthetic. Parametric study was carried out by varying the width of basal geogrid, geogrid tensile modulus, embankment height, slope of embankment, Young's modulus of embankment fill and Young's modulus of foundation soil. The optimum width of basal geogrid is identified based on crest settlements, toe lateral displacements and lateral displacements at the crest.

7.2 UNDER STATIC LOAD

7.2.1 Effect of basal geogrid stiffness

Figure 7.1 presents the effect of geogrid tensile modulus on crest centre settlements for 6 m high embankment having 1V:1H side slope subjected to static loading. Increase in basal geogrid tensile modulus reduces the crest centre settlements. For geogrid tensile modulus above 500 kN/m, the crest centre settlements observed are very less (Fig.7.1). Increase in geogrid tensile modulus from 0 kN/m to 50 kN/m reduces about 11 % of crest centre settlements. Also, increase in geogrid tensile modulus from 0 kN/m to 100 kN/m, 250 kN/m, and 500 kN/m reduces about 13 %, 14.6 % and 15.25 % of crest centre settlements. Less than 0.5 % reduction of crest centre settlements are observed with increase in geogrid tensile modulus beyond 500 kN/m.

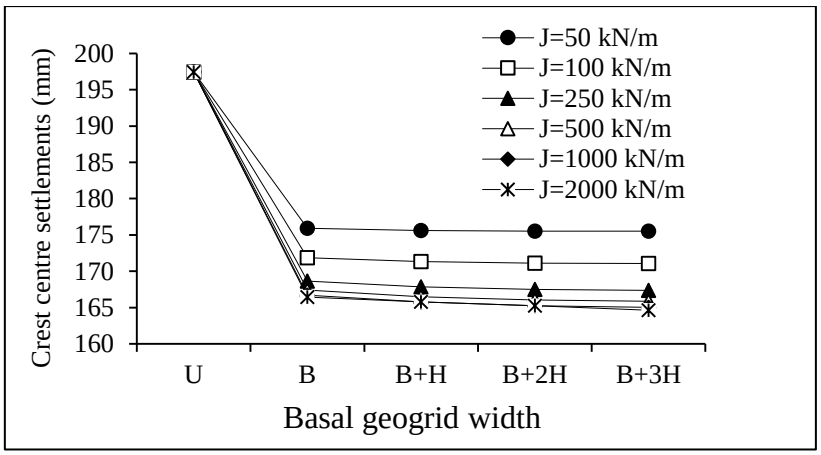

Figure 7.1 Effect of basal geogrid stiffness on crest centre settlements

Figure 7.2 shows the effect of basal geogrid stiffness on differential settlements at embankment crest. Differential settlements also reduce with an increase in geogrid tensile modulus. The differential settlements are nearly zero for geogrid of tensile modulus above 500 kN/m. About 10 % reduction of differential settlements are observed by increasing the basal geogrid tensile modulus from 50 kN/m to 100 kN/m and 100 kN/m to 250 kN/m. Further increase in geogrid tensile modulus from 250 kN/m to 500 kN/m reduces about 4 % of differential settlements. Less than 2 % reduction of differential settlements are observed with the increase of basal geogrid tensile modulus beyond 500 kN/m.

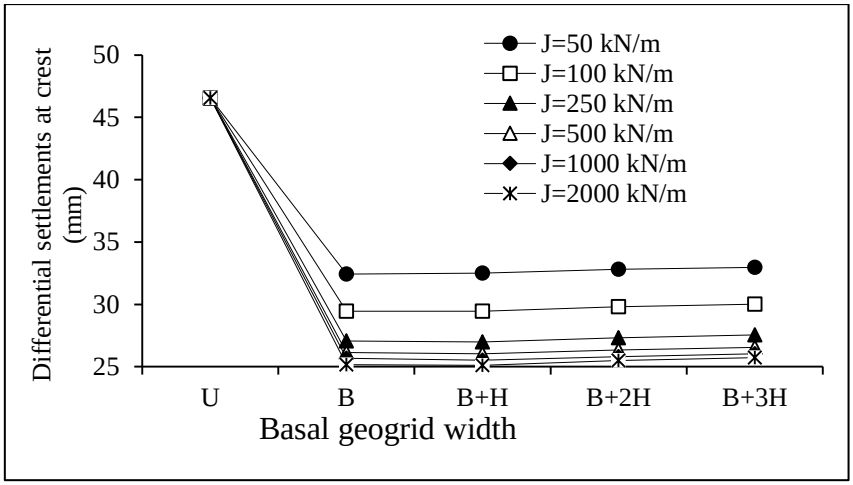

Figure 7.2 Effect of basal geogrid stiffness on differential settlements at crest

Toe lateral displacements reduction with increase in geogrid tensile modulus is observed from Fig.7.3. Provision of extra-wide geogrid more than base width of embankment (B) is not needed to reduce the toe lateral displacements further (Fig.7.3).

60 % to 80 % reduction in toe lateral displacements are observed by increasing the basal geogrid tensile modulus from 50 kN/m to 100 kN/m and 100 kN/m to 250 kN/m. Further reduction of about 35 % in toe lateral displacement is observed by increasing the geogrid tensile modulus from 250 kN/m to 500 kN/m. Further increase in tensile modulus above 500 kN/m reduces about 4 % of toe lateral displacements

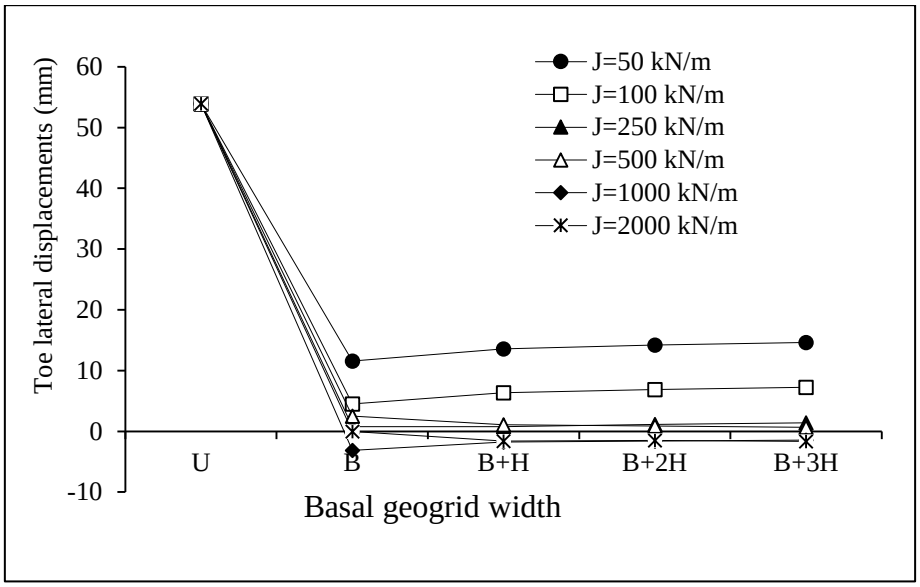

Figure 7.3 Effect of basal geogrid stiffness on toe lateral displacements

Based on these findings the basal geogrid with tensile modulus of 500 kN/m has been selected for analysing the response variation due to other parameters.

7.2.2 Effect of foundation soil stiffness

Figure 7.4 depicts the effect of stiffness of foundation soil on settlements at crest centre considering the basal geogrid width and embankment side slope under static loading conditions. 6 m high embankment having basal geogrid of 500 kN/m tensile modulus was considered to study the effect of foundation soil stiffness. From Fig.7.4 it is noticed that increase in foundation soil stiffness reduces the crest centre settlements. About 65 %, 75 % and 82% reduction of crest centre settlements are observed by changing the FS1foundation soil to FS2, FS3 and FS4 (Table 4.4) irrespective of embankment side slope. About 15.2 %, 11.92 %, 10 % and 6.8 % crest centre settlement reduction is observed by the addition of basal geogrid of width ‘B’ in FS1, FS2, FS3 and FS4 foundation soils. Further increase in geogrid width do not reduce embankment crest settlements. This shows that the provision of basal geogrid is no longer required for stiffer foundation soils (FS4) irrespective of embankment side slopes.

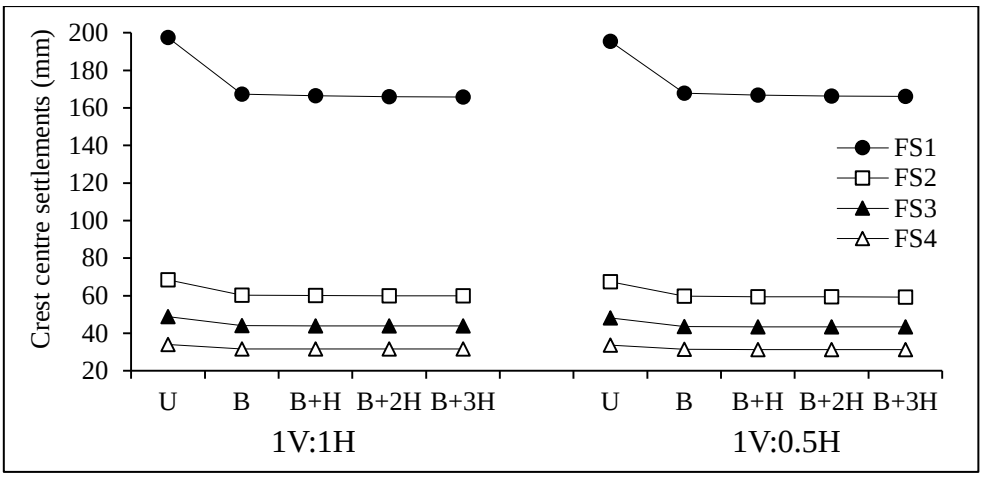

Figure 7.4 Effect of foundation soil stiffness on crest centre settlements

Similar as crest centre settlements, differential settlements (Fig.7.5) and toe lateral displacements (Fig.7.6) also reduce with increase in foundation soil stiffness. It is also observed from Fig.7.5 and Fig.7.6 that, the basal geogrid width equal to the base width of embankment (B) is sufficient to reduce the displacements. Further increase in width of basal geogrid will not have any influence in reducing the displacements caused by static loads. About 86 % and 87 % reduction of differential settlements are observed in 1V:1H and 1V:0.5H side slope by changing the foundation soil stiffness FS1to FS4.

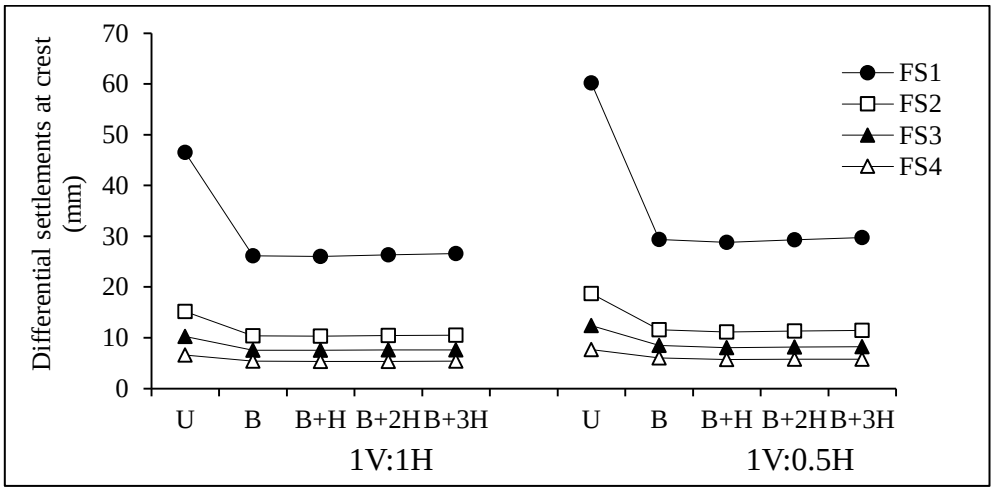

Figure 7.5 Effect of foundation soil stiffness on differential settlements at crest

Maximum reduction of toe lateral displacements (>95%) are observed by the addition of basal geogrid of width ‘B’ for the considered foundation soil stiffness and embankment side slope (Fig.7.6).

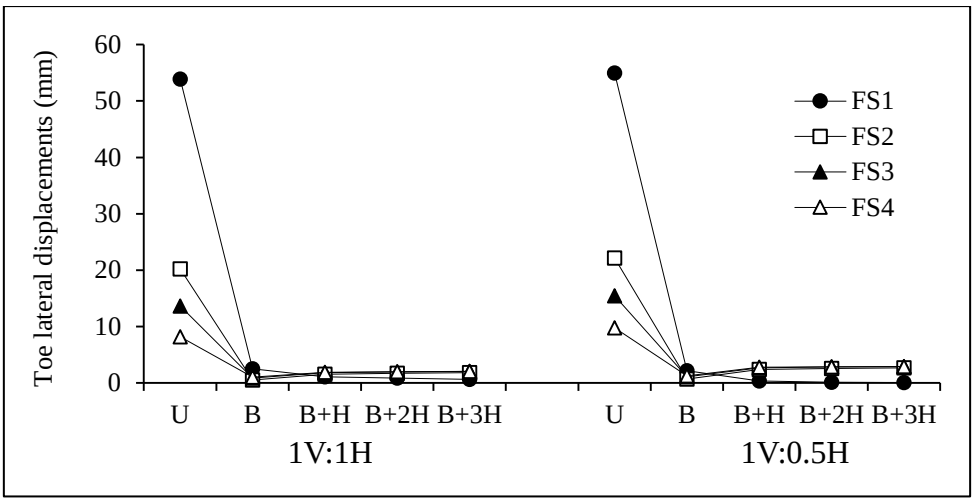

Figure 7.6 Effect of foundation soil stiffness on toe lateral displacements

7.2.3 Effect of embankment soil stiffness

Figure 7.7 presents the effect of embankment soil stiffness on crest centre settlements for 6 m high embankment having 1V:1H side slope with basal geogrid tensile modulus of 500 kN/m. From Fig.7.7 it is observed that, the increase in embankment soil stiffness reduces the crest centre settlements. About 5 %, 8 % and 10 % reduction in crest settlements are observed by varying the embankment stiffness from ES1 to ES2, ES3 and ES4 (Table 4.4). Also, irrespective of embankment soil stiffness, the addition of basal geogrid reduces the settlements (15 %) at crest centre.

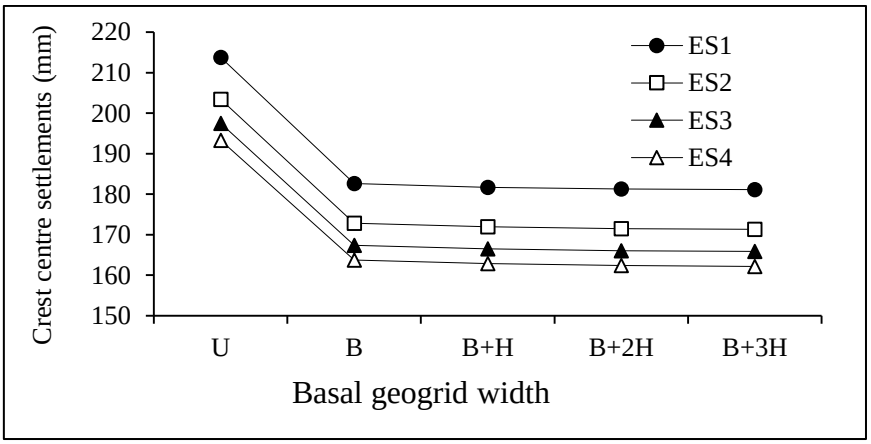

Figure 7.7 Effect of embankment soil stiffness on crest centre settlements

Like crest centre settlements, differential settlements also reduce with increase in embankment soil stiffness and the addition of basal geogrid further reduces the differential settlements (40% to 45 %) at crest subjected to static loads (Fig.7.8).

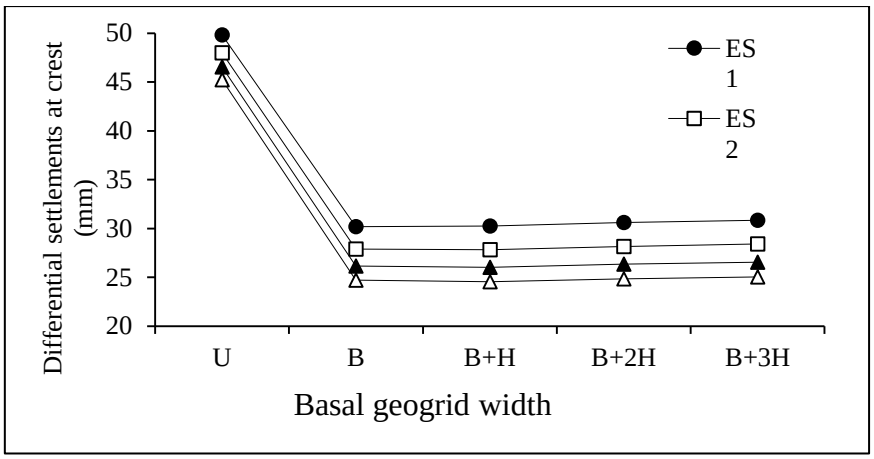

Figure 7.8 Effect of embankment soil stiffness on differential settlements at crest

Figure 7.9 shows the effect of embankment soil stiffness on toe lateral displacements. The embankment soil stiffness has some influence (7 % to 15 %) on toe lateral displacements only in the absence of basal geogrid. Addition of basal geogrid having width equal to the bottom width of embankment (B) is optimum to reduce (>95 %) toe lateral displacements while the embankment is subjected to static loading (Fig.7.9).

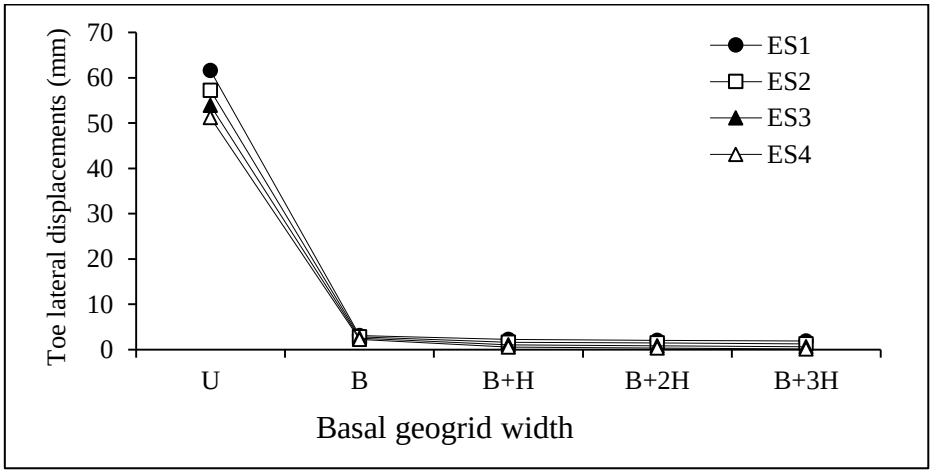

Figure 7.9 Effect of embankment soil stiffness on toe lateral displacements

7.2.4 Effect of height of embankment

Effect of embankment height on crest centre settlements having basal geogrid tensile modulus of 500 kN/m and 1V:1H side slope with ES3 and FS1 is shown in Fig.7.10. It is observed from Fig.7.10 that, the increase in embankment height increases the crest centre settlements. For 4 m and 6 m high embankments, nearly 10 % and 15 % reduction in settlement is observed by adding the basal geogrid. About 17

% settlement reductions are observed for both 8 m and 10 m high embankments by the addition of basal geogrid.

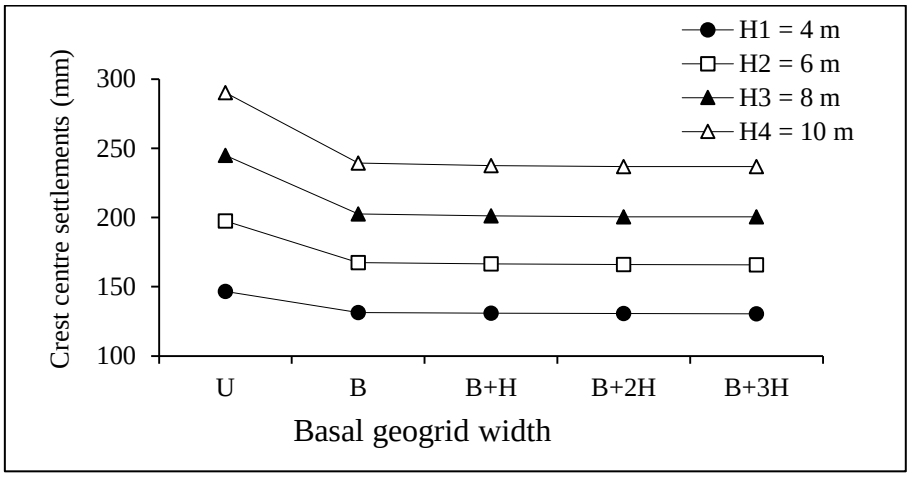

Figure 7.10 Effect of embankment height on crest centre settlements

Figure 7.11 gives the differential settlements for various embankment heights. Differential settlements at crest for 4 m high embankment with basal geogrid are almost zero (Fig.7.11). This is due to less embankment height; the embankment weight acting on the foundation soil is less as compared with the other embankment heights considered. Hence the provided basal geogrid (J = 500 kN/m) is sufficient to withstand and spread the embankment weight evenly to the foundation soil. This results in negligible differential settlements in 4 m high embankment. For 6 m, 8 m and 10 m high basal geogrid-reinforced embankments, the differential settlements are almost same (Fig.7.11).

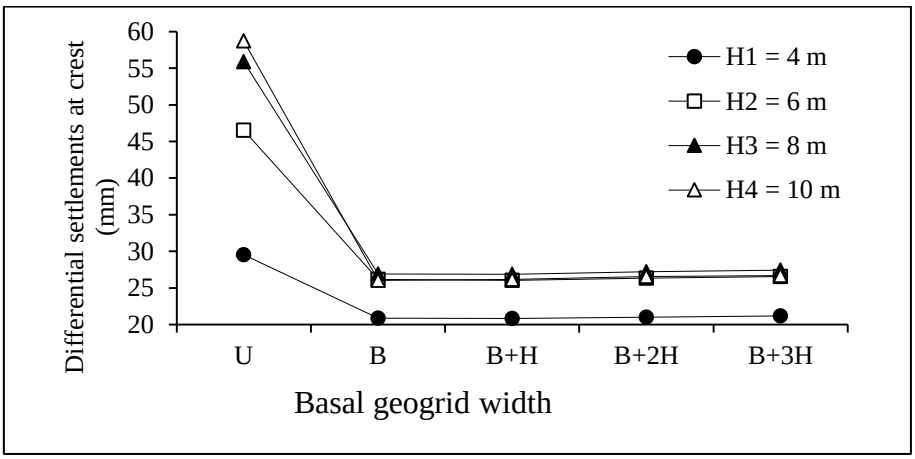

Figure 7.11 Effect of embankment height on differential settlements at crest

Variation of toe lateral displacements with embankment height and basal geogrid width is seen in Fig.7.12. Addition of basal geogrid reduces the toe lateral displacements to almost zero irrespective of the embankment height (Fig.7.12).

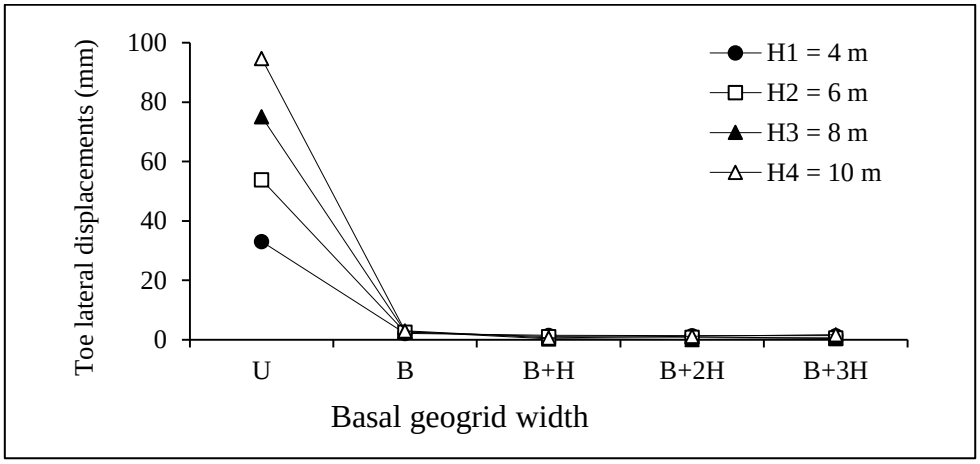

Figure 7.12 Effect of embankment height on toe lateral displacements

7.2.5 Vertical deformation plots under static loading

Figure 7.13 depicts the vector plot of settlements in a 6 m high embankment with ES3 and FS1 having 1V:1H side slope with and without basal geogrid reinforcement of different width subjected to static loading. The deformation profile of the embankments for various width of geogrid are clearly seen here. From Fig.7.13 it is observed that, the addition of basal geogrid reduces the vertical displacements. About 15 % reduction in vertical displacements are seen by the addition of basal geogrid of width 'B'. Further increase in basal geogrid width is ineffective in reducing the vertical displacements under static loading conditions.

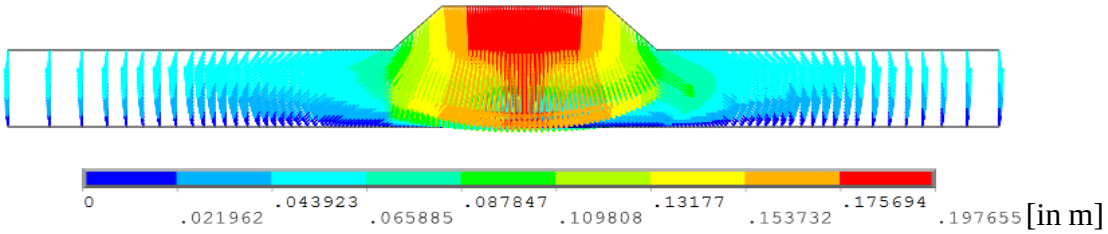

(a) 6 m high unreinforced embankment

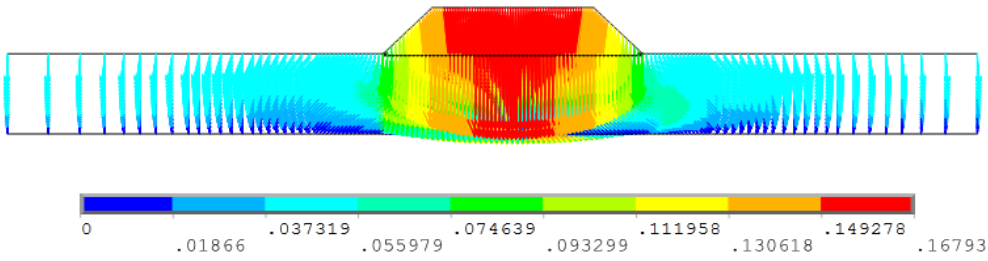

(b) 6 m high embankment having basal geogrid of width B

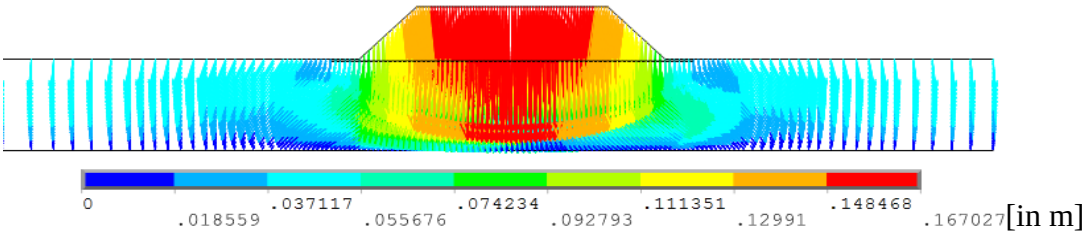

(c) 6 m high embankment having basal geogrid of width B+H

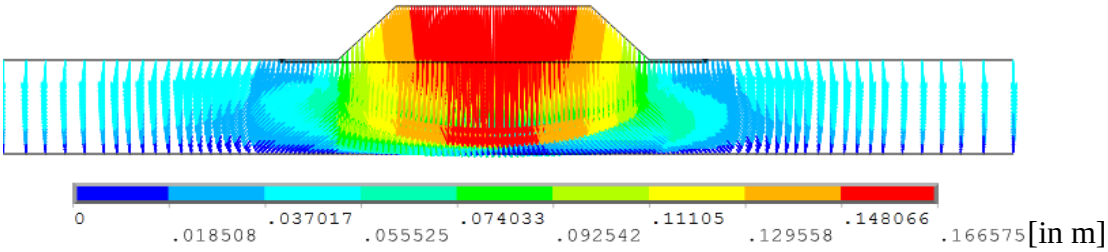

(d) 6 m high embankment having basal geogrid of width B+2H

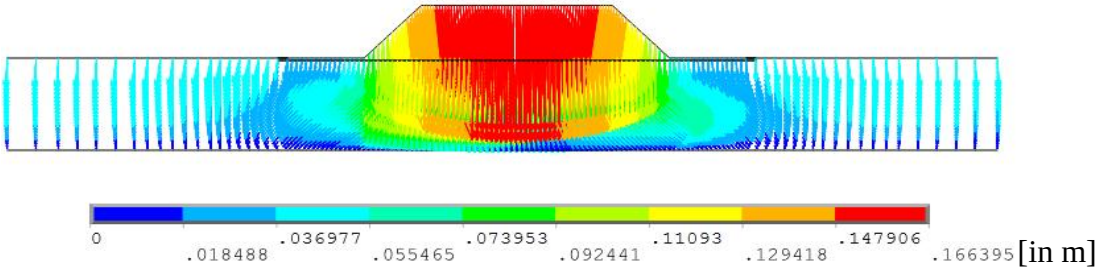

(e) 6 m high embankment having basal geogrid of width B+3H

Figure 7.13 Vector plot of vertical deformations in 6 m high unreinforced and reinforced embankment subjected to static loading

7.3 UNDER FREE VIBRATION AND SEISMIC LOADING

7.3.1 Variation in Natural Frequency

The equation for fundamental period of embankment as given in IS 1893(Part 5):1984 is

$$T = 2.9H\sqrt{\frac{\rho}{G}} \qquad (7.1)$$

Where; T is the fundamental period in s. $T = \frac{1}{f}$

f is the natural frequency in Hz.

H is the embankment height in m.

ρ is the mass density of embankment fill in kg/m^3

G is the shear modulus of embankment fill in N/m^2

Eq. (7.1) assumes that the embankment rests over a rigid base.

The natural frequencies were obtained for 6 m high embankment having 1V:1H side slope with ES3 and different foundation soil stiffness and different basal geogrid (J = 500 kN/m) width. Fig. 7.14 (a) depicts the natural frequency variation with the foundation soil stiffness obtained from finite element analysis. It is observed from Fig.7.14 (a) that, the increase in foundation soil stiffness increases the natural frequency of the embankment. But the natural frequency calculated using Eq. (7.1) is 3.67 Hz. Since the equation assumes that the embankment rests over rigid base and ignores the presence of basal geogrid, the natural frequency obtained from Eq. (7.1) is high as compared to the natural frequency obtained from numerical simulations. Thus Fig. 7.14 (a) shows that the stiffness of foundation soil has considerable effect (upto 80 % in FS1) on dynamic characteristics of the embankment.

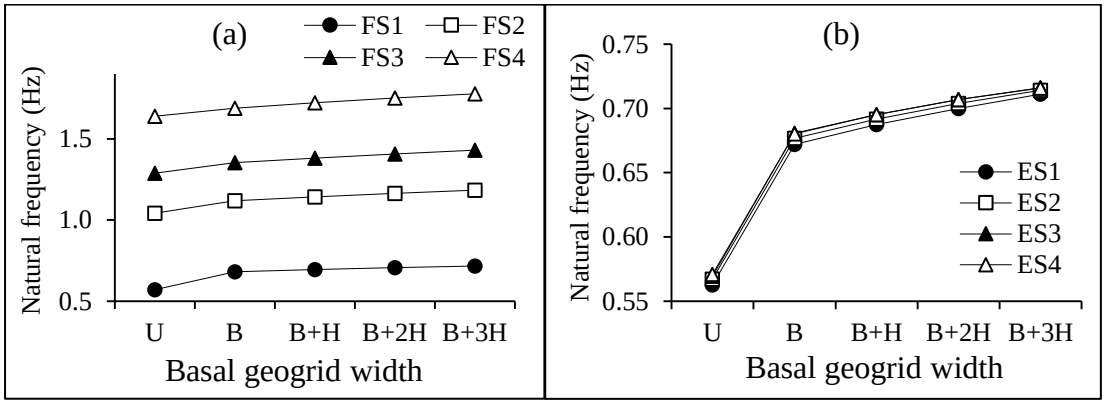

Figure 7.14 Natural frequency variation with (a) Foundation soil stiffness (b) Embankment soil stiffness

Figure 7.14 (b) shows the natural frequency variation with the embankment soil stiffness. The natural frequency was obtained for 6 m high embankment having 1V:1H side slope with FS1 and different embankment soil stiffness and different basal geogrid (J = 500 kN/m) width. The effect of stiffness of embankment soil is much less as compared to foundation soil stiffness on the natural frequency. The natural

frequencies obtained from numerical analysis (Fig.7.14 (b)) are lower as compared with the natural frequencies calculated using Eq. (7.1) and seen in Table 7.1. This is due to the consideration of supporting subsoil in numerical analysis. The addition of geogrid increases the natural frequency and the increase in width of geogrid causes slightly higher natural frequency.

Table 7. 1 Natural frequency as per Eq. (7.1) for various embankment soil stiffnesses

Notation	Embankment soil Young's modulus	Natural frequency from Eq.(7.1)
	MN/m^2	Hz
ES1	10	2.6
ES2	15	3.18
ES3	20	3.67
ES4	25	4.10

Figure 7.15 (a) shows the natural frequency variation with the basal geogrid stiffness for 6 m high embankment having ES3, FS1 and 1V:1H side slope. Increase in geogrid tensile modulus increases the natural frequency. For J = 1000 kN/m and above, negligible increase in natural frequencies are observed (Fig.7.15 (a)).

Increase in embankment side slope causes negligible increase in the natural frequency of the embankment (Fig.7.15 (b)). Eq. (7.1) also does not account for the effect of the embankment side slope. Hence, from the numerical analysis it is found that the effect of side slope on the natural frequency of the embankment is insignificant for the considered range of side slopes in embankments.

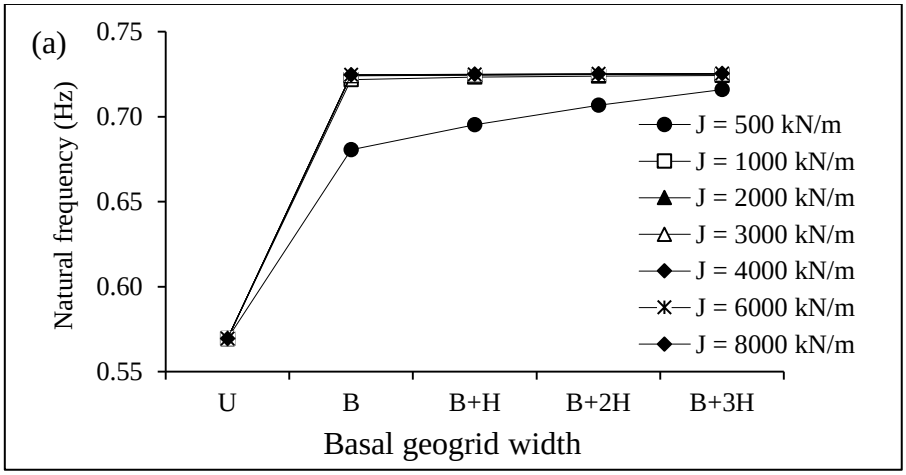

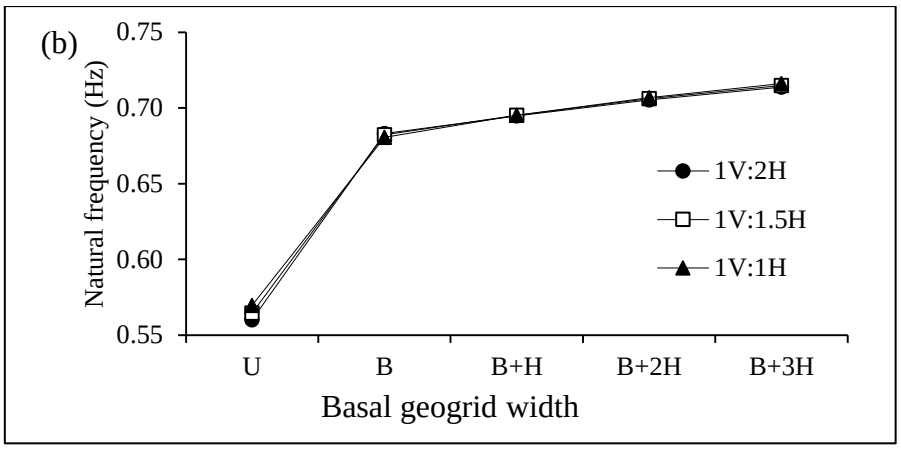

Figure 7.15 Natural frequency variation with (a) Basal geogrid stiffness (b) Embankment side slope

Table 7.2 presents the natural frequency for various embankment heights calculated using Eq.(7.1). Fig.7.16 shows the natural frequency variation with embankment height and basal geogrid width obtained from numerical analysis. Since Eq.(7.1) assumes the embankment rests over rigid base, the natural frequency values obtained using Eq. (7.1) are high compared to Fig.7.16.

In general it is seen that there is considerable difference in the natural frequency of reinforced and unreinforced embankments. The foundation soil stiffness, geogrid tensile modulus, slope and height of embankment influences the natural frequency of embankments

Table 7. 2 Natural frequency as per Eq. (7.1) for various embankment heights

Embankment Height	Natural frequency from Eq.(7.1)
m	Hz
4	5.5
6	3.67
8	2.75
10	2.2

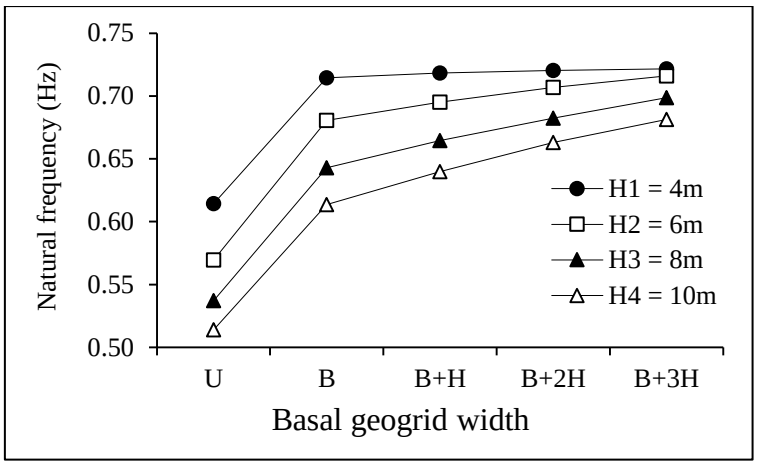

Figure 7.16 Natural frequency variation with embankment height

7.3.2 Lateral Displacement Reduction Ratio

In order to study the effect of basal geogrid width on embankment crest lateral displacements, a parameter Lateral Displacement Reduction Ratio (LDRR) is introduced. LDRR is defined as the lateral displacement of unreinforced embankment to the lateral displacement of basal geogrid-reinforced embankment measured at the instant (t) of peak lateral displacement of unreinforced embankment.

i.e; $$\text{LDRR} = \frac{\text{UR}_x}{\text{R}_x} \tag{7.2}$$

Where; UR_x is the peak lateral displacement of unreinforced embankment at time 't' and

R_x is the lateral displacement of basal geogrid-reinforced embankment at time 't'.

Figure 7.17 shows the variation of LDRR at crest edge with foundation soil stiffness for 6 m high embankment having 1V:1H side slope and ES3 reinforced with a basal geogrid having tensile modulus of 500 kN/m subjected to IS Zone III ground motion with a PGA of 0.1 g. From Fig.7.17 it is observed that, LDRR is more for very soft foundation soil (FS1) and LDRR is less than 1 and almost parallel to abscissa for stiff foundation soil (FS4). This means the addition of basal geogrid is more effective in very soft foundation soils and stiffer foundation soils don't require any basal reinforcement. The LDRR for FS2 is slightly less when compared to the LDRR values of FS3 with increase in basal geogrid width. This maybe due to the natural frequency of embankment resting over FS2 type foundation soil (Fig.7.14 (a)) nearly matches with the high amplitude frequency content (1.1 Hz) of the ground motion as seen from the Fourier spectrum (Fig.4.9 (b)).

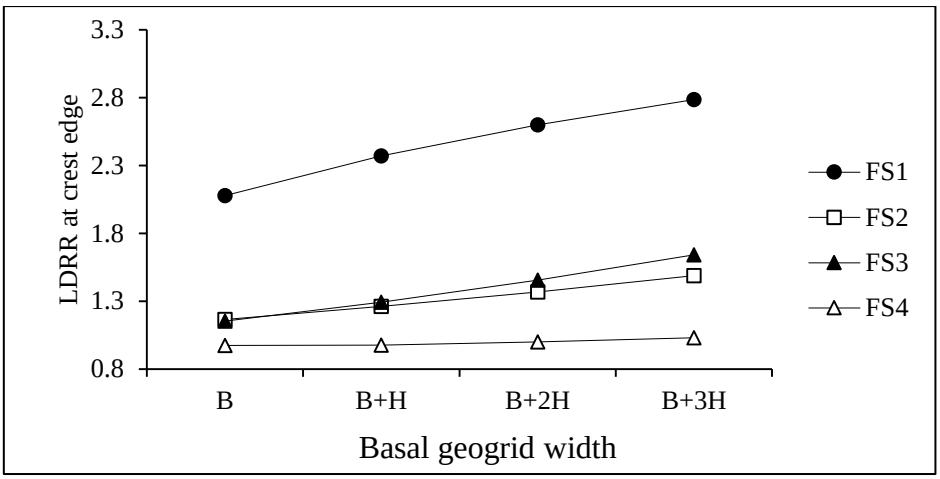

Figure 7.17 LDRR variation with foundation soil stiffness

The variation of LDRR with embankment soil stiffness for 6 m high, 1V:1H side sloped, basal geogrid (J = 500 kN/m) reinforced embankment resting over FS1 soil is depicted in Fig.7.18. From Fig.7.18 it is observed that the LDRR is very less for embankment with ES1 soil. Also increase in embankment soil stiffness increases the LDRR at crest edge and reaches the maximum for ES3 soil and further increase in embankment soil stiffness does not vary the LDRR. It is also observed from Fig.7.18 that the LDRR values increase with the increase in basal geogrid width irrespective of embankment soil stiffness.

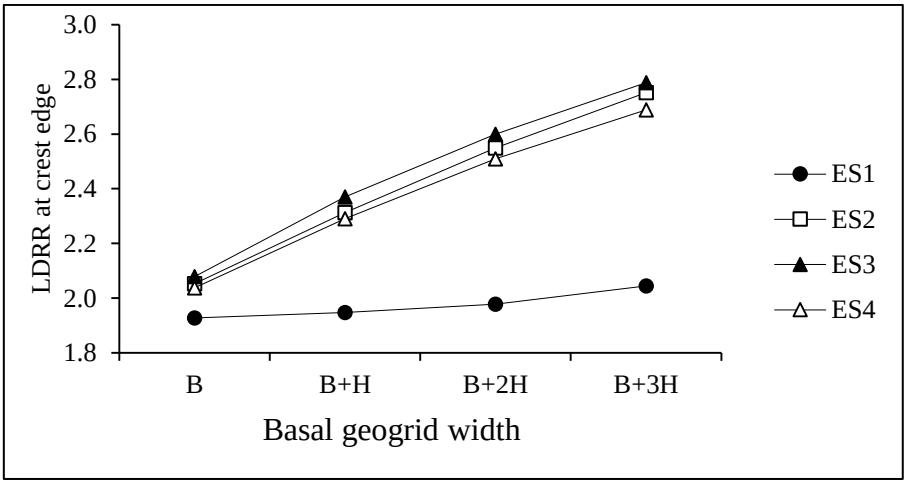

Figure 7.18 LDRR variation with embankment soil stiffness

Figure 7.19 shows the variation of LDRR with basal geogrid stiffness for 6 m high embankment having 1V:1H side slope, ES3 and FS1 soils subjected to IS Zone III ground motion. For geogrid tensile modulus upto 3000 kN/m, increase in basal geogrid width increases the LDRR at crest edge. For geogrid tensile modulus of 4000

kN/m, the LDRR increases upto the geogrid width equal to 'B+H' and further increase in width doesn't vary the LDRR value. For geogrid tensile modulus above 4000 kN/m, increase in basal geogrid width more than 'B+H' reduces the LDRR value (Fig.7.19). From Fig.7.19, it can be inferred that the basal geogrid having tensile modulus of 4000 kN/m and width of 'B+H' is best suited for reducing the lateral displacements at crest edge to the maximum. Similar trend in LDRR is seen even for embankment having shallow slope of 1V:2H (Fig.7.20).

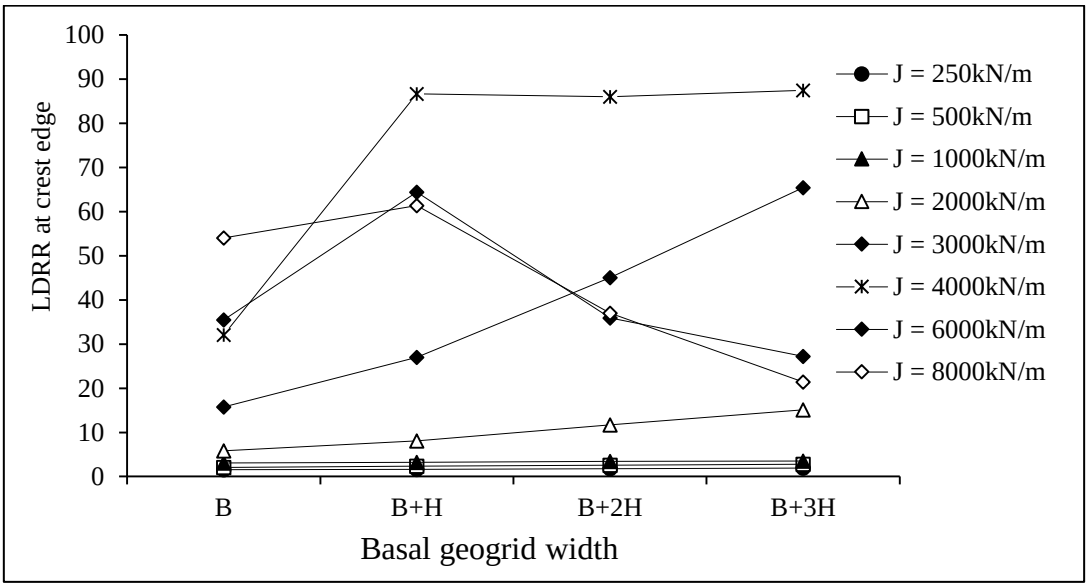

Figure 7.19 LDRR variation with basal geogrid stiffness

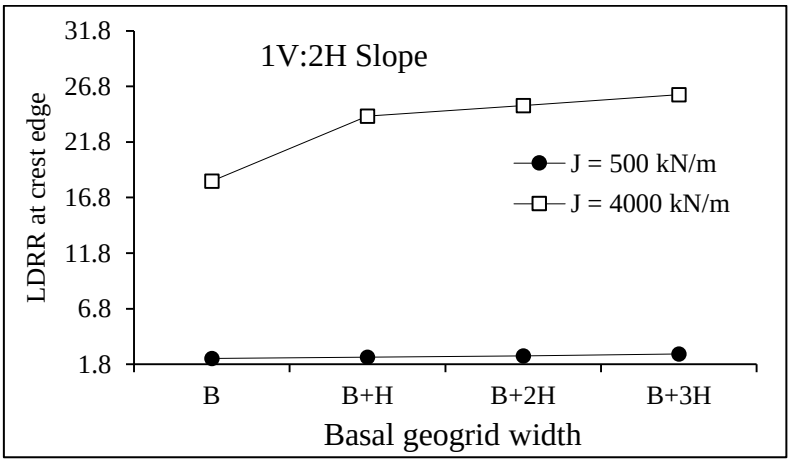

Figure 7.20 LDRR variation with basal geogrid stiffness for 1V:2H slope subjected to IS Zone III ground motion

Fig.7.21 shows the LDRR results of embankments with 1 layer of basal geogrid of 4000 kN/m tensile modulus as compared to those with 4 layers of basal geogrid of 1000 kN/m tensile modulus. In both the cases, 6 m high embankment made of ES3 soil

having 1V:1H side slope supported over FS1 foundation soil subjected to IS Zone III ground motion is considered. From Fig.7.21 it is observed that, the LDRR values for 4 layers basal geogrid-reinforced embankment are higher than the LDRR values of single layer basal geogrid-reinforced embankment irrespective of the basal geogrid width. About 20 % increase in LDRR values are observed in 4 layers basal geogrid-reinforced embankment compared to single layer basal geogrid-reinforced embankment. Similar to the response in the case of single layer basal geogrid-reinforced embankment, the LDRR values in 4 layers geogrid-reinforced embankment increases upto a basal geogrid width of 'B+H' and further increase in basal geogrid width leads to negligible increase in LDRR value.

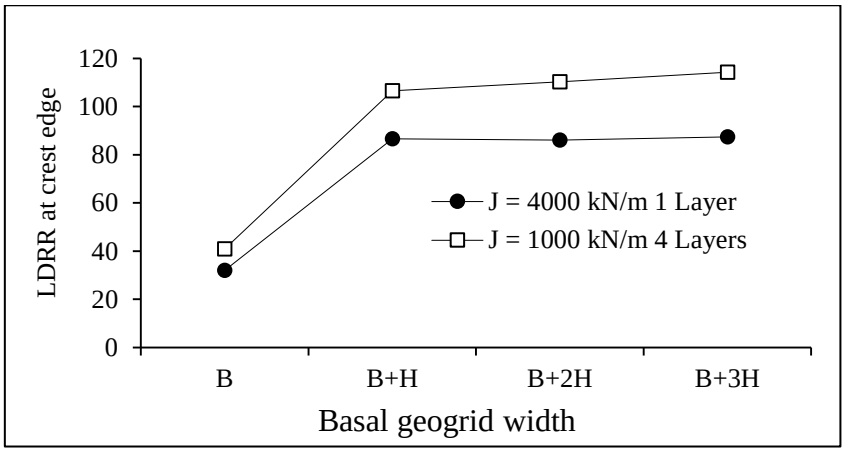

Figure 7.21 LDRR variation with number of basal geogrid layers for 1V:1H slope subjected to IS Zone III ground motion

Figure 7.22 shows the variation of LDRR with various ground motion intensity for 6 m high embankment having 1V:1H side slope constructed with ES3 and supported on FS1 and basal geogrid with 500 kN/m tensile modulus. As the ground motion intensity increases, the lateral displacement in the embankment also increases. But the addition of basal geogrid could reduce the lateral displacements effectively for IS Zone III ground motion intensity than IS (0.35 g) and IS (0.6 g). This is observed by the higher LDRR value for IS Zone III (0.1 g) from Fig.7.23. It is also observed from Fig.7.22 that, the LDRR for IS (0.35 g) and IS (0.6 g) is almost equal; this indicates that the lateral displacement reduction is same at high ground motion intensities.

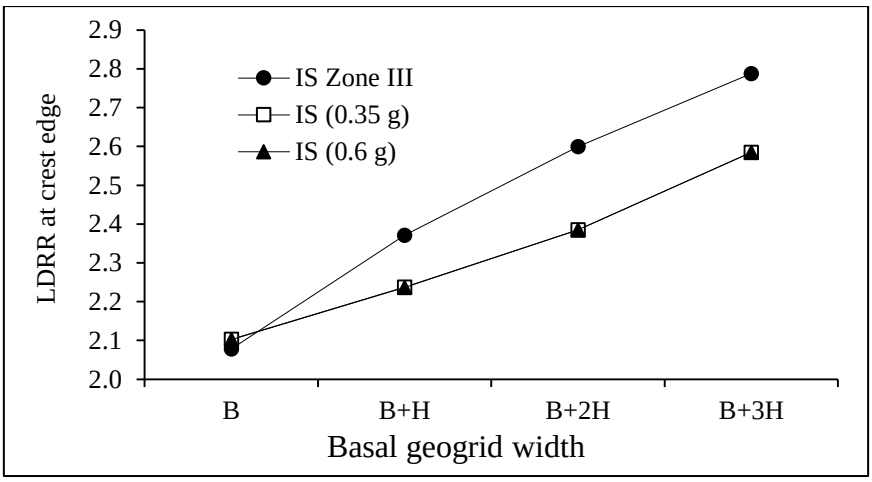

Figure 7. 22 LDRR variation with intensity of ground motions

The effect of embankment side slope on the LDRR value for 6 m high basal geogrid (J = 500 kN/m) reinforced embankment made of ES3 and supported over FS1 soil is presented in Fig.7.23. It is observed from Fig.7.23 that, for the considered side slopes, increase in basal geogrid width increases the LDRR at crest edge. This is because in case of shallow slopes, lateral spread of slope is more likely to occur and less likelihood of face failure of slope. Hence the provision of additional width of basal geogrid beyond the base width of embankment 'B' could reduce lateral displacements further.

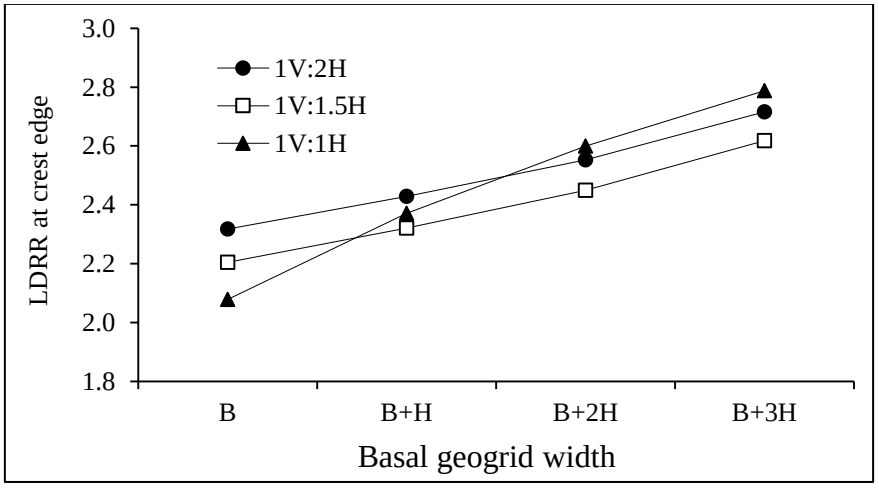

Figure 7. 23 LDRR variation with embankment side slope

Figure 7.24 shows the variation of LDRR with the height of embankment having 1V:1H side slope and basal geogrid tensile modulus of 500 kN/m subjected to IS Zone III ground motion with 0.1g PGA. From Fig.7.24 it is seen that, as the embankment height increases the LDRR value reduces. This is because increased

embankment height increases the lateral displacements hence the LDRR value reduces. It is also observed from Fig.7.24 that in high embankments (8 m and 10 m) the basal geogrid width beyond 'B+H' will not have much effect (< 5%) on LDRR. This could be because the basal geogrid of width 'B+H' provided is able to transfer (and also withstand) the lateral spreading forces of toe, whether it be 6 m high or 10 m high embankment.

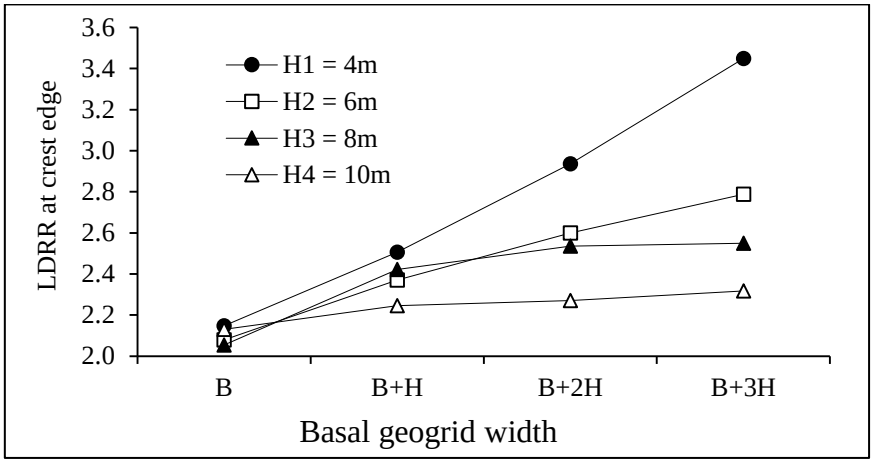

Figure 7. 24 LDRR variation with height of embankment

7.3.3 Toe Lateral Displacements

Figure 7.25 depicts the variation of toe lateral displacements with basal geogrid width and foundation soil stiffness subjected to IS Zone III ground motions with 0.1g PGA. The effect of foundation soil stiffness was analysed for 6 m high 1V:1H side sloped basal geogrid (J = 500 kN/m) reinforced embankment constructed with ES3 soil. From Fig.7.25 it is observed that increase in foundation soil stiffness reduces the toe lateral displacements. In soft foundation soil (FS1) about 48.5 % reduction in toe lateral displacement is observed by the addition of basal geogrid having width 'B'. A toe lateral displacement reduction of 55.2 %, 59.3 % and 54 5 % is observed by the addition of basal geogrid having width equal to 'B+H', 'B+2H' and 'B+3H'. It is also observed from Fig.7.25 that the presence of basal geogrid in stiff foundation soil (FS4) causes a small increase in the toe lateral displacements. About 4.6 % increase in toe lateral displacement is observed by the addition of basal geogrid having width 'B'. An increase of 1.5 % and a reduction of 2.7 % in toe lateral displacement is observed for basal geogrid having width of 'B+H' and 'B+3H'. No difference in toe lateral

displacement is observed for basal geogrid having width ‘B+2H’ compared to the unreinforced case.

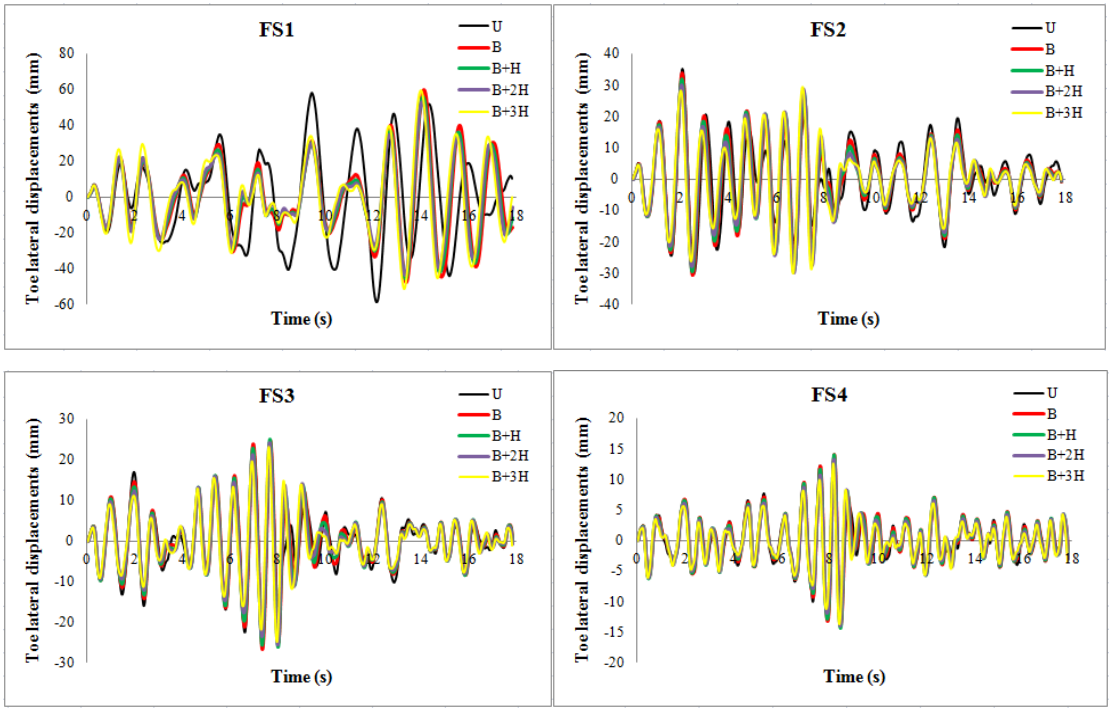

Figure 7. 25 Time-history of toe lateral displacements considering the effect of basal geogrid width and foundation soil stiffness

Figure 7.26 shows the variation of toe lateral displacements with basal geogrid width and embankment soil stiffness. Embankment having 6 m height, 1V:1H side slope and basal geogrid with a tensile modulus of 500 kN/m supported by FS1 soil subjected to IS Zone III ground motion (0.1 g PGA) is considered for the analysis. About 1 % increase in maximum toe lateral displacements are observed with increase in embankment soil stiffness regardless of basal geogrid width. Maximum toe lateral displacements are increased to about 2.2 % when an unreinforced embankment is reinforced with a basal geogrid having width ‘B’. But further increase in basal geogrid width ‘B+H’, ‘B+2H’ and ‘B+3H’ reduces the maximum toe lateral displacements to about 3.5 %, 8.5 % and 13.5 % respectively, irrespective of embankment soil stiffness (Fig.7.26). This indicates that the basal geogrid width to reduce the toe lateral displacements under seismic excitations should be more than the base width (B) of the embankment.

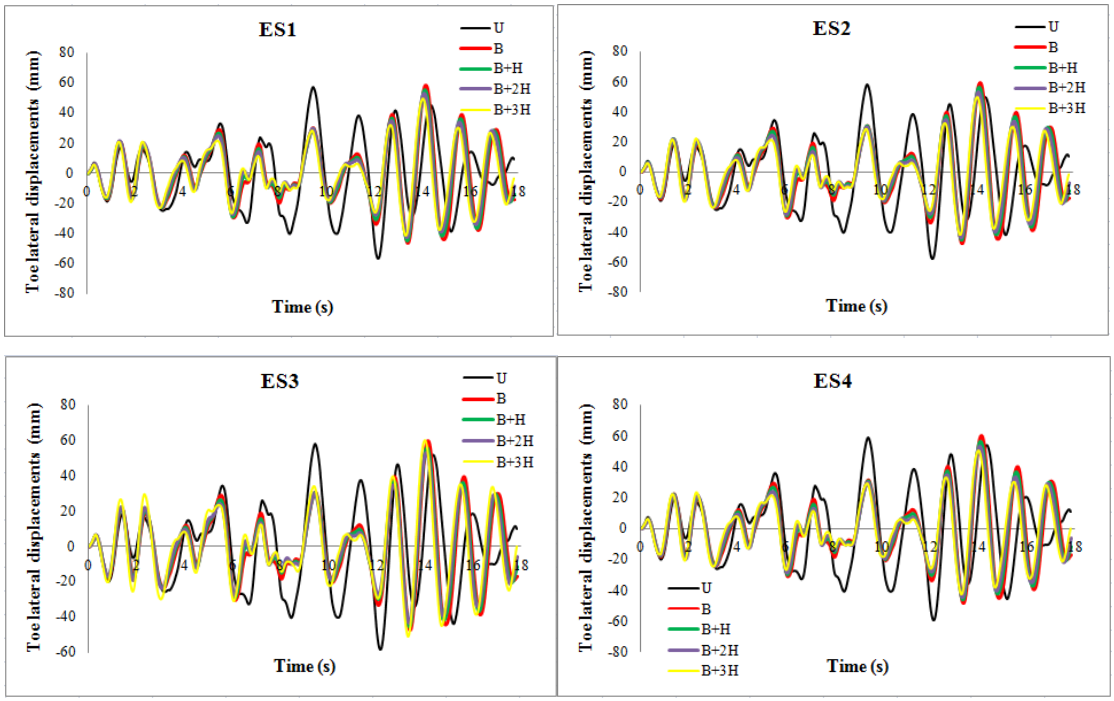

Figure 7. 26 Time-history of toe lateral displacements considering the effect of basal geogrid width and embankment soil stiffness

Time-history of variation of toe lateral displacements with basal geogrid width and embankment side slope subjected to IS Zone III ground motion (0.1 g PGA) is shown in Fig.7.27 (Fig.7.25 FS1 is for 1V:1H slope). 6 m high embankment made of ES3 soil having basal geogrid of tensile modulus 500 kN/m and resting over FS1 soil is considered for the analysis. Table 7.3 presents the percentage reduction of maximum toe lateral displacements considering the embankment side slope and basal geogrid width. It is seen from Table 7.3 that, increase in basal geogrid width reduces toe lateral displacements significantly for embankment with 1V:2H slope (a flat slope). It is also observed from Fig.7.27 and Table 7.3 that, increase in basal geogrid width reduces the toe lateral displacements for the slopes considered.

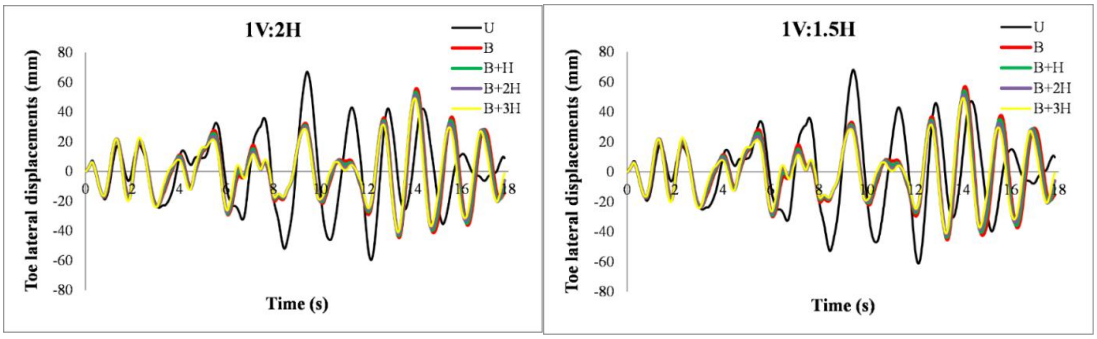

Figure 7. 27 Time-history of toe lateral displacements considering the effect of basal geogrid width and embankment side slope

Table 7. 3 Percentage reduction in the maximum toe lateral displacements for 6 m high embankment considering the effect of side slope and basal geogrid width

Basal geogrid width	Percentage reduction in the maximum toe lateral displacements		
	Embankment side slope		
	1V:1H	1V:1.5H	1V:2H
B	48.55 %	53.57 %	54.55 %
B+H	55.2 %	56.2 %	56.8 %
B+2H	59.3 %	58.75 %	59.14 %
B+3H	61.5 %	61.54 %	61.66 %

Figure 7.28 shows the time-history of toe lateral displacements variation with basal geogrid width and embankment height. Embankment made of ES3 having 1V:1H side slope reinforced with a basal geogrid of 500 kN/m tensile modulus supported over FS1 soil subjected to IS Zone III ground motions (0.1 g PGA) is considered. From Fig.7.28 it is observed that, the increase in the embankment height increases the toe lateral displacements to about 1 %. In 4 m high embankment about 48.7 %, 55.94 %, 62.1 % and 67.36 % reduction in maximum toe lateral displacements are observed by the addition of basal geogrid of width 'B', 'B+H', 'B+2H' and 'B+3H'. Similarly, in 6 m high embankment about 48.55 %, 55.2 %, 59.3 %, 61.5 % reduction and in 8 m high embankment about 53.77 %, 57.4 %, 58.6 %, 59.9 % reduction and in 10 m high embankment about 55.58 %, 64.58 %, 67.92 %, 69.23 % reduction in maximum toe lateral displacements are observed by the addition of basal geogrid of width 'B', 'B+H', 'B+2H' and 'B+3H' respectively.

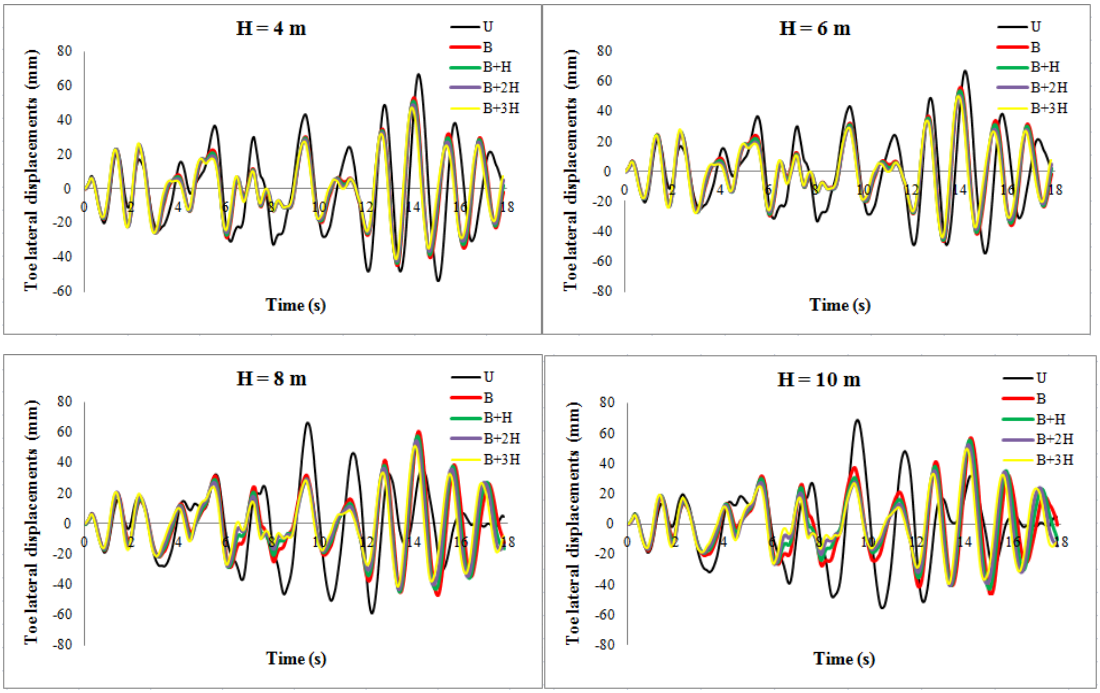

Figure 7. 28 Time-history of toe lateral displacements considering the effect of basal geogrid width and embankment height

Figure 7.29 presents the time-history plot of toe lateral displacements variation with basal geogrid width and earthquake intensity. 6 m high embankment having 1V:1H side slope made of ES3 soil reinforced with a basal geogrid of tensile modulus 500 kN/m resting over FS1 soil is considered for the analysis. By increasing the earthquake intensity from 0.1 g (Fig.25 FS1) to IS (0.35 g) and IS (0.6 g), more than 250 % and 500 % increase in maximum toe lateral displacements are observed (Fig.7.29). For IS Zone III excitations (Fig.7.25 FS1), about 48.55 %, 55.2 %, 59.3 % and 61.5 % reduction in maximum toe lateral displacement is seen by the addition of basal geogrid having width 'B', 'B+H', 'B+2H' and 'B+3H' respectively. And for both IS (0.35 g) and IS (0.6 g) excitations, about 52.3 %, 55.7 %, 58.8 % and 62.3 % reduction in maximum toe lateral displacement is seen by the addition of basal geogrid having width 'B', 'B+H', 'B+2H' and 'B+3H' respectively. This shows that the addition of basal geogrid reduces the toe lateral displacements regardless of earthquake intensity and at high intensity the percentage reduction of displacement is same for the considered case.

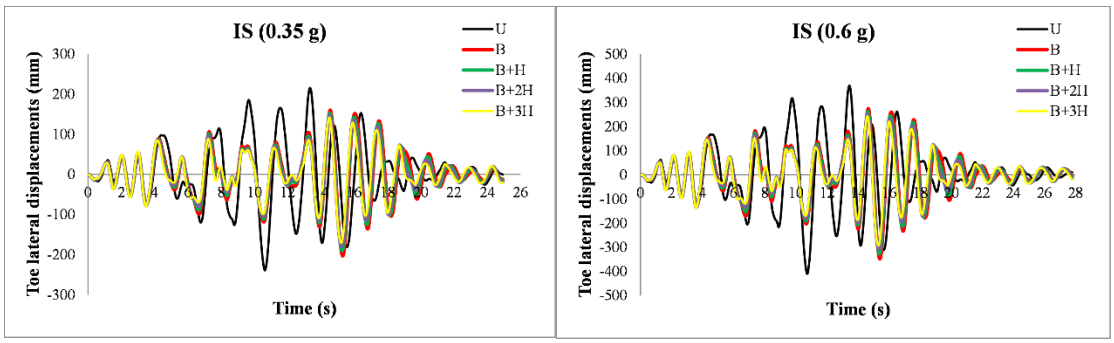

Figure 7. 29 Time-history of toe lateral displacements considering the effect of basal geogrid width and earthquake intensity

Time-history plot of toe lateral displacements variation with width and stiffness of basal geogrid is shown in Fig.7.30. It is observed that increase in both basal geogrid stiffness and width reduces the toe lateral displacements. About 25.5 % to 37.3 % toe lateral displacements reduction is observed for basal geogrid width 'B' to 'B+3H' and tensile modulus 1000 kN/m. Similarly 56.5 % to 58.7 %, 72 % to 76 % and 81 % to 85 % toe lateral displacements reductions are observed for basal geogrid width 'B' to 'B+3H' and tensile modulus of 2000 kN/m, 4000 kN/m and 6000 kN/m respectively.

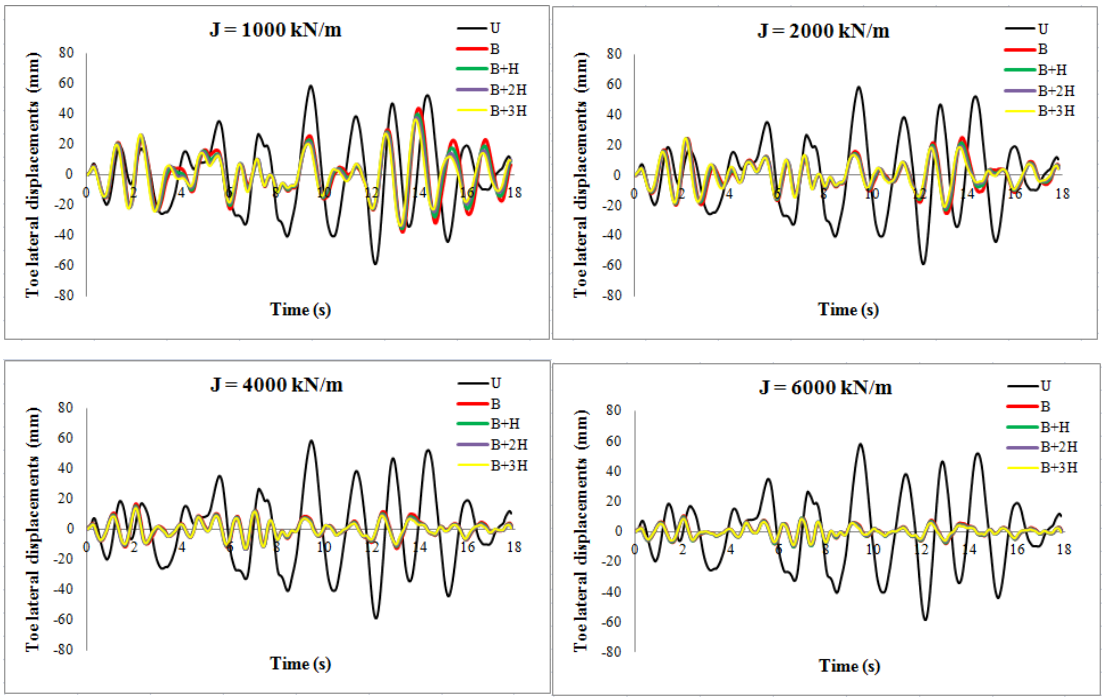

Figure 7. 30 Time-history of toe lateral displacements considering the effect of width and stiffness of basal geogrid

Figure 7.31 shows the time-history plot of toe lateral displacements for 6 m high 4 layers basal geogrid-reinforced embankment having 1V:1H side slope subjected

to IS Zone III ground motion. The embankment is made of ES3 soil and constructed over FS1 foundation soil. From Fig.7.31 and Fig.7.31 (1 Layer, J = 4000 kN/m) it is noticed that, the embankment resting over 4 layers basal geogrid having tensile modulus of 1000 kN/m performs better in reducing toe lateral displacements than the embankment resting over single layer basal geogrid having 4000 kN/m tensile modulus. Further reduction in maximum toe lateral displacements of about 6 % is observed for embankment supported over 4 layers basal geogrid (J = 1000 kN/m) when compared with embankment supported over 1 layer geogrid (J = 4000 kN/m) under seismic loading conditions.

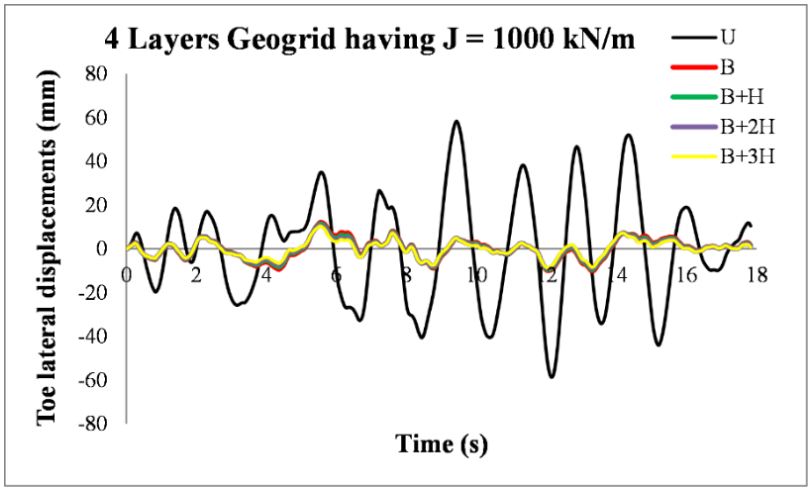

Figure 7. 31 Time-history of toe lateral displacements for 4 layers basal geogrid-reinforced 6m high embankment

7.3.4 Effect of pore water pressure

Figure 7.32 shows the pore water pressure contours (in N/m^2) for 6 m high embankment taken at the instant of occurrence of PGA. From Fig.7.32 it is observed that in the basal geogrid-reinforced embankments, the maximum pore water pressure is located just below the edge of basal geogrid. For the embankment with basal geogrid of width 'B' the maximum pore water pressure is observed just below embankment toe and the provision of additional width of basal geogrid moves the maximum pore water pressure point away from embankment toe. Hence to keep the embankment toe safe from excess pore water pressure, a minimum width of basal geogrid 'B+H' is needed in active seismic regions.

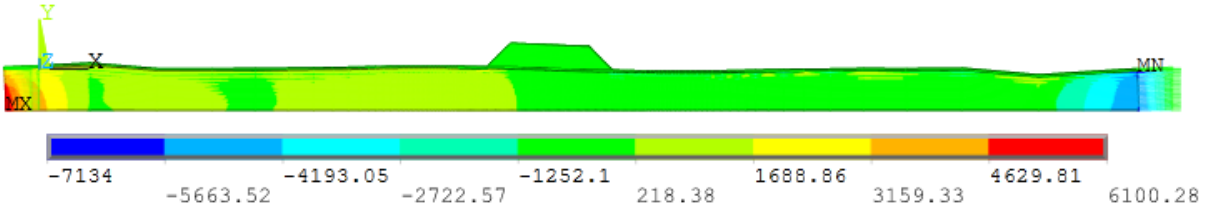

(a) Unreinforced 6 m high embankment having 1V:1H side slope

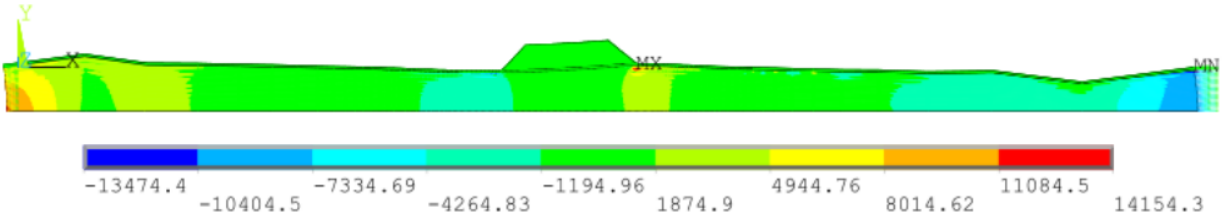

(b) Basal geogrid (width B) reinforced 6 m high embankment having 1V:1H side slope

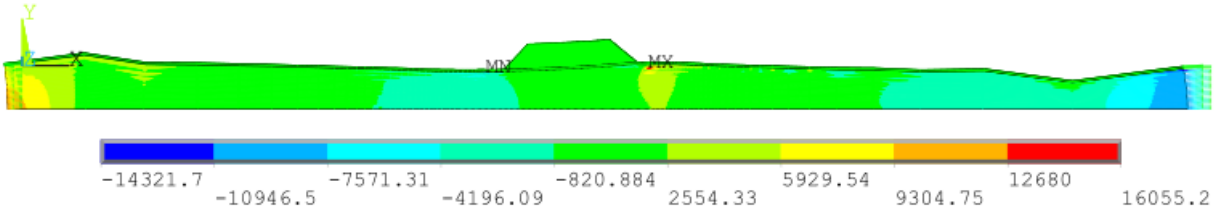

(c) Basal geogrid (width B+H) reinforced 6 m high embankment having 1V:1H side slope

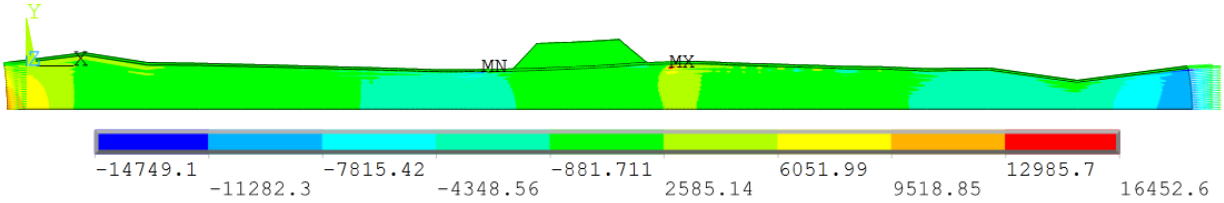

(d) Basal geogrid (width B+2H) reinforced 6 m high embankment having 1V:1H side slope

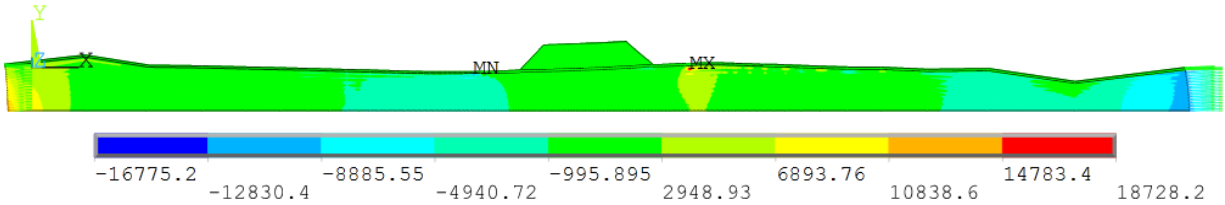

(e) Basal geogrid (width B+3H) reinforced 6 m high embankment having 1V:1H side slope

Figure 7. 32 Pore water pressure contours in embankments at the instant of occurrence of PGA for IS Zone III ground motion (0.1g)

7.3.5 Lateral Displacements contours at the instant of occurrence of PGA

Figure 7.33 shows the lateral displacement contours of 6 m high embankment having 1V:1H side slope made of ES3 soil and supported over FS1 soil reinforced with a basal geogrid (J = 500 kN/m) subjected to IS Zone III ground motions. From Fig.7.33 it is observed that, the addition of basal geogrid reduces the lateral displacements of embankment. Further reductions of lateral displacements are seen by increasing the basal geogrid width. About 49.8%, 54%, 56.58% and 65.7% lateral displacement reduction in the embankment is observed by the addition of basal geogrid of width 'B', 'B+H', 'B+2H' and 'B+3H' respectively at the instant of occurrence of PGA.

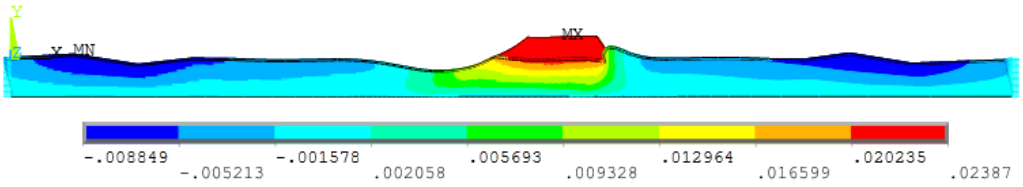

[in m]

(a) Unreinforced 6 m high embankment having 1V:1H side slope

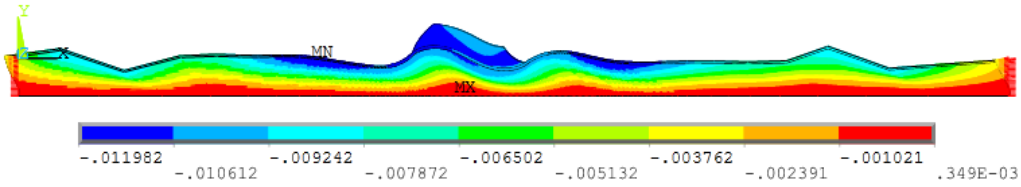

[in m]

(b) Basal geogrid (width B) reinforced 6 m high embankment having 1V:1H side slope

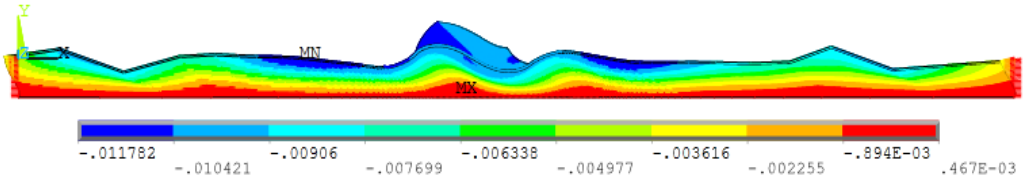

[in m]

(c) Basal geogrid (width B+H) reinforced 6 m high embankment having 1V:1H side slope

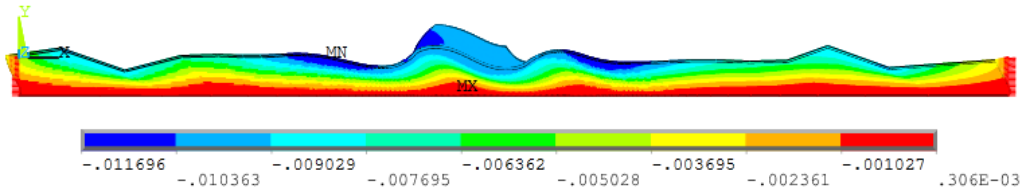

[in m]

(d) Basal geogrid (width B+2H) reinforced 6 m high embankment having 1V:1H side slope

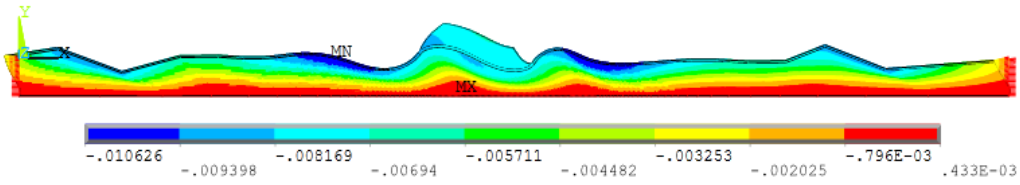

[in m]

(f) Basal geogrid (width B+3H) reinforced 6 m high embankment having 1V:1H side slope

Figure 7. 33 Lateral displacement contours in embankments at the instant of occurrence of PGA for IS Zone III ground motion (0.1g)

7.4 SUMMARY

Static and time-history analysis of basal geosynthetic-reinforced embankments is presented in this chapter. The effect of geogrid tensile modulus, embankment height, slope of embankment, Young's modulus of embankment fill, Young's modulus of foundation soil, number of layers of basal geogrid and intensity of seismic loading in determining the optimum width of basal geogrid are discussed. Based on the results of crest settlements, toe lateral displacements and lateral displacements at the crest the required width and tensile modulus of basal geogrid are identified.

From above discussions, basal geogrid having minimum tensile modulus of 500 kN/m with a width equal to base width (B) of embankment is sufficient to reduce settlements at places where static loading is predominant or in low seismic regions. Basal geogrid of width equal to 'B+H' having tensile modulus of 4000 kN/m is recommended to reduce the lateral displacements in embankments at active seismic regions. Further reduction in lateral displacements are seen by providing 4 layers of basal geogrid with a total tensile modulus equal to 4000 kN/m.

CHAPTER 8

RESPONSE VARIATION OF BODY-REINFORCED EMBANKMENTS SUBJECTED TO SEISMIC LOAD

8.1 INTRODUCTION

At places where the land restrictions exists, the construction of embankments with flat side slope is an issue. During such circumstances, the embankment side slopes are steepened by providing the geosynthetic reinforcements to the embankment body. The stability of these body reinforced embankments under static loading conditions is well explained in the literature. Though there are studies on the behaviour of these body-reinforced embankments subjected to seismic excitations, the behaviour of these embankments supported on different foundation soils and provision of very steep slopes under seismic loading need to be studied.

6 m high embankment having 1V:1H side slope supported over soft foundation soil subjected to the time-history of IS (0.35 g) ground motion was considered as reference model. The model was analysed for the effect of body reinforcement, slope inclination and foundation soil property. Body reinforcements of tensile stiffness 500 kN/m was designed using simple wedge method. The embankment body was reinforced with 6 layers of geogrid reinforcement with 1 m vertical spacing along the embankment elevation on both sides of the embankment slope. The crest centre accelerations, face lateral displacements and crest vertical displacements were observed.

8.2 EFFECT OF BODY REINFORCEMENT

6m high embankment of side slopes 1V:1H on 20m thick soft soil was given seismic load. Both reinforced and unreinforced models were analysed. The acceleration response at crest centre of embankment for both reinforced and unreinforced case is shown in Fig.8.1. Compared to the input time history, acceleration amplification is more pronounced for unreinforced model. Thus inclusion of reinforcement caused attenuation of acceleration in the embankment**.**

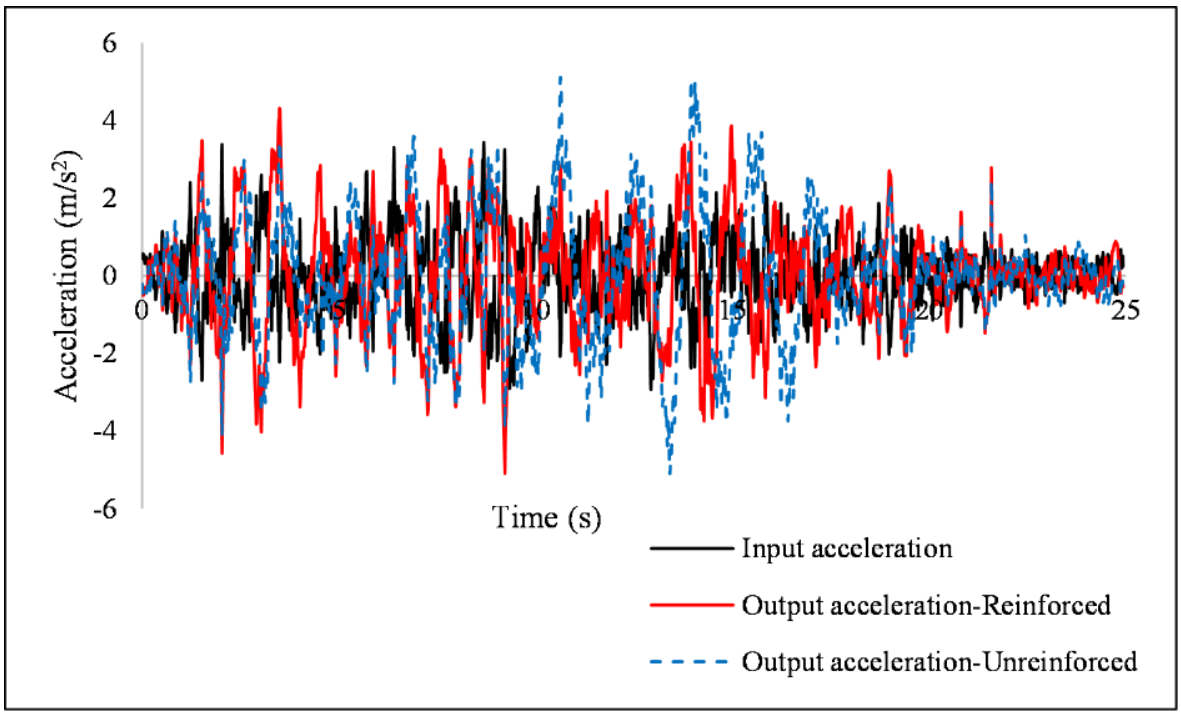

Figure 8.1 Acceleration response at crest centre

Figures 8.2 to 8.4 presents the lateral displacements of reinforced and unreinforced embankments at crest centre, toe and crest edge. Obviously, the displacements of reinforced embankments are smaller than that of unreinforced case. The inclusion of body-reinforcements at the embankment slopes without extending throughout the embankment width could reduce more than 80 % of crest centre lateral displacements. But there is an average reduction of 84.58% and 70.61% in crest edge and toe lateral displacements due to the reinforcements. It can be seen in Fig.8.1 that unreinforced slopes shows higher acceleration amplification than reinforced slopes. Thus the attenuation of acceleration and shear resistance developed on the interface of reinforcement and soil helped in reducing lateral displacements.

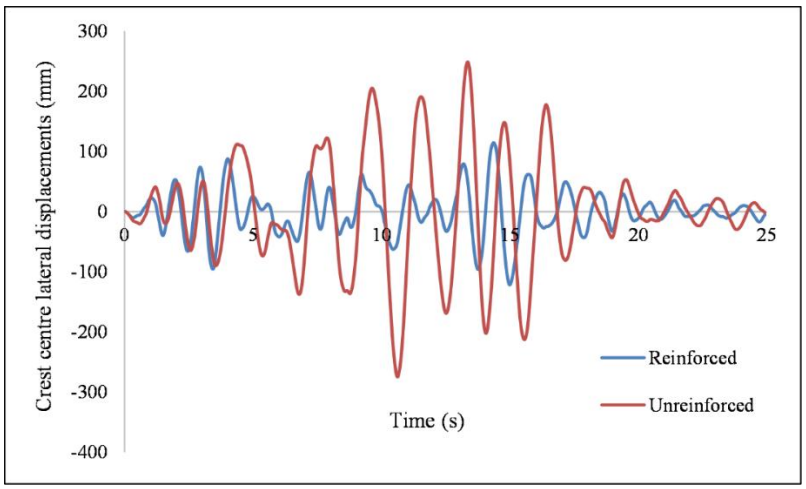

Figure 8.2 Crest centre lateral displacement for reinforced and unreinforced case

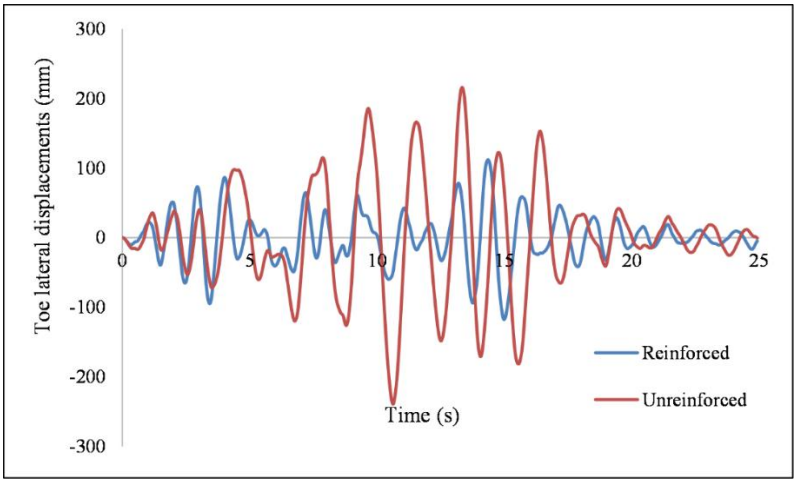

Figure 8.3 Toe lateral displacement for reinforced and unreinforced case

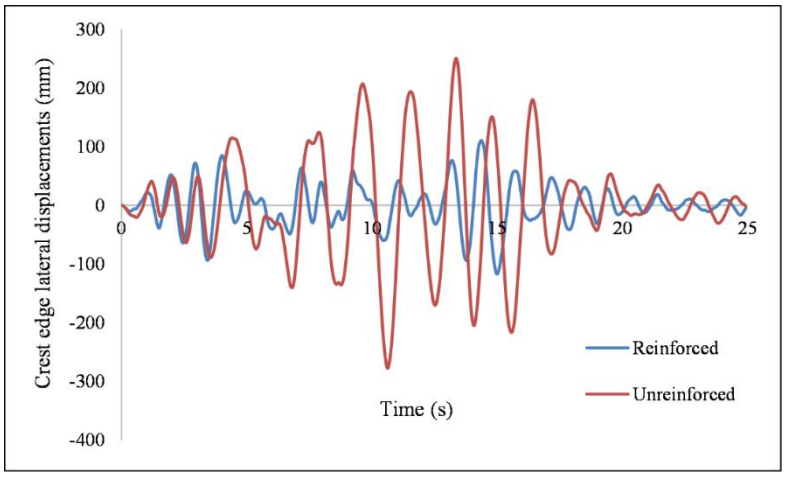

Figure 8.4 Crest edge lateral displacement for reinforced and unreinforced case

Analysing the face horizontal displacements at different elevations of the slope at PGA of the IS (0.35 g) ground motion, the reduction due to reinforcement can be seen (Fig.8.5). This reduction is more at higher elevations. About 92.5 % reduction at the top and about 90 % reduction of face horizontal displacement at the bottom level are observed.

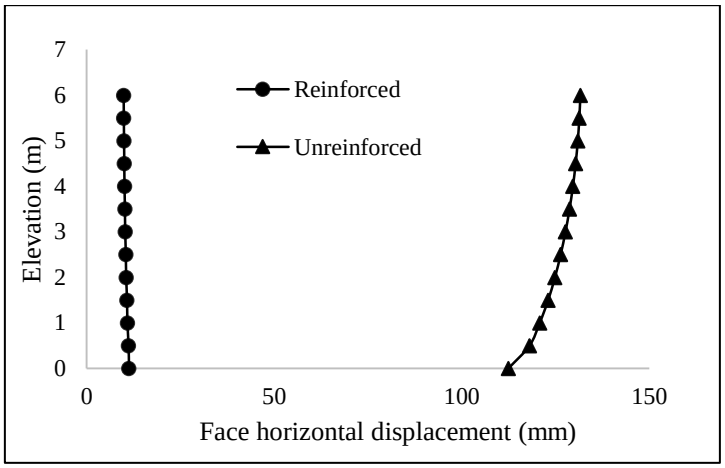

Figure 8.5 Face horizontal displacement for reinforced and unreinforced case

8.3 EFFECT OF SLOPE OF EMBANKMENT

The embankment slope was varied and reinforcements designed accordingly. The horizontal displacements at the face of the slope at each elevation measured from embankment base are plotted. These are the displacements at the instant of maximum ground acceleration.

Figure 8.6 presents the face horizontal displacements along the embankment elevation for the considered embankment slopes with and without reinforcement measured at the instant of occurrence of PGA. In unreinforced embankments the face lateral displacements increase as the steepness of slope increases. This can be due to increase of downslope driving force caused by embankment weight. The reduction of face horizontal displacements due to the inclusion of reinforcement is much effective in steep slopes than in shallow slopes. About 92.5%, 92.75 % and 93 % reduction of face horizontal displacements are observed for 1V:1H, 1V:0.5H and 1V:0H sloped embankments at the embankment top.

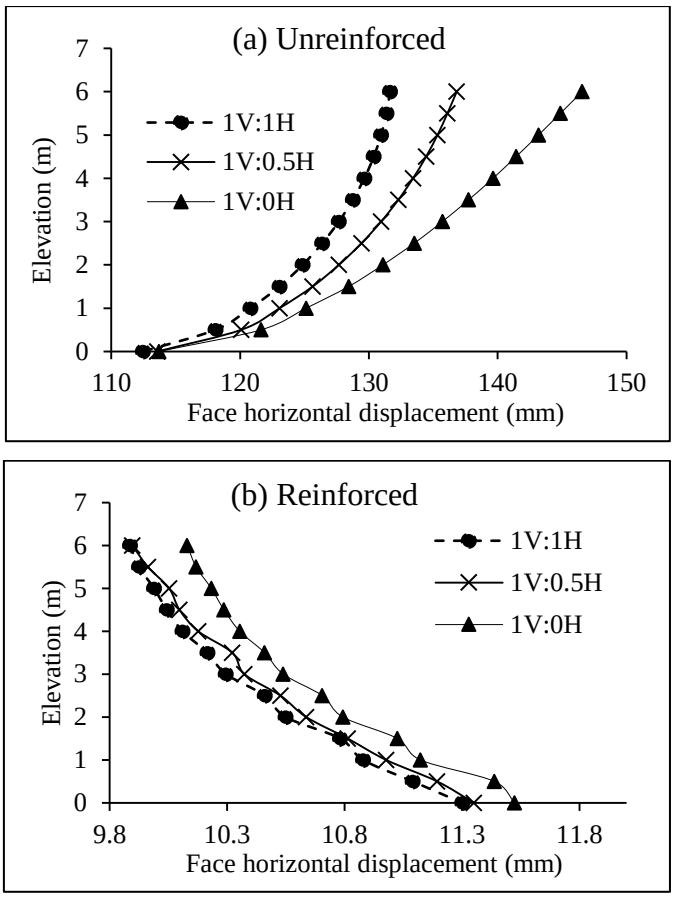

Figure 8.6 Face horizontal displacement for different slope of embankment

The lateral displacement of crest edge of the embankment resting on soft soil corresponding to the PGA of earthquake is given in Fig.8.7. The increase in displacements with steepness of slope is seen in the case of unreinforced slope.

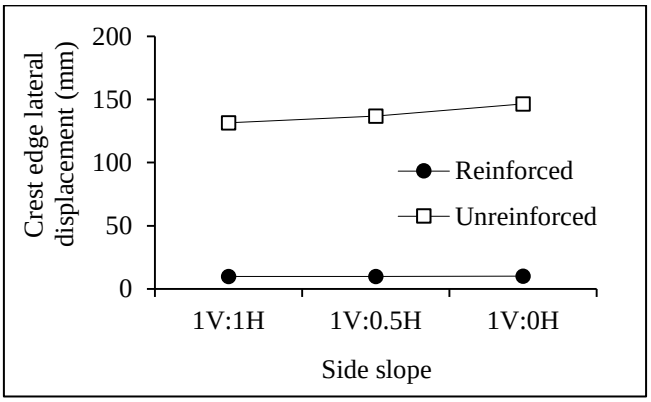

Figure 8.7 Crest edge lateral displacement for varying slope of embankment

8.4 EFFECT OF FOUNDATION SOIL STIFFNESS

Both reinforced and unreinforced embankments of slope 1V:1H was subjected to IS (0.35 g) ground motion considering different properties of foundation soil. Soft

has a density of 14 kN/m^3 and Young's modulus of 4 MPa whereas stiff soil is of density 21 kN/m^3 and Young's modulus 50 MPa.

During earthquakes, soft soils can amplify the seismic motion (Fig.8.8) and can significantly influence the amplitude, frequency and duration of ground motion that reaches the foundations and hence the subsequent dynamic response of the superstructure. Since the shear resistance of soft foundation soil is less, the lateral displacements are larger for embankments on soft soil for both unreinforced and reinforced case, even though reinforcements could cause reduction in displacements. Thus embankment above soft soil displaces more than embankment on stiff soil. Fig. 8.9 shows the toe lateral displacement for reinforced embankment on soft and stiff foundation soil. About 50 % increase in toe lateral displacements are observed for the embankment resting over soft foundation soil when compared with the embankment resting over stiff foundation soil.

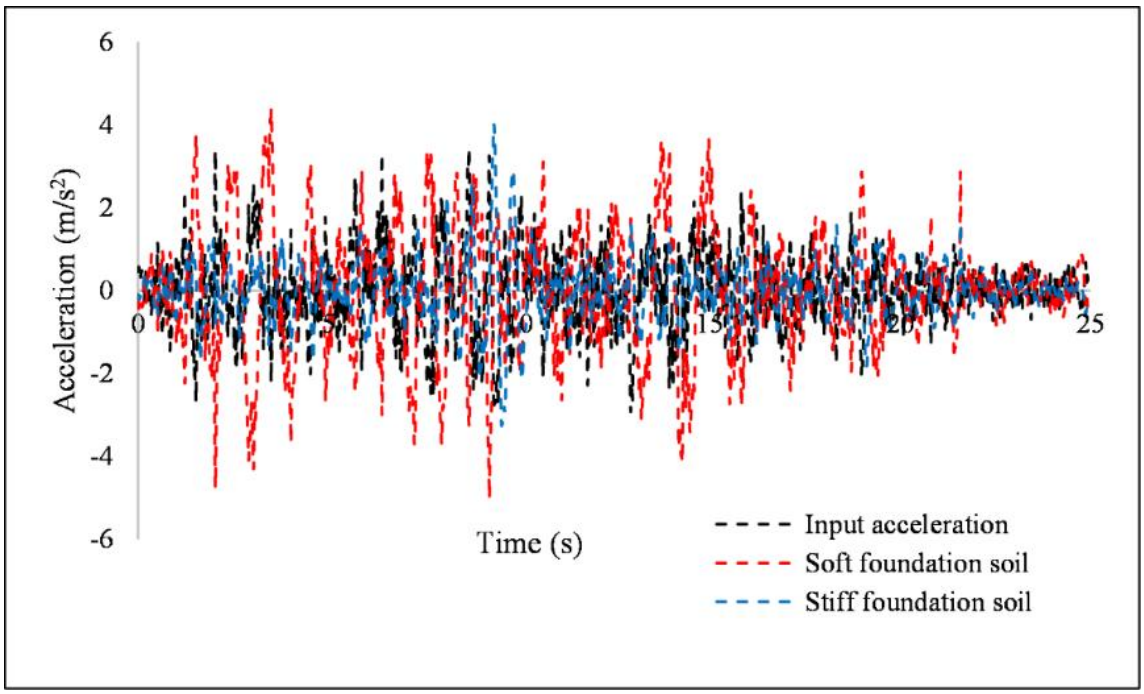

Figure 8.8 Acceleration response at the interface of embankment and foundation soil

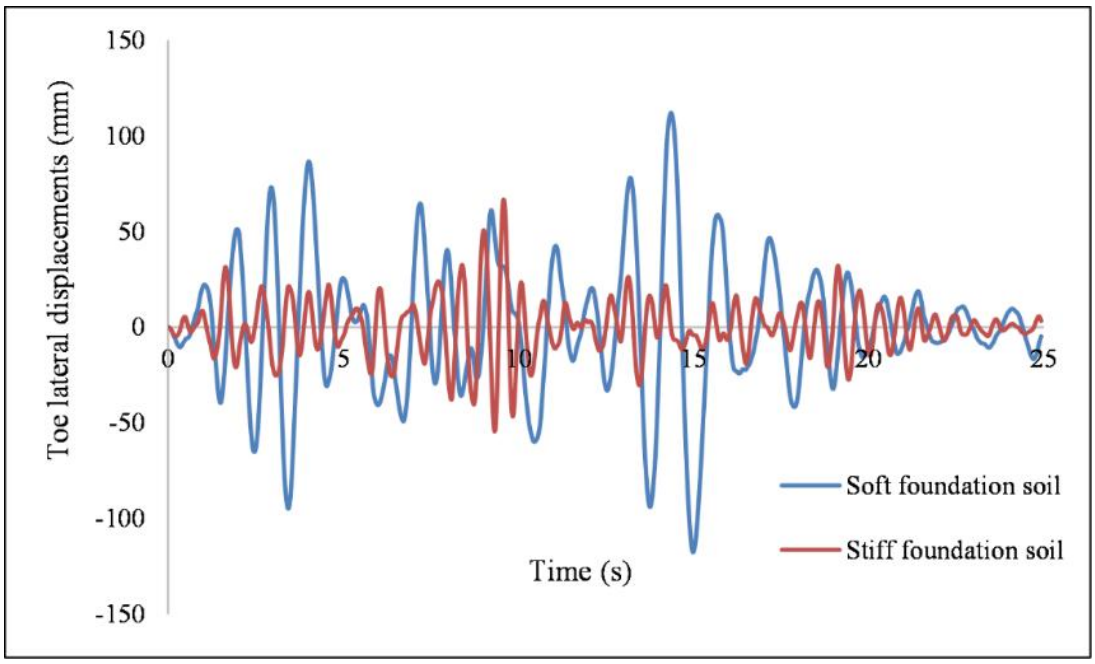

Figure 8. 9 Toe lateral displacements for varying foundation soil type (Reinforced case)

8.5 SUMMARY

This chapter presented the time-history analysis results of body-reinforced embankments. Effect of embankment side slope and foundation soil stiffness on the lateral displacements and lateral accelerations of embankment with and without reinforcement are presented. The following observations are drawn from the analysis.

Even though the reinforcements are provided at the side slope and not extended throughout the embankment body, addition of reinforcement could reduce more than 80 % of the lateral displacements at crest centre.

In unreinforced embankments the face lateral displacements increase as the steepness of slope increases. This can be due to increase of downslope driving force caused by embankment weight. The reduction of face horizontal displacements due to the inclusion of reinforcement is much effective in steep slopes than in shallow slopes. About 92.5%, 92.75 % and 93 % reduction of face horizontal displacements are observed for 1V:1H, 1V:0.5H and 1V:0H sloped embankments at crest edge.

In soft foundation soils, the seismic waves get amplified and this causes adverse effect on highways resting over it. Hence, the lateral displacements are larger for embankments on soft soil for both unreinforced and reinforced case, even though reinforcements could cause reduction in displacements.

CHAPTER 9
CONCLUSIONS

An attempt has been made to study the behaviour of embankments constructed over soft clays subjected to self-weight, traffic and seismic loading. Depending on the importance, type and depth of foundation soil several ground improvement techniques like embankments supported over piles or basal geogrid or the combination of both piles and basal geogrid were analysed. At land restricted areas, the embankments side slopes were steepened using geosynthetic reinforcements in the embankment body. Hence, the behaviour of body-reinforced embankments under seismic excitations has also been analysed.

Parametric studies were conducted considering embankment height, pile length, pile spacing, pile type and geogrid tensile modulus subjected to static and seismic loads. Response of embankments in terms of settlements, toe lateral displacements, differential settlements, stress distribution ratio, lateral stress distribution ratio and coefficient of lateral pressure were analysed for self-weight. Based on numerical analysis, modifications to the soil arching coefficient (C_c) were also proposed for self-weight of embankment.

The following conclusions were drawn from the self-weight and traffic load analysis of basal geogrid-reinforced pile-supported embankments:

9.1 STATIC ANALYSIS OF BASAL GEOGRID-REINFORCED PILE-SUPPORTED EMBANKMENTS

1) For embankments supported over end-bearing/floating piles, a minimum geogrid tensile modulus of 500 kN/m is sufficient to reduce the maximum settlements and beyond tensile modulus of 4000 kN/m, further increase in tensile modulus do not have any effect in reducing settlements.
2) Increase in embankment height, increase in pile spacing and decrease in pile length increases the crest settlements irrespective of presence or absence of basal geogrid. End bearing piles (28 m) are more effective in reducing settlements than floating piles. About 82.3 % reduction in settlement is observed by increasing the pile length from 22 m to 28 m. Based on the analysis, 5D spaced end-bearing pile supported embankments with basal geogrid (J = 4000 kN/m) are most suited for reducing crest settlements.

3) Presence of basal geogrid (J = 4000 kN/m) could reduce more than 70 % of toe lateral displacements for embankments supported on end-bearing (28 m) piles. Increase in embankment height, increase in pile spacing and decrease in pile length increases the toe lateral displacements. Embankments supported over 3D spaced end-bearing piles with basal geogrid are recommended to reduce the toe lateral displacements to a maximum extent.
4) Increase in embankment height, increase in pile length and decrease in pile spacing increases the SDR values. Also, increase in geogrid tensile modulus upto 4000 kN/m increases the SDR values and further increase in geogrid tensile modulus could lead to negligible increase in SDR. The presence of basal geogrid transfers additional embankment loads to the piles. The SDR values increases by more than 90 % due to the addition of basal geogrid.
5) Increase in basal geogrid stiffness increases the SDR value at foundation level, as the depth increases the SDR values for the considered range of geogrid stiffness becomes equal. Similar trend is observed for various embankment height, pile length and pile spacing considered.
6) The self-weight of embankment exerts more vertical stress on piles. This leads to less LSDR values with increase in embankment height and geogrid tensile modulus. Hence the LSDR values are inversely proportional with SDR values and also the LDSR values are negligible compared to SDR values.
7) Increase in pile spacing and decrease in pile length increases the differential settlements at crest irrespective of presence or absence of basal geogrid. Differential settlements are very much dependent on the embankment height. In low embankments, the direct load transfer on piles causes more differential settlements and in high embankments, differential settlements increases due to increased embankment weight. 28 m pile supported 3 m high embankment without basal geogrid experiences maximum differential settlements but the addition of basal geogrid reduces the differential settlements. Also 28 m pile supported 6 m high embankment experiences more differential settlements than the other embankment heights considered. 4 m high embankment supported on 3D spaced 28 m piles with basal geogrid of tensile modulus 4000 kN/m experiences negligible differential

settlements. This combination is recommended for reducing the differential settlements at crest due to self-weight.

8) Higher K values are observed above foundation soil when compared with the K values above piles taken along the embankment elevation. Also, addition of basal geogrid helps to maintain the K values along embankment elevation nearly equal to pressure at rest (K_0).
9) The foundation soil beside piles just after embankment toe move towards the piles due to consolidation settlement by its own weight causing negative lateral displacement in the foundation soil. But in the case of embankment without pile supports, consolidation occurs due to embankment load and causes a positive lateral displacement. Also the addition of basal geogrid reduces about 10 % to 15 % of lateral displacements of foundation soil in the presence of pile supports.
10) The proposed C_c values based on 3-dimensoinal numerical analysis are capable of predicting the load shared over piles more accurately when compared to other methods.
11) Inclusion of traffic load leads to further increase of settlements and lateral displacements in the embankment.
12) In variable head diameter pile supported embankment, both negative and positive skin frictions at the head and toe of piles are increasing with the increase of floating pile length and spacing. But more than 50% increase in skin friction is seen for the embankments supported on end bearing piles.

The time-history analysis was conducted on 3-Dimensional FE model of basal geogrid reinforced pile-supported embankments to analyse the lateral and vertical stress distribution between piles and surrounding foundation soil, displacements in the embankment and the soil arching under seismic excitations. From the results, the following conclusions are arrived at:

9.2 SEISMIC ANALYSIS OF BASAL GEOGRID-REINFORCED PILE-SUPPORTED EMBANKMENTS

1) Under seismic loading conditions, for (H/s) less than or equal to 4.5, basal geogrid tensile modulus of 3000 kN/m is sufficient to distribute vertical stresses on pile foundations and soft foundation soil and for (H/s) greater than 4.5, increase in basal geogrid tensile modulus increases the vertical stresses on piles.

2) To withstand the lateral stresses due to earthquakes, basal geogrid tensile modulus less than 4000 kN/m is best suited for (H/s) less than or equal to 4.5.
3) Increase in embankment height increases the Amplification Coefficient value and increase in geogrid tensile modulus reduces the Amplification Coefficient value.
4) Geogrid tensile modulus of 3000 kN/m is found sufficient in reducing the differential settlements under seismic loading conditions for all embankment heights considered in the present study.
5) For the considered embankment heights and pile diameters when (H/s) nearly equal to 4.5, differential settlements are very less irrespective of seismic excitations.
6) Addition of basal geogrid reduces the lateral displacements at crest centre and toe by about 10 %.
7) Embankment without basal geogrid experiences more vertical displacements causing more differential settlements at crest. Basal geogrids even with small geogrid tensile modulus of 1000 kN/m, reduce vertical displacements at crest. This reduces the differential settlements at crest.
8) Embankment without pile supports and basal geogrid experiencs maximum toe lateral displacements. Embankment with only basal geogrid reinforcement reduces only 8 % of toe lateral displacements. But the embankment with pile supports reduces 40.8 % and the embankment with pile supports and basal geogrid could reduce 46.1 % of toe lateral displacements.
9) The embankment supported over vertical and 5º batter piles experiences very less differential settlements, toe lateral displacements and accelerations. Beyond this further increase in angle of batter piles increases the differential settlements. Hence combination of vertical and 5º batter piles are best suited.
10) The variation of coefficient of lateral pressure (K) along the embankment elevation is random for the considered embankment height, pile length, pile spacing and geogrid tensile modulus. This indicates that the formation of soil arching in a geogrid-reinforced pile-supported embankment subjected to seismic loading is not uniform like in the case of self-weight analysis.

Static and time-history analysis was conducted on finite element model of basal geogrid-reinforced embankments to identify the suitable width of basal geogrid by

considering the toe lateral displacements, lateral displacement reduction ratio at crest edge and differential settlements at crest. The following conclusions are listed from the analysis of results:

9.3 STATIC AND SEISMIC ANALYSIS OF BASAL GEOGRID-REINFORCED EMBANKMENTS

1) Basal geogrid having tensile modulus of 500 kN/m with a width equal to base width (B) of embankment is sufficient to reduce settlements at places where static loading is predominant or in low seismic regions.
2) Under static loading conditions, basal geogrid reinforcements are no longer required for embankments with very stiff foundation soil irrespective of embankment soil stiffness, embankment height and embankment side slope.
3) The type of foundation soil, slope of embankment and presence of geogrid influences the natural frequency of embankments considerably and hence the formula for natural frequency of embankments given in IS1893(Part 5):1984 need to be modified incorporating these parameters to account for nonrigid base conditions.
4) Increase in foundation soil stiffness reduces the LDRR values. But the embankment resting over FS2 soil has slightly less LDRR values than the embankment resting over FS3 soil. This maybe due to the natural frequency of embankment resting over FS2 type foundation soil nearly matching with the high Fourier amplitude frequency content of ground motion.
5) In seismic regions with peak ground acceleration 0.1 g to 0.6 g range, basal geogrid having tensile modulus of 4000 kN/m with a minimum width of ‘B+H’ is the best suited.
6) About 6 % of further reduction in lateral displacements are seen for 4 layers basal geogrid-reinforced embankment (with J = 1000 kN/m) when compared with single layer basal geogrid reinforced embankment (with J = 4000 kN/m) for all the basal geogrid width considered under seismic loading conditions.
7) Maximum pore water pressure is observed below the basal geogrid edge. Hence for embankment having basal geogrid of width ‘B’, maximum pore water pressure is seen just below embankment toe. In order keep the embankment toe safe from

excess pore water pressure, a minimum width of basal geogrid 'B+H' is needed in active seismic regions

8) In seismic regions having PGA ranging from 0.35 g to 0.6 g, percentage reduction of embankment lateral displacement is almost same by the addition of basal geogrid.

Numerical modelling of body-reinforced embankment was also done to study the effect of reinforcement, slope inclination and foundation soil property. The following conclusions were derived from the dynamic analysis of body-reinforced embankments:

9.4 SEISMIC ANALYSIS OF BODY-REINFORCED EMBANKMENTS

1) Even though the reinforcements are provided at the side slope and not extended throughout the embankment body, addition of reinforcement could reduce more than 80 % of the lateral displacements at crest centre.
2) The displacements of reinforced embankments are lesser than that of unreinforced case. There is an average reduction of 84.58% and 70.61% in crest edge and toe lateral displacements respectively due to the reinforcements.
3) In unreinforced embankments, the face lateral displacements increase as the steepness of slope increases. This can be due to increase of downslope driving force caused by embankment weight.
4) The reduction of face horizontal displacements due to the inclusion of reinforcement is much effective in steep slopes than in shallow slopes. About 92.5%, 92.75 % and 93 % reduction of face horizontal displacements are observed for 1V:1H, 1V:0.5H and 1V:0H sloped embankments at crest edge.
5) During earthquakes, soft soils can amplify the seismic motion and hence the subsequent dynamic response of the structure resting on soft soil. Thus embankment above soft soil displaces more than embankment on hard soil. Provision of body reinforcement improves the seismic response of the embankment.

9.5 CONTRIBUTIONS FROM THE STUDY

The present study analyses the static and seismic response of embankments supported over pile improved soft grounds with or without basal geogrid using 3-Dimensional finite element models. Based on the study, several parameters are identified which help in the development of new design methods and also to better understand the behaviour of these embankments under seismic excitations.

Based on the numerical analysis, the soil arching coefficient (C_c) including the effect of pile length and pile spacing are proposed for the basal geogrid-reinforced pile-supported embankment subjected to static loading conditions.

In basal geogrid-reinforced pile-supported embankments, to withstand the lateral stresses due to earthquakes, basal geogrid tensile modulus less than 4000 kN/m is best suited for (H/s) less than or equal to 4.5.

In seismic regions with peak ground acceleration 0.1 g to 0.6 g range, basal geogrid having tensile modulus of 4000 kN/m with a minimum width of 'B+H' is the best suited for a basal geogrid-reinforced embankment.

9.6 SCOPE OF FUTURE RESEARCH

This work can be extended in the following ways:

1. Experimental and field investigations can be conducted on basal geosynthetic-reinforced pile supported embankments subjected to seismic excitations.
2. Piles can be replaced with stone columns and the basal geogrid can be replaced with geocells and the seismic behaviour of this combination can be analysed.
3. Basal geogrid-reinforced pile-supported embankments in liquefaction zone can be analysed to study their response to liquefaction.
4. Naturally available materials like coir and jute can be used instead of basal geogrid and the behaviour can be analysed in terms of load transfer to the piles.
5. The behaviour of basal geogrid-reinforced pile-supported embankments subjected to moving train loads can be analysed.

APPENDIX I
3-DIMENSIONAL FINITE ELEMENT ANALYSIS OF VARIABLE HEAD DIAMETER PILE-SUPPORTED EMBANKMENT

I. INTRODUCTION

With rapid increase in industrialization and urbanization, the movement of raw materials, agricultural products and most importantly manpower from resource regions to urban areas has become essential. This leads to the expansion of infrastructures such as highways, bridges, railways, etc. on soft unfavourable grounds also. The most appropriate solution to construct embankments and roads over these unfavourable grounds is reinforced piled embankments especially when the depth of soft soil is more or differential settlements at junctions of approach embankments and bridge deck are a major concern. The embankment cannot be constructed in a single stage. In case of pile supported and geogrid reinforced embankment, most of the embankment loads will be transferred by pile foundations irrespective of field soil conditions.

Russell and Pierpoint (1997), Han and Gabr (2002) and Yoo and Kim (2009) studied the performance of conventional pile supported embankments using the unit cell concept. Liu et al. (2007) conducted a case study on a geogrid reinforced pile supported highway embankment. van Eekelen et al. (2011) analyzed and modified British Standard BS8006 for the design of piled embankments. Bhasi and Rajagopal (2015) conducted a numerical study on Geosynthetic-Reinforced Piled Embankments (GRPES) using three modeling approaches, such as a) axisymmetric b) Three-dimensional (3D) column and c) full 3D models. Also they compared these results with various analytical methods. Bhasi and Rajagopal (2015) performed numerical study on basal reinforced embankments supported on floating and end bearing piles considering pile-soil interaction. They reported that, the embankment load transferred through the piles to the foundation soil depends very much on length of piles. Dias and Grippon, (2017) conducted numerical analysis of embankment supported by variable inertia piles using unit cell concept.

Many of these studies have been conducted on conventional cylindrical piles with or without pile caps. Hardly one or two studies were seen on variable head diameter piles using unit cell concept. Based on the literature survey, three-dimensional

finite element analyses were carried out to study the settlements of bridge approaching embankment constructed over floating/end bearing piles with variable head diameter subjected to traffic loading along with its weight.

II. METHODOLOGY

A. Numerical Analysis

A 5 m high embankment with 20 m crest width and 1V:1.5H side slope constructed over 25 m thick soft clay stratum is considered for the present study. Hard stratum exists below clay layer. The embankment geometry is shown in Fig.AI-1. The analysis is done using general purpose finite element software ANSYS.

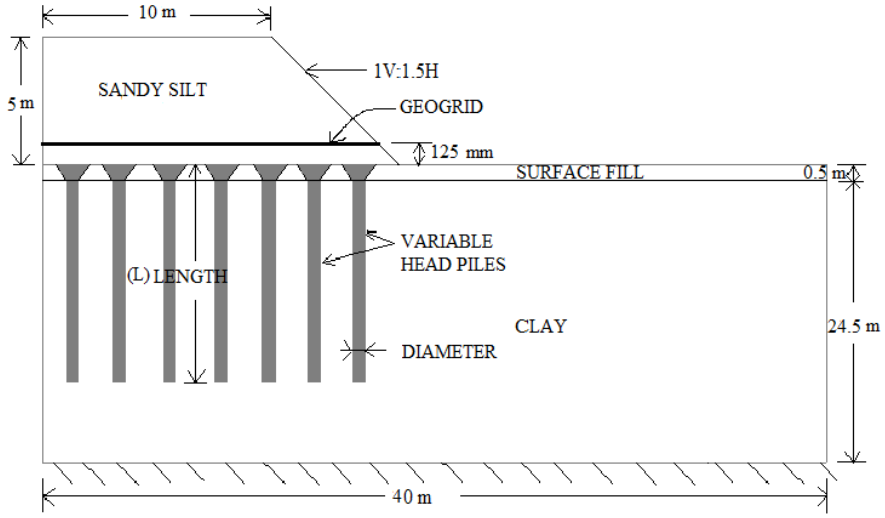

Figure AI- 1 Embankment geometry

B. Properties of soil

Homogeneous clay strata of depth 25 m is considered beneath the 5m high sandy silt embankment. Both embankment and foundation soils were modelled as Drucker-Prager elasto-plastic material model. Different parameters considered for soil modelling are listed in Table AI-1 [Bowles (2012)].

Table AI-1 Soil parameters

Material	Sandy silt	Soft Clay	Surface fill
Density (kN/m^3)	18	17	21
Modulus of elasticity (MPa)	40	10	120
Poisson's ratio	0.3	0.4	0.3
Cohesion (kPa)	25	10	10
Angle of internal friction (φ)	32°	25°	40°

C. Properties of Piles

Variable head diameter pile having head diameter (D) of 1 m and shaft diameter 400 mm with centre to centre spacing 2D, 3D and 4D arranged in square pattern are considered. Length of pile (L) considered are 7.5 m, 12.5 m, 17.5 m and 25 m (End bearing piles) based on critical length of pile given by Satibi (2009). Piles are modelled as linear isotropic elastic material with modulus of elasticity of 25000 MPa, Poisson's ratio of 0.15 and density of 25 kN/m^3.

D. Properties of Geogrid

One layer of geogrid at the base of embankment was sandwiched between 125 mm thick hard soil (i.e., surface fill). Geogrid is also modelled as linear isotropic elastic material with Poisson's ratio of 0.3 and modulus of elasticity, $E = T/\varepsilon$ where, T is the tensile strength of geogrid (1500 kN/m^2) and ε is the strain in geogrid (2%).

E. Modelling

The analysis of a piled embankment is truly a three-dimensional problem. Two-dimensional finite element models do not appropriately represent the realistic conditions because they assume that piles are continuous in the out-of-plane direction and behave as walls Ariyarathne and Liyanapathirana (2015). Hence in the present study, three-dimensional finite element modelling was performed using ANSYS. Both soil and piles were modelled using SOLID65 element. It is an eight noded element with three degrees of freedom at each node: translations in the nodal x, y, and z directions. Geogrid was modelled using SHELL181 element with membrane effect. It is a four noded element with 3 translational degrees of freedom at each node. The surface to surface interaction between soil and pile has been established with CONTA174 and TARGE170 elements with coefficient of friction $\mu = \tan(\varphi)$ (Table AI-1). The target-contact elements and the coupling of degrees of freedom make possible the interaction between pile and soil. 3D Finite element model of embankment, pile and geogrid are shown in Fig.AI-2

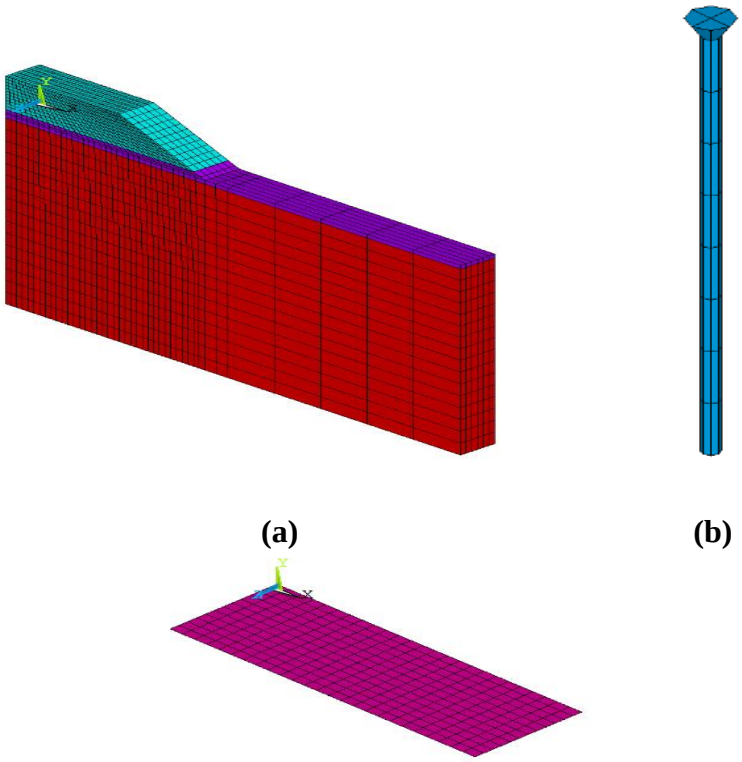

(a) **(b)**

(c)

Figure AI- 2 Three-Dimensional Finite element model of (a) a slice of embankment (b) Pile (c) Geogrid.

F. Boundary conditions

Due to symmetry of embankment geometry, only right half of the embankment is considered for the analysis. Since the soil is assumed as semi-infinite, the vertical boundaries were restrained for the horizontal deformations and the bottom surface is fixed for all the three deformations.

G. Loads

Initially the embankment was analysed for its self-weight by applying the gravitational acceleration of 9.81 m/s^2 in the vertical direction. Later it was analyzed for a traffic load of 24 kN/m^2 over the embankment crest [IRC:75-2015].

III. Results and discussions

H. Settlement Reduction Ratio

Settlement reduction ratio is the ratio between the settlements of reinforced and unreinforced embankments expressed in percentage.

Given by $SRR = 1 - \frac{S_{reinf}}{S_{unreinf}}$ (1)

Where, S_{reinf} is the settlement of soil with pile and geogrid reinforcement and $S_{unreinf}$ is the settlement of soil without pile and geogrid reinforcement.

From Fig.AI-3 and Table AI-2 it is observed that end bearing piles are very effective in reducing settlements. About 35% to 43% settlement reduction ratio is observed in floating piles with different length and spacing. A settlement reduction ratio of 7% is observed for only basal geogrid reinforced embankment. But end bearing piles with 2D spacing gives 93%, 3D spacing gives 85% and 4D spacing gives 77% settlement reduction ratio.

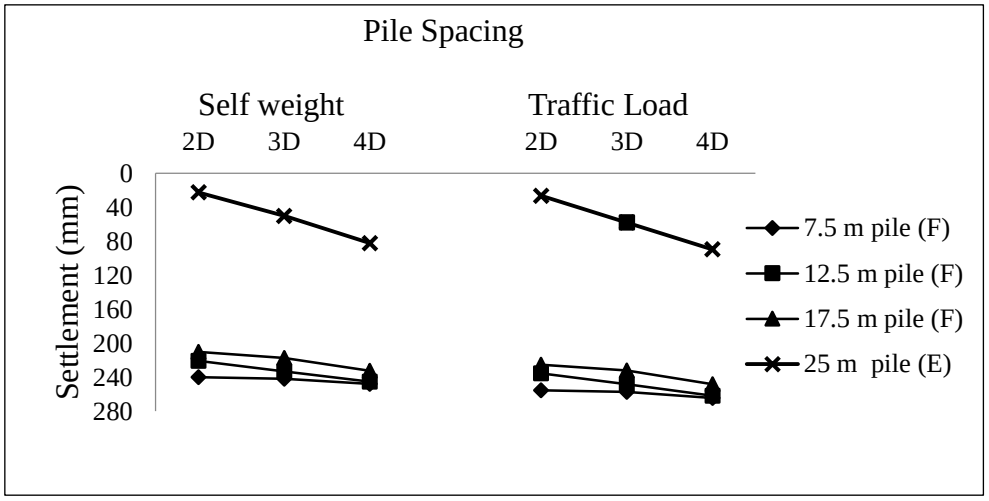

Figure AI- 3 Surface settlements at the centre of the embankment (F-Floating pile, E-End bearing pile)

Table AI-2 Settlements at different locations of embankment subjected to traffic load along with self-weight.

Embankment type		Embankment Surface Settlements (mm)	
		At centre of crest	At edge of crest
No pile No geogrid		398.74	359.31
With basal Geogrid		348.84	334.78
Pile Spacing	Length of pile (m)		
2D	7.5 m	255.63	239.12
	12.5 m	235.63	219.96
	17.5 m	225.21	210.53
	25 m	26.4	26.16

3D	7.5 m	257.18	241.06
	12.5 m	248.47	232.38
	17.5 m	232.23	216.6
	25 m	57.977	56.934
4D	7.5 m	264.32	248.7
	12.5 m	261.66	245.98
	17.5 m	248.22	232.74
	25 m	89.66	85.8

B. Differential Settlement Ratio

Differential settlement ratio is the ratio between surface settlements measured at centre of embankment crest and at edge of embankment crest expressed in percentage.

$$\text{Given by,} \quad DSR = 1 - \frac{S_{edge}}{S_{centre}} \tag{2}$$

Where, S_{edge} is the settlement of soil at the edge of embankment crest and S_{centre} is the settlement of soil at the centre of embankment crest

Settlements at the crest centre are more than at the crest edge because soil at the centre will be subjected to more stresses than at edge. An unreinforced embankment shows 10% of differential settlement ratio whereas geogrid reinforced embankment shows 4% of differential settlement ratio. About 6% differential settlement ratios at surface level were observed for all floating pile lengths and for all spacing combinations considered (Table AI-2). But in the case of end bearing piles less than 1% of differential settlements were seen.

C. Pile Skin Friction

At the foundation level, the soft soil settles more than the piles causing negative skin friction on the pile head. At the pile base level the pile toe punches into the soil stratum and settle more than the surrounding soft soil, which tends to positive skin friction at pile toe [Jenck et al (2009)]. Table AI-3 shows the settlement difference between centre of pile and middle of pile spacing measured at pile head and toe level subjected to traffic load along with the embankment weight. Increase in settlement difference is observed with the increase in floating pile length and spacing, which

shows the increase in both negative and positive skin friction with increase in pile length and spacing. In floating piles, very less settlement difference is seen at pile head level, which leads to lower negative skin friction and at toe level higher difference in settlements leads to very high positive skin friction. Hence extra care should be taken while designing the pile toe for positive skin friction. End bearing piles show very high negative skin friction values at pile head level than floating piles.

Table I-3 Settlement difference between centre of pile and middle of pile spacing subjected to traffic load along with the embankment weight

Pile Spacing	Length of pile (m)	Settlement difference (mm)	
		At pile head level	At pile toe level
2D	7.5 m	-1.4	+32.1
	12.5 m	-3.3	+52.2
	17.5 m	-7.2	+94.6
	25 m	-11	--
3D	7.5 m	-2.2	+33.9
	12.5 m	-4.5	+71.7
	17.5 m	-9.4	+108.5
	25 m	-55.5	--
4D	7.5 m	-4.7	+42.4
	12.5 m	-8.6	+81.3
	17.5 m	-13.1	+143.8
	25 m	-65.4	--

D. Stress Concentration Ratio

Stress concentration ratio (SCR) is defined as the ratio of vertical stress on the pile head to that on the surrounding soil. Given by, $SCR = \frac{\sigma_p}{\sigma_s}$ (3)

Where, σ_p is the vertical stress on pile head in N/m^2 and σ_s is the vertical stress on the soil surrounding pile in N/m^2.

From Table AI-4 it is seen that the stress concentration ratio for all the piles with 2D spacing is higher than the 3D and 4D spaced piles. In 4D spaced floating piles,

smaller values of stress concentration ratios were observed, because of large spacing between piles, the soil between the piles were also subjected to considerable amount of stresses. End bearing piles show higher stress concentration ratios than the floating piles due to continuous transfer of loads transferred from embankment to the hard stratum.

TableAI-4. Stress concentration ratios for different pile length and spacing subjected to traffic load along with the weight of the embankment

Spacing	Pile Length (m)	SCR
2D	7.5 m	9
	12.5 m	9.2
	17.5 m	9.3
	25 m	9.8
3D	7.5 m	7.2
	12.5 m	7.6
	17.5 m	7.7
	25 m	8.3
4D	7.5 m	6.3
	12.5 m	6.8
	17.5 m	7
	25 m	7.4

IV. Conclusions

End bearing piles are very much effective in reducing settlements even at 4D spacing. A maximum of 43% settlement reduction ratio is observed for floating piles, but more than 90% settlement reduction ratio is observed for 2D spaced end bearing piles.

An unreinforced embankment shows about 10% of differential settlement ratio. All the floating piles with different spacing considered for the present study shows 6% of differential settlement ratio. But in the case of end bearing piles, less than 1% of differential settlement ratios were seen.

Negative and positive skin frictions at the head and toe of piles are increasing with the increase of floating pile length and spacing. But more than 50% increase in skin friction is seen for the embankments supported on end bearing piles.

4D spaced floating piles gives smaller values of stress concentration ratios than 2D and 3D spaced floating piles, because of large spacing between piles, the soil between the piles are also subjected to considerable amount of stresses. End bearing piles are showing higher stress concentration ratios than the floating piles due to continuous transfer of loads transferred from embankment to the hard stratum.

APPENDIX II
DESIGN OF GEOGRID AS BODY-REINFORCEMENT USING SIMPLE WEDGE METHODS

Two part wedge, or bilinear, limit equilibrium models provide a method for quickly checking the computer-generated results. Design charts were developed based upon simplified analysis methods of two-part and one-part wedge-type failure surfaces and are limited by the following assumptions:

- Extensible reinforcement elements are used.
- Slopes are constructed with uniform, cohesionless soil; ϕ', c'=0, analysis appropriate,
- No pore pressures within the slope,
- Competent, level foundations,
- Flat slope face and horizontal slope crest,
- Uniform surcharge load at the top of the slope, and
- Horizontal reinforcement layers with coefficient of interaction (C_i) equal to 0.9.

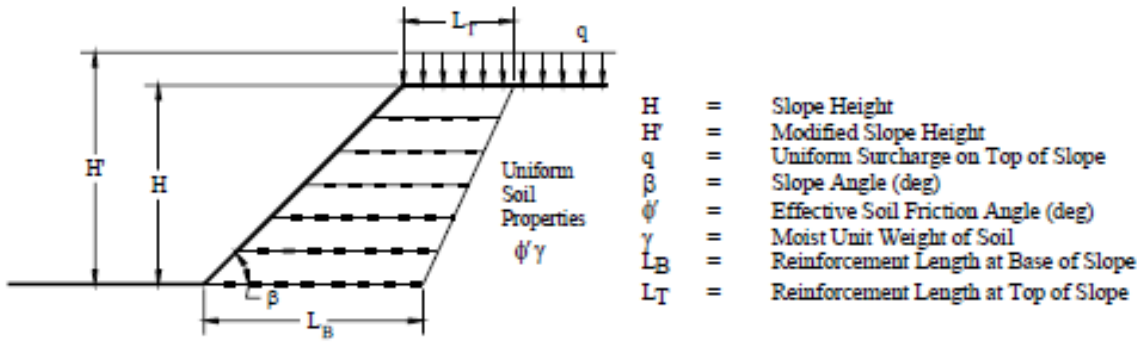

Figure AII- 1 Slope geometry and definitions (Schmertmann et al. 1987)

By definition, solutions for limit equilibrium models are for a factor of safety (FS) equal to unity. The target, or desired, overall FS is taken into account by factoring or reducing the soil shear strengths and is calculated as follows:

$$\emptyset'_f = \tan^{-1}\left(\frac{\tan \emptyset'}{FS}\right)$$

Where

Φ' = soil friction angle

Φ'_f = factored soil friction angle

The next step is to calculate the modified slope height (H') to take into account any uniform surcharge loading at the top of the slope. The modified slope height is calculated as follows:

$$H' = H + \frac{q}{\gamma}$$

Where H, q and γ are defined on Fig.AII-1.

From the chart on Fig.AII-3, determine the force coefficient K and calculate the maximum tensile force requirement (T_{max}) from the following.

$$T_{max} = 0.5 \times K \times \gamma \times (H')^2$$

From the chart on Fig. AII-2, determine the required reinforcement length at the top (L_T) and at the bottom (L_B) of the reinforced section.

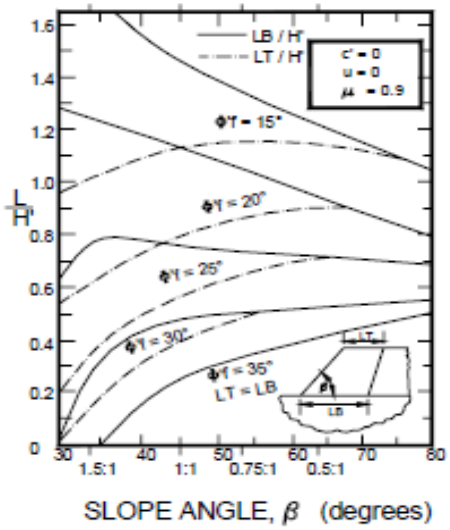

Figure AII- 2 Reinforcement length ratio, L_T and L_B (Schmertmann et al. 1987)

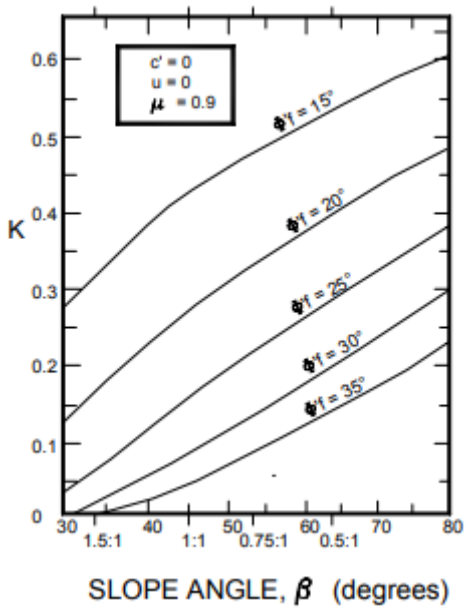

Figure AII- 3 Reinforcement Coefficient K (Schmertmann et al. 1987)

The next step in the procedure is to select the appropriate primary geogrid and calculate the number. The term "primary" geogrid layer refers to the geogrid required to satisfy internal, external and global stability requirements. At this point in the analysis, the designer must choose a geogrid so that the resulting spacing calculations yield acceptable values. For example, the spacing of primary geogrid layers at the bottom of slope should not be less than 200 mm to 300 mm. This corresponds to typical earthworks fill thickness. Conversely, the primary geogrid spacing should be no greater than 1220 mm. If calculations yield geogrid spacing less than the practical limit, then a stronger primary geogrid should be chosen. Alternatively, if the calculations yield geogrid spacing greater than 1220 mm, a lighter geogrid can be selected.

To determine the appropriate geogrid, calculate the long-term design strength (LTDS) of the material as follows:

$$LTDS = \frac{T_{ult}}{RF_{CR} \times RF_{ID} \times RF_{D}}$$

Where,

T_{ult} = ultimate tensile strength of the reinforcement as per ASTM D6637

RF_{CR} = reduction factor due to creep,

RF_{ID} = reduction factor due to installation damage, and

RF_{D} = reduction factor due to durability.

The minimum number of geogrid layers for the reinforced section, is then calculated as follows assuming 100% coverage of the geogrid vertical elevation:

$N = \frac{T_{max}}{LTDS}$ and $S_v = \frac{H}{N}$

Where

N = number of geogrid layers (rounded up to the next integer)

T_{max} = the total geogrid force (for a given section)

Note that T_{max} for a section of slope is equal to the geogrid force requirement for the entire height of the slope. For higher slope sections, T_{max} can be distributed over several zones. For example for a three zone section, one can distribute T_{max} as follows:

$$T_{Bottom} = \frac{1}{2} T_{max}$$

$$T_{MIddle} = \frac{1}{3} T_{max}$$

$$T_{Top} = \frac{1}{6} T_{max}$$

In other words, the section is divided into three zones where there will be three different spacing and geogrid requirements. This results in an efficient and cost-effective design. Pull-out embedment lengths have been taken into consideration in the total length, L_T and L_B in the chart in Fig.AII-2.

APPENDIX III

I COEFFICIENT OF LATERAL PRESSURE ON PILES UNDER SEISMIC LOADING CONDITIONS

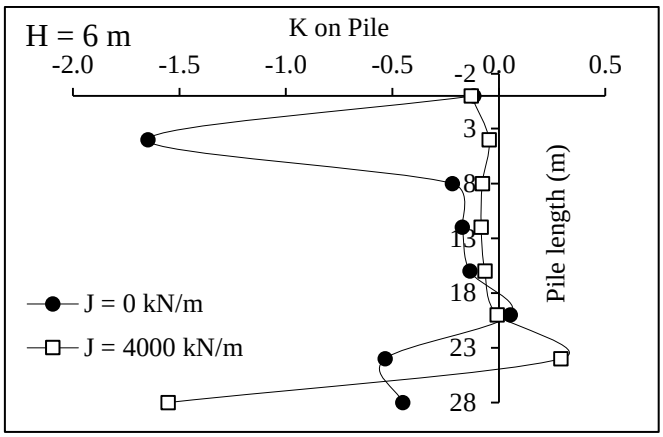

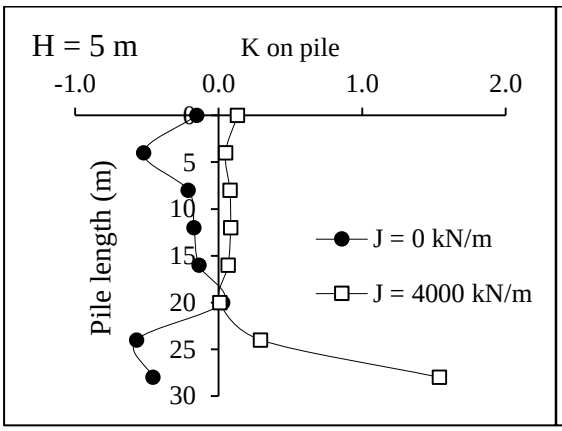

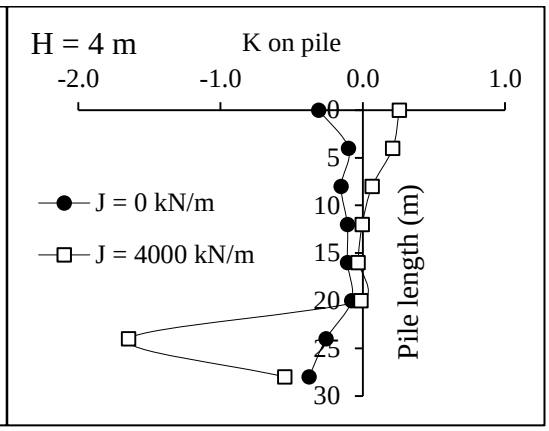

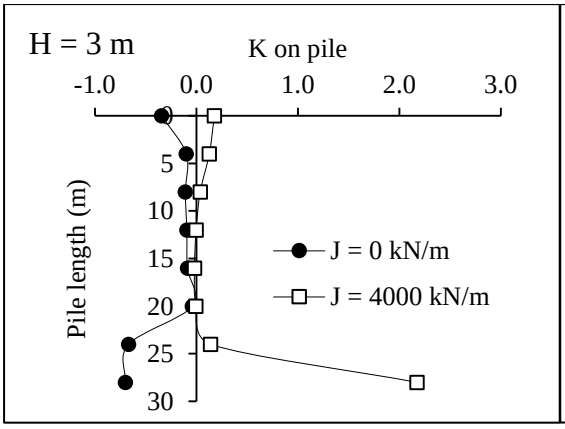

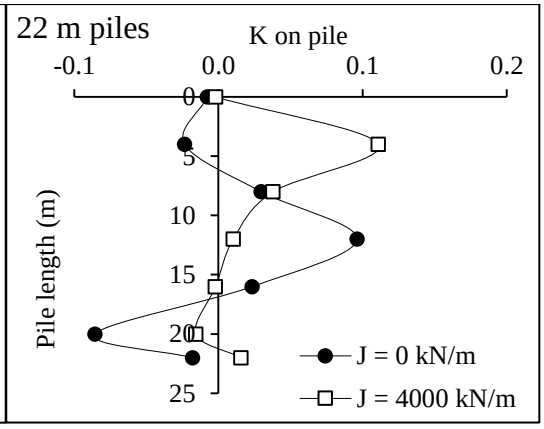

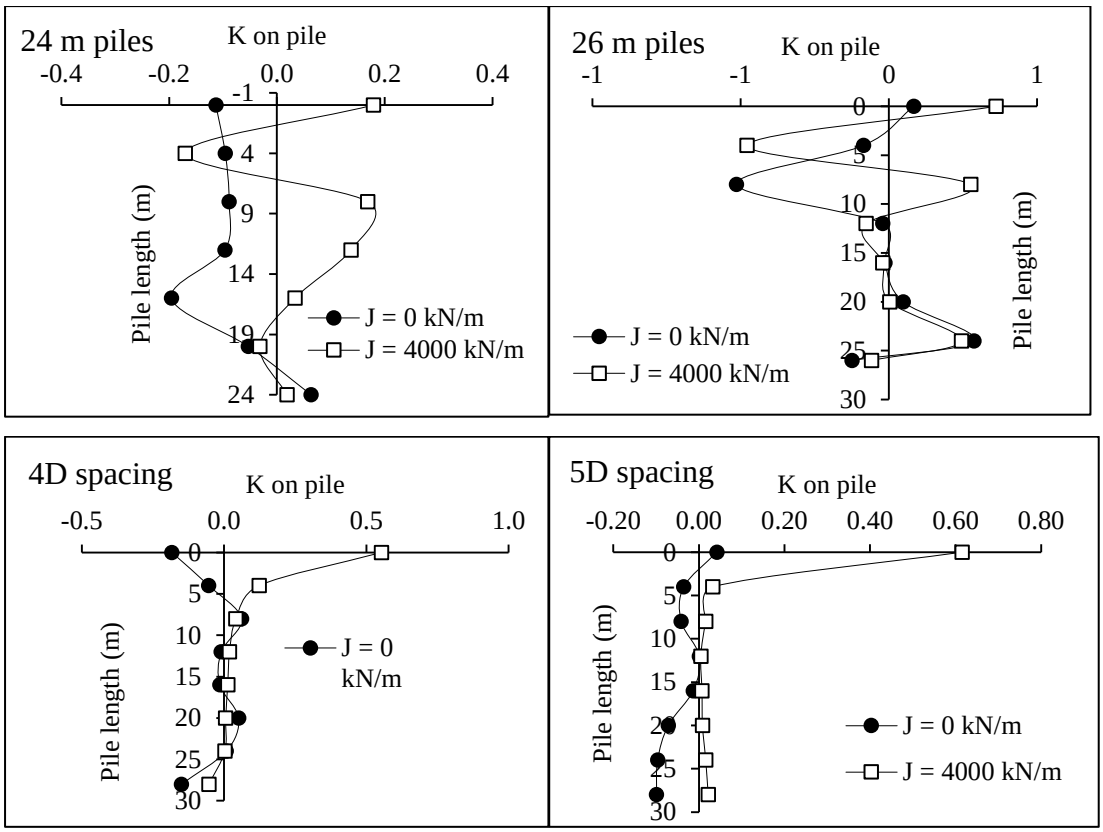

Figure AIII- 1 K along the length of pile at the instant of occurrence of PGA subjected to IS (0.35 g) ground motion

II COEFFICIENT OF LATERAL PRESSURE ON FOUNDATION SOIL UNDER SEISMIC LOADING CONDITIONS

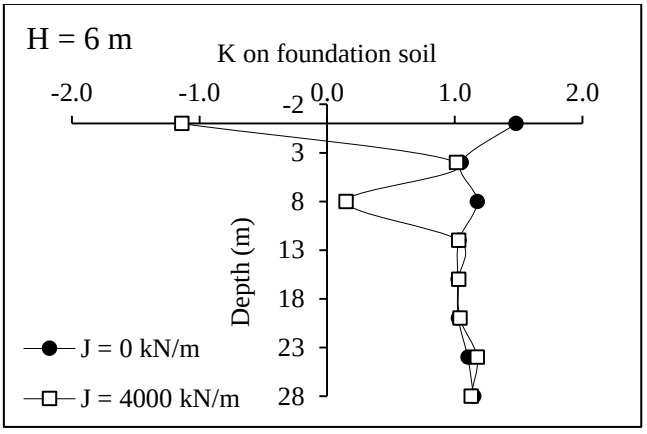

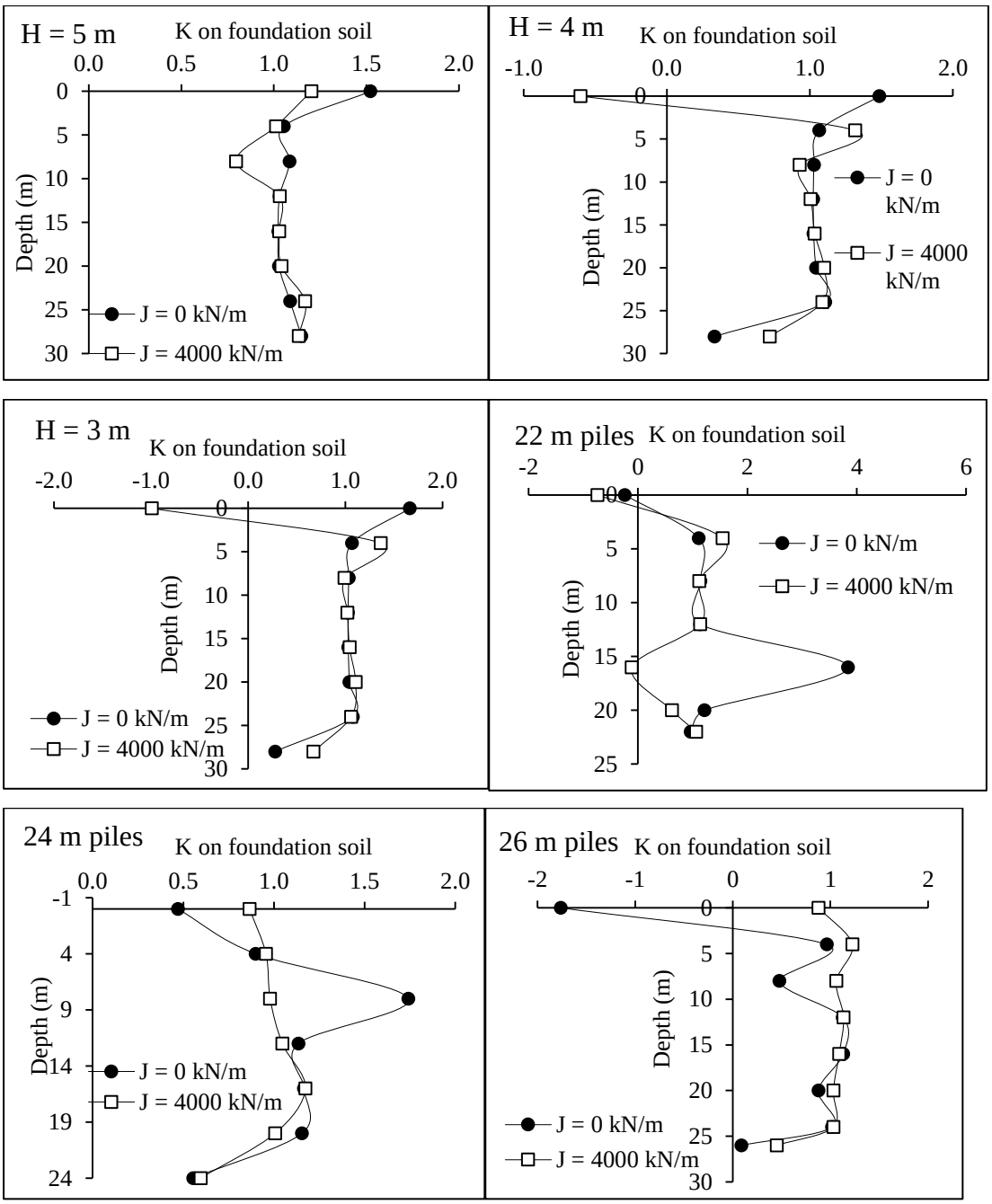
H = 5 m
K on foundation soil
0.0
0.5
1.0
1.5
2.0
Depth (m)
J = 0 kN/m
J = 4000 kN/m
H = 4 m
K on foundation soil
-1.0
0.0
1.0
2.0
Depth (m)
J = 0 kN/m
J = 4000 kN/m
H = 3 m
K on foundation soil
-2.0
-1.0
0.0
1.0
2.0
Depth (m)
J = 0 kN/m
J = 4000 kN/m
22 m piles
K on foundation soil
-2
0
2
4
6
Depth (m)
J = 0 kN/m
J = 4000 kN/m
24 m piles
K on foundation soil
0.0
0.5
1.0
1.5
2.0
Depth (m)
J = 0 kN/m
J = 4000 kN/m
26 m piles
K on foundation soil
-2
-1
0
1
2
Depth (m)
J = 0 kN/m
J = 4000 kN/m

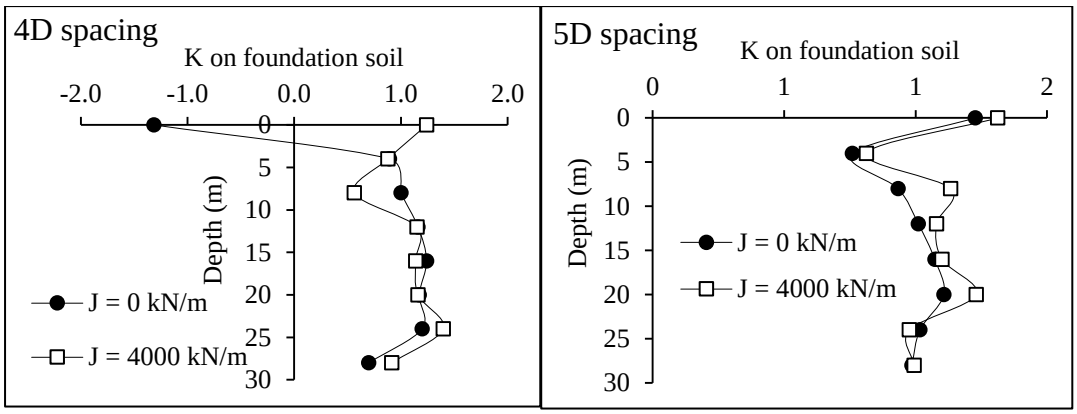

Figure AIII- 2 K along the depth of foundation soil at the instant of occurrence of PGA subjected IS (0.35 g) ground motion

REFERENCES

Abdullah, C.H. and Edil, T.B. (2007). "Behaviour of geogrid-reinforced load transfer platforms for embankment on rammed aggregate piers." *Geosynthetics International*, 14(3), 141-153.

ANSYS, Inc. (2019). "ANSYS Mechanical APDL user's manual, Canonsburg."

Ariyarathne, P. and Liyanapathirana, D. S. (2015). "Review of existing design methods for geosynthetic-reinforced pile-supported embankments." *Soils and Foundations*, 55(1), 17-34.

Ariyarathne, P., Liyanapathirana, D.S. and Leo, C.J., (2013). "A comparison of different two-dimensional idealizations for a geosynthetic reinforced pile- supported embankment." *International Journal of Geomechanics*, 13(6), 754–768.

Armstrong, R. J., Boulanger, R. W. and Beaty, M. H. (2013). "Liquefaction Effects on Piled Bridge Abutments: Centrifuge Tests and Numerical Analyses." *Journal of geotechnical and geoenvironmental engineering*, ASCE 139(3): 433–443.

Bathurst, R.J., Blatz, J.A. and Burger, M.H. (2003). "Performance of instrumented large-scale unreinforced and reinforced embankments loaded by a strip footing to failure." *Canadian Geotechnical Journal*, 40(6), 1067-1083.

Benmebarek, S., Berrabah, F. and Benmebarek, N. (2015). "Effect of geosynthetic reinforced embankment on locally weak zones by numerical approach." *Computers and Geotechnics*, 65:115-125

Bhasi, A., & Rajagopal, K. (2013). "Study of the effect of pile type for supporting basal reinforced embankments constructed on soft clay soil." *Indian Geotechnical Journal*, *43*(4), 344-353.

Bhasi, A., and Rajagopal, K. (2013). "Numerical investigation of time dependent behavior of geosynthetic reinforced piled embankments." *International Journal of Geotechnical Engineering*, *7*(3), 232-240.

Bhasi, A., and Rajagopal, K. (2015). "Geosynthetic-Reinforced Piled Embankments: Comparison of Numerical and Analytical Methods." *International Journal of Geomechanics*, ASCE. 15(5): 04014074.

Bhasi, A., and Rajagopal, K. (2015). "Numerical study of basal reinforced embankments supported on floating/end bearing piles considering pile-soil interaction." *Geotextiles and Geomembranes* 43:524-536.

Bonaparte, R., & Christopher, B. R. (1987). "Design and construction of reinforced embankments over weak foundations." *Transportation Research Record*, 1153, 26-39.

Bowles, J.E. (2012). "Foundation analysis and design." *Fifth Indian edition, Mc Graw-Hill education*, London

Briançon, L. and Simon, B. (2012). "Performance of pile-supported embankment over soft soil: full-scale experiment." *Journal of Geotechnical and Geoenvironmental Engineering*, 138(4), 551-561.

BS 8006:2010. "Code of Practice for Strengthened/Reinforced Soils and Other Fills." *British Standard Institution*, UK.

BS 8006: 1995. "Code of Practice for Strengthened/Reinforced Soils and Other Fills." *British Standard Institution*, UK.

Carlsson, B. (1987). "Reinforced soil, principles for calculation." *Terratema AB, Linköping.*

cement and clay drain tile and sewer pipe. Bulletin No. 31, Iowa Engineering Experiment design methods for piled embankment." *Proceedings of Geo-Frontiers*, Austin, USA.

Chai, J.C., Miura, N. and Shen, S.L. (2002). "Performance of embankments with and without reinforcement on soft subsoil." *Canadian Geotechnical Journal*, 39(4), 838-848

Chaiyaput, S., Bergado, D.T. and Artidteang, S. (2014). "Measured and simulated results of a Kenaf Limited Life Geosynthetics (LLGs) reinforced test embankment on soft clay." *Geotextiles and Geomembranes*, 42(1), 39-47

Chandrasekaran, S. S., Boominathan, A., and Dodagoudar, G. R. (2010). "Group interaction effects on laterally loaded piles in clay." *Journal of geotechnical and geoenvironmental engineering*, *136*(4), 573-582.

Chen, R. P., Wang, Y. W., Ye, X. W., Bian, X. C. and Dong, X. P., (2015). "Tensile force of geogrids embedded in pile-supported reinforced embankment: A full-scale experimental study." *Geotextiles and Geomembranes*, 44,157-169.

Dias, D, and Grippon, J. (2017). "Numerical modelling of a pile-supported embankment using variable inertia piles." *Structural Engineering and Mechanics*, 61(2), 245-253.

Dutch CUR design guideline for piled embankments. CUR 226 2010, ISBN 978-90-376-0518-1

EBGEO, (2010). "German Standard recommendation for Design and Analysis of Earth Structures Using Geosynthetic Reinforcements." *German Geotechnical Society, Ernst &Sohn GmbH &Co*.

Elsawy, M.B.D. (2018). "Soft soil improvement with conventional and geogrid-encased stone piles under an embankment." GeoMEast 2017. *Advances in Reinforced Soil Structures, Sustainable Civil Infrastructures*, Springer, Egypt, 110-125

Faizi, K., Armaghani, D.J, Kassim, A. and Lonbani, M. (2013). "Evaluation of geotextiles on embankment displacement under seismic Load." *Electronic Journal of Geotechnical Engineering*, 18: 439-449

Gangakhedkar, R. (2004). "Geosynthetic reinforced pile supported embankments." (Doctoral dissertation, University of Florida).

Gao, X. J., Qian, H., Guo, Y. C., and Wang, F. (2016). "Seismic response analysis of GRPS embankment under oblique incident P wave." *Journal of Central South University*, *23*(3), 721-728.

Ghosh, S, and Wilson, E.L. (1969). "Analysis of axi-symmetric structures under arbitrary loading." (No. 69-10) EERC Report

Ghosh, B., Fatahi, B., Khabbaz, H., and Yin, J. H. (2017). "Analytical study for double-layer geosynthetic reinforced load transfer platform on column improved soft soil." *Geotextiles and Geomembranes*, 45(5), 508-536

Ghosh, S. and Wilson, E. L. (1969). "Analysis of axi-symmetric structures under arbitrary loading." (No. 69-10) EERC Report.

Guido, V.A, Kneuppel, J. D., and Sweeney, M. A., (1987). "Plate loading tests on geogrid reinforced earth slabs." *Proceedings of Geosynthetics conference,* 87, 216–225.

Han, J., Oztoprak, S., Parsons, R. L., and Huang, J. (2007). "Numerical analysis of foundation columns to support widening of embankments." *Computers and Geotechnics*, *34*(6), 435-448.

Han, G. X., Gong, Q. M. and Zhou, S. H. (2015). "Soil arching in a piled embankment under dynamic load." *International Journal of Geomechanics*, 15(6), 04014094.

Han, J., and Gabr, M. A. (2002). "A numerical study of load transfer mechanisms in geosynthetic reinforced and pile supported embankments over soft soil." *Journal of Geotechnical and Geoenvironmental Engineering*, ASCE 128(1):44-53.

Han, J., Bhandari, A., and Wang, F. (2012). "DEM analysis of stresses and deformations of geogrid-reinforced embankments over piles." *International Journal of Geomechanics*, 12(4), 340-350

Hata, Y., Ichii, K., Tsuchida, T., Kano, S., and Yamashita, N. (2008). "A practical method for identifying parameters in the seismic design of embankments." *Geori*sk, 2(1) 28-40

Helwany, S. M. B., Jonathan, T.H. Wu., and Burkhard, Froessl. (2003). "GRS bridge abutments-an effective means to alleviate bridge approach settlement." *Geotextiles and Geomembranes*, 21, 177-196.

Hewlett, W. J., and Randolph, M. F. (1988). "Analysis of piled embankments." *Ground Engineering*, 21(3), 12-18.

Huang, J., and Han, J. (2009). "3D coupled mechanical and hydraulic modeling of a geosynthetic-reinforced deep mixed column-supported embankment." *Geotextiles and Geomembranes*, 27, 272-280.

IRC 113-2013 "Guidelines for the design and construction of geosynthetic reinforced embankments on soft subsoils."

IRC: 6-2014. "Standard specifications and code of practice for road bridges. Section: II Loads and stresses."

IRC: 75-2015 "Guidelines for the Design of High Embankments."

IS 1893 (Part 1). (2016). "Criteria for earthquake resistant design of structures."

IS 1893 (Part 5). (1984). "Criteria for earthquake resistant design of structures."

IS 2911 (Part 1/Sec 1). (2010). "Design and construction of pile foundations - code of practice."

IS 456 (2000). "Plain and reinforced concrete - Code of practice."

IS: 1498-1970 (reaffirmed 2007). "Classification and identification of soils for general engineering purposes."

Jenck, O., Daniel, D., and Richard, K. (2009). "Three-dimensional numerical modeling of a piled embankment." *International Journal of Geomechanics*, 9 (3), 102-112.

Jing, Z. D., Liu, L., Zheng, G., and Jiang, Y. (2008). "Numerical analysis of pile lateral behavior of pile supported embankment." *Journal of Central South University of Technology*, 15(2), 87-92.

Jones, C. J. F. P., Lawson, C. R., and Ayres, D. J. (1990). "Geotextile reinforced piled embankments." *Proceedings, 4th International Conference on Geotextiles, Geomembranes, and Related Products*, Vol. 1, G. Den Hoedt (ed), The Hague, May - June 1990, 155-160.

Jose, B. T., Sridharan, A., and Abraham, B. M. (1988). "A study of geotechnical properties of Cochin marine clays." *Marine Georesources & Geotechnology*, 7(3), 189-209.

Kempfert, H. G., Stadel, M., and Zaeske, D. (1997). "Design of geosynthetic-reinforced bearing layers over piles." *Bautechnik,* 74(12), 818-825.

Kianoush, M. R., and Ghaemmaghami, A. R. (2011). "The effect of earthquake frequency content on the seismic behavior of concrete rectangular liquid tanks using the finite element method incorporating soil–structure interaction." *Engineering Structures,* 33(7), 2186-2200.

King, D. J., Bouazza, A., Gniel, J. R., Rowe, R. K., and Bui, H. H. (2017). "Serviceability design for geosynthetic reinforced column supported embankments". *Geotextiles and Geomembranes*, *45*(4), 261-279.

Komak Panah A., Yazdi, M., and Ghalandarzadeh, A. (2015). "Shaking table tests on soil retaining walls reinforced by polymeric Strips." *Geotextiles and Geomembranes*, 43, 148-161

Lawson, C.R. (1992). "Soil Reinforcement with Geosynthetics." *Applied Ground Improvement Techniques*. Southeast Asian Geotechnical Society (SEAGS) 55–74.

Leshchinsky, D., Imamoglu, B., and Meehan C. L. (2010). "Exhumed Geogrid-Reinforced Retaining Wall." *J. Geotech. Geoenviron. Eng., ASCE.* 136(10), 1311-1323.

Lin, Y.L, Leng, W.M., Yang, G.L., Li, L., and Yang, J.S. (2015). "Seismic response of embankment slopes with different reinforcing measures in shaking table tests." *Natural Hazards,* 76(2) 791-810.

Lin, Y.L., and Yang, G.L. (2013). "Dynamic behavior of railway embankment slope subjected to seismic excitation." *Natural hazards*, 69(1), 219-235

Liu, H. L., Charles, W. W. Ng., and Fei, K. (2007). "Performance of a Geogrid-Reinforced and Pile-Supported Highway Embankment over Soft Clay: Case Study." *Journal of Geotechnical and Geoenvironmental Engineering, ASCE.* 133(12), 1483-1493.

Liu, K. W., Rowe, R. K., Su, Q., Liu, B., and Yang, Z. (2017). "Long-term reinforcement strains for column supported embankments with viscous reinforcement by FEM." *Geotextiles and Geomembranes*, 45(4), 307-319.

Lu, W., and Miao, L. (2015). "A simplified 2-D evaluation method of the arching effect for geosynthetic-reinforced and pile-supported embankments." *Computers and Geotechnics*, 65, 97-103.

Madhavi Latha, G., and Nandhi Varman, A.M. (2014). "Shaking table studies on geosynthetic reinforced soil slopes." *International Journal of Geotechnical Engineering*, 8(3), 299-306.

Magnani, H.O., Almeida, M.S.S., and Ehrlich, M. (2009). "Behaviour of two reinforced test embankments on soft clay." *Geosynthetics International*, 16(3), 127-138

Marston, A., and Anderson, A. O. (1913). "The theory of loads on pipes in ditches and tests of cement and clay drain tile and sewer pipe." B*ulletin No. 31, Iowa Engineering Experiment Station*, Ames, Iowa.

Matsuo, O., Shimazu, T., Uzuoka, R., Mihara, M., and Nishi, K. (2000). "Numerical analysis of seismic behavior of embankments founded on liquefiable soils." *Soils and Foundations* 40(2), 21-39

Meena, N. K., Nimbalkar, S., Fatahi, B., and Yang, G. (2020). "Effects of soil arching on behavior of pile-supported railway embankment: 2D FEM approach." *Computers and Geotechnics, 123,* 103601.

McNulty, J. W. (1965). "An Experimental study of arching in sand." *Technical Report No. I-674, U.S. Army Engineer Waterways Experiment Station, Corps of Engineers, Vicksburg, Mississippi,* 170.

Modoni, G., Albano, M., Salvatore, E., and Koseki, J. (2018). "Effects of compaction on the seismic performance of embankments built with gravel." *Soil Dynamics and Earthquake Engineering,* 106, 231-242

Mwasha, A., and Petersen, A. (2010). “Thinking outside the box: The time dependent behaviour of a reinforced embankment on soft soil.” *Materials & Design*, (1980-2015), 31(5), 2360-2367.

Niu, T., Liu, H., Ding, X., and Zheng, C. (2018). “Model tests on XCC-piled embankment under dynamic train load of high-speed railways.” *Earthquake Engineering and Engineering Vibration*, 17(3) 581-594.

Naughton, P. J., & Kempton, G. T. (2005). “Comparison of analytical and numerical analysis design methods for piled embankments.” *Contemporary Issues in Foundation Engineering* (pp. 1-10).

Oh, Y. I., and Shin, E. C. (2007). “Reinforcement and arching effect of geogrid-reinforced and pile-supported embankment on marine soft ground.” *Marine Georesources and Geotechnology*, 25(2), 97-118.

Okamura, M., Tamamura, S., and Yamamoto, R. (2013). “Seismic stability of embankments subjected to pre-deformation due to foundation consolidation.” *Soils and foundations*, 53(1) 11-22.

Oliveira, H.M., Ehrlich, M., and Almeida, M.S. (2010). “Embankments over soft clay deposits: Contribution of basal reinforcement and surface sand layer to stability.” *Journal of geotechnical and geoenvironmental engineering*, 136(1), 260-264.

Oser, C., Cinicioglu, S.F., and Cinicioglu, O. (2020). “Design method for quantifying embankment safety against lateral spreading and determining contribution of basal reinforcements.” *Geotextiles and Geomembranes*, 48(3), 297-305.

Ousta, R., and Shahrour, I. (2001). “Three-dimensional analysis of the seismic behavior of micropiles used in the reinforcement of saturated soil.” *International Journal for Numerical and Analytical Methods in Geomechanics*, 25: 183–196.

Panah, A. K., Yazdi, M., and Ghalandarzadeh, A. (2015). “Shaking table tests on soil retaining walls reinforced by polymeric strips.” *Geotextiles and Geomembranes*, 43(2), 148-161.

Papadimitriou, A.G., Bouckovalas, G.D., and Andrianopoulos, K.I. (2014). “Methodology for estimating seismic coefficients for performance-based design of earthdams and tall embankments.” *Soil Dynamics and Earthquake Engineering*, 56, 57-73.

Pham, H. V., and Dias, D. (2019). "3D Numerical Modeling of a Piled Embankment under Cyclic Loading." *International Journal of Geomechanics*, 19(4) 04019010

Richard, J. Armstrong., Ross, W., Boulanger, and M. H. Beaty. (2013). "Liquefaction Effects on Piled Bridge Abutments:Centrifuge Tests and Numerical Analyses." *Journal of Geotechnical and Geoenvironmental Engineering, ASCE*, 139(3). 433–443.

Rowe, R.K., and Li A.L. (2005). "Geosynthetic-reinforced embankments over soft foundations." *Geosynthetics International*, 12(1), 50-85.

Rowe, R.K., and Li A.L. (1999). "Reinforced embankments over soft foundations under undrained and partially drained conditions." *Geotextiles and Geomembranes* 17(3) 129-146

Rowe, R.K., and Soderman, K.L. (1987). "Stabilization of very soft soils using high strength geosynthetics: the role of finite element analyses." *Geotextiles and Geomembranes* 6(1-3), 53-80.

Rowe, R. K., and Skinner, G. D. (2001). "Numerical analysis of geosynthetic reinforced retaining wall constructed on a layered soil foundation." *Geotextiles and geomembranes*, 19(7), 387-412.

Rui, R., Han, J., van Eekelen, S. J. M. and Wan, Y. (2019). "Experimental investigation of soil-arching development in unreinforced and geosynthetic-reinforced pile-supported embankments." *Journal of Geotechnical and Geoenvironmental Engineering*, 145(1), 04018103

Rui, R., Van Tol, A. F., Xia, Y. Y., Van Eekelen, S. J. M., and Hu, G. (2016). "Investigation of soil-arching development in dense sand by 2D model tests." *Geotechnical Testing Journal*, 39(3), 415-430

Russell, D., and Pierpoint, N. (1997). "An assessment of design methods for piled embankments." *Ground Engineering,* November, 39-44.

Sarsby, R.W. (2007). "Use of 'Limited Life Geotextiles' (LLGs) for basal reinforcement of embankments built on soft clay." *Geotextiles and Geomembranes*, 25(4-5), 302-310

Schmertmann, G. R., Chouery-Curtis, V. E., Johnson, R. D. and Bonaparte, R. (1987). "Design charts for geogrid-reinforced slopes." *Proc Geosynthetics '87,* Vol 1, New Orleans: 108-120.

Shen, P., Xu, C. and Han, J. (2017). "Model tests investigating spatial tensile behavior of simulated geosynthetic reinforcement material over rigid supports." *Journal of Materials in Civil Engineering*, 30(2), 04017288.

Sheta, N.O., and Frizzi, R.P. (2018). "Analysis and design of piled geogrid-reinforced-earth embankment." *GeoMEast 2017, Advances in Reinforced Soil Structures, Sustainable Civil Infrastructures,* Springer, Egypt, 126-136.

Shukla, S.K., and Kumar, R. (2008). "Overall slope stability of prestressed geosynthetic-reinforced embankments on soft ground." *Geosynthetics International*, 15(2), 165-171

Skinner, G. D., and Rowe, R. K. (2005). "Design and behaviour of a geosynthetic reinforced retaining wall and bridge abutment on a yielding foundation." *Geotextiles and Geomembranes*, 23(3), 234-260.

Smith, C.C., and Tatari, A. (2016). "Limit analysis of reinforced embankments on soft soil." *Geotextiles and Geomembranes*, 44(4), 504-514

Smith, M., and Filz, G. (2007). "Axisymmetric numerical modeling of a unit cell in geosynthetic-reinforced, column-supported embankments." *Geosynthetics International*, 14(1), 13-22.

Stewart, M.E., and Filz, G.M. (2005). "Influence of clay compressibility on geosynthetic loads in bridging layers for column supported embankments." *Geotech. Spec. Publ, 131*, 447-460.

Svano**,** G., Ilstad, T., Eiksund, G., and Want, A. (2000). "Alternative calculation principles for design of piled embankment with base reinforcement." *Proceedings of 4th International Conference on Ground Improvement Geosystems,* Helsinki.

Syawal, Satibi. (2009). "Numerical analysis and design criteria of embankments on floating piles." *(A PhD Thesis submitted to the University of Stuttgart, Germany).*

Taechakumthorn, C., and Rowe, R.K. (2013). "Reinforced embankments on soft deposits: behaviour, analysis and design." *Geotechnical Engineering. Journal of the Southeast Asian Geotechnical Society*, 44(4), 69-76.

Taha, A., El Naggar, M. H., and Turan, A. (2015). "Numerical modeling of the dynamic lateral behavior of geosynthetics-reinforced pile foundation system." *Soil Dynamics and Earthquake Engineering*, 77, 254-266.

Tang, Y., Xiao, S., and Yang, Q. (2020). “The behaviour of geosynthetic-reinforced pile foundation under long-term dynamic loads: model tests.” *Acta Geotechnica*, *15*(8), 2205-2225.

Terzaghi, K. (1965). “Theoretical soil mechanics.” *John Wiley and Sons*

Thach, P. N., Liu, H. L., and Kong, G. Q. (2013). “Vibration analysis of pile-supported embankments under high-speed train passage.” *Soil Dynamics and Earthquake Engineering*, 55:92-99.

Thach, P. N., Liu, H. L., and Kong, G. Q. (2013). “Evaluation of PCC pile method in mitigating embankment vibrations from a high-speed train.” *Journal of Geotechnical and Geoenvironmental Engineering*, 139(12), 2225-2228.

Thach, P. N., Liu, H. L., and Kong, G. Q. (2013). “Vibration analysis of pile-supported embankments under high-speed train passage.” *Soil Dynamics and Earthquake Engineering*, 55, 92-99

Van Eekelen, S .J. M., Bezuijen, A., and Van, Tol, A. F. (2011). “Analysis and modification of the British Standard BS8006 for the design of piled Embankments” *Geotextiles and Geomembranes* 29(3), 345-359.

Van Eekelen, S .J. M., Bezuijen, A., and Van Tol, A. F. (2013). “An analytical model for arching in piled embankments.” *Geotextiles and Geomembranes* 39, 78-102.

Van Eekelen, S .J. M., Bezuijen, A., and Van Tol, A. F. (2014). “Validation of analytical models for the design of basal reinforced piled Embankments.” *Geotextiles and Geomembranes* 43, 56-81.

Van Eekelen, S. J., Bezuijen, A., Lodder, H. J., and van Tol, E. A. (2012). “Model experiments on piled embankments.” Part I. *Geotextiles and Geomembranes*, 32, 69-81

Van Eekelen, S. J., Bezuijen, A., Lodder, H. J., and van Tol, E. (2012). “A Model experiments on piled embankments. Part II.” *Geotextiles and Geomembranes*, 32, 82-94

Vijayasri, T., Raychowdhury, P., Patra, N.R. (2017). “Seismic response analysis of Renusagar pond ash embankment in Northern India.” *International Journal of Geomechanics*, 17(6), 04016141

Wachman, G. S., Biolzi, L., and Labuz, J. F. (2009). “Structural behavior of a pile-supported embankment.” *Journal of geotechnical and geoenvironmental engineering*, 136(1), 26-34.

Wang, C., Wang, B., Guo, P., and Zhou, S. (2015). "Experimental analysis on settlement controlling of geogrid-reinforced pile-raft-supported embankments in high-speed railway." *Acta Geotechnica*, 10(2), 231-242

Wang, K. Y., Zhuang, Y., Liu, H., and Miao, Y. (2018) "Soil arching in highway piled embankments subjected to moving shakedown limit loads." *European Journal of Environmental and Civil Engineering*, 1-15

Wang, L., and Yuan, X. (2005). "Decline and dynamic characteristics of micropiles reinforced foundation." *Journal of Hydraulic Engineering*,12: 1193–1199.

Wang, L., Chen, G., and Chen, S. (2015). "Experimental study on seismic response of geogrid reinforced rigid retaining walls with saturated backfill sand." *Geotextiles and Geomembranes*, *43*(1), 35-45.

Wang, Z., and Mei, G. (2012). "Numerical analysis of seismic performance of embankment supported by micropiles." *Marine Georesources & Geotechnology*, *30*(1), 52-62.

Wang, L., Liu, H., and Wang, C. (2018) "Earth pressure coefficients for reinforcement loads of vertical geosynthetic reinforced soil retaining walls under working stress conditions." *Geotextiles and Geomembranes.* 46, 486-496.

Wijerathna, M., and Liyanapathirana, D. S. (2021). "Simplified modelling approaches for DCM column-supported embankments." *International Journal of Geotechnical Engineering*, *15*(5), 553-562.

Xie, Yonggui., and Leshchinsky, Ben. (2015). "MSE walls as bridge abutments: Optimal reinforcement density." *J. Geotextiles and Geomembranes,* 43, 128-138.

Xing, H., Zhang, Z., Liu, H., and Wei, H. (2014). "Large-scale tests of pile-supported earth platform with and without geogrid." *Geotextiles and Geomembranes*, 42(6), 586-598

Yoo, C., and Jung, H. S. (2004). "Measured behavior of a geosynthetic-reinforced segmental retaining wall in a tiered configuration." *Geotextiles and Geomembranes*, 22(5), 359-376.

Yoo, C., and Kim, S. B. (2008). "Performance of a two-tier geosynthetic reinforced segmental retaining wall under a surcharge load: full-scale load test and 3D finite element analysis." *Geotextiles and Geomembranes*, 26(6), 460-472.

Yoo, C., and Kim, S. B. (2009). “Numerical modeling of geosynthetic-encased stone column-reinforced ground.” *Geosynthetics International*, 16(3), 116-126.

Yu, Y., and Bathurst, R. J. (2017). “Modelling of geosynthetic-reinforced column-supported embankments using 2D full-width model and modified unit cell approach.” *Geotextiles and Geomembranes*, 45(2), 103-120.

Zhang, C., Jiang, G., Liu, X., and Buzzi, O. (2016). “Arching in geogrid-reinforced pile-supported embankments over silty clay of medium compressibility: Field data and analytical solution.” *Computers and Geotechnics*, 77, 11-25.

Zhang, L., Zhou, S., Zhao, H., and Deng, Y. (2018). “Performance of geosynthetic-reinforced and pile-supported embankment with consideration of soil arching.” *Journal of Engineering Mechanics*, 144(12), 06018005.

Zhang, N., Shen, S.L., Wu, H.N., Chai, J.C., Xu, Y.S., and Yin, Z.Y. (2015). “Evaluation of effect of basal geotextile reinforcement under embankment loading on soft marine deposits.” *Geotextiles and Geomembranes*, 43(6), 506-514

Zhang, Z., Wang, M., Ye, G. B., and Han, J. (2019). “A novel 2D-3D conversion method for calculating maximum strain of geosynthetic reinforcement in pile-supported embankments.” *Geotextiles and Geomembranes*, 47(3), 336-351.

Zhao, L. S., Zhou, W. H., and Yuen, K. V. (2017). “A simplified axisymmetric model for column supported embankment systems.” *Computers and Geotechnics*, 92, 96-107.

Zhuang, Y., and Wang, K. (2017). “Analytical solution for reinforced piled embankments on elastoplastic consolidated soil.” *International Journal of Geomechanics, ASCE. 17*(9), 06017010.

Zhuang, Y., Wang, K. Y., and Liu, H. L. (2014). “A simplified model to analyze the reinforced piled embankments.” *Geotextiles and Geomembranes*, 42(2), 154-165.

Zhuang, Y., and Wang, K. (2018). “Finite element analysis on the dynamic behavior of soil arching effect in piled embankment.” *Transportation Geotechnics*, *14*, 8-21.

Zhuang, Y., Cui, X., Zhang, S., Dai, G., and Zhao, X. (2020). “The load transfer mechanism in reinforced piled embankment under cyclic loading and unloading.” *European Journal of Environmental and Civil Engineering*, 1-15.

LIST OF PUBLICATIONS

JOURNALS

1. Patel, R.M., Jayalekshmi, B.R., and Shivashankar, R. (2021). "Stress Distribution in Basal Geogrid Reinforced Pile-Supported Embankments Under Seismic Loads." *Transportation Infrastructure Geotechnology.* https://doi.org/10.1007/s40515-021-00148-9 (SCOPUS indexed)
2. Radhika, M. Patel, B. R. Jayalekshmi., and R. Shivashankar. (2017). "Finite Element Analysis of Geogrid Reinforced Pile Supported Embankment Considering the Effect of Pile Length." *International Journal of Engineering and Advanced Technology* (IJEAT)', ISSN: 2249-8958, Volume-7 Issue-ICMSC17, Pg. 137-140, December 2017. https://www.ijeat.org/download/volume-7-issue-icmsc17/
3. Patel, R.M., Jayalekshmi, B.R. and Shivashankar, R. (2021). "Effect of Reinforcement Width on Dynamic response of Basal Geosynthetic-Reinforced Embankment." *Transportation Infrastructure Geotechnology*, https://doi.org/10.1007/s40515-021-00188-1 (SCOPUS indexed)

BOOK CHAPTERS

1. Patel, R. M., Jayalekshmi, B. R., and Shivashankar, R. (2020). "A Study on the Seismic Behaviour of Embankments with Pile Supports and Basal Geogrid." *Advances in Computer Methods and Geomechanics* (pp.257-268). Lecture Notes in Civil Engineering, vol 56. Springer, Singapore. https://doi.org/10.1007/978-981-15-0890-5_22 (SCOPUS indexed)
2. Patel, R. M., Jayalekshmi, B. R., and Shivashankar, R. (2020). "Seismic Response of Basal Geogrid Reinforced Embankments Supported over Floating and End Bearing Piles." *Silvestri & Moraci (Eds), Earthquake Geotechnical Engineering for Protection and Development of Environment and Constructions*, ISBN 978-0-367-14328-2 pp. 4620-4628. Rome, Italy. (SCOPUS indexed)
3. Patel, R. M., Jayalekshmi, B. R., and Shivashankar, R. (2020). "Seismic Response of Basal Geogrid Reinforced Embankments Supported on a Group of Vertical and Batter Piles." *Local Site Effects and Ground Failures: Select Proceedings of 7th ICRAGEE*, 145. https://doi.org/10.1007/978-981-15-9984-2_13. (SCOPUS indexed)

CONFERENCE PUBLICATIONS

1. Radhika, M. Patel, B. R. Jayalekshmi., and R. Shivashankar. (2016). "Settlement Analysis of Pile Supported Embankments", *10th International Symposium on Lowland Technology,* Mangalore, India. p. 209-214. (Presented by First Author)
2. Jayalekshmi, B. R., Radhika, M. Patel., and Shivashankar R. (2018). "Seismic response of Geogrid Reinforced Piled Embankment Slopes." *International Symposium on Lowland Technology, Sept. 26 – 28, 2018,* Hanoi, Vietnam. ISBN: 978.604.82.2483.7(Presented by First Author)
3. Radhika, M. Patel, Jayalekshmi, B. R., and Shivashankar, R. (2018). "Seismic Response Analysis of Geogrid Reinforced Pile Supported Embankments." *16th Symposium on Earthquake Engineering, Dec.20-22, 2018,* IIT Roorkee, India. p-206(1-10). (Presented by First Author)
4. Sreelekshmy, S., Radhika, M. Patel., B. R. Jayalekshmi., and R. Shivashankar. (2016). "Finite Element Analysis of Geogrid Reinforced Piled Embankments Under Traffic Load", *10th International Symposium on Lowland Technology,* Mangalore, India. p. 250-255. (Presented by First Author)
5. Sreelekshmy, S., Radhika, M. Patel., B. R. Jayalekshmi., and R. Shivashankar. (2017). "Effect of pile aspect ratio on geogrid reinforced piled embankments", *6thInternational Engineering Symposium – IES. March 1-3, 2017, Kumamoto University, Japan* (Presented by First Author)
6. Patel, R. M., Jayalekshmi, B. R., and Shivashankar, R. (2020). "A Study on the Seismic Behaviour of Embankments with Pile Supports and Basal Geogrid." *Advances in Computer Methods and Geomechanics* (pp.257-268). Lecture Notes in Civil Engineering, vol 56. Springer, Singapore. https://doi.org/10.1007/978-981-15-0890-5_22 (Presented by First Author)
7. Patel, R. M., Jayalekshmi, B. R., and Shivashankar, R. (2020). "Seismic Response of Basal Geogrid Reinforced Embankments Supported over Floating and End Bearing Piles." *Silvestri & Moraci (Eds), Earthquake Geotechnical Engineering for Protection and Development of Environment and Constructions,* ISBN 978-0-367-14328-2 pp. 4620-4628. Rome, Italy. (Presented by Third Author)

RESUME

Radhika.M.Patel
W/o Avinash A S
Adigere, Biselere post
Kadur taluk
Chikmagalur dist **Email:radikagmpatel@gmail.com**
Karnataka-577116 **Contact-no: +91-9880545979**

CAREER OBJECTIVE

To work as a intend to build a career with leading corporate of hi-tech environment with committed and dedicated people, which will help me to explore myself fully and realize my potential simultaneously being willing key player in a challenging and creativity environment.

EDUCATIONAL QUALIFICATIONS

Name of the course	College/School	University/ Board	Year of Passing	Aggregate/ Percentage
PhD (Civil Engineering-Geotechnical engineering)	NITK, Surathkal	NITK, Surathkal	On going	**8.46 CGPA (based on course work)**
M.Tech(Geotechnical Engineering)	NIT, Warangal.	NIT, Warangal	2015	**7.54 CGPA**
BE(civil engineering)	SJM Institute of Technology, Chitradurga	Visvesvaraya technological university	2012	**76.94%**
PUC	Govt PU.College, Kadur	Karnataka Pre-University Board	2008	**68%**

SSLC	Govt. Junior College, Kadur	Karnataka State Secondary Education Board	2005	**75.52%**

GATE RANKING

Scored 971 ranking in GATE-2012

WORK EXPERIENCE

One year teaching Experience as Lecturer at SRSIT, Chikkajala, Bangalore.

PROJECT PROFILE

Study on "**Effect of Pile Aspect Ratio on Pile Supported Building Frame Considering Soil-Structure Interaction**."- (M.Tech)

Presently doing **Ph.D.** in the department of Civil Engineering NITK, Surathkal, Mangalore.

Research Area- Numerical analysis of pile-supported geogrid-reinforced Embankments on soft grounds.

Publications based on PhD work

Journals-3

Book chapters-3

Conference publications-5